AD-775 391

TAIL ROTOR DESIGN GUIDE

Wayne Wiesner, et al

Boeing Vertol Company

Prepared for:

Army Air Mobility Research and Development
Laboratory

January 1974

DISCLAIMERS

The findings in this report are not to be construed as an official Department of the Army position unless so designated by other authorized documents.

When Government drawings, specifications, or other data are used for any purpose other than in connection with a definitely related Government procurement operation, the United States Government thereby incurs no responsibility nor any obligation whatsoever; and the fact that the Government may have formulated, furnished, or in any way supplied the said drawings, specifications, or other data is not to be regarded by implication or otherwise as in any manner licensing the holder or any other person or corporation, or conveying any rights or permission, to manufacture, use, or sell any patented invention that may in any way be related thereto.

Trade names cited in this report do not constitute an official endorsement or approval of the use of such commercial hardware or software.

DISPOSITION INSTRUCTIONS

Destroy this report when no longer needed. Do not return it to the originator.

ii

This report has been reviewed by the Eustis Directorate, U. S. Army Air Mobility Research and Development Laboratory and is considered to be technically sound.

This program was initiated to develop guidelines for tail rotor design by using wind tunnel test data for a tail rotor in the proximity of a main rotor and fin. The tests were conducted to study the aerodynamics of the tail rotor in hover and in low-speed forward and rearward flight, in and out of ground effect.

The technical monitor for this contract was Mr. Patrick A. Cancro, Aeromechanics, Technology Applications Division.

Task 1F162204AA4304
Contract DAAJ02-73-C-0010
USAAMRDL Technical Report 73-99
January 1974

TAIL ROTOR DESIGN GUIDE

By

Wayne Wiesner
Gary Kohler

Prepared by

BOEING VERTOL COMPANY
A Division of The Boeing Company
Philadelphia, Pennsylvania

for

EUSTIS DIRECTORATE
U.S. ARMY AIR MOBILITY RESEARCH AND DEVELOPMENT LABORATORY
FORT EUSTIS, VIRGINIA

AD - 775 391

DOCUMENT CONTROL DATA - R & D

(Security classification of title, body of abstract and indexing annotation must be entered when the overall report is classified)

1. ORIGINATING ACTIVITY (Corporate author)	2a. REPORT SECURITY CLASSIFICATION
Boeing Vertol Company A Division of The Boeing Company P.O. Box 16858 Philadelphia, Pa. 19142	Unclassified
	2b. GROUP

3. REPORT TITLE

TAIL ROTOR DESIGN GUIDE

4. DESCRIPTIVE NOTES *(Type of report and inclusive dates)*

Final report -- November 1972 - August 1973

5. AUTHOR(S) *(First name, middle initial, last name)*

Wayne Wiesner
Gary Kohler

6. REPORT DATE	7a. TOTAL NO. OF PAGES	7b. NO OF REFS
January 1974	256	17

8a. CONTRACT OR GRANT NO. DAAJ02-73-C-0019 b. PROJECT NO. c. Task 1F162204AA4304 d.	9a. ORIGINATOR'S REPORT NUMBER(S) USAAMRDL Technical Report 73-99 9b. OTHER REPORT NO(S) *(Any other numbers that may be assigned this report)* D210-10687-1

10. DISTRIBUTION STATEMENT

Approved for public release; distribution unlimited.

11. SUPPLEMENTARY NOTES	12. SPONSORING MILITARY ACTIVITY Eustis Directorate U.S. Army Air Mobility Research and Development Laboratory Fort Eustis, VA

13. ABSTRACT

This report presents guidelines for the preliminary design of tail rotors for single-rotor helicopters in low-speed and hover flight. Application of these guidelines should alleviate the directional control problems of single-rotor helicopters under certain conditions of wind speed and direction, height above the ground, gross weight, and altitude. The data base used to develop the guidelines is wind tunnel tests of a tail rotor helicopter model. These tests were run in and out of ground effect, in various wind speeds to 35 knots, and with varying wind azimuths. Some of the significant results concern selection of an optimum tail rotor configuration and the critical operating conditions. The configuration which gives the highest thrust for a given collective pitch, the lowest power required, and the least thrust excursion with wind azimuth is that with the hub in the plane of the main rotor, with bottom-blade-forward rotation, and with the wake directed away from the fin. The operating conditions which are critical with respect to solidity and maximum blade pitch selection are 20-knot wind speed, wind direction from the right front, and main rotor height-to-diameter ratio of 0.45. Procedures are included for calculation of the effect of the tail rotor on the main rotor power required. With a tailwind in ground effect, the main rotor power required can increase by 22 percent over that of an isolated rotor with no wind. A design chart predicts the effect of the fin on the tail rotor thrust. The guide includes calculations for the tail rotor thrust required and the solidity and maximum blade incidence necessary to achieve that thrust; power required by the tail rotor in the presence of the fin and main rotor is also included. Factors involved in blade design are discussed, as are tip speed and number of blades from sound detection criteria. Other parameters that affect flying qualities and structural loads are also discussed: pitch-flap coupling, tail rotor shaft sweep, pedal control rate limiting, etc. Of special significance is the effect of tail rotor disc loading on pedal movement in sideward flight. A sample problem is presented.

DD FORM NOV 65 1473

14. KEY WORDS	LINK A		LINK B		LINK C	
	ROLE	WT	ROLE	WT	ROLE	WT
Design of tail rotors						
Single-rotor helicopters						
Low-speed and hover flight						
Directional control problems						
Wind tunnel tests						
Tail rotor model						
Optimum tail rotor configuration						
Critical operating conditions						
Flying qualities						
Structural loads						
Sample problems						

SUMMARY

This report presents general guidelines for the preliminary design of tail rotors for single-rotor helicopters in low-speed and hover flight. Application of these guidelines should alleviate the directional control problems of single-rotor helicopters under certain conditions of wind speed and direction, height above the ground, gross weight, and altitude.

The main data base used to develop the guidelines is the results of a wind tunnel test of a tail rotor helicopter model conducted by Boeing. These tests were conducted in and out of ground effect, in various wind speeds to 35 knots, and with varying wind azimuths.

Some of the more significant results concern the selection of an optimum tail rotor configuration and the critical operating conditions. The configuration which gives the highest level of thrust for a given collective pitch, the lowest power required, and the least thrust excursion with wind azimuth is the design with the hub in the plane of the main rotor, with bottom blade forward rotation and in the pusher position; i.e. with the wake directed away from the fin. The operating conditions which have been found to be critical with respect to solidity and maximum blade pitch selection are 20-knot wind speed, wind direction from the right front, and main rotor height to diameter ratio of 0.45.

Procedures based on test data are included for calculation of the effect of the tail rotor on the main rotor power required. With a tailwind in ground effect, the main rotor power required can increase as much as 22 percent over that of an isolated rotor with no wind. Also, a design chart predicts the effect of the fin on the tail rotor thrust.

Presented are methods for calculating the tail rotor thrust required and the solidity and maximum blade incidence necessary to achieve that thrust. Power required by the tail rotor in the presence of the fin and main rotor is also included.

Factors involved in blade design (airfoil selection and blade twist) are discussed, as are tip speed and number of blades based on acoustic detection criteria.

Other parameters that affect flying qualities and structural loads are also discussed: pitch-flap coupling, tail rotor shaft sweep, pedal control rate limiting, etc. Of special significance is the effect of tail rotor disc loading on pedal movement in sideward flight.

A sample problem is presented to show how each guideline is used in the selection of tail rotor parameters.

FOREWORD

This document was prepared for the Eustis Directorate, U.S.
Army Air Mobility Research and Development Laboratory, Fort
Eustis, Virginia, by Boeing Vertol Company under Contract
DAAJ02-73-C-0010, Task 1F162204AA4304, during the period
November 1972 through August 1973.

USAAMRDL technical direction was provided by Mr. P. A. Cancro,
Eustis Directorate. Boeing Vertol program management was pro-
vided by W. W. Walls, Chief of Aerodynamics.

The principal investigators for this study were Messrs. Wayne
Wiesner, Project Engineer; Gary Kohler, Research Engineer; and
Rodger Mann, Research Technician. Technical contributions
were also made by the following Boeing Vertol personnel:

- David Carmichael   - Acoustics

- Leo Dadone   - Aerodynamics

- Eugene Kieselowski   - Aerodynamics

- Warren Larson   - Flying Qualities

- Stanley Mills   - Aerodynamics

TABLE OF CONTENTS

Preceding page blank

LIST OF ILLUSTRATIONS

x

LIST OF TABLES

SYMBOLS

A	rotor disc area, ft^2
$\bar{A}$	fin blockage ratio, S/A
A_{FIN}	area of fin, ft^2
BA	bottom aft rotation
BF	bottom forward rotation
B_1	longitudinal cyclic pitch, deg
b	number of blades
C	induced velocity ratio
c_d	drag coefficient
c_{do}	minimum section profile drag coefficient
c_f	fin force coefficient, fin force$/\rho A_{TR}(\omega r)^2$
c_ℓ	section lift coefficient
$c_{\ell_{max}}$	maximum section lift coefficient
c_{m_0}	zero lift section pitching moment coefficient
$c_{P_{REF}}$	power required by a tail rotor producing a thrust of $c_{T_{REF}}$
c_p	power coefficient, $P/\rho A V_T^3$
c_{R_M}	tail rotor rolling moment coefficient
c_T	thrust coefficient, $T/\rho A V_T^2$
c_{T_M}	thrust coefficient of tail rotor in presence of main rotor with no fin installed
c_{T_0}	thrust coefficient of isolated tail rotor
$c_{T_{REF}}$	a constant reference thrust coefficient

C_{YM}	tail rotor yaw moment coefficient
C_σ	trim thrust coefficient, ℓT_{TR}/vehicle torque
d	main rotor diameter, ft
d_{TR}	tail rotor diameter, ft
FM	figure of merit, $0.707\ C_T^{3/2}/C_p$
GW	gross weight, lb
h	height of main rotor above the ground, ft
IGE	in ground effect (see definitions)
I_p	blade polar moment of inertia, slug-ft^2
I_z	aircraft yaw moment of inertia, slug-ft^2
K_T, K_M, K_g	constants defined in Section 13
K_p	multiplying factor applied to isolated tail rotor power to give actual power in presence of the main rotor and fin
ℓ	tail arm, longitudinal distance between main rotor shaft and tail rotor shaft (the main rotor shaft location is assumed to be the longitudinal center of gravity), ft
M	Mach number
M_{DD}	drag divergence Mach number
N_r	yaw rate damping, sec^{-1}
OGE	out of ground effect
P	power, lb ft/sec
P_O	isolated tail rotor power, lb ft/sec
Q	shaft torque, lb/ft^2
R, r	main rotor radius (R), tail rotor radius (r), ft
R_e	Reynolds number
S	disc area blocked by fin, ft^2

SHP	shaft horsepower
SL	sea level
s	distance between fin and tail rotor, ft
T	thrust, lb
t	time, sec
u	induced velocity, ft/sec
u_O	uniform downwash induced velocity in hover, ft/sec
V	wind velocity, ft/sec
V_T	tip speed, ft/sec
v	velocity at fin
w	main rotor disc loading, lb/ft^2
w'	blade weight per square foot, lb/ft^2
x	blade radial station, ft
$Y_{.0125}/c$	upper surface nose shape parameter
δ	main rotor average profile drag coefficient
δ_{TAB}	trailing-edge tab deflection, deg
δ_3	pitch-flap coupling, deg
θ	collective pitch, referred to airfoil zero lift line, deg
ρ	air density, $slugs/ft^3$
ρ_O	air density at sea level, $slugs/ft^3$
σ	rotor solidity
μ	main rotor advance ratio

μ_{TR}	tail rotor advance ratio
ψ	wind azimuth, deg; $= 0°$ for headwind, $= 90°$ for wind from right
Ω	main rotor rotational speed, rad/sec
ω	tail rotor rotational speed, rad/sec

Subscripts:

d	design
i	induced
MR	main rotor
N	net
SL	sea level
TR	tail rotor

DEFINITIONS

Alternate Gross Weight - The maximum gross weight at which
an aircraft can hover in ground effect at a specified
ceiling

Excursion - The deviation of tail rotor thrust or power from
a smooth mean curve versus wind azimuth

Fin Blockage Ratio - Ratio of disc area blocked by fin to
total disc area

Fin Separation Distance - Distance from centerline of fin to
plane of rotation of tail rotor

In Ground Effect - Main rotor height diameter less than 1.0

Net Thrust - Shaft thrust of the tail rotor less the fin
force

Out of Ground Effect - Defined as main rotor height diameter
ratio greater than or equal to 1.0

Pusher - Tail rotor located downstream of the vertical fin
so that its wake does not strike the fin

Shaft Thrust - Thrust of the tail rotor as measured on the
tail rotor shaft

Tractor - Tail rotor located so that its wake strikes the
vertical fin

Wing Tip Vortex - That vortex shed from the lateral portions
of the main rotor similar to the wing tip vortices of a
lifting fixed wing

INTRODUCTION

This report establishes 23 general guidelines for preliminary design of the tail rotor for single-rotor helicopters.

Single-rotor helicopters, within the past decade, have experienced directional control irregularities or loss or have had failures of the tail rotor drive system during certain overload or extreme maneuver conditions. The intensity and magnitude of such failures or control losses have varied from model to model, usually under certain operating conditions of wind, ground proximity, and altitude. Examples of such service experiences are summarized in Appendix I of this report. In general, the cause of such failures can be related to:

● Tail rotors not effective enough to produce the required thrust without stall under certain conditions of maneuver, wind magnitude and azimuth, ground proximity and flight altitude, and temperature.

● Tail rotor drive systems not designed to the proper strength to transmit the torque required under such conditions.

These guidelines are based on service data analysis and wind tunnel test data which have been accumulated in recent years by NASA and Boeing (References 1, 2, and Appendix II). Unless otherwise specified, all data in this report is from the Boeing tests. The current report presents 23 such guidelines, covering the most critical aspects of tail rotor design, such as placement with respect to the main rotor, placement with respect to the fin, and direction of rotation (see Figure 1). Although not all design conditions have been covered, such as high-speed flight regime, sufficient data is presented to permit the designers to perform trade-off studies and to select basic tail rotor design parameters.

The report is organized in a handbook format allowing easy accessibility to each specific guideline. This also provides flexibility for possible revision or inclusion of additional data with a minimum disturbance to the remainder of the material. The guidelines section is preceded by detailed discussion of the tail rotor flow-field environment and is followed by a sample application of the guidelines to a specific tail rotor design.

The substantiating data for the guidelines is presented in Appendix III.

1

FIN-TAIL ROTOR
SEPARATION

DIRECTION OF
ROTATION

TAiL ROTOR PLACEMENT
WITH RESPECT TO
THE MAIN ROTOR

THRUST
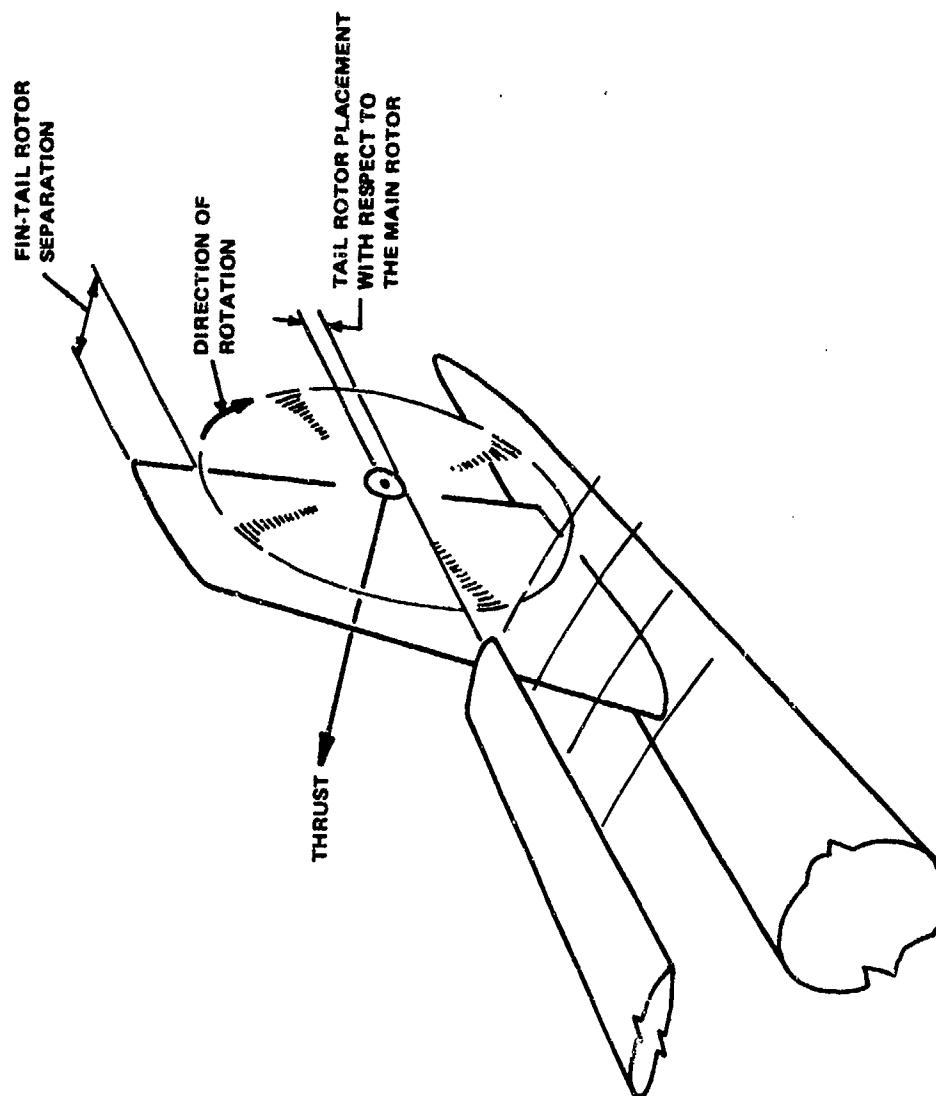
Figure 1. Major Tail Rotor Design Parameters.

2

FLOW ENVIRONMENT OF TAIL ROTOR

The recent flight tests (Reference 3), the wind tunnel tests (Reference 2), and the water tunnel tests of Reference 4 have shown a wide range of mixing of the wind, the main rotor downwash, and the tail rotor wash flow. Such tests have shown that at least six flow phenomena will affect tail rotor thrust and power performance. They are:

● Momentum flow of main rotor

● Main rotor trailing vortices (see Reference 4)

● Ground vortex from meeting of main rotor momentum flow and wind

● Vortex ring from tail rotor

● Wind

These items are illustrated in Figure 2.

a. MOMENTUM FLOW OF MAIN ROTOR
b. MAIN ROTOR TRAILING VORTEX
c. GROUND VORTEX
d. VORTEX RING FROM TAIL ROTOR
e. WIND
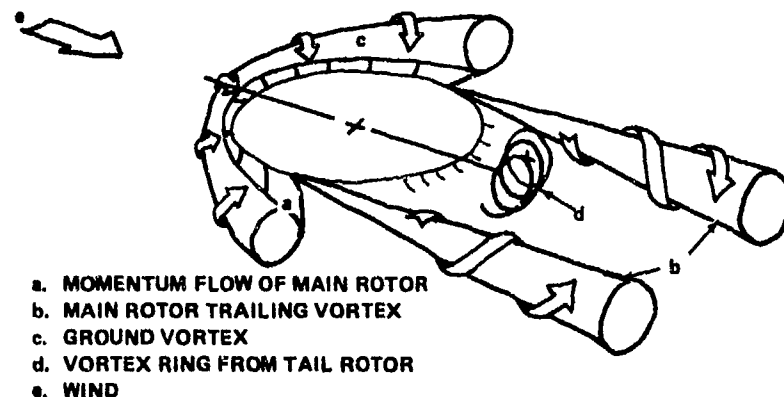
Figure 2. Flow Environment of Tail Rotor.

Because of the interaction of all these flows, the problem of determining the critical conditions of wind speed, wind direction, and height above the ground is difficult. The tests conducted by Boeing (Reference 2), on which most of these major guidelines are based, are believed to have covered the critical combinations, but they in no way covered all combinations. The Boeing test model and test conditions are described in Appendix II.

The main rotor momentum flow (IGE) affects the tail rotor at those wind azimuths at which the tail rotor is partially immersed in the main rotor wake as it spreads along the ground. Its effects can be seen in Figure 3, which shows the trend of

3
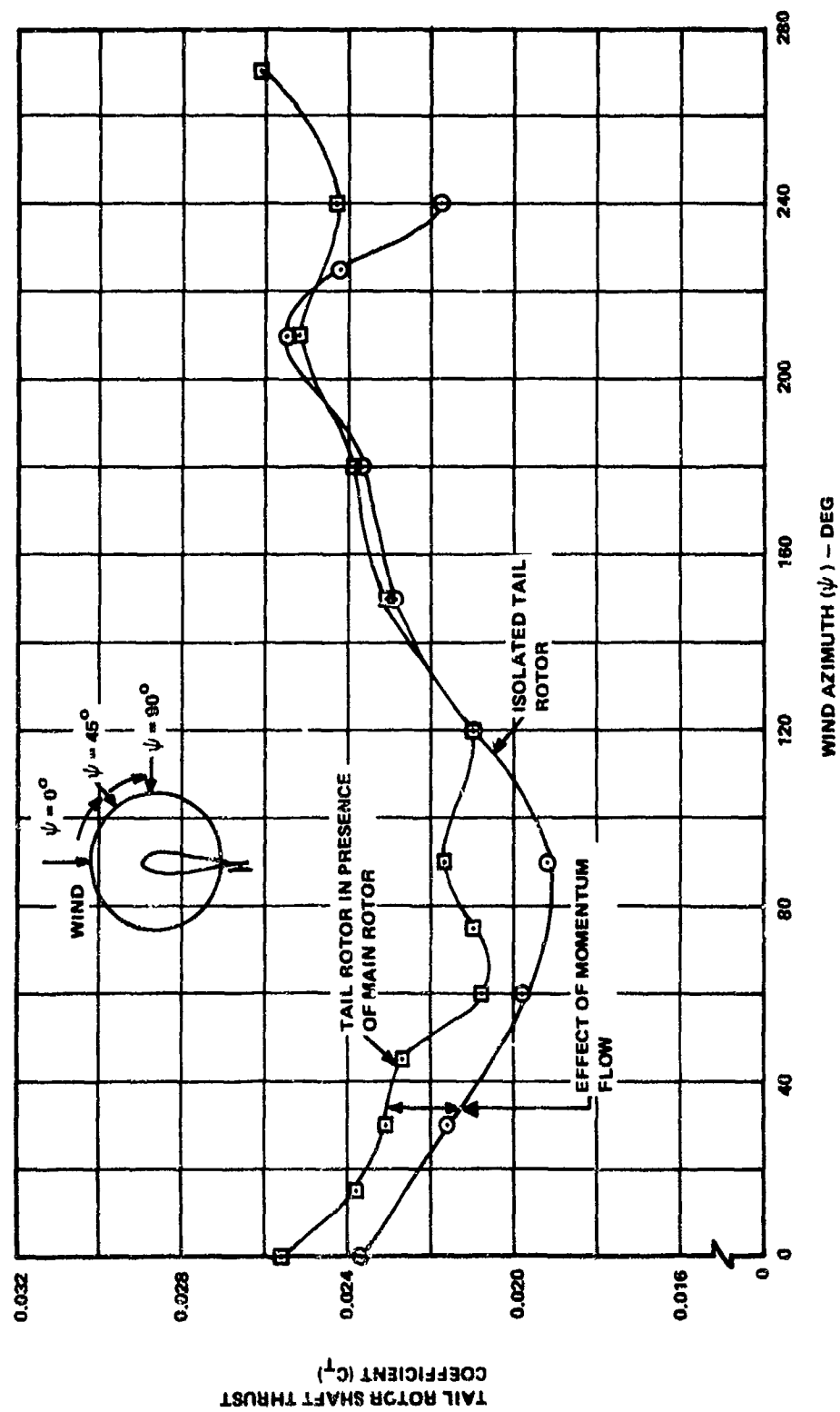
Figure 3. Effect of Main Rotor Momentum Flow on Tail Rotor Thrust —
V = 35 Kn, h/d = 0.3, Rotation = BF, IGE.

4

tail rotor thrust at constant blade incidence versus wind
azimuth. This figure compares headwind azimuths ($\psi = 0$ to
30^0), where the tail rotor is partially immersed in the main
rotor wake, to the tailwind azimuths ($\psi = 150^0$ to 210^0), where
it is not immersed. With the bottom forward rotation of the
tail rotor, the dynamic pressure is increased over that part
of the disc which is immersed; consequently, the thrust is
increased. With bottom aft rotation, the dynamic pressure and
the thrust are decreased. The vertical position of the tail
rotor also affects thrust output, since a high position (hub
above plane of main rotor) has less disc area immersed; there-
fore, the tail rotor has less thrust increase for bottom forward
rotation than a low position (hub below plane of main rotor).

The interaction of the tail rotor with the main rotor trailing
vortex has a great effect on tail rotor performance. This
vortex, of the same type that trails from the wing-tips of a
fixed-wing aircraft, is very powerful. It can be observed be-
hind a helicopter flying through smoke or agricultural dust.
Army tests of the AH-1G (Reference 3) determined its effects
with different directions of rotation. Its effect can also be
seen from Boeing test results in Figure 4. At $\psi = 45^0$, the
tail rotor is operating within the wing tip vortex. Since its
bottom aft rotation is in the same direction as the vortex,
the tail rotor suffers a loss of dynamic pressure and thrust.

The main rotor trailing vortex is evident at 20 knots and is
fully formed at 35 knots. Its angle of deflection is approxi-
mately 45^0 in ground effect. As the height above the ground
increases, the deflection angle (between main rotor disc plane
and the vortex) increases in a 20-knot wind, but it is nearly
constant in a 35-knot wind. Vortex strength and probably de-
flection angle are dependent on main rotor disc loading, but
no quantitative data is available to determine these effects.

The effect of the ground vortex on tail rotor performance in
rearward flight was reported by NASA (Reference 1). The
ground vortex is generated by the interaction of the main
rotor wake and the wind when the aircraft is in ground effect.
At certain azimuths and wind velocities, the tail rotor oper-
ates within this vortex, producing adverse effects on thrust,
fin force, and power when the tail rotor direction of rotation
is the same as that of the vortex (bottom aft) (see Figure 5).
The ground vortex also acts on the horizontal stabilizer and
is the major cause of ground skittishness in rearward flight.
The location of the ground vortex is plotted later in this
report (Figures 23-3 and 23-4) for a main rotor disc loading
of 7 psf.

Tail rotor thrust is decreased in left-side flight due to the
formation of the vortex ring state on the tail rotor. However,
when the tail rotor with bottom forward rotation is positioned
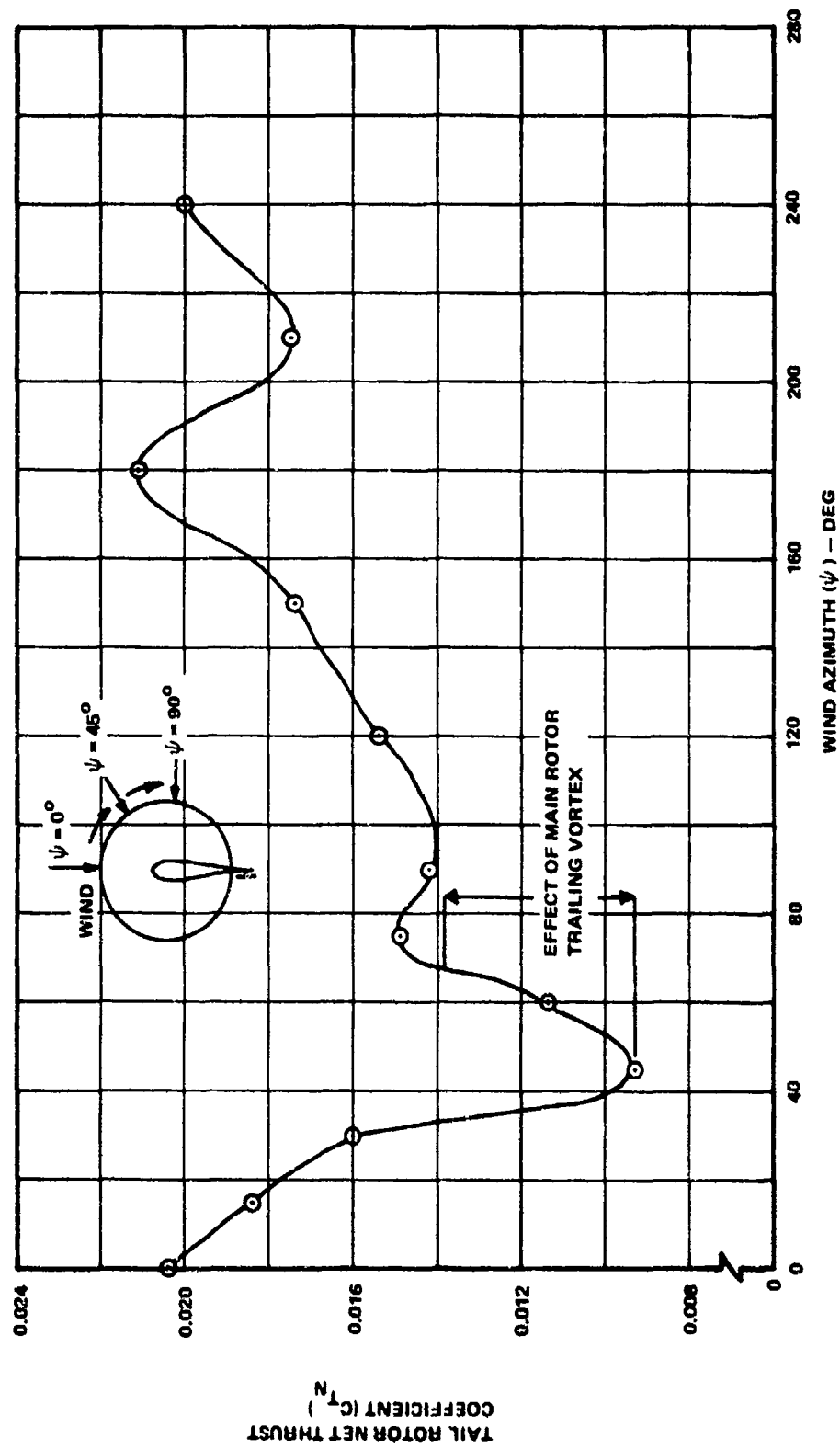
Figure 4. Effect of Main Rotor Trailing Vortex on Tail Rotor Thrust — V = 35 Kn, h/d = 1.0, Rotation = BA.

6
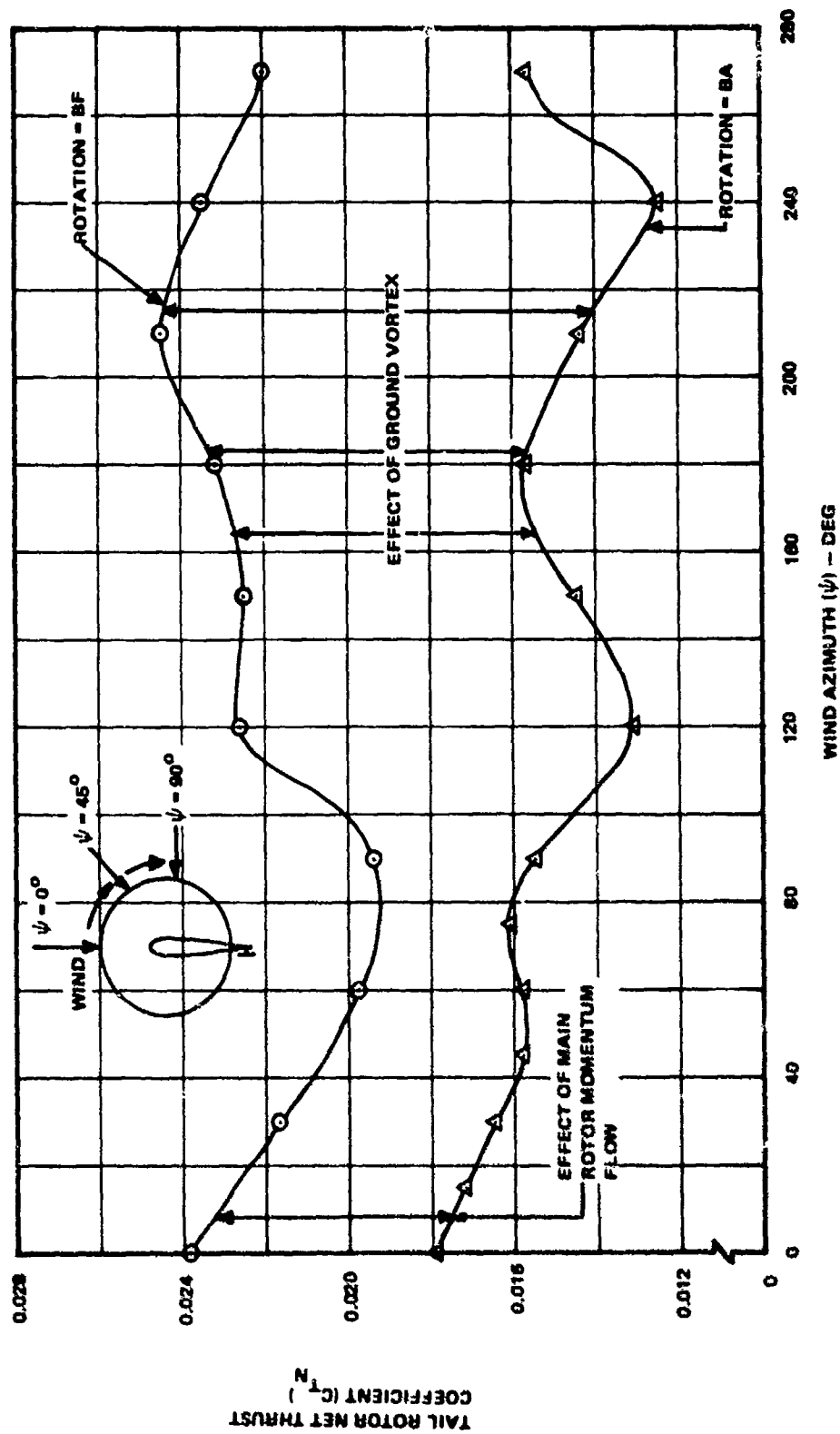
Figure 5. Effect of Ground Vortex on Tail Rotor Thrust — V = 20 Kn, h/d = 0.3.

7

near the main rotor blade tip, the main rotor wake retards formation of the vortex ring state of the tail rotor. This can be seen in Figure 6 by comparing the thrust of the aft and mid positions (both in the plane of the main rotor) at $\psi = 240^\circ$. When the tail rotor is further from the main rotor wake, as it is in the aft position, the thrust for constant blade pitch is considerably reduced, indicating stronger vortex ring formation.

Reference 5 shows the effect on transient rudder pedal motion required when the tail rotor is in the vortex ring state. It was found that reversing the direction of rotation to bottom forward greatly reduced this transient pedal motion. A major conclusion of the Boeing wind tunnel test is that the vortex ring leaves the tail rotor in a helical manner rather than in a donut-like pulse. The helix revolves slowly in the direction of rotation of the tail rotor, and when that rotation is such that the tips of the tail rotor move in the same direction as the main rotor flow field (bottom aft), the vortex ring is accented and thrust transients increase. The inverse is true for bottom forward rotation (see Figure 7).
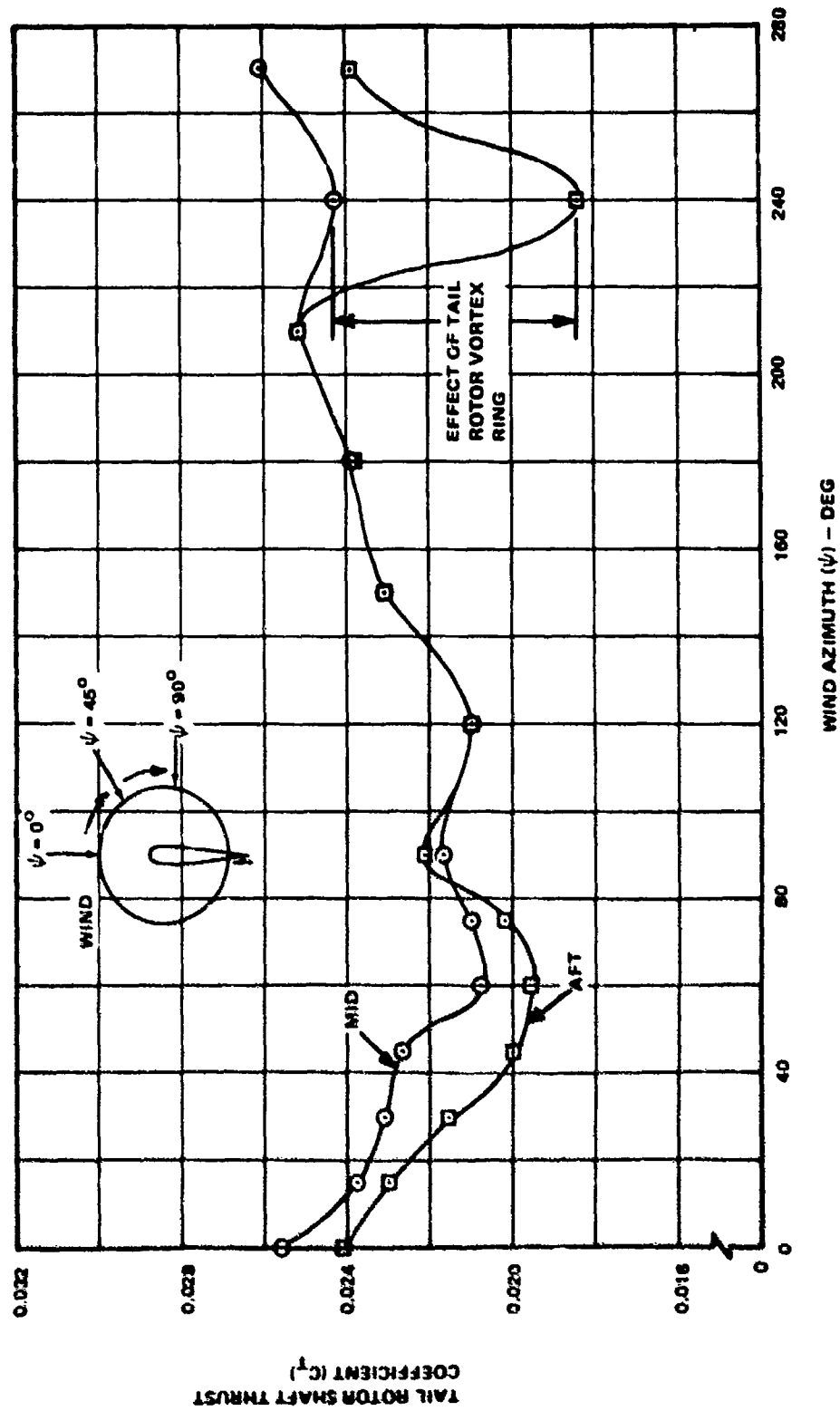
Figure 6. Effect of Tail Rotor Vortex Ring on Tail Rotor Thrust — V = 25 Kn, h/d = 0.3, Rotation = BF.

9

TAIL ROTOR ROTATION = BA

VORTEX RING HELICAL ROTATION ACCENTED

MAIN ROTOR DISC PLANE

TAIL ROTOR ROTATION = BF

VORTEX RING HELICAL ROTATION DIMINISHED
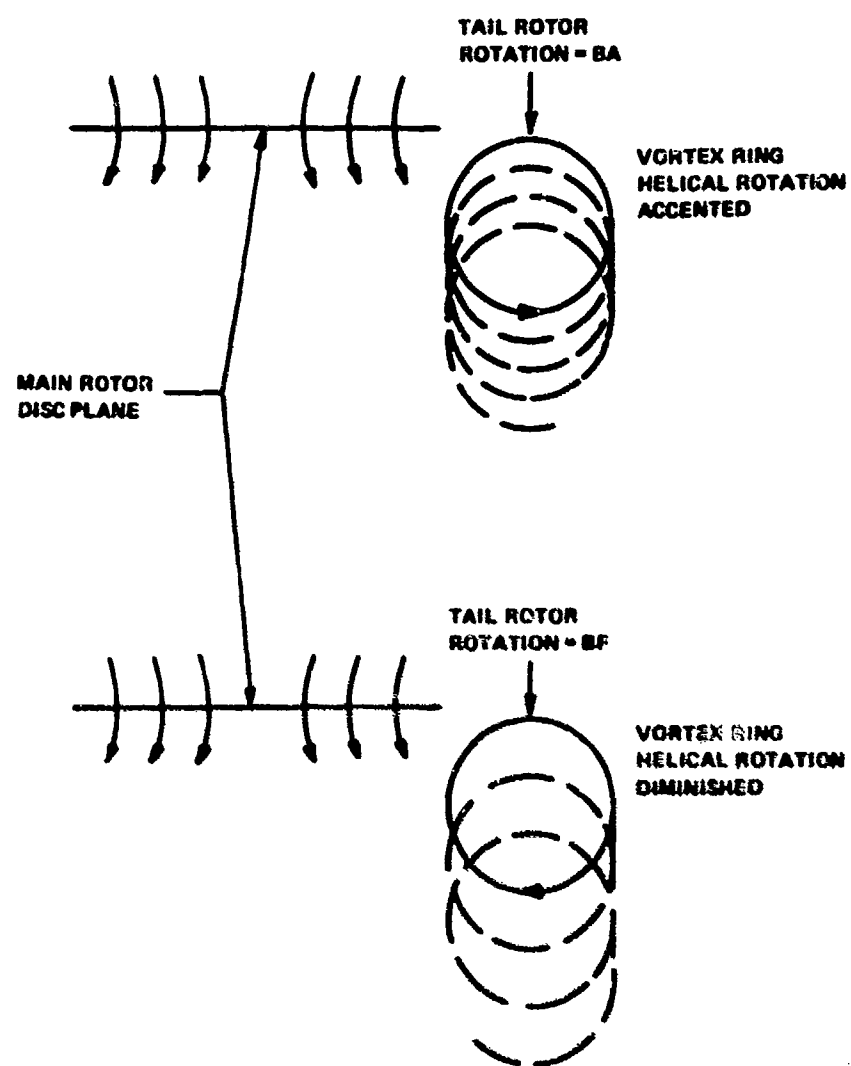
Figure 7. Effect of Direction of Rotation on Tail Rotor Thrust in Vortex Ring State.

TAIL ROTOR DESIGN GUIDELINES

The 23 guidelines have been developed to provide helicopter designers and program managers with the most current information and guidance for the preliminary design of tail rotors.

These guidelines are not all-inclusive, but it is believed that proper emphasis has been placed on the variables that govern tail rotor parameter design selection. For example, considerable attention has been given to the calculation and method to quantify the design thrust required (i.e., the thrust that designs the solidity) so that parameters such as solidity and blade incidence can be selected which do not permit stall of the tail rotor in low-speed yaw maneuvers. Further effort has been made to present means of obtaining design power so that recurrent drive system failures may be eliminated.

USE OF GUIDELINES

There are many combinations of the following parameters that can affect the flow field of the main rotor and tail rotor and, therefore, affect the thrust output of tail rotor and power required for that output.

- wind magnitude

- main rotor disc loading

- tail rotor disc loading

- magnitude of tail rotor thrust

- h/d of main rotor

- wind azimuth

- fin location

- fin size

- placement of tail rotor with respect to main rotor

The conditions on which the guidelines are based are main rotor disc loading (7 psf), a C_Q generally of maneuver (approximately 2.0), winds generally of 20 and 35 knots, and an h/d of 0.3 and 1.0.

The guidelines herein quantify these effects from limited data. Judgments therefore had to be made at times as to the

11

most critical conditions. Thus, although the basis for tail rotor design is far from complete, it is believed that these criteria are a significant improvement over those previously developed. If the criteria are used, a better tail rotor will evolve.

Before attempting to use these guidelines, the designer should become familiar with each guideline and its background.

In the guidelines that follow, the critical condition for optimum tail rotor design (selection of solidity and maximum blade incidence) is evolved. This condition includes tail rotor in mid position, bottom forward rotation, pusher configuration, 20-knot wind, 60° azimuth, and h/d = 0.45.

This condition will assure the designer that the solidity and left pedal blade incidence are adequate to meet required control margins at conditions of specified maneuver and altitude. This condition will not, however, yield a conservative solidity so as to produce a large static design power for the tail rotor system.

The guidelines have been presented in the approximate order in which they should be used to select the tail rotor characteristics for a given helicopter. In general, the first half of the guidelines are of major importance in the selection of parameters, while the second half are concerned with the secondary design items that should be considered. In order to provide a straightforward usage of these guidelines, a sample design selection is completely outlined in the section Example Use of Guidelines. It is suggested that the following guidelines be reviewed first, then the sample design problem be reviewed. The sample design section also discusses penalties for selection of parameters such as direction of rotation that are not optimum.

12

1.0 PLACEMENT OF TAIL ROTOR WITH RESPECT TO MAIN ROTOR

The objective of this section is to formulate a guideline for optimum placement of the tail rotor with respect to the main rotor. A diagram of tail rotor positions tested by Boeing (Reference 2) is given in Figure 1-1. The determination of the optimum placement is based on the following considerations (definition of terms is given in Figure 1-2):

- The tail rotor position that gives the highest level of thrust (such a position will require the least collective pitch or solidity and therefore minimum weight for equal thrust outputs)

- The lowest level of power required

- The least excursion of thrust and power required from a mean curve (the position with the least excursion of thrust will require the least rudder pedal excursion in a hover turn)

1.1 DISCUSSION

Thrust and power data versus wind azimuth for the four positions tested by Boeing are shown in Figures 1-3 through 1-11. Test conditions included main rotor h/d ratios of 0.3 (IGE) and 1.0 (OGE) for V = 35 knots and h/d = 0.3 for V = 20 knots. These tests were conducted without the fin installed and with bottom forward rotation. The Boeing tests were conducted at a constant tail rotor collective pitch. Since in actual flight the trim thrust would be held approximately constant with azimuth, induced power corrections have been made to adjust C_T/C_p for a constant reference thrust. These adjusted values are shown in Figures 1-5, 1-8, and 1-11. For the methods used to reduce such data, refer to Appendix III.

Examination of Figures 1-3 through 1-11 yields the relative rankings given in Table 1-I on page 27.

The major findings from Table 1-I are:

- **Thrust** The low position has highest level at 20 knots while the mid position is highest at 35 knots for h/d of 0.3. At h/d of 0.45 (Figure 1-12), both the mid and low position produced the same amount of thrust at 20 knots; at 20 knots, both are equivalent. As will be shown in Guideline 5, 20 to 25 knots is the critical design velocity. However, because of the severe thrust excursion of the low position at 35 knots, the mid position is selected over the low position. Little or no penalty in solidity or maximum

13

blade incidence would be incurred, however, for any position between mid and low. The high and aft positions are eliminated due to their poor thrust levels at $\psi = 45^0$ and 240^0, respectively (the aft position thrust is very much decreased in the vortex ring state at $\psi = 240^0$).

● <u>Power</u> Due to instrumentation failure when the tail rotor was in the low position, power level and excursion comparisons between the low and other positions cannot be made. The high, aft, and mid positions have approximately the same power-required level and the same power excursions.

Changing the separation between the main rotor tip path plane and the tail rotor by changing the trim cyclic has the same effect as raising or lowering the tail rotor (Reference 2). Thus the effect of longitudinal helicopter cg location on tail rotor performance should be considered.

1.2 <u>GUIDELINE</u>

To minimize the collective pitch and solidity required for a given yaw maneuver, to minimize the rudder pedal excursions during a hover turn, and to minimize the power requirements, the tail rotor hub should be located in the plane of rotation of the main rotor and located aft and as close to the main rotor as practical limitations allow.
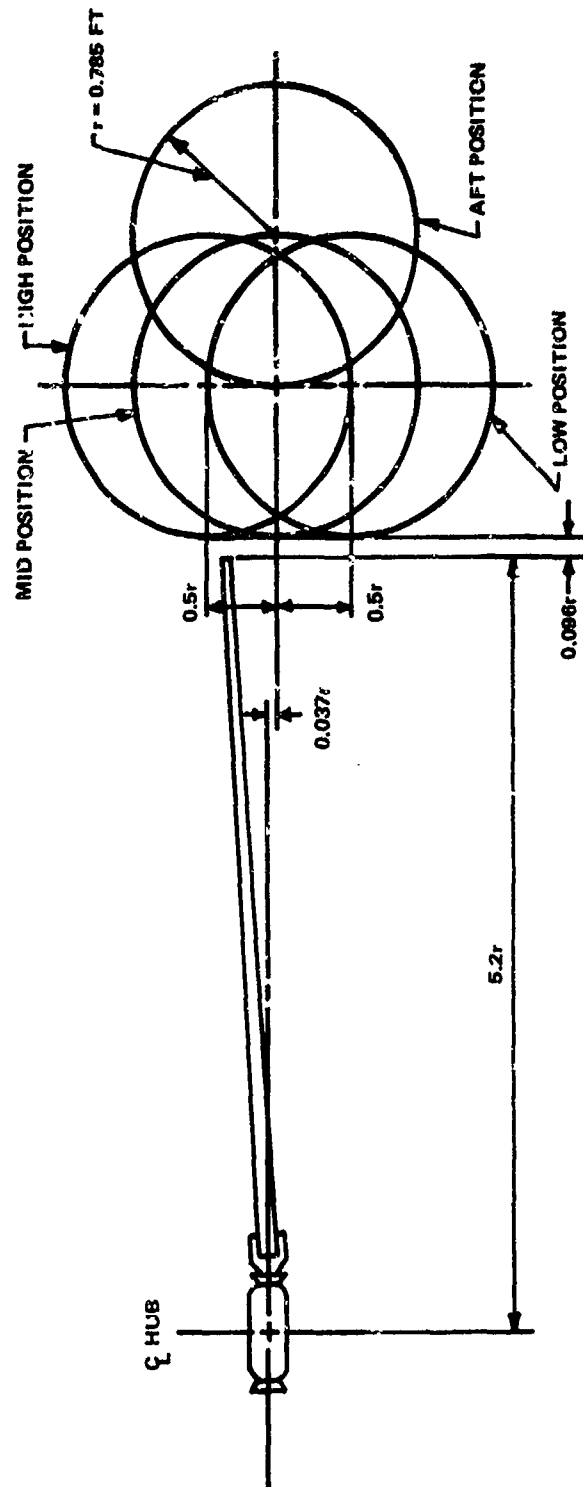
Figure 1-1. Tail Rotor Positions.

15
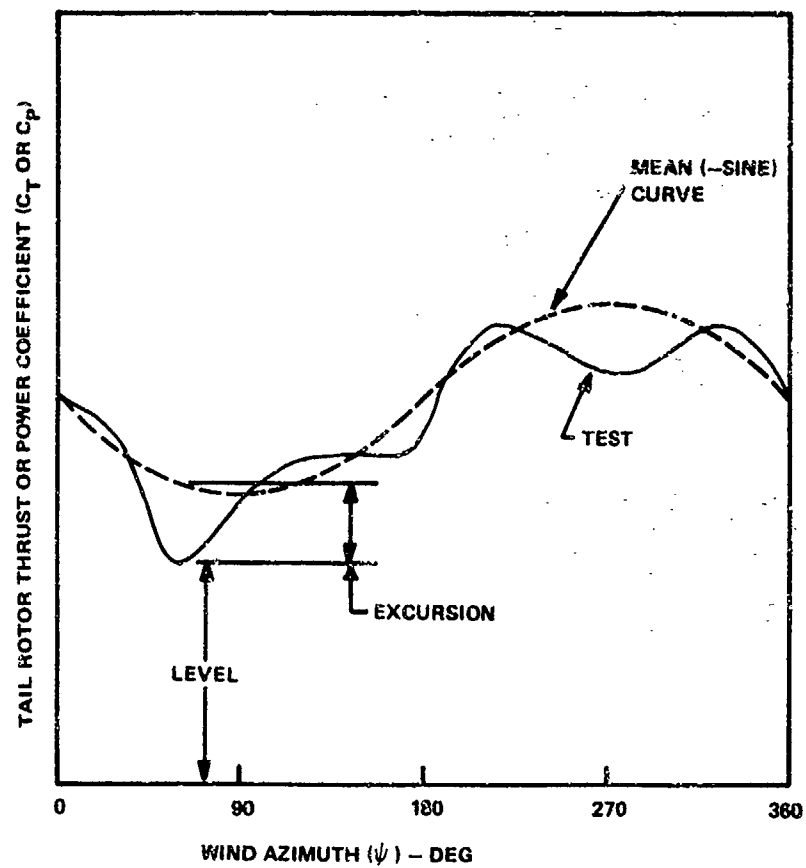
Figure 1—2. Definition of Guideline Selection Parameters.
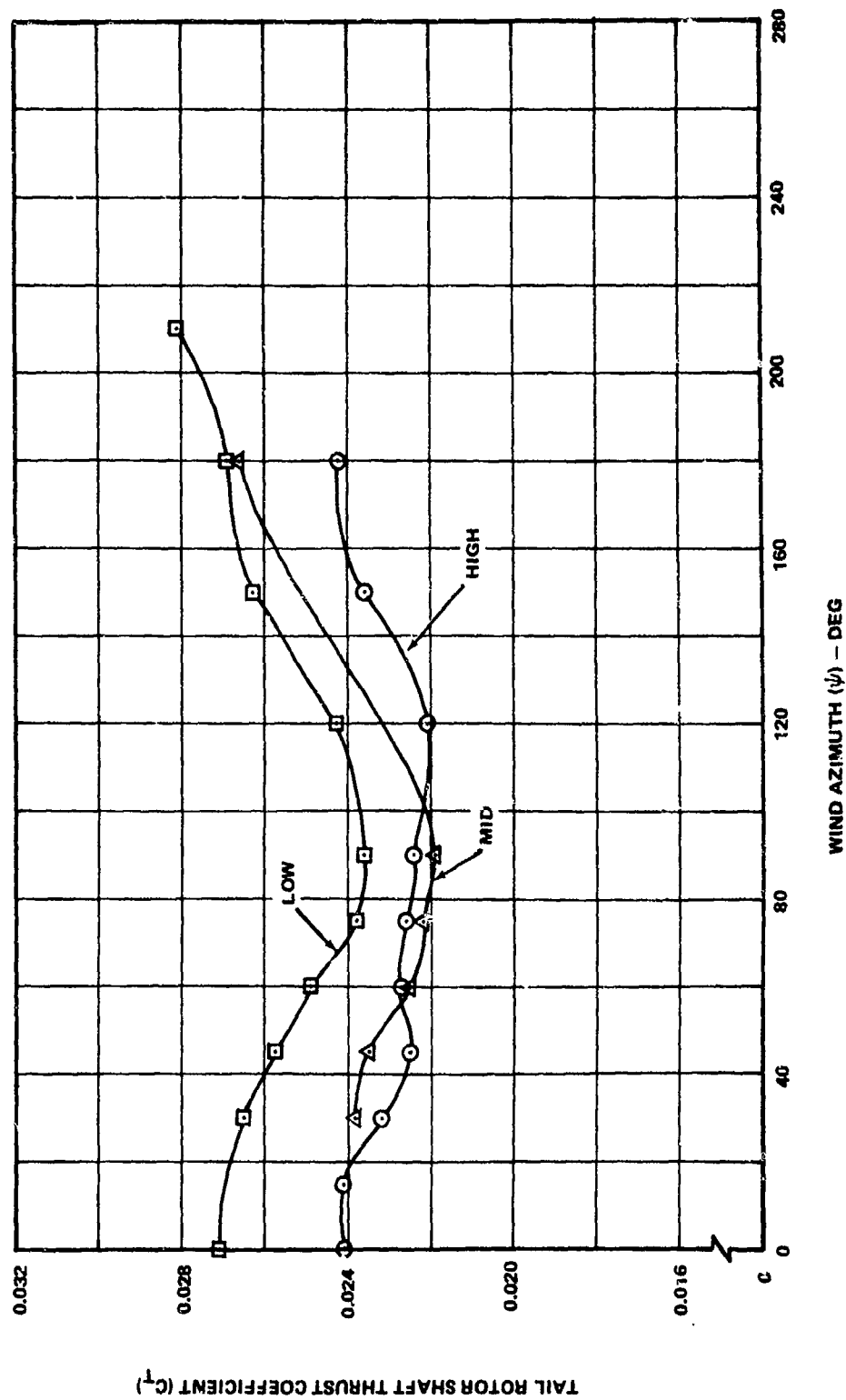
Figure 1–3. Effect of Tail Rotor Position on Tail Rotor Shaft Thrust — V = 20 Kn, h/d = 0.3, θ = 20°, Fin = OFF, Rotation = BF.

17
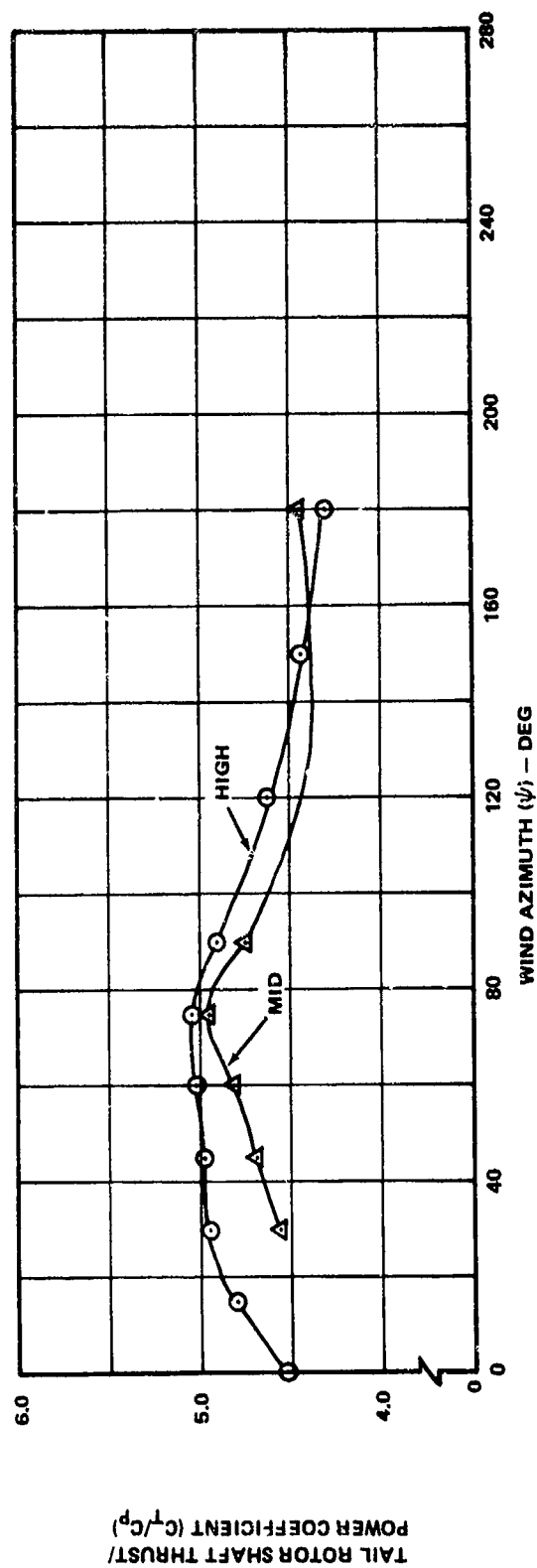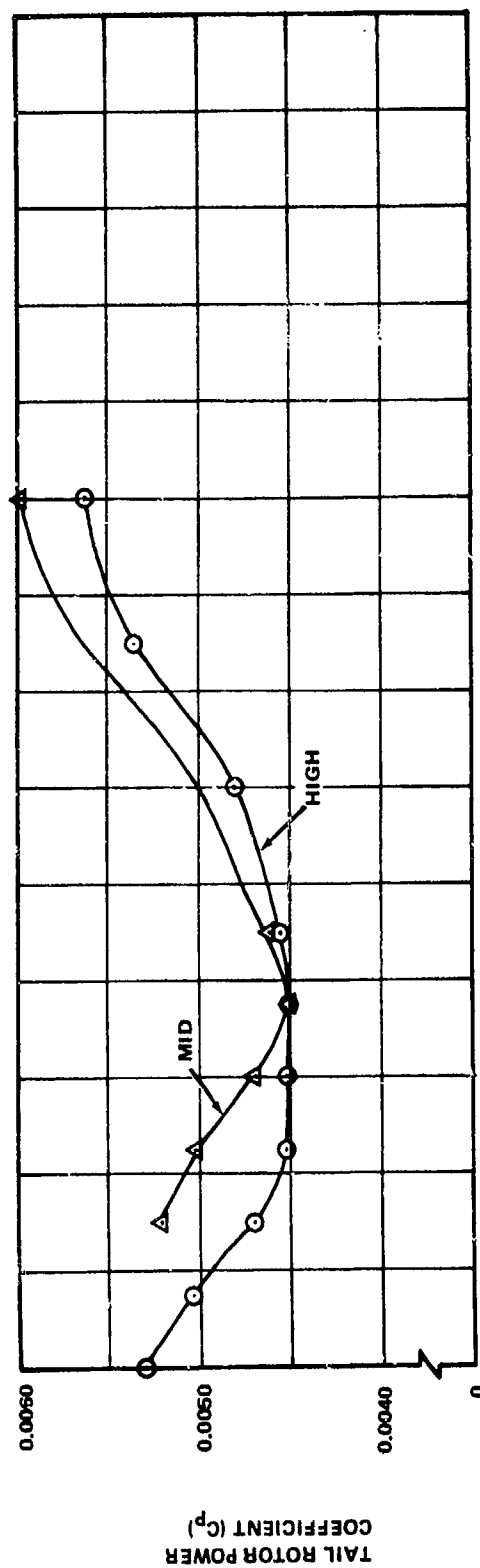
Figure 1—4. Effect of Tail Rotor Position on Tail Rotor Power and Shaft Thrust/Power — V = 20 Kn, h/d = 0.3. $\theta = 20°$, Fin = OFF, Rotation = BF.

18
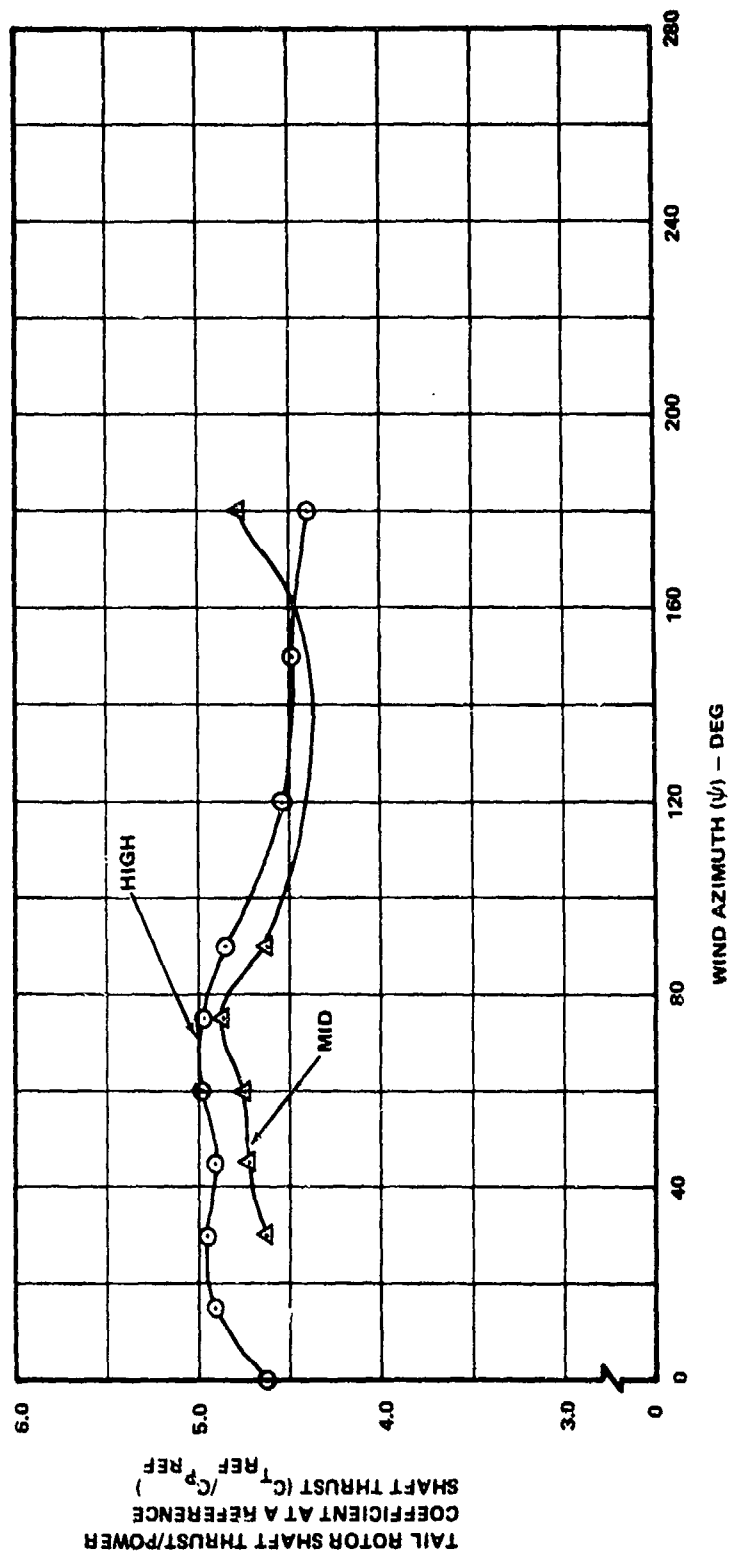
Figure 1–5. Effect of Tail Rotor Position on Tail Rotor Shaft Thrust/Power at a Reference Shaft Thrust — V = 20 kn, h/d = 0.3, $\theta = 20°$, Fin = OFF, Rotation = BF, $C_{T_{REF}} = 0.023$.
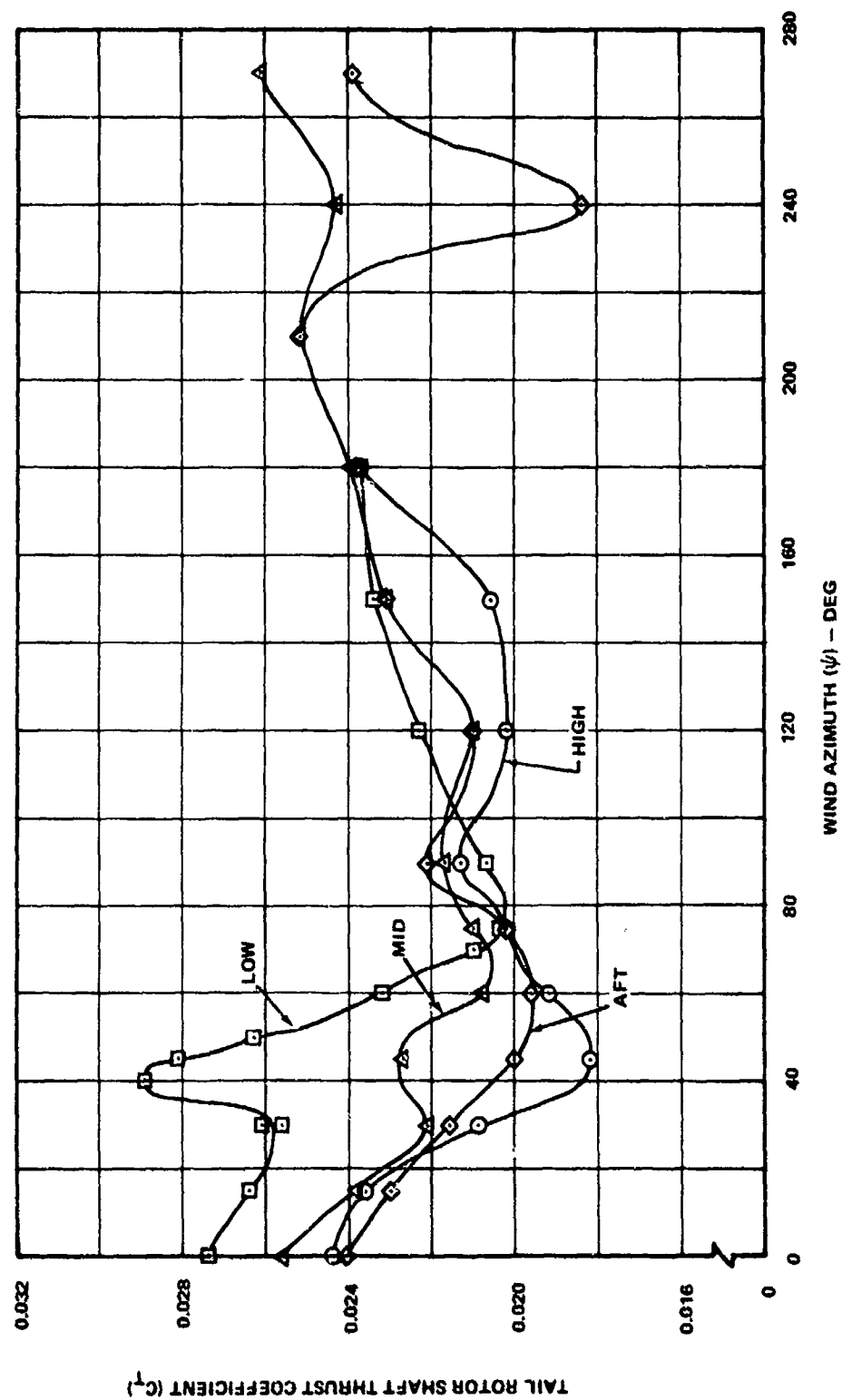
Figure 1—6. Effect of Tail Rotor Position on Tail Rotor Shaft Thrust — V = 35 kn, h/d = 0.3, θ = 20°, Fin = OFF, Rotation = BF.

20
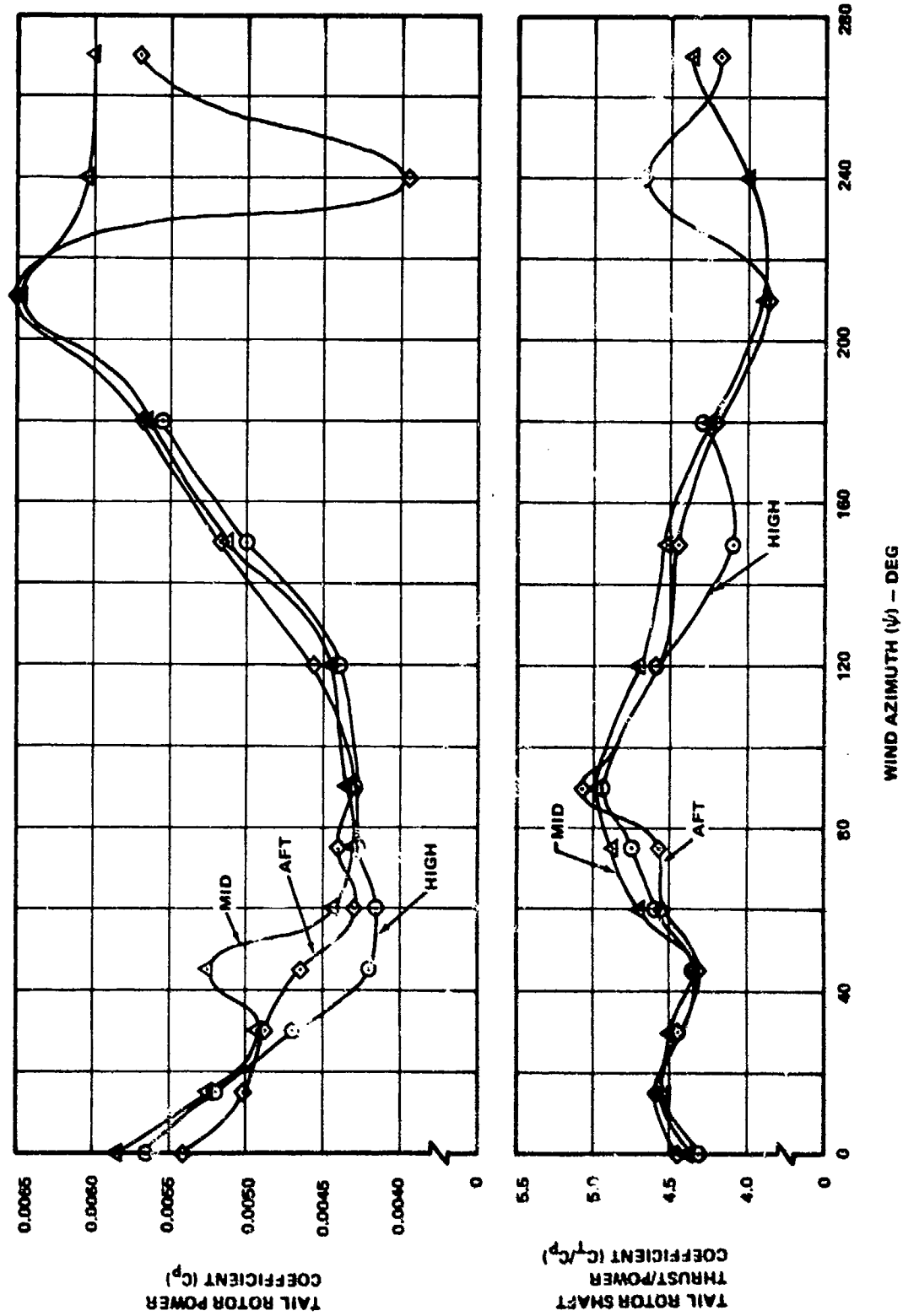
Figure 1-7. Effect of Tail Rotor Position on Tail Rotor Power and Shaft Thrust/Power — V = 35 kn, h/d = 0.3, θ = 20°, Fin = OFF, Rotation = BF.

21
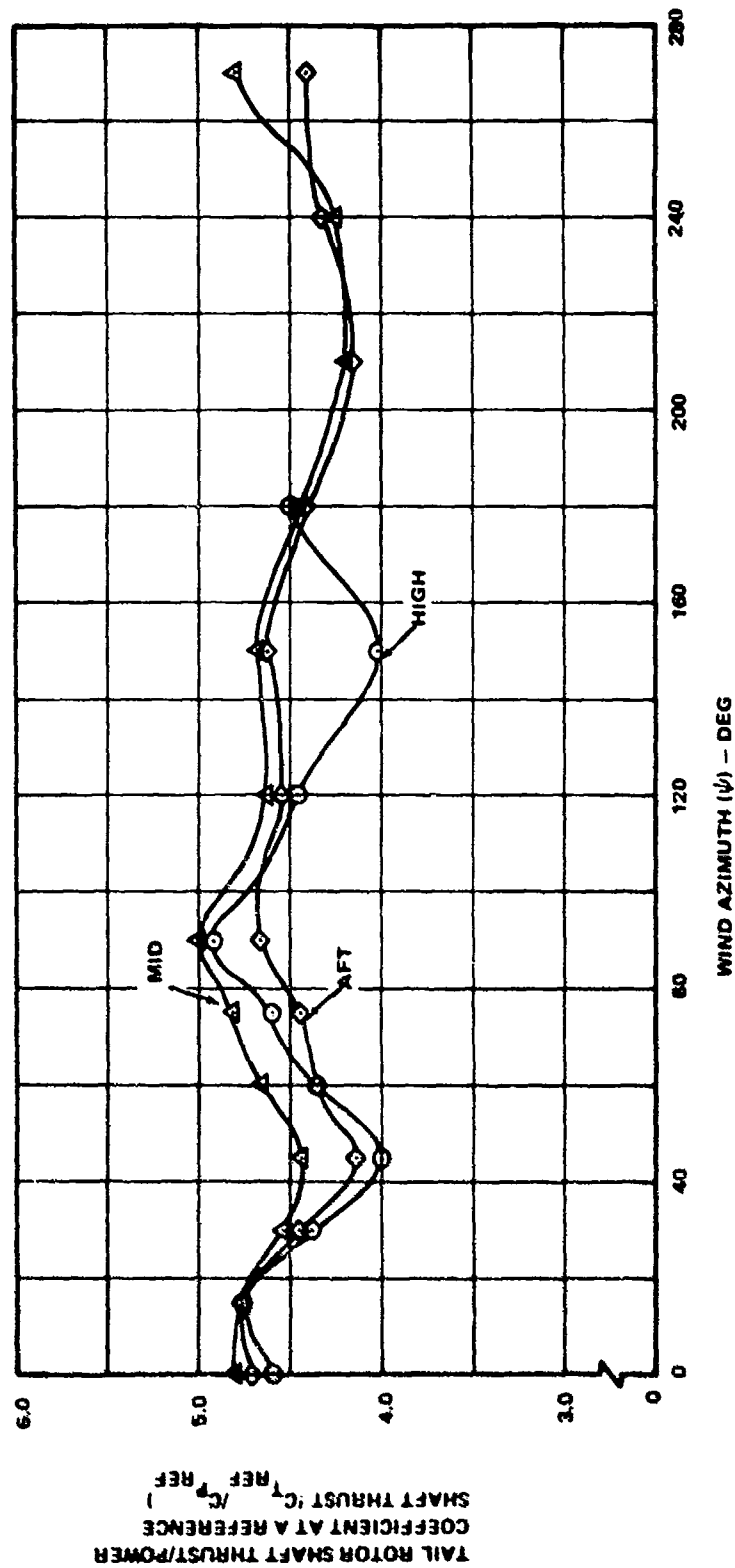
Figure 1—8. Effect of Tail Rotor Position on Tail Rotor Shaft Thrust/Power at a Reference Shaft Thrust — V = 35 kn, h/d = 0.3, θ = 20°, Fin = OFF, Rotation = BF, $C_{T_{REF}}$ = 0.0215.
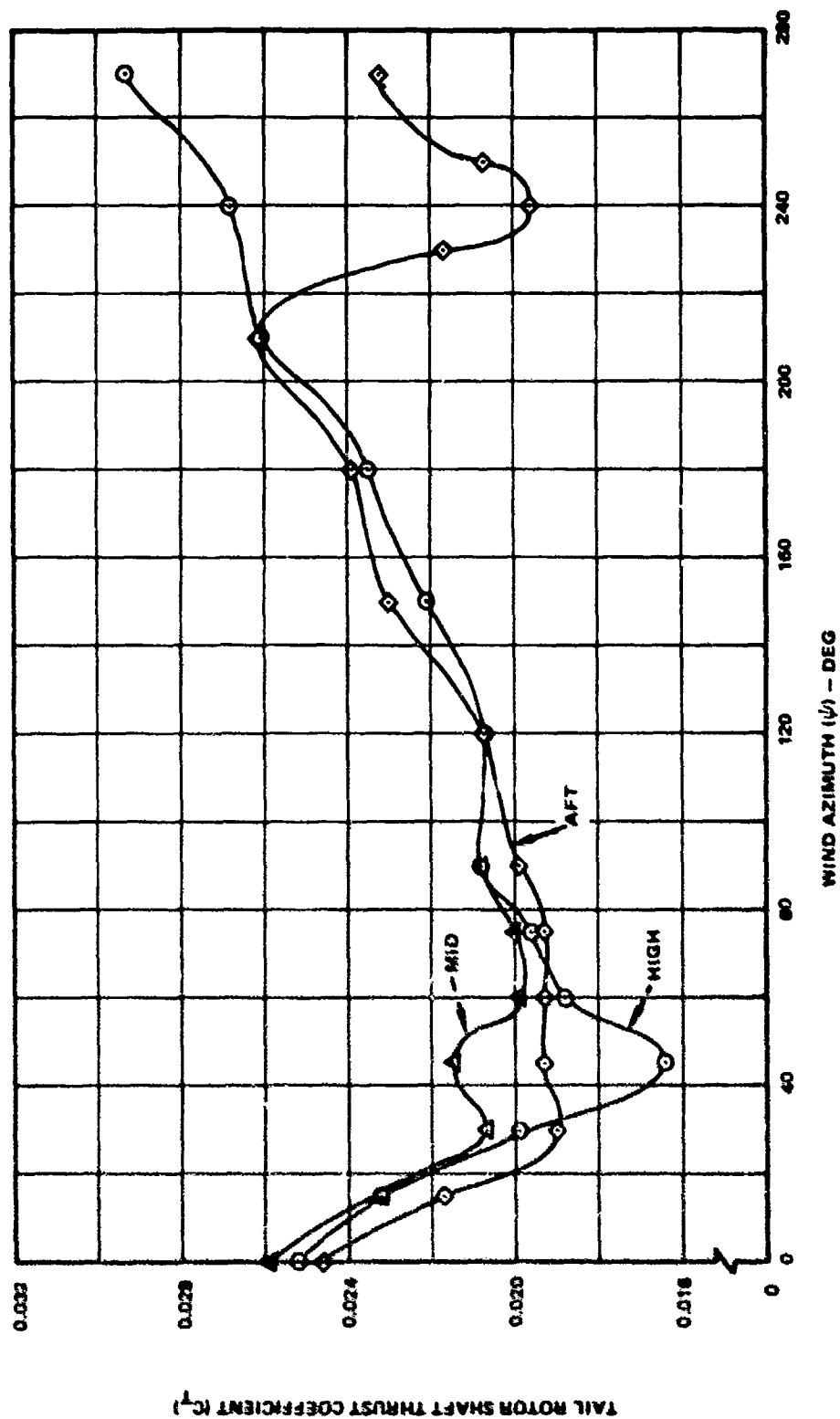
TAIL ROTOR SHAFT THRUST/POWER
COEFFICIENT AT A REFERENCE
SHAFT THRUST $(C_{T_{REF}}/C_{P_{REF}})$

WIND AZIMUTH (ψ) — DEG

22

Figure 1-9. Effect of Tail Rotor Position on Tail Rotor Shaft Thrust — V = 35 kn, h/d = 1.0, θ = 20°, Fin = OFF, Rotation = BF.

23
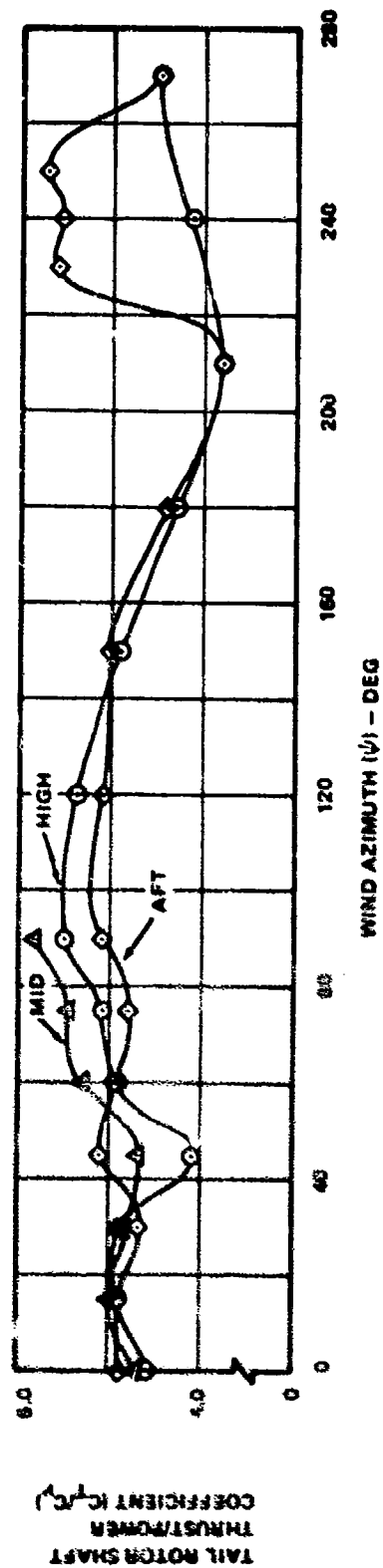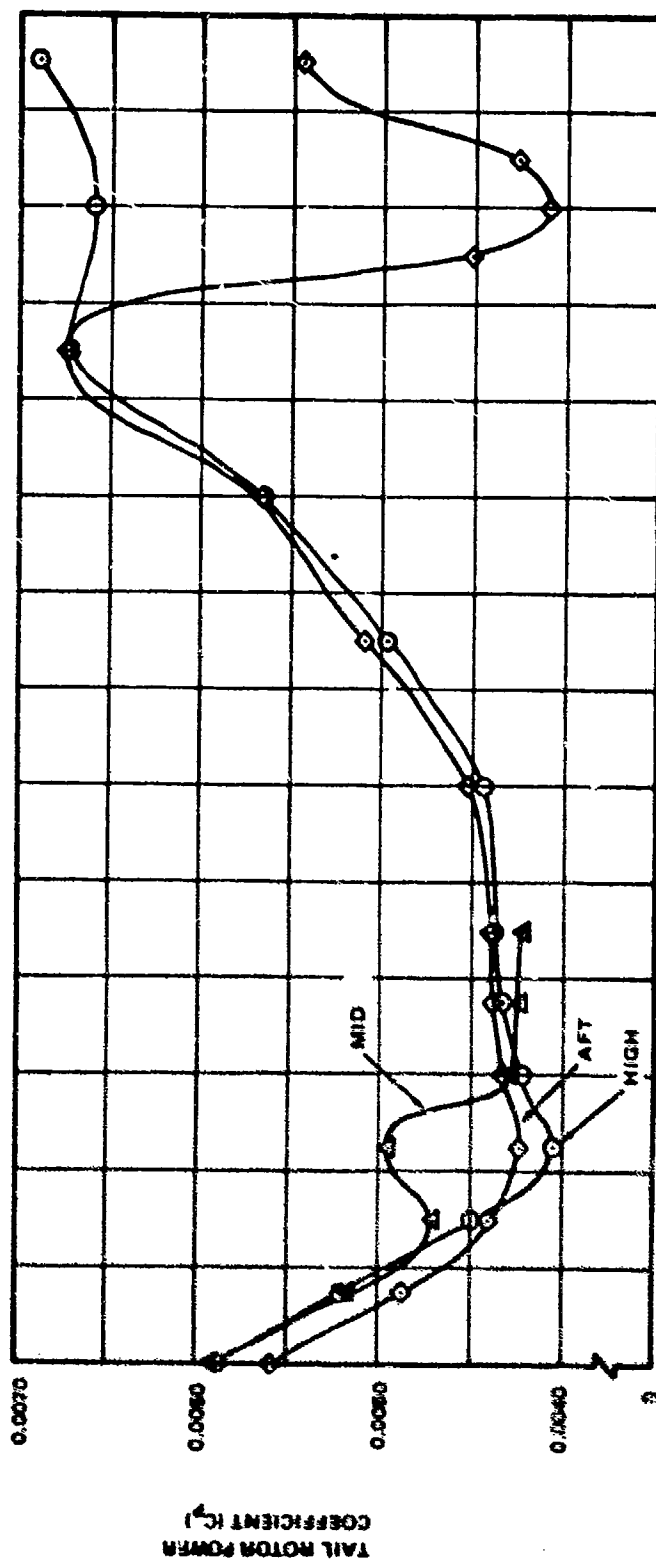
Figure 1 – 10. Effect of Tail Rotor Position on Tail Rotor Power and Shaft Thrust/Power – V = 35 kn, h/d = 1.0, θ = 20°, Fin = OFF, Rotation = BF.

24
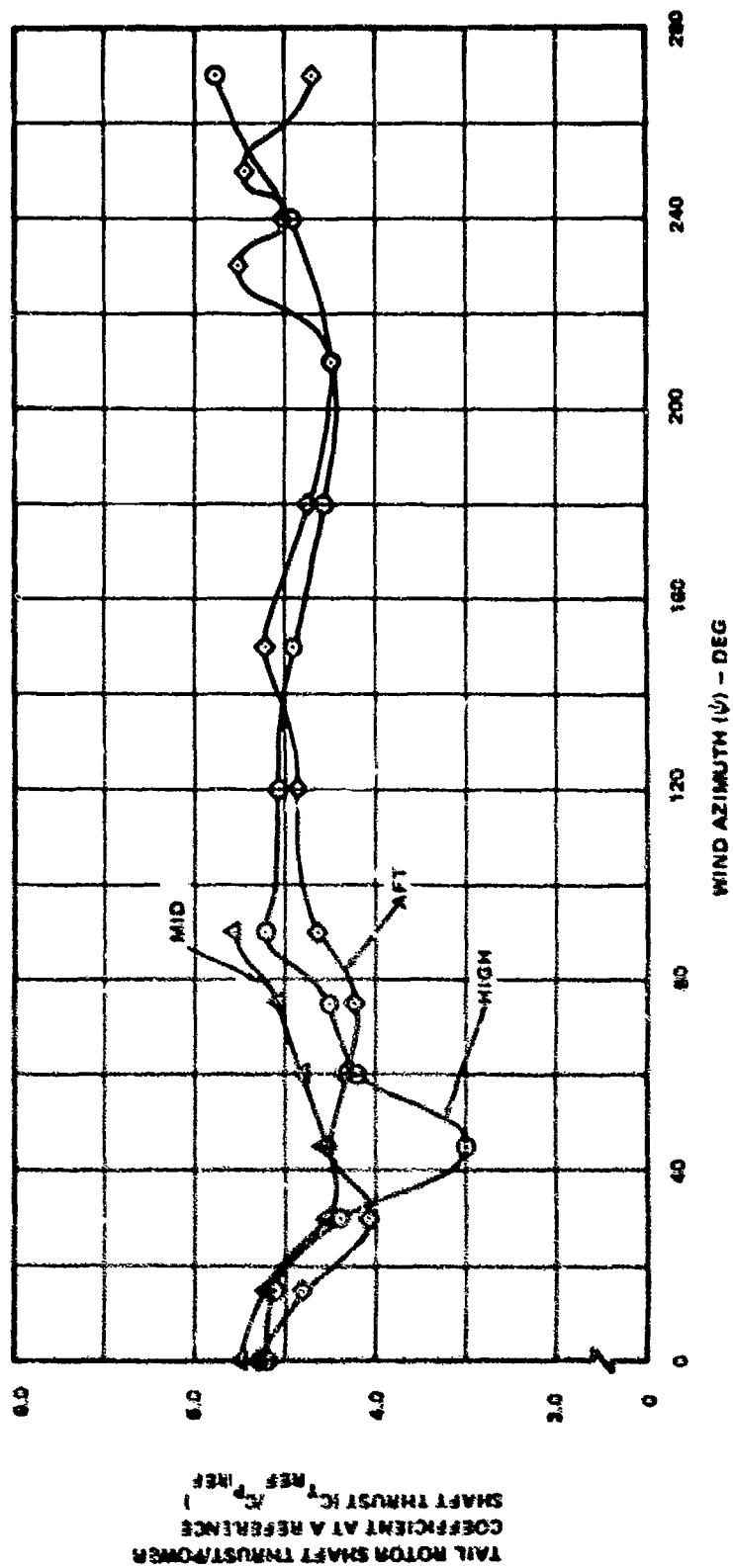
Figure 1–11. Effect of Tail Rotor Position on Tail Rotor Shaft Thrust/Power at a Reference Shaft Thrust — V = 35 kn, h/d = 1.6, θ = 20°, Fin = OFF, Rotation = BF, $C_{T_{REF}}$ = 0.022.
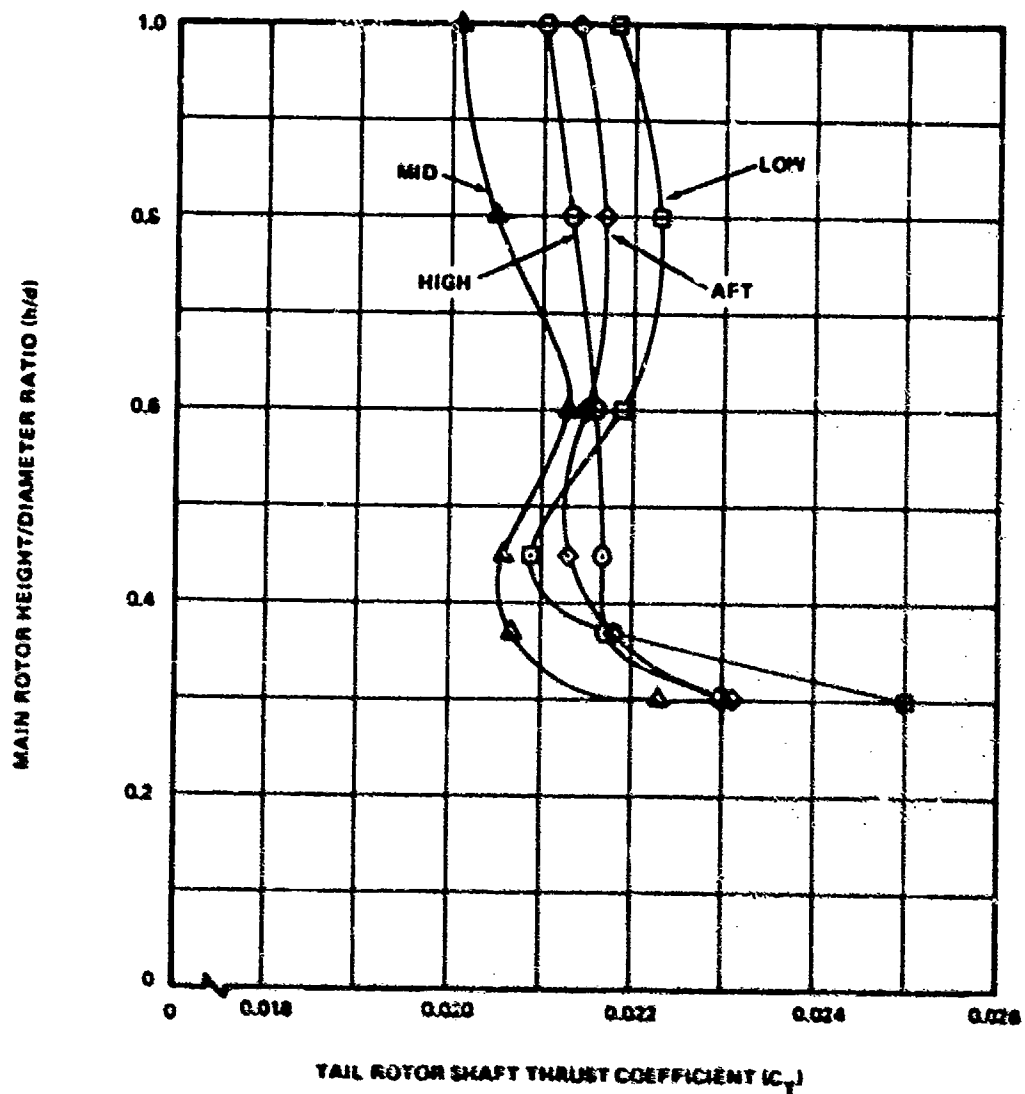
Figure 1-12. Effect of Tail Rotor Position and Main Rotor Height/Diameter Ratio on Tail Rotor Shaft Thrust — V = 20 kn. $\psi = 60^\circ$, $\theta = 20^\circ$, Fin = OFF, Rotation = DF.

26

TABLE 1-I. RELATIVE RANKINGS OF TAIL ROTOR POSITIONS WITH RESPECT TO MAIN ROTOR

	V = 20 IGE				V = 35 IGE				V = 35 OGE			
	High	Mid	Low	Aft	High	Mid	Low	Aft	High	Mid	Low	Aft
High Thrust Level (Figures 1-3, 1-6, 1-9)	2	2	1	NA	4	1	2	3	3	1	NA	2
Low Power Level* (Figures 1-4, 1-7, 1-10)	1	2	NA	NA	1	1	NA	1	1	1	NA	1
Low Thrust Excursion (Figures 1-3, 1-6, 1-9)	1	1	3	NA	3	1	4	2	3	1	NA	2
Low Power Excursion* (Figures 1-4, 1-9, 1-10)	1	1	NA	NA	1	1	NA	1	3	2	NA	1

*Based on the highest $C_{T_{N_{Ref}}}/C_{P_{Ref}}$ ratio

1 is best; 4 is worst

NA indicates data not available

27

2.0 PLACEMENT OF TAIL ROTOR WITH RESPECT TO FIN

The objective of this guideline is to determine the optimum
lateral placement of the tail rotor with respect to the fin.
Possible configurations to be selected include pusher and
tractor, with fin-tail rotor separation distance a variable.
The optimum placement is determined on the same basis as
Guideline 1, that is:

● The fin placement that gives the highest level of net
  thrust, defined as shaft thrust less fin force

● The lowest level of power required

● The least excursion of thrust and power required from a
  mean curve

2.1 DISCUSSION

The two configurations, tractor and pusher, were each tested
at a fin-tail rotor separation ratio of s/r = 0.45.

Thrust and power comparisons of the tractor and pusher
configurations are shown in Figures 2-1 through 2-6. Test
conditions were V = 20 and 35 knots IGE (h/d = 0.3).

Examination of Figures 2-1 through 2-6 yields the relative
rankings given in Table 2-1 below.

TABLE 2-1. RELATIVE RANKINGS OF PUSHER AND TRACTOR
CONFIGURATIONS, s/r = 0.45

Item	V = 20 IGE		V = 35 IGE	
	Pusher	Tractor	Pusher	Tractor
High Thrust Level (Figures 2-1,2-4)	x		x	
Low Power Level* (Figures 2-3,2-6)	x		x	
Low Thrust Excursion (Figures 2-1,2-4)	0	0	x	
Low Power Excursion* (Figures 2-3,2-6)	0	0	x	

x indicates the better configuration
0 indicates no advantage for either configuration
* Based on the higher $C_{T_{N_{Ref}}}/C_{P_{Ref}}$ ratio

29

The major findings from Table 2-I are:

- The pusher position gives the higher level of net thrust with less power

- Neither configuration has excessive net thrust excursion at 20 knots, while the pusher has considerably less thrust excursion than the tractor at 35 knots.

Since the tractor must develop more shaft thrust for a given net thrust because of higher fin forces, the tail rotor in the tractor position will stall sooner than a pusher of the same solidity.

The effects of fin-tail rotor separation distance on tail rotor net and shaft thrust are shown in Figure 2-7. This data is for the pusher configuration with a bottom forward rotation and blockage ratio of 0.207. As the separation distance decreases, both the fin force and shaft thrust increase, so that the net thrust output remains approximately constant. The configuration with the lesser s/r, however, will stall at a lower net thrust level. Thus, for equal stall tail rotors, the greater the fin-tail rotor separation, the less solidity is required.

2.2 GUIDELINE

To minimize collective pitch required for a given thrust, solidity, tip speed, pedal excursions during hover turns in high winds, and power required, the tail rotor should be placed so that it acts as a pusher (the tail rotor wake does not strike the fin).

To minimize solidity, the fin-tail rotor separation distance should be as large as possible within weight restrictions.
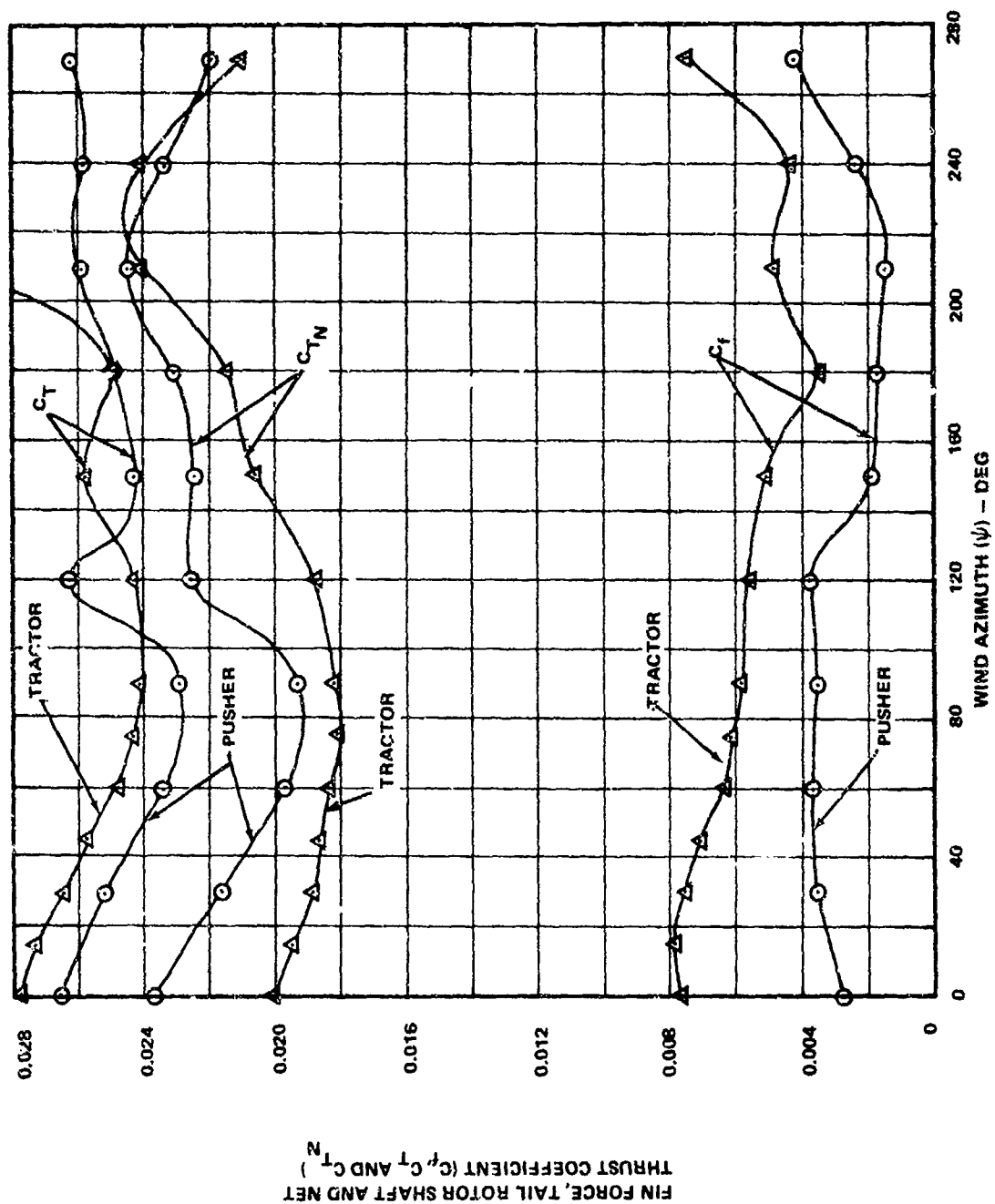
Figure 2–1. Effect of Fin Location on Fin Force, Tail Rotor Shaft and Net Thrust — V = 20 kn, h/d = 0.3, $\theta = 20^{0}$, Position = MID. Fin = ON, Rotation = BF, s/r = .45.

THRUST COEFFICIENT (C_f, C_T AND C_{T_N})
FIN FORCE, TAIL ROTOR SHAFT AND NET

31
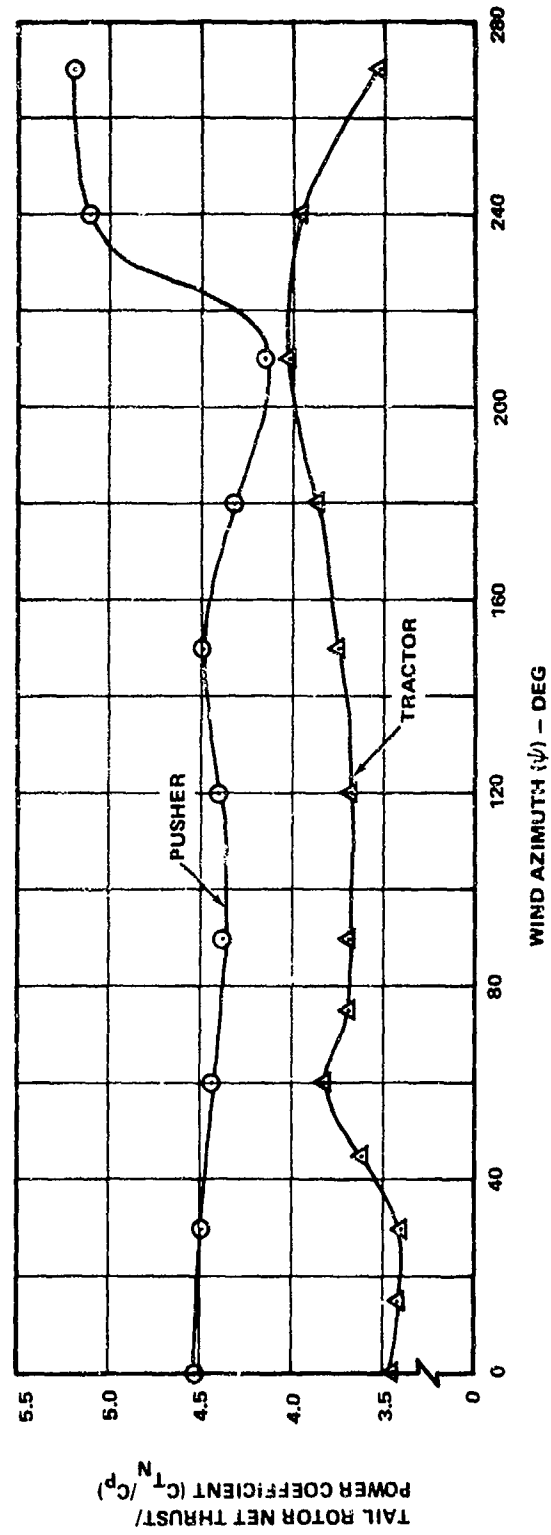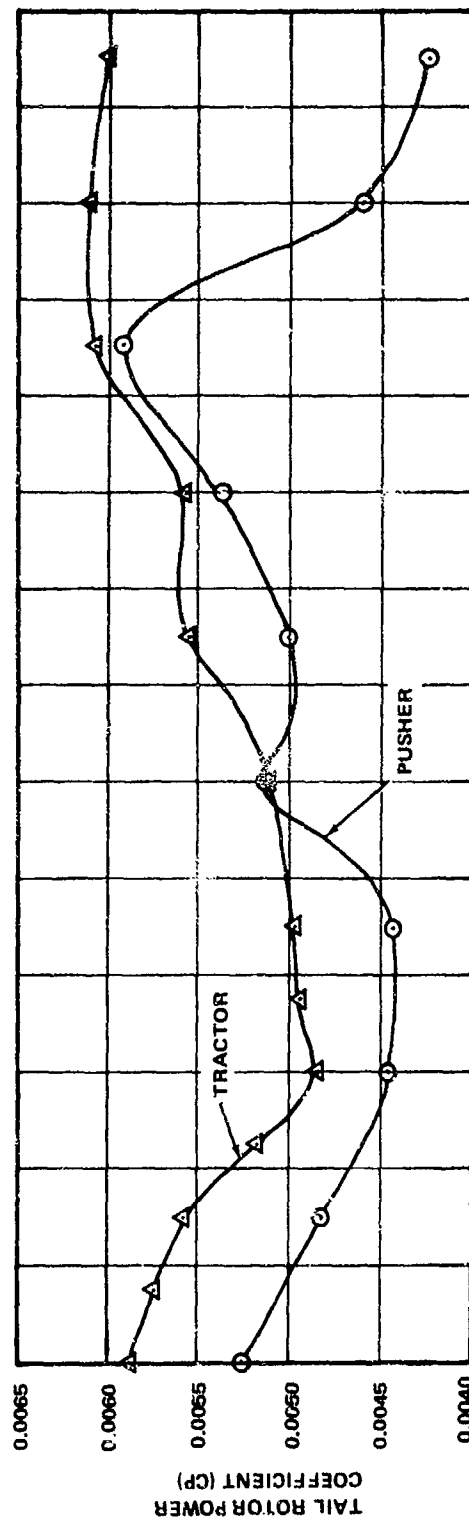
Figure 2-2. Effect of Fin Location on Tail Rotor Power and Net Thrust/Power — V = 20 kn, h/d = 0.3, θ = 20°, Position = MID, Fin = ON, Rotation = BF, s/r = 0.45.

32
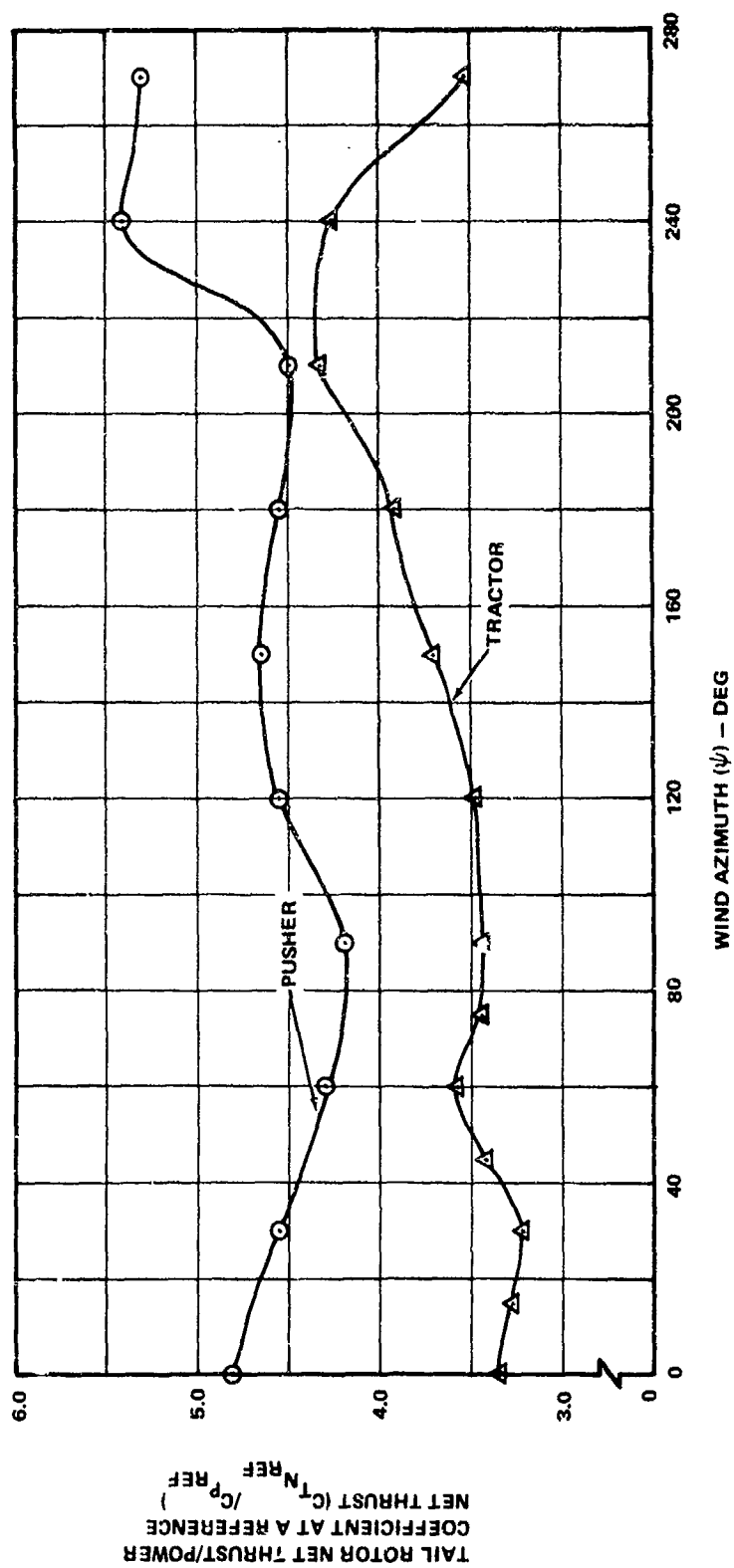
Figure 2–3. Effect of Fin Location on Tail Rotor Net Thrust/Power at a Reference Net Thrust — V = 20 kn, h/d = 0.3, $\theta = 20^{\circ}$, Position = MID, Fin = ON, Rotation = BF, s/r = 0.45, $C_{T_{N_{REF}}} = 0.021$.

33
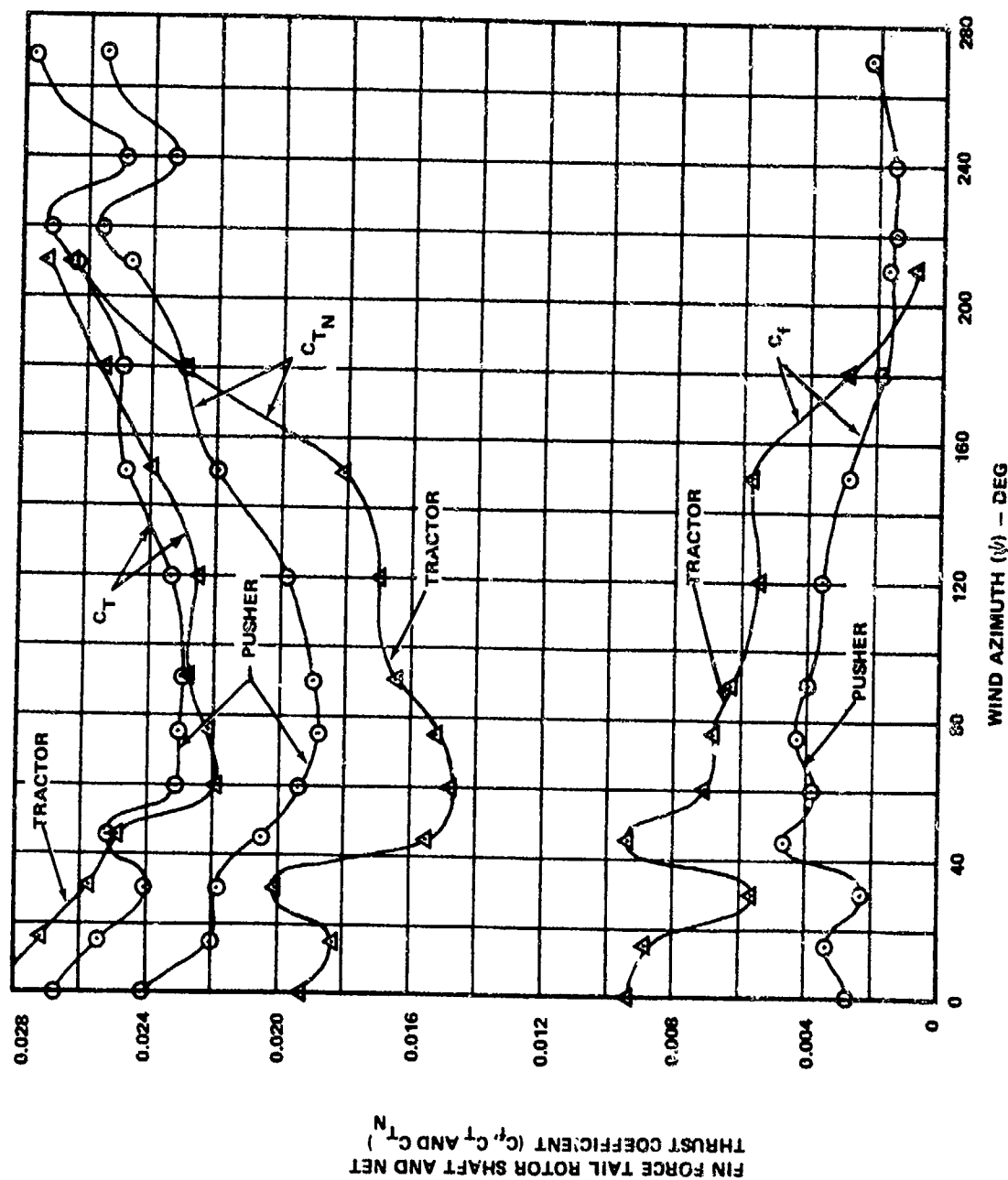
Figure 2—4. Effect of Fin Location on Fin Force, Tail Rotor Shaft and Net Thrust — V = 35 kn, h/d = 0.3, θ = 20°, Position = MID, Fin = ON, Rotation = BF, s/r = 0.45.

34
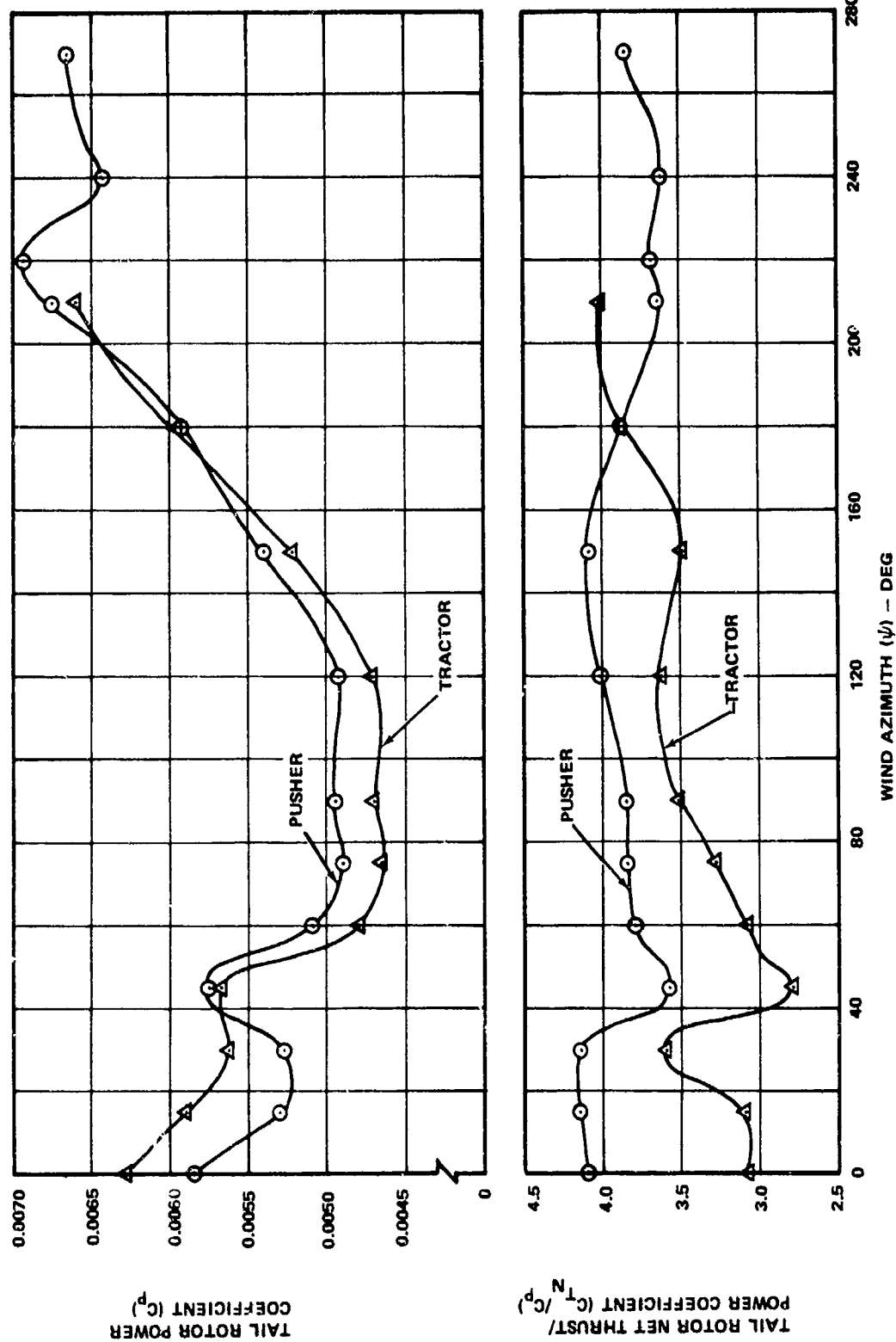
Figure 2—5. Effect of Fin Location on Tail Rotor Power and Net Thrust/Power — V = 35 kn, h/d = 0.3, θ = 20°, Position = MID, Fin = ON, Rotation = BF, s/r = 0.45.

35

WIND AZIMUTH (ψ) – DEG

TAIL ROTOR NET THRUST/POWER
COEFFICIENT AT A REFERENCE
NET THRUST ($c_{T_{N_{REF}}}/c_{P_{REF}}$)
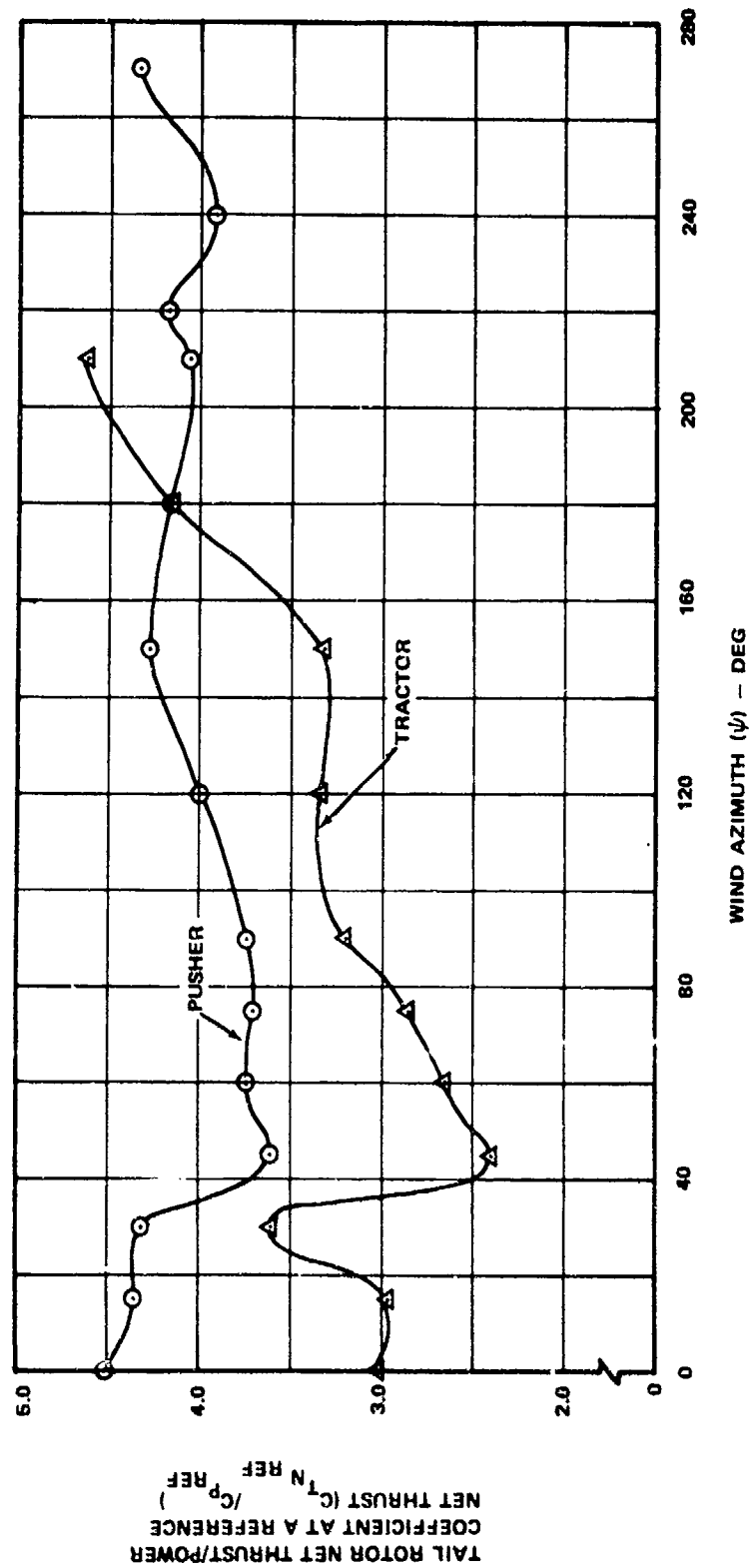
Figure 2–6. Effect of Fin Location on Tail Rotor Net Thrust/Power s: a Reference Net Thrust – V = 35 kn, h/d = 0.3, θ = 20°, Position = MID, Fin = ON, Rotation = BF, s/r = 0.45, $C_{T_{N_{REF}}}$ = 0.020.

36
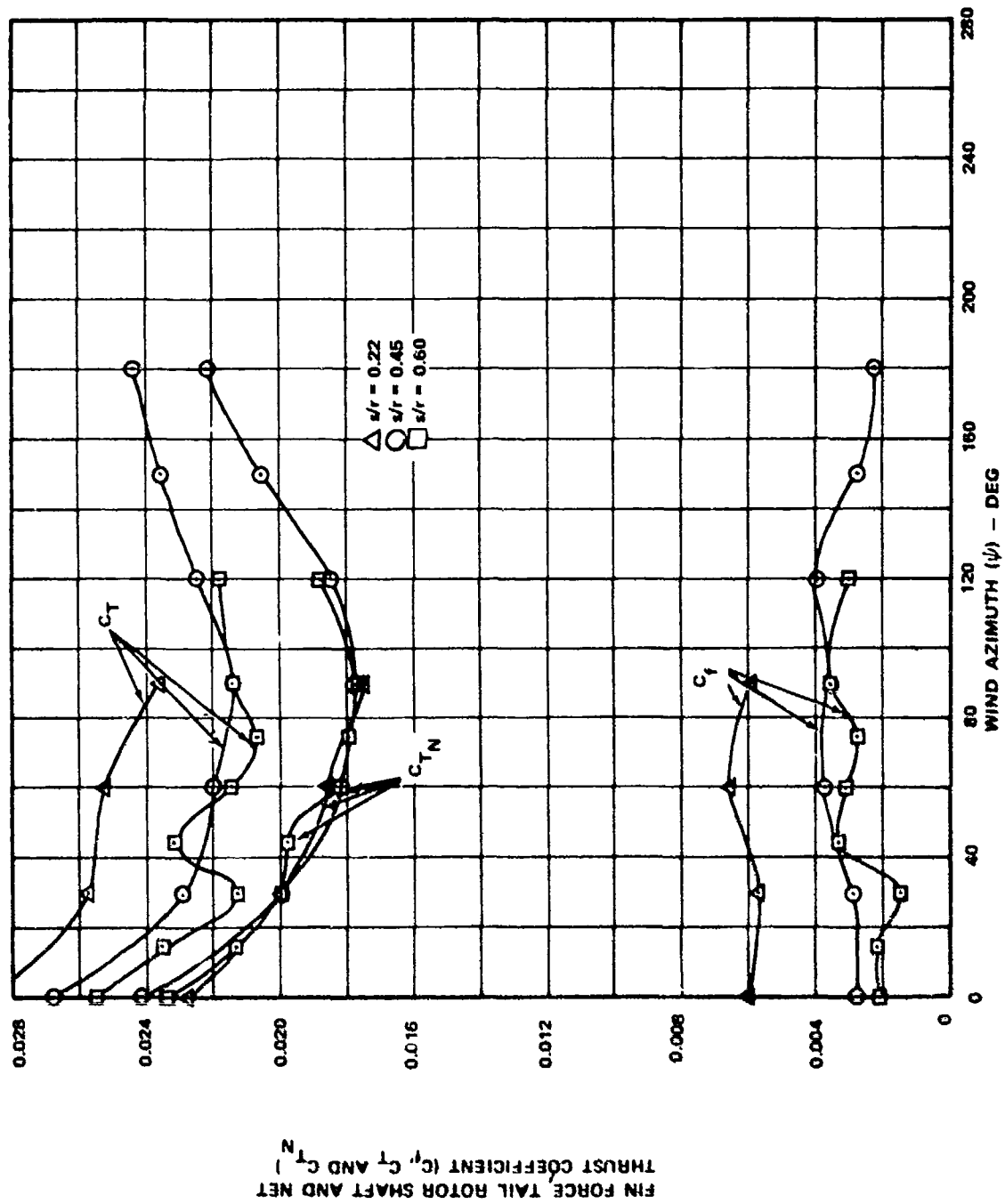
Figure 2-7. Effect of Fin-Tail Rotor Separation on Pusher Tail Rotor — V = 35 kn, h/d = 1.0, θ = 20°. Position = MID, Fin = ON, Rotation = BF.

37

3.0 DIRECTION OF ROTATION

The objective of this guideline is to select the tail rotor direction of rotation. The selection of the direction of rotation is to be determined on the same basis as Guideline 1, that is:

● The direction of rotation that gives the highest level of net thrust

● The lowest level of power required

● The least excursion of thrust and power required from a mean curve

3.1 DISCUSSION

Thrust and power comparisons between bottom aft and bottom forward directions of rotation are shown in Figures 3-1 through 3-9. This data is for the mid-position pusher configuration in 20-knot winds IGE and in 35-knot winds IGE and OGE. Examination of Figures 3-1 through 3-9 yields the relative rankings of Table 3-I.

TABLE 3-I. RELATIVE RANKINGS OF TAIL ROTOR DIRECTIONS OF ROTATION

Item	V = 20 IGE		V = 35 IGE		V = 35 OGE	
	Bottom Forward	Bottom Aft	Bottom Forward	Bottom Aft	Bottom Forward	Bottom Aft
High Thrust Level (Figures 3-1,3-4,3-7)	x		x		x	
Low Power Level* (Figures 3-3,3-6,3-9)	x		x		0	0
Low Thrust Excursion (Figures 3-1,3-4,3-7)	x		x		x	
Low Power Excursion* (Figures 3-3,3-6,3-9)	0	0	x		0	0

x indicates the better configuration
o indicates no advantage for either configuration
* Based on the higher $C_{T_{N_{Ref}}}/C_{P_{Ref}}$ ratio

39

Preceding page blank

The major findings from Table 3-I are:

- Bottom forward rotation gives the higher level of net thrust with less power.

- Bottom forward rotation results in less net thrust and power excursion.

3.2 GUIDELINE

The tail rotor direction of rotation should be bottom forward to minimize:

- collective pitch required for a given thrust, solidity, and tip speed

- pedal excursions during hover turns in winds and left sideward flight

- power required
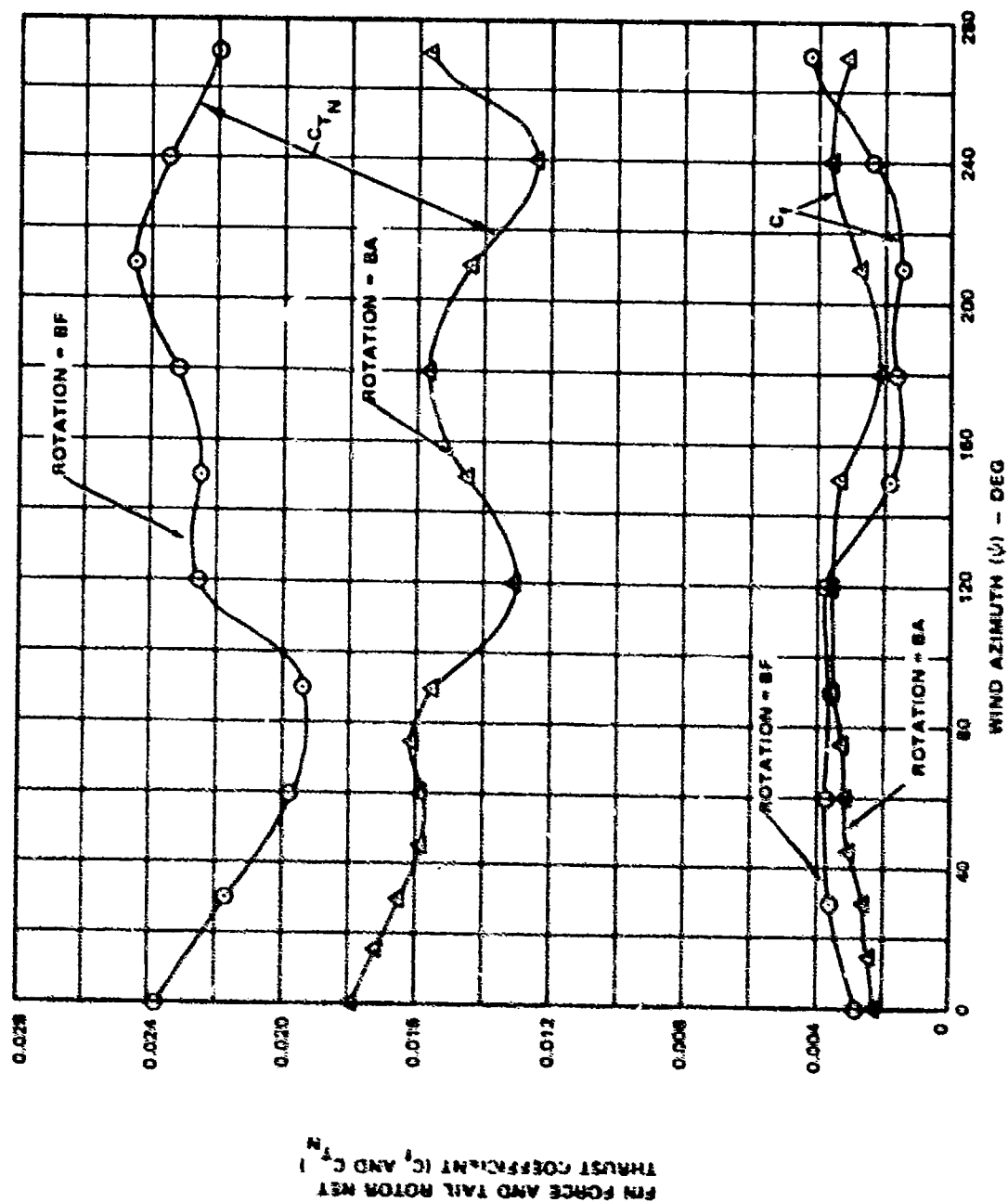
Figure 3—1. Effect of Direction of Rotation on Fin Force and Tail Rotor Net Thrust — V = 20 kn, R/d = 0.3, θ = 25°, Position = Mid, Fin = ON.
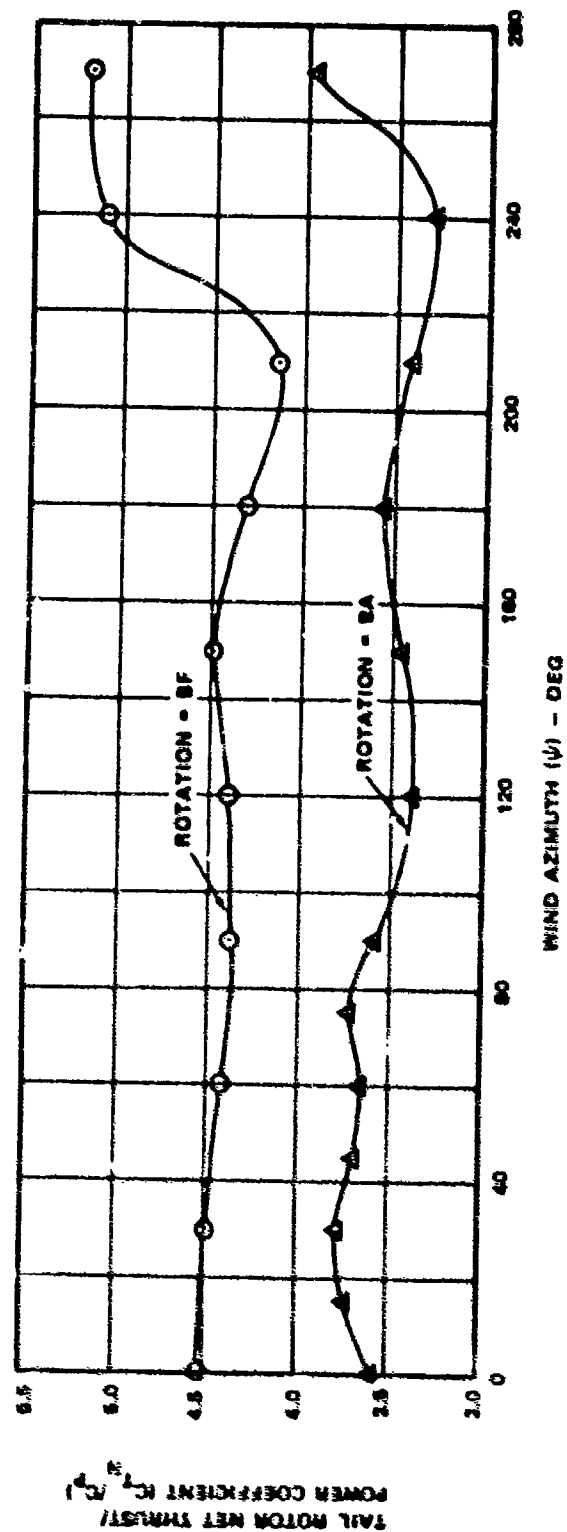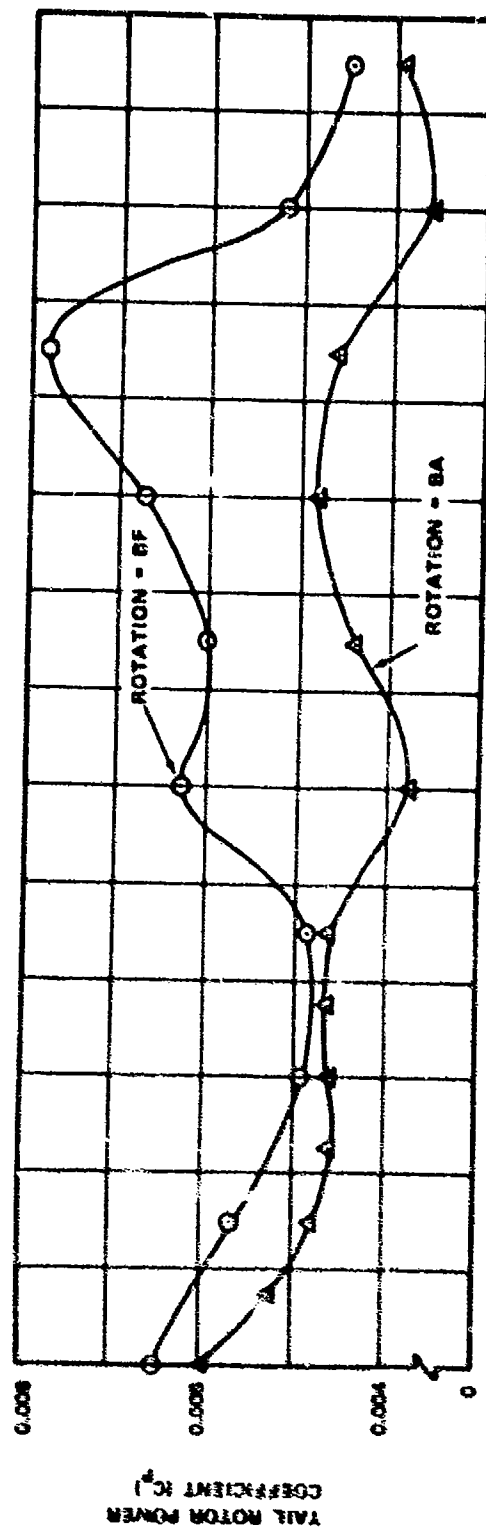
Figure 3-2. Effect of Direction of Rotation on Tail Rotor Power and Net Thrust/Power — V = 20 kn, h/d = 0.3, θ = 20°, Position = MID, Fin = ON.

Figure 2-3. Effect of Direction of Rotation on Tail Rotor Net Thrust/Power at a Reference Net Thrust — $V = 20$ kn, $h/d = 0.3$, $\theta = 20^\circ$, Position = MID, Fin = ON, $C_{T_{N\text{ REF}}} = 0.018$.

43
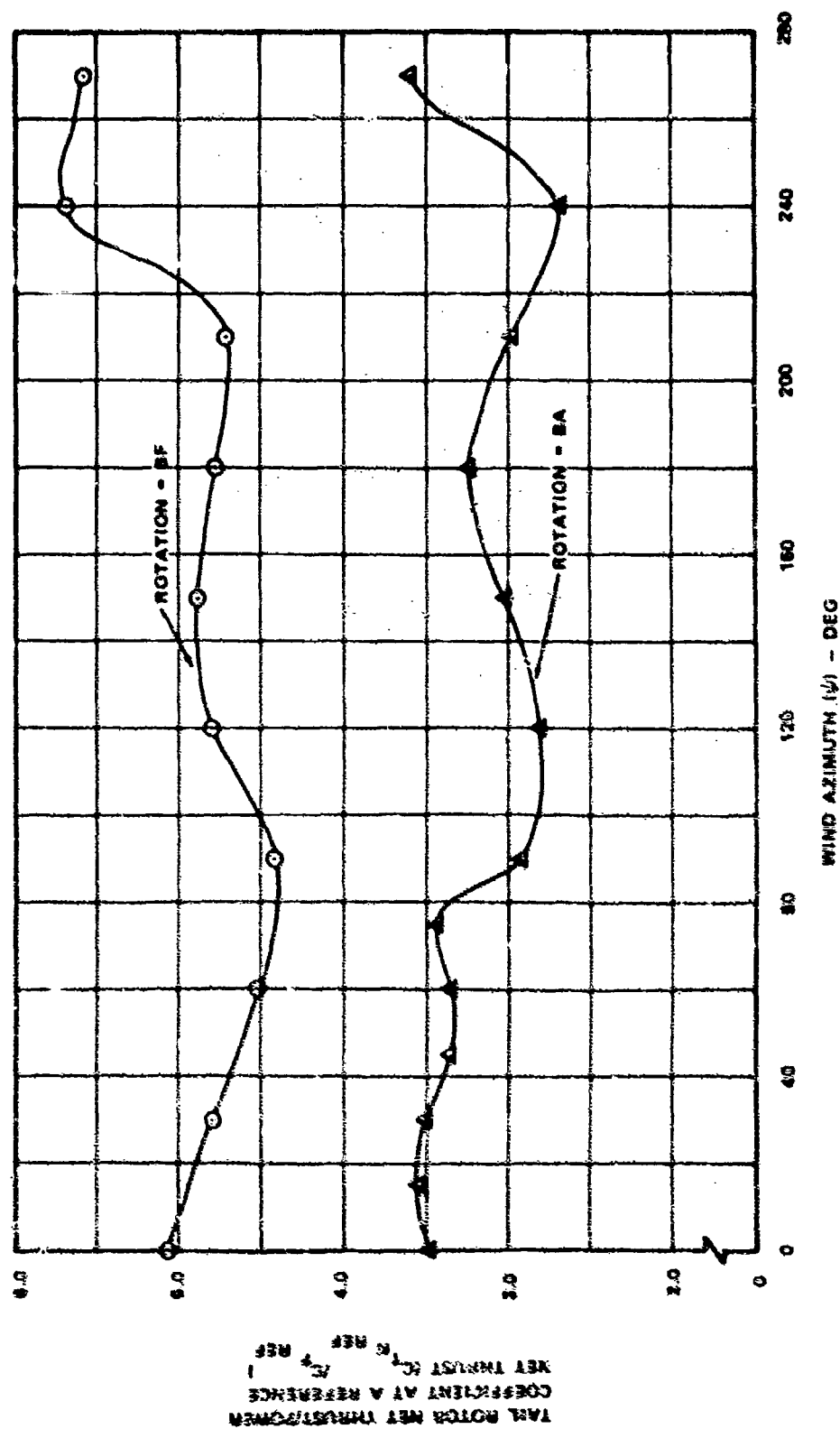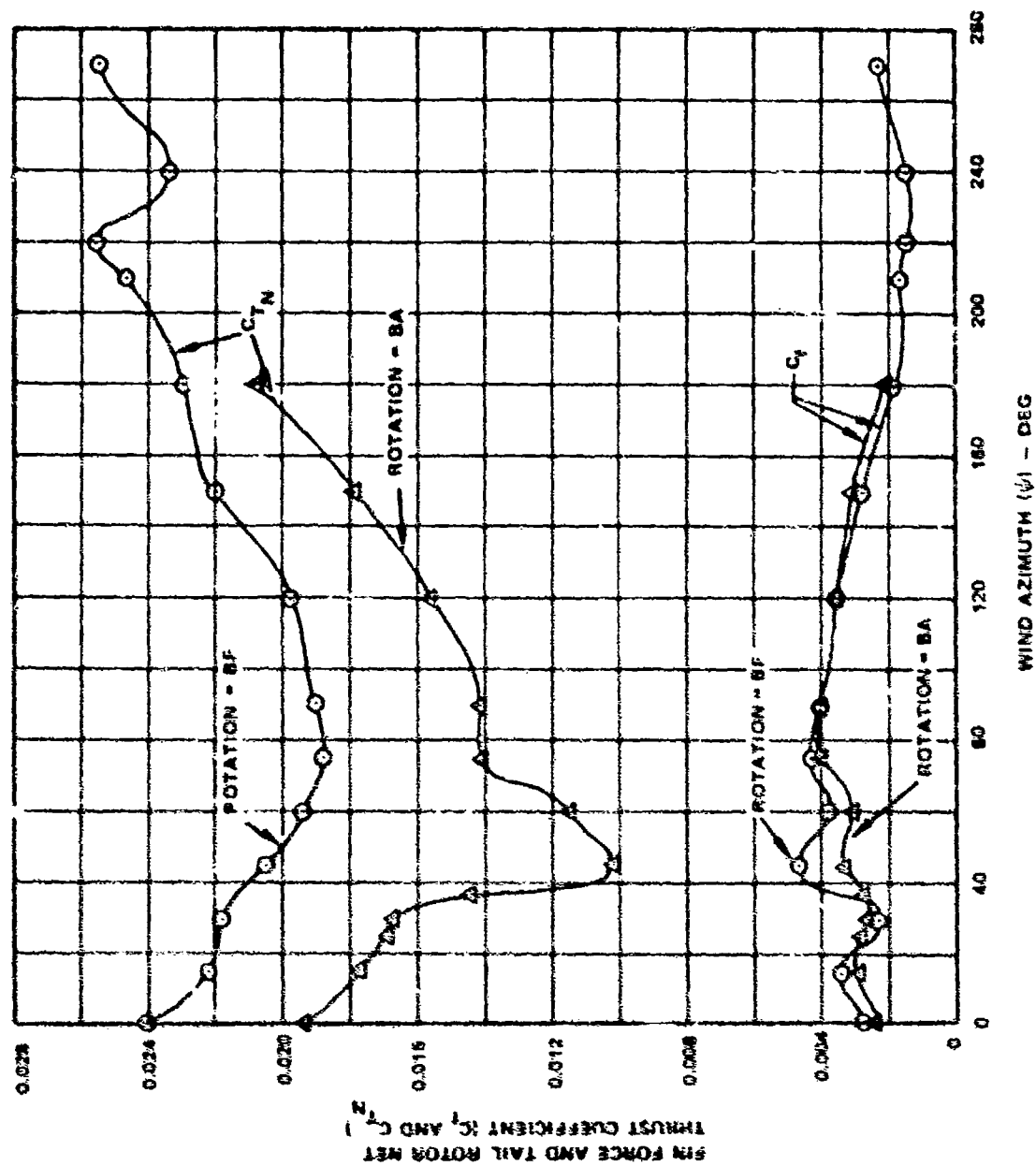
Figure 3-4. Effect of Direction of Rotation on Fin Force and Tail Rotor Net Thrust — V = 35 kn, h/d = 0.3, θ = 20°. Position = MID, Fin = ON.
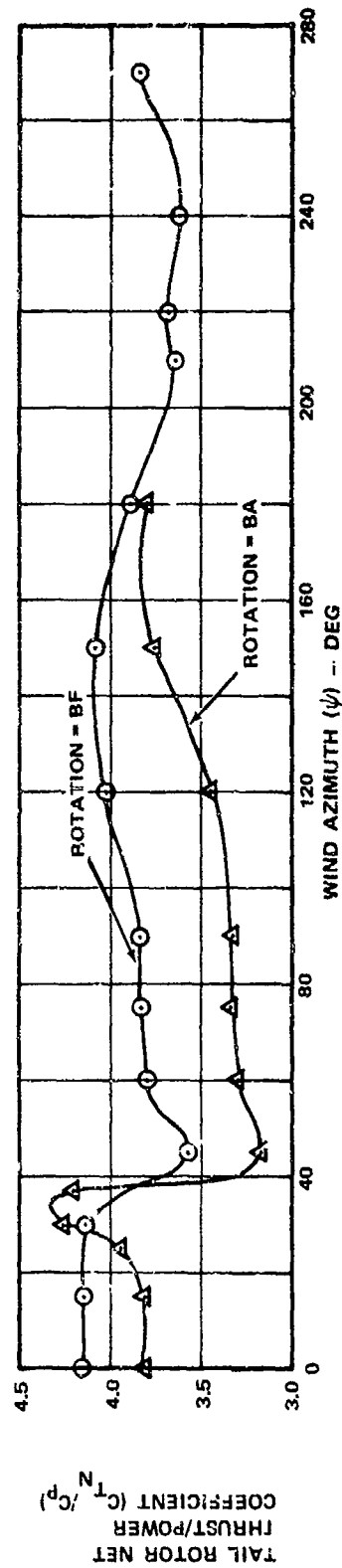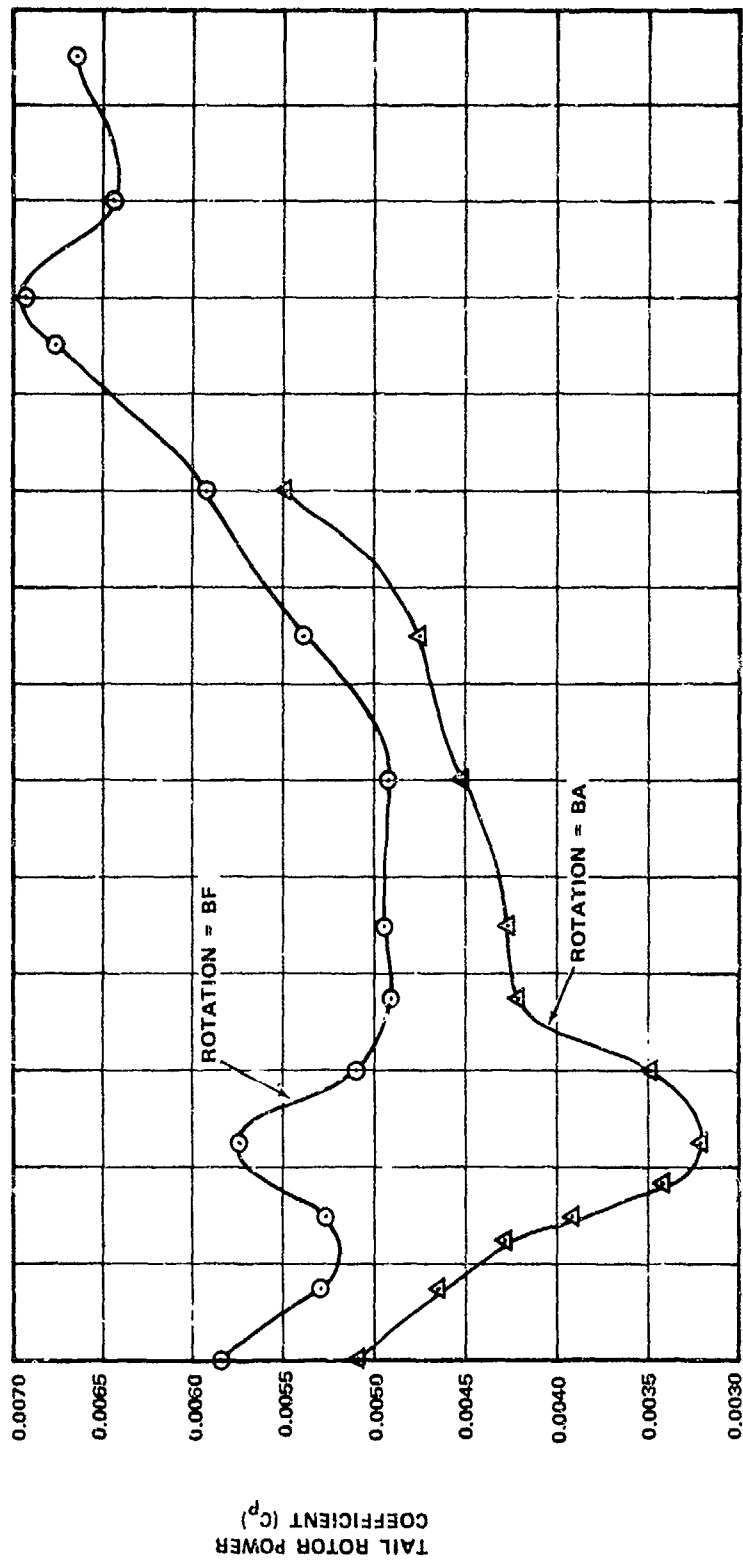
Figure 3-5. Effect of Direction of Rotation on Tail Rotor Power and Net Thrust/Power — V = 35 kn, h/d = 0.3, θ = 20°, Position = MID, Fin = ON.

45
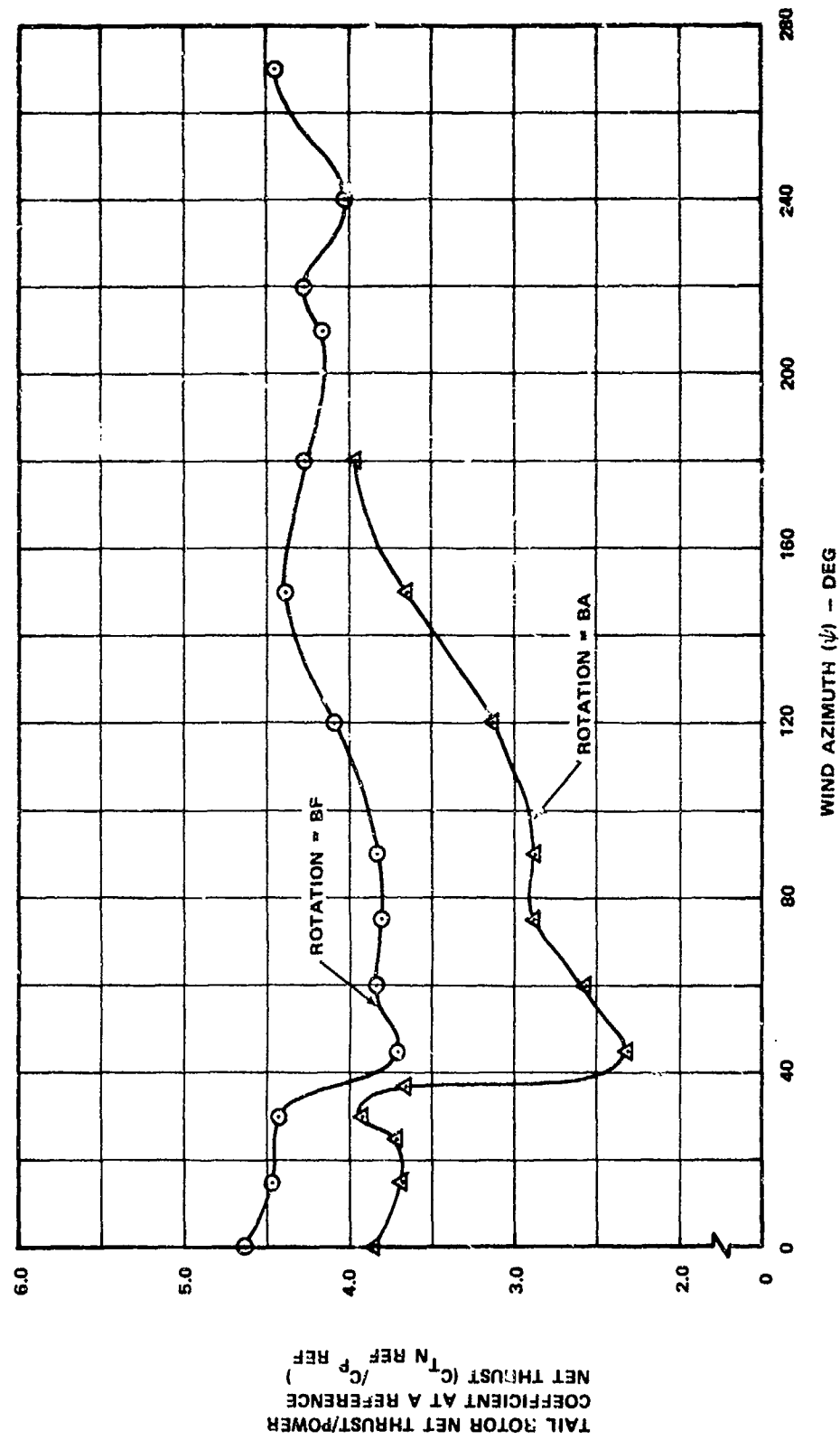
Figure 3–6. Effect of Direction of Rotation on Tail Rotor Net Thrust/Power at a Reference Net Thrust –
V = 35 kn, h/d = 0.3, θ = 20°, Position = MID, Fin = ON, $C_{T_{N_{REF}}}$ = 0.012.

WIND AZIMUTH (ψ) – DEG

TAIL ROTOR NET THRUST/POWER
COEFFICIENT AT A REFERENCE
NET THRUST ($C_{T_N REF}/C_{P_{REF}}$)

46
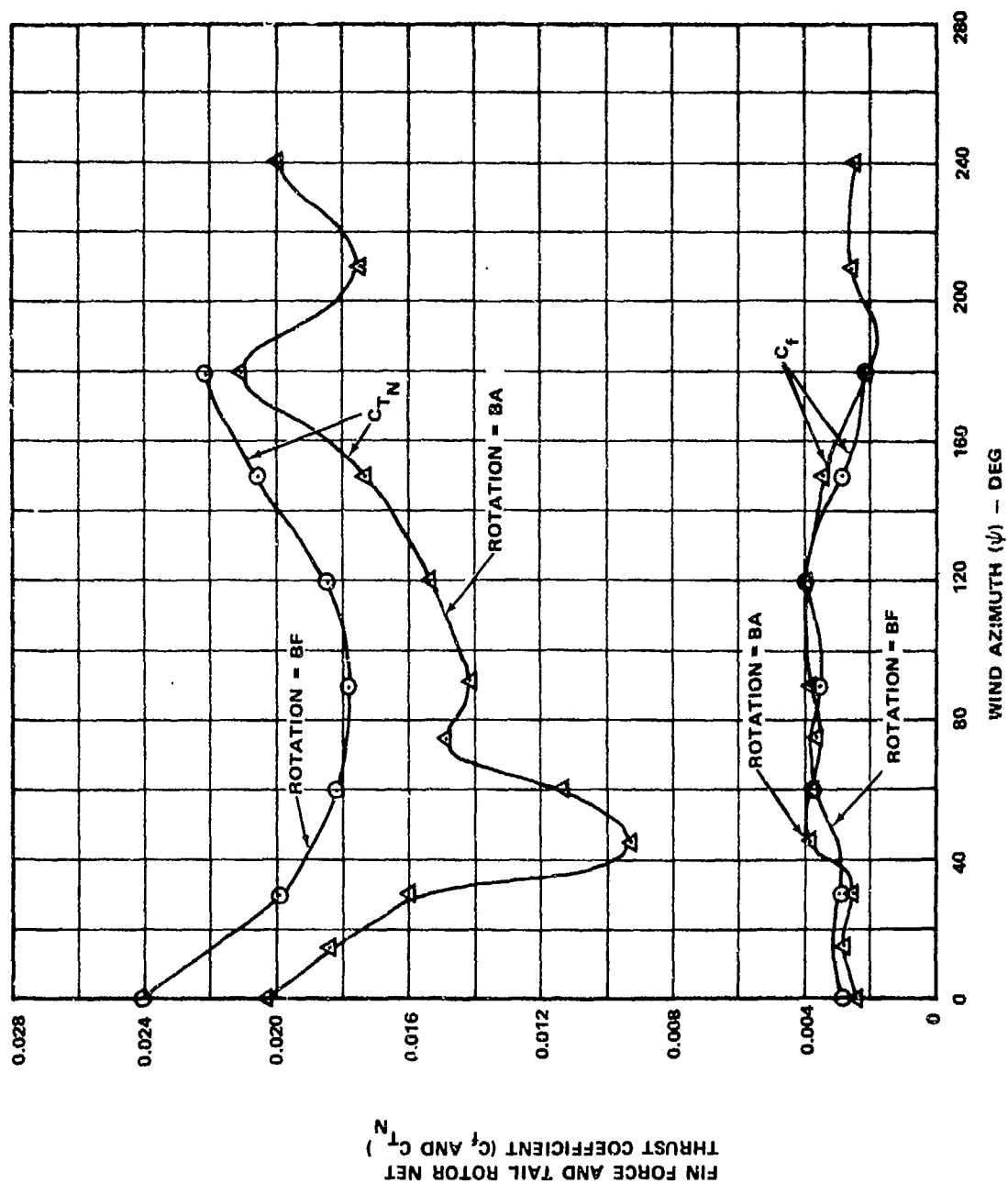
Figure 3—7. Effect of Direction of Rotation on Fin Force and Tail Rotor Net Thrust — V = 35 kn, h/d = 1.0, $\theta = 20^\circ$, Position = MID, Fin = ON.

47
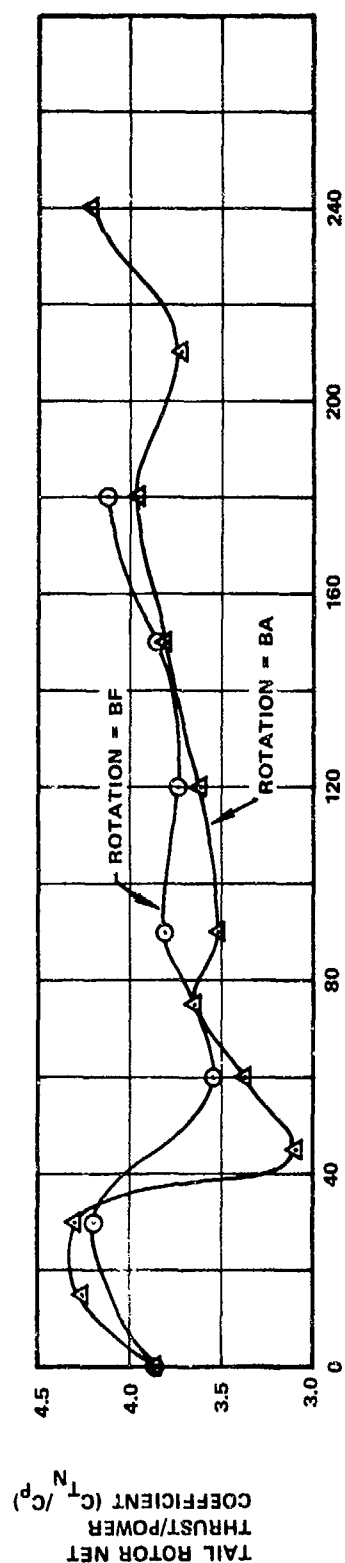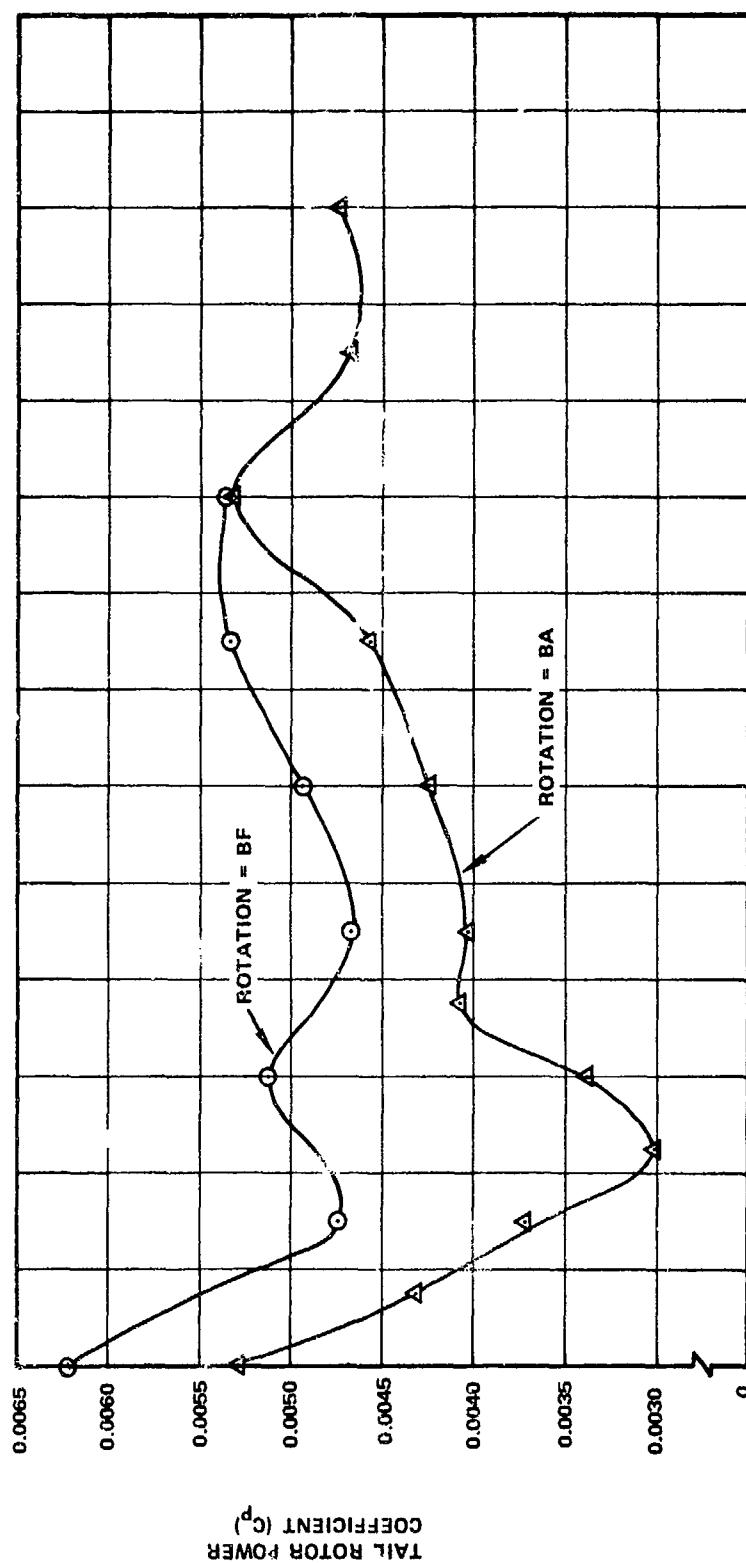
Figure 3-8. Effect of Direction of Rotation on Tail Rotor Power and Net Thrust/Power — V = 35 kn, h/d = 1.0, θ = 20°, Position = MID, Fin = ON.

48
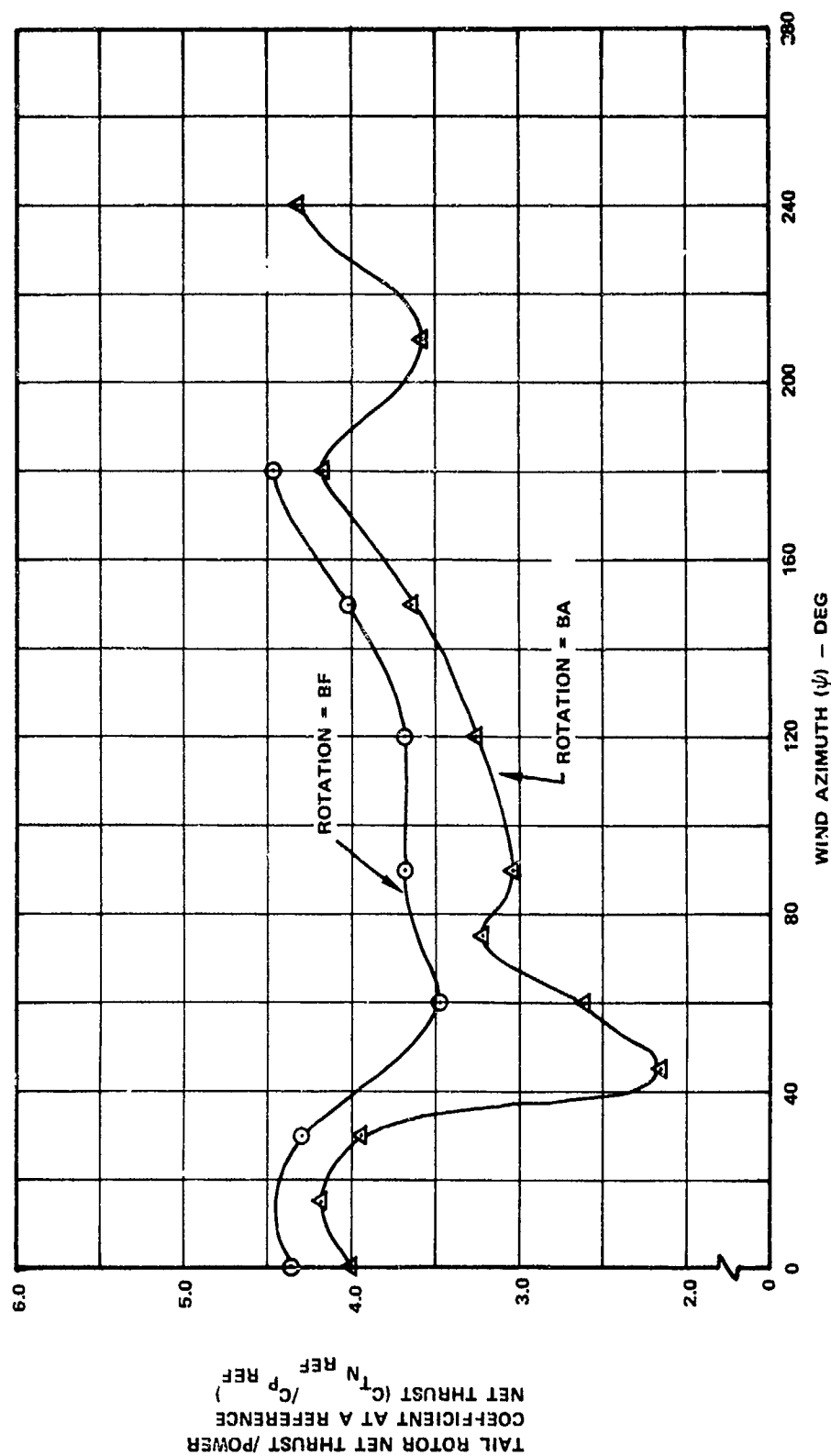
Figure 3–9. Effect of Direction of Rotation on Tail Rotor Net Thrust/Power at a Reference Net Thrust — $V = 35$ kn, h/d = 1.0, $\theta = 20^0$, Position = MID, Fin = ON, $C_{T_{N \text{ REF}}}$ = 0.019.

4.0 CRITICAL THRUST AND POWER AZIMUTHS

The objective of this guideline is to define the critical wind azimuth, wherein the tail rotor produces the least thrust and the power required for a given thrust is highest for a given set of flight conditions and tail rotor parameters. For a tail rotor with a given diameter and tip speed, maximum blade incidence and solidity selection is based on the thrust available at the critical thrust azimuth. The critical power azimuth must be known to determine tail rotor power requirements.

4.1 DISCUSSION

The data from which this guideline is developed is included in Figures 1-3 through 3-9 and 4-4 for wind velocities of 20 and 35 knots and Figures 4-1 through 4-3 for wind velocity of 12 knots. The critical thrust and power azimuths determined from these figures are tabulated in Table 4-I on page 57.

At low wind velocities (12 knots) the critical direction for thrust is anywhere between wind azimuths of 30° and 240° (Figure 4-1). As the wind velocity is increased to 20 knots, the critical direction for bottom forward rotation becomes wind from the right, $\psi = 90°$ IGE (Figures 1-3 and 2-1), and $\psi = 60°$ OGE (Figure 4-4). For bottom aft, the left rear quadrant is critical (Figure 3-1).

For high-velocity winds (35 knots), the critical thrust azimuth is $\psi = 45$ to $90°$, the right front quadrant. The only exception is the aft position (without fin) IGE, where the thrust is lower at $\psi = 240°$ (Figures 1-6, 1-9, 2-4, 3-4 and 3-7).

The tests used to determine the critical azimuth were conducted at $\theta = 20°$, which corresponds to C_σ values between 2.0 and 2.5. Tests conducted with the mid-position IGE at lower collectives (Figures 4-5 and 4-6) confirm that the critical thrust azimuth remains near $\psi = 90°$ for low values of C_σ (at $\theta = 11°$, $C_\sigma = 0.7$).

The critical power azimuth can occur with wind either from the right front or from the left rear, depending upon the configuration, wind speed, and height above the ground. Generally, on configurations with fin installed and with bottom forward rotation, the critical azimuth occurs between $\psi = 30°$ and $90°$ (Figures 2-3, 2-6, 3-9, and 4-3).

51

4.2 GUIDELINE

Maximum blade incidence should be determined at the critical thrust azimuths listed in Table 4-I, which are generally between $\psi = 30^\circ$ and 240° at low wind velocity (12 knots), from $\psi = 60^\circ$ OGE and $\psi = 90^\circ$ IGE at 20 knots, and from the right ($\psi = 90^\circ$) at higher velocities.

Maximum tail rotor power requirements occur at the critical power azimuths listed in Table 4-I. These azimuths are generally wind from the right front for configurations with fin installed and with bottom forward rotation.
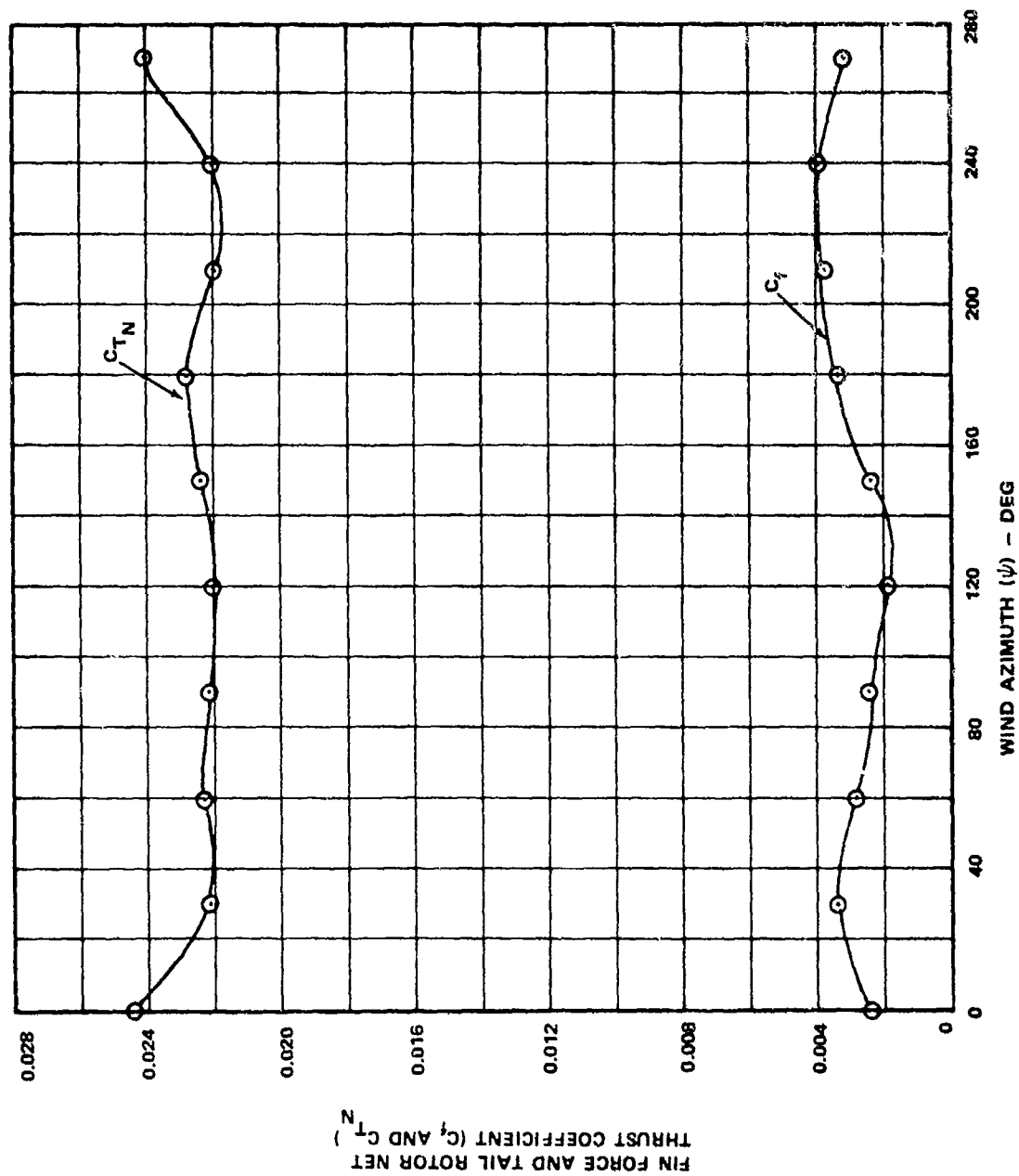
Figure 4—1. Fin Force and Tail Rotor Net Thrust — V = 12 kn, h/d = 0.3, ϑ = 20°, Position = MID, Fin = ON, Rotation = BF.

53
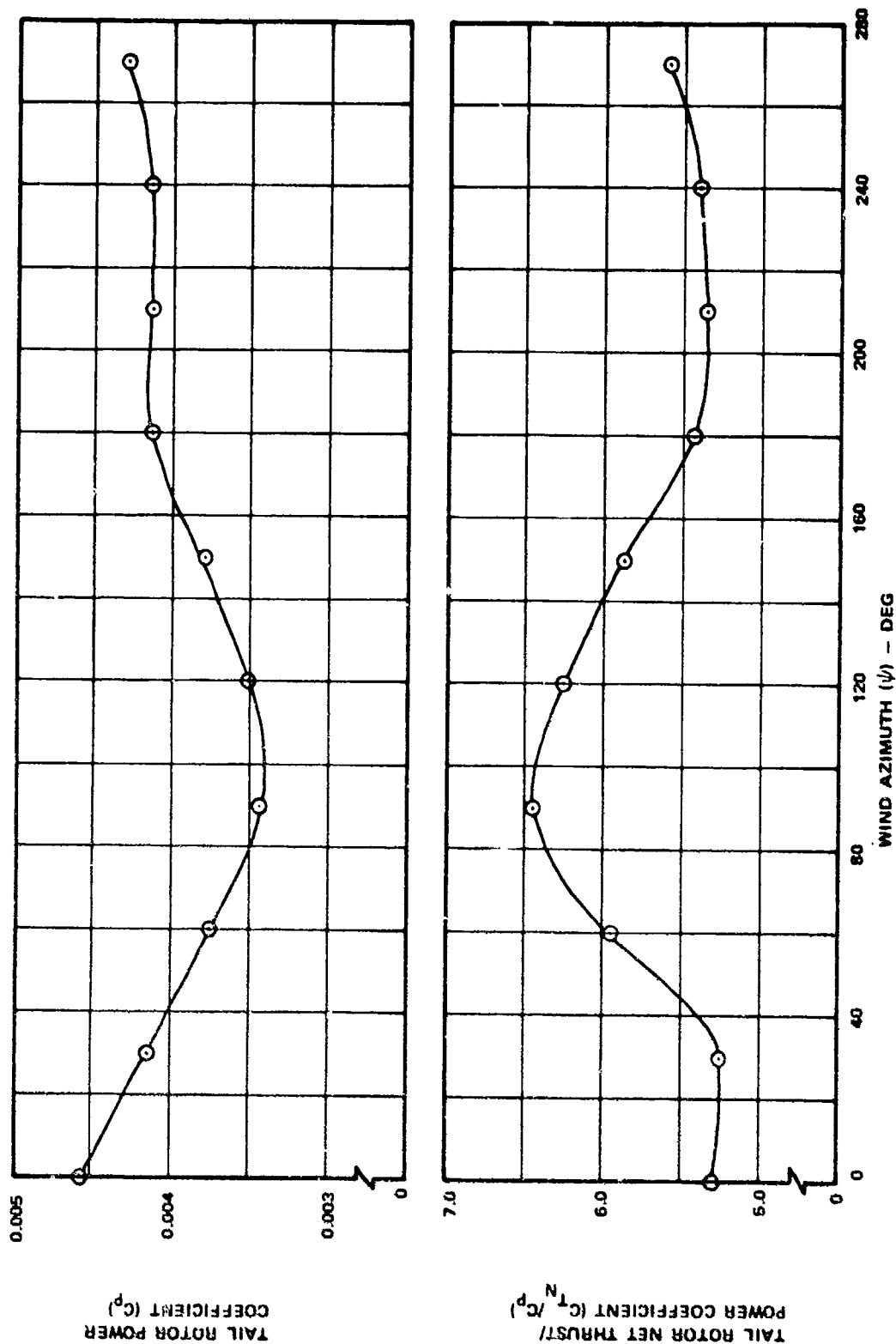
Figure 4-2. Tail Rotor Power and Net Thrust/Power — V = 12 kn, h/d = 0.3, θ = 20°, Position = MID, Fin = ON, Rotation = BF.
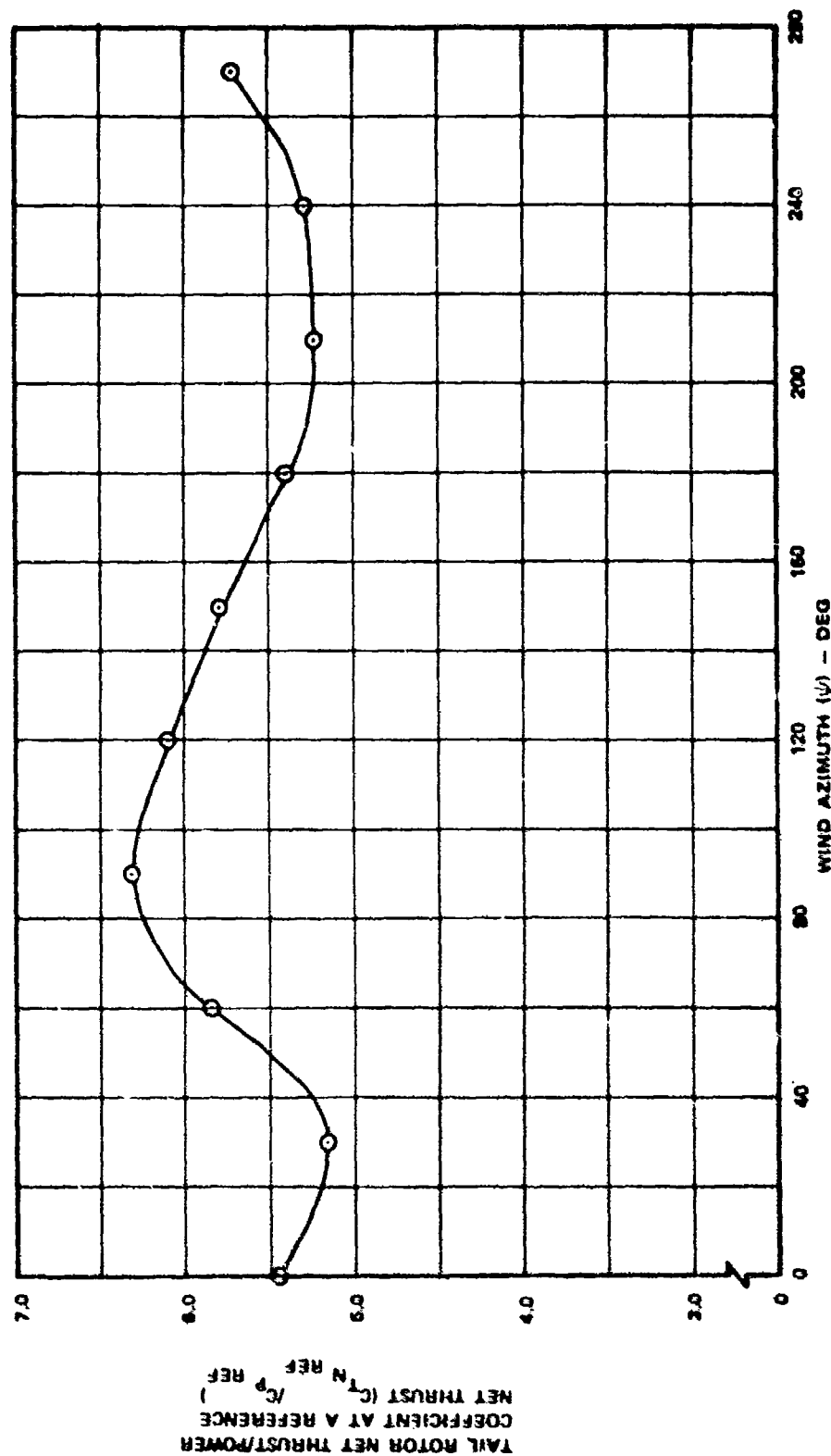
Figure 4-3. Tail Rotor Net Thrust/Power at a Reference Net Thrust -- V = 12 kn, h/d = 0.3, θ = 20°.
Position = MID, Fin = ON, Rotation = BF, $C_{T_{N \, REF}}$ = 0.023.
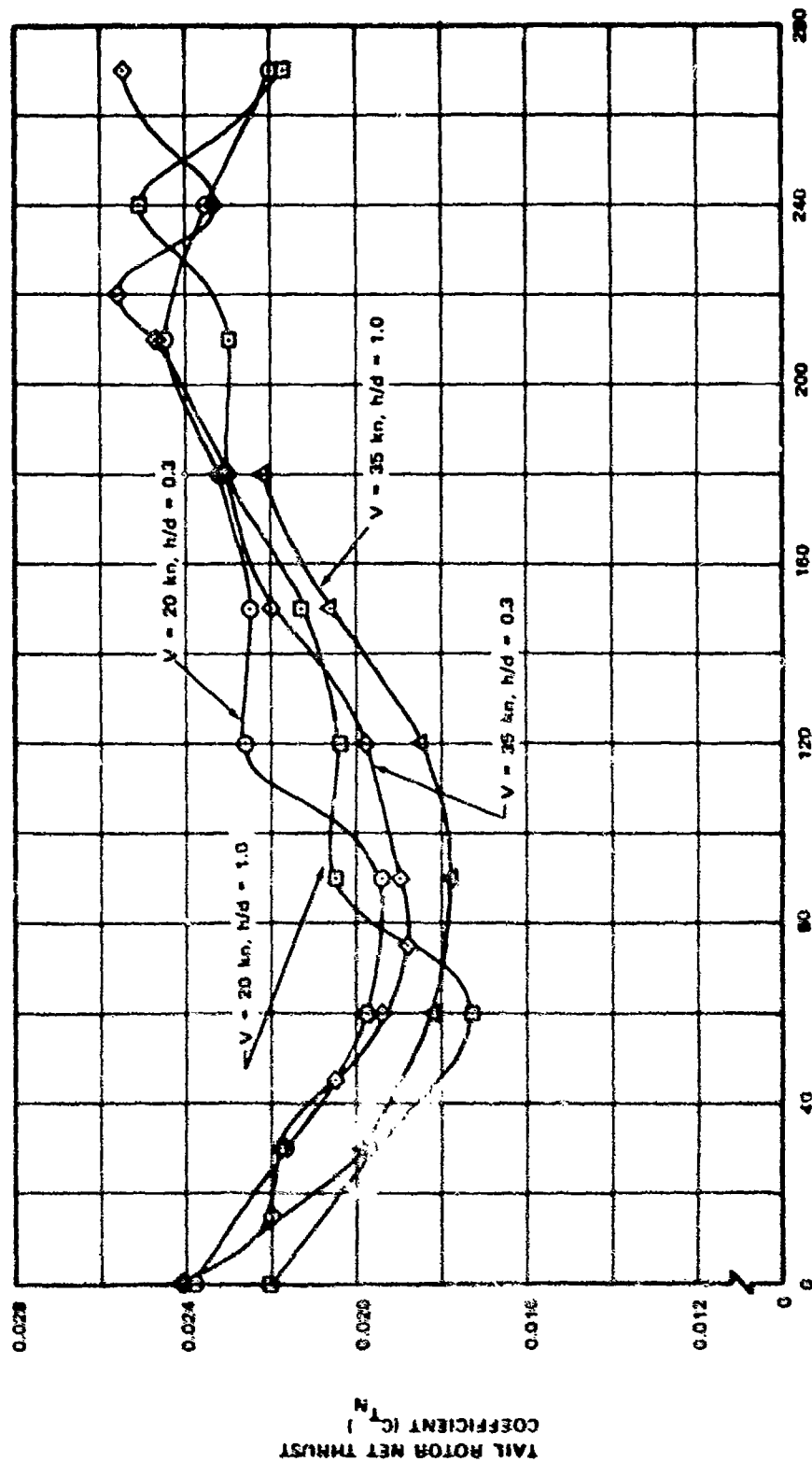
Figure 4-4. Effect of Wind Velocity and Main Rotor Height/Diameter Ratio on Tail Rotor Net Thrust –
$\theta = 20^\circ$, Position = MID, Fin = ON, Rotation = BF.

WIND AZIMUTH (ψ) – DEG

TAIL ROTOR NET THRUST
COEFFICIENT (C_{T_N})

56

TABLE 4-I. CRITICAL THRUST AND POWER AZIMUTHS

Velocity (Kn) h/d	12 0.3		20 0.3		20 1.0		35 0.3		35 1.0	
Configuration	Thrust	Power	Thrust	Power	Thrust	Power	Thrust	Power	Thrust	Power
High Position[1] (Reference Figure)			120 (1.3)	210(estimated)[3] (1 4)			45 (1.6)	210 (1.7)	45 (1.9)	210 (1.10)
Mid Position[1] (Reference Figure)			90 (1.3)	210(estimated) (1.4)			70 (1.6)	210 (1.7)	60 (1.9)	210(estimated)[3] (1.10)
Low Position[1] (Reference Figure)			90 (1.3)	NA			80 (1.6)	NA	NA	NA
Aft Position[1] (Reference Figure)			NA	NA			240 (1.6)	210 (1.7)	30 (1.9)	210 (1.10)
Pusher[2] Bottom Forward Rotation (Reference Figure)	120 (4.1)	30 (4.2)	90 (2.1)	210 (2.2)	60 (4.4)	NA	75 (2.4)	45 (2.5)	90 (3.7)	45(estimated) (3.8)
Tractor[2] Bottom Forward Rotation (Reference Figure)			75 (2.1)	30 (2.2)			60 (2.4)	45 (2.5)	NA	NA
Pusher[2] Bottom Aft Rotation (Reference Figure)			240 (3.1)	240 (3.2)			45 (3.4)	45 (3.5)	45 (3.7)	45 (3.8)

[1] Fin off, bottom forward rotation
[2] Mid position, fin on, θ = 20°, for all configurations
NA indicates data not available

[3] Data not specifically available but estimated from examination of all velocity and position curves
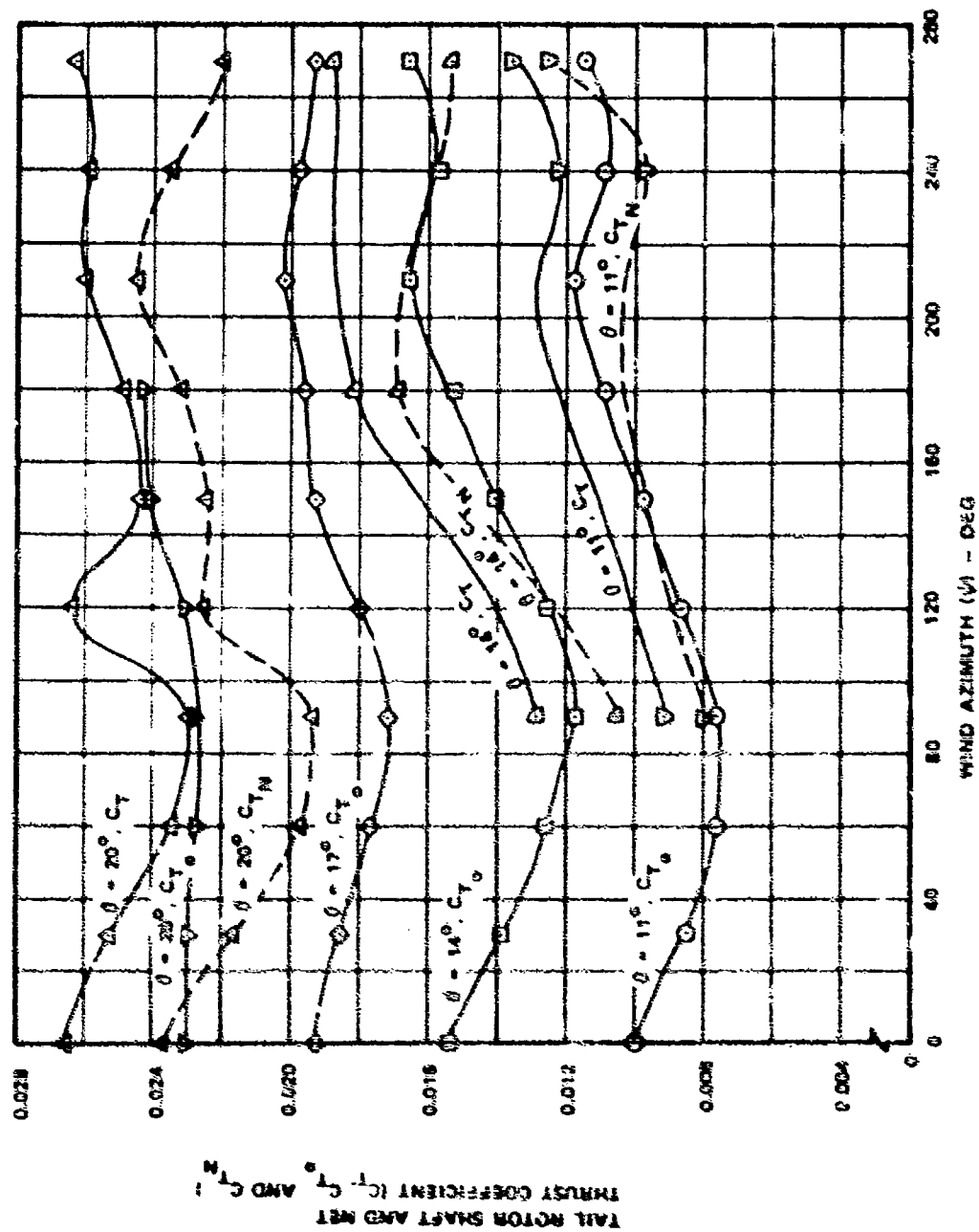
Figure 4-6. Effect of Tail Rotor Collective Pitch on Tail Rotor Shaft and Net Thrust — $\gamma = 20$ ft, $\mu = 0.3$, Position = MID, Rotation = BF.
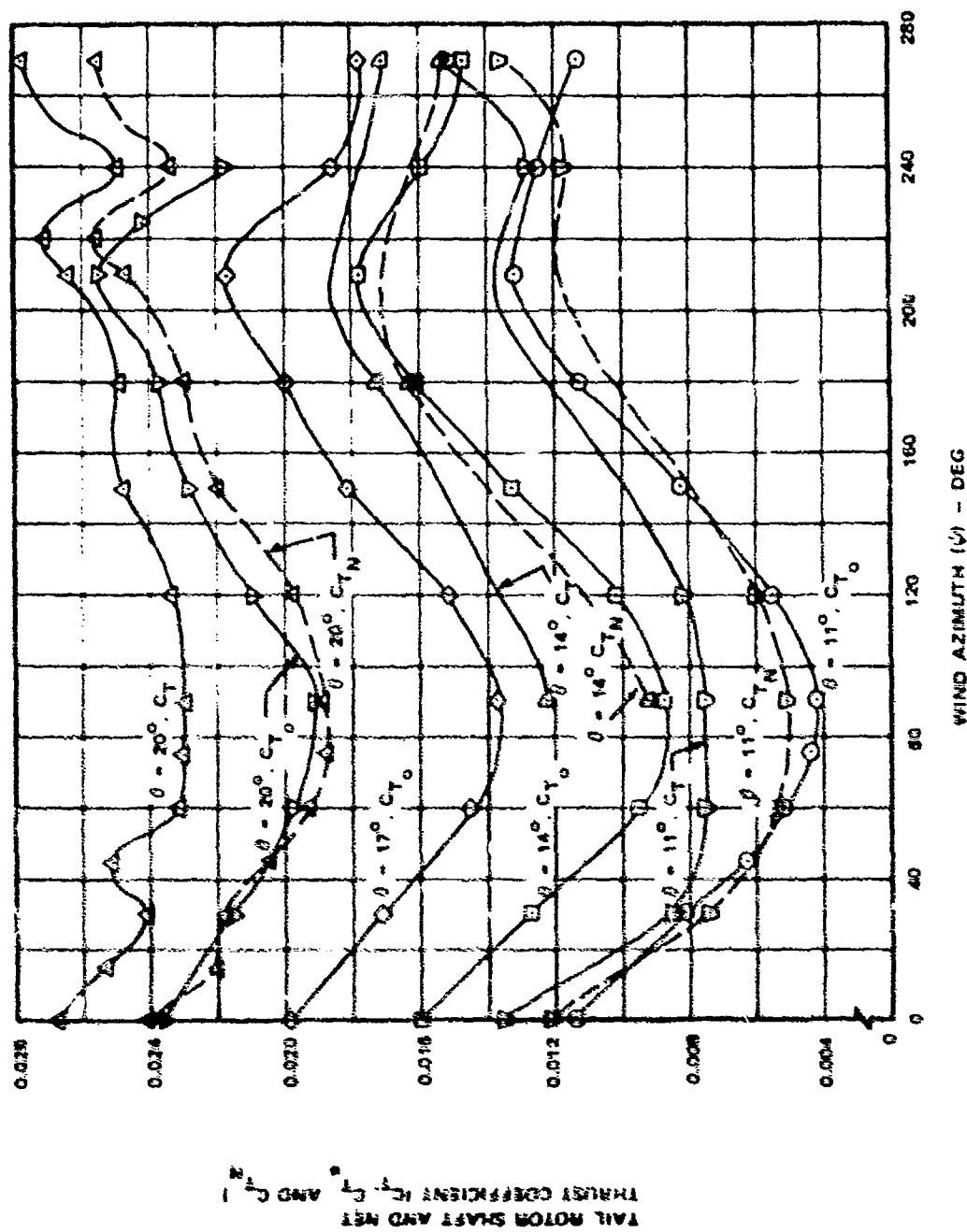
Figure 4-4. Effect of Tail Rotor Collective Pitch on Tail Rotor Shaft and Net Thrust – V = 35 kn, h/d = 0.3, Position – MID, Rotation – BF.

5.0 CRITICAL WIND VELOCITY

The critical wind velocity is defined as the velocity at which
the net tail rotor thrust level is a minimum for a given wind
azimuth, main rotor height above the ground, and constant tail
rotor blade incidence. As with critical wind azimuth and
critical h/d, the critical wind velocity must be known to de-
sign the tail rotor solidity and maximum blade incidence.

5.1 DISCUSSION

Net thrust and fin force results from the Boeing tests of wind
azimuth sweeps at various velocities or mid position only are
presented in Figures 5-1 and 5-2 for IGE and OGE conditions,
respectively. Note that the lowest thrust level occurs at
$V = 20$ knots OGE at $\psi = 60^\circ$.

As evident from Figure 5-3, the critical wind velocity depends
on h/d. The wing tip vortex deflection changes with h/d in
20- to 25-knot winds; t' its effect on tail rotor thrust
production depends on h,

5.2 GUIDELINE

The critical velocity (lowest level of thrust production) for
low-speed flight occurs between $V = 20$ and 25 knots, depending
on main rotor height. Because of the higher trim thrust re-
quired at 20 knots, a 20-knot velocity, in conjunction with
the critical azimuth and critical h/d, is used to design tail
rotor solidity and maximum blade incidence for both in- and
out-of-ground-effect conditions.
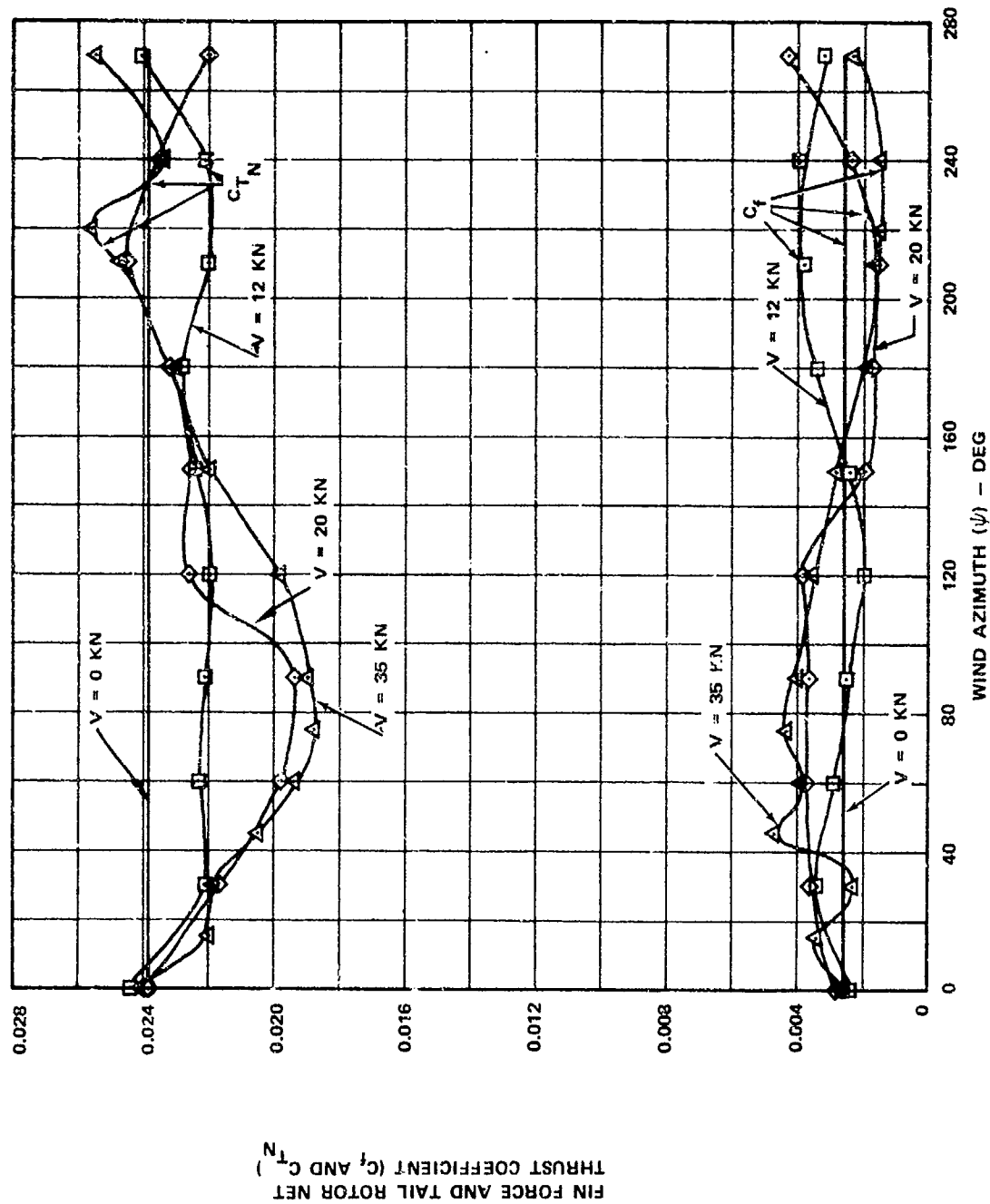
Figure 5—1. Effect of Wind Velocity on Fin Force and Tail Rotor Net Thrust — h/d = 0.3, θ = 20°, Position = MID, Fin = ON, Rotation = BF.

62
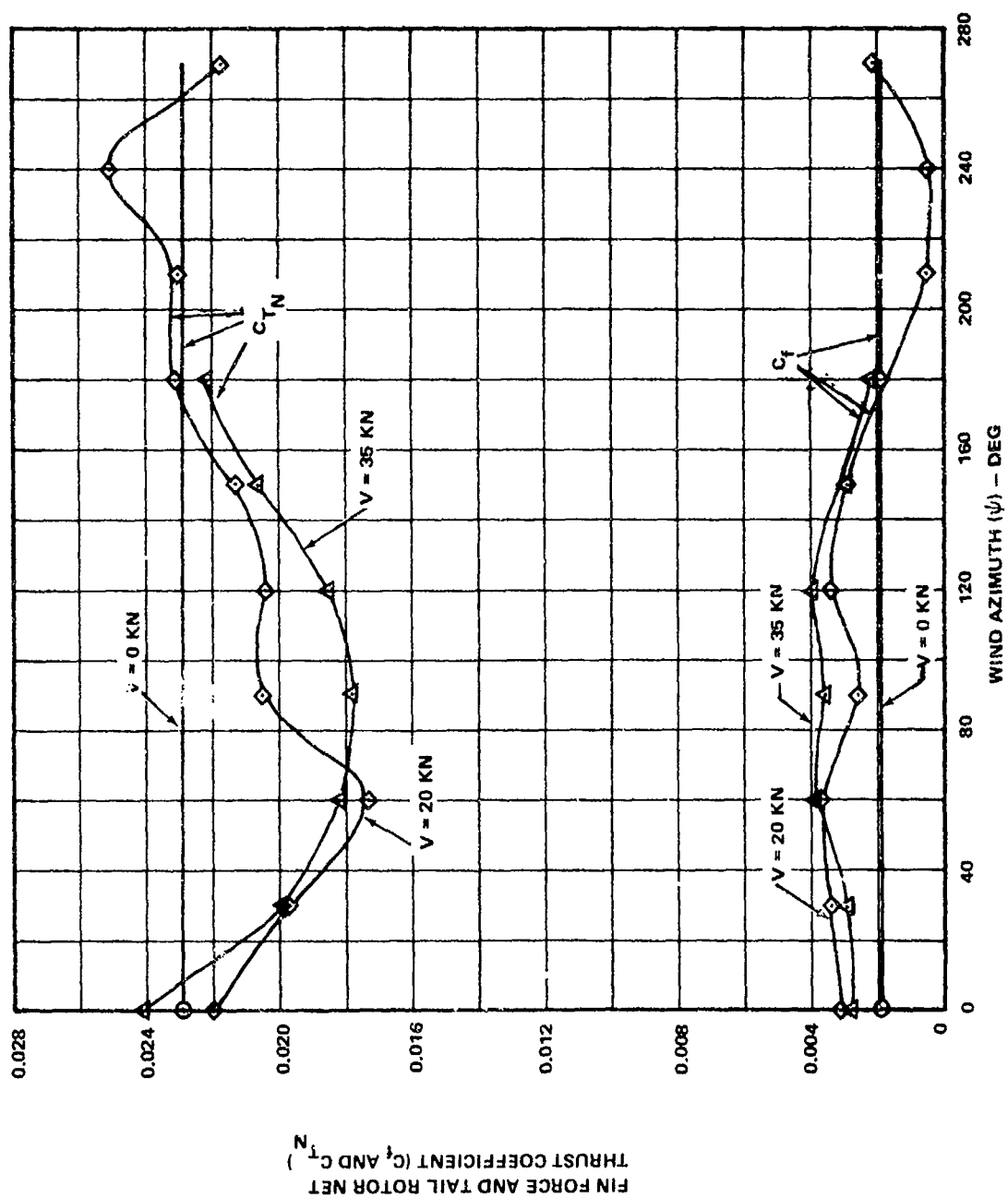
Figure 5–2. Effect of Wind Velocity on Fin Force and Tail Rotor Net Thrust — h/d = 1.0, θ = 20°, Position =MID, Fin = ON, Rotation = BF.

63
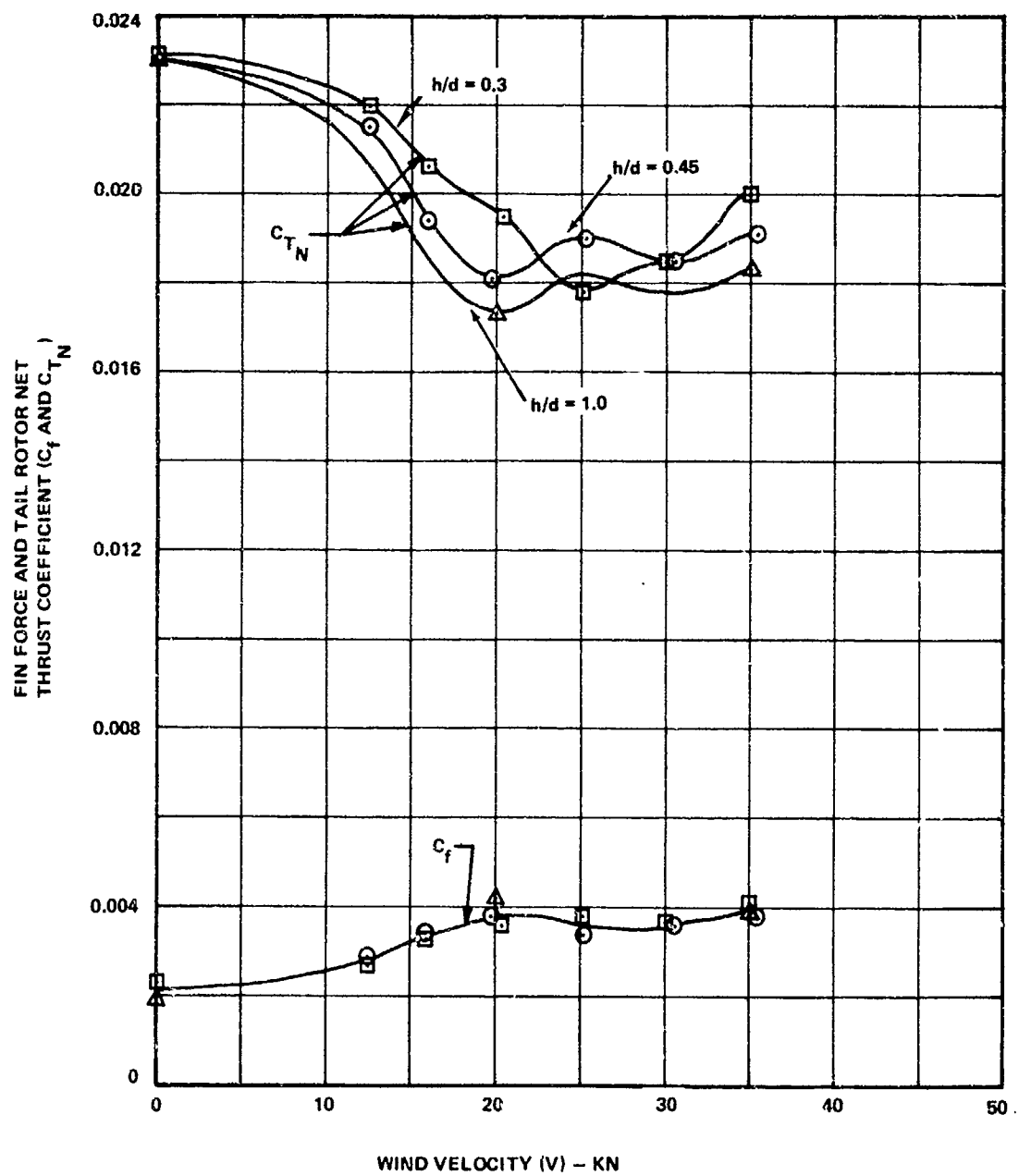
Figure 5–3. Effect of Main Rotor Height/Diameter Ratio on Fin Force and Tail Rotor Net Thrust — $\psi = 60^o$, $\theta = 20^o$, Position = MID, Fin = ON, Rotation = BF.

64
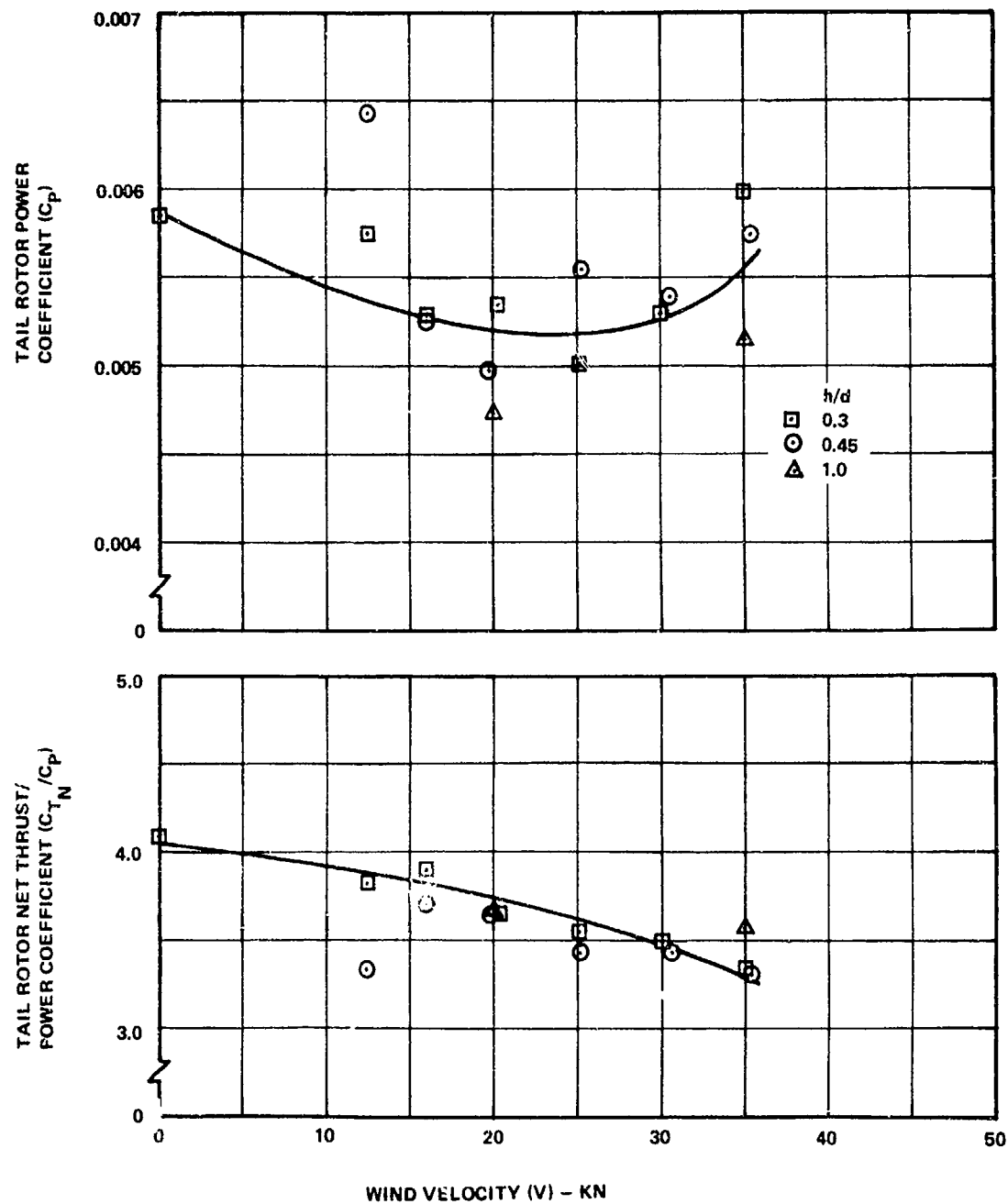
Figure 5-4. Effect of Main Rotor Height/Diameter Ratio on Tail Rotor Power and Net Thrust/Power — $\psi = 60^{o}$, $\theta = 20^{o}$, Position = MID, Fin = ON, Rotation = BF.

65

6.0 CRITICAL IGE HOVER HEIGHT

Critical IGE thrust hover height is defined as that main rotor height above the ground (for h/d ≤ 0.6) at which the tail rotor thrust is a minimum for a given wind velocity and azimuth. Similarly, critical IGE power hover height is the main rotor height at which the ratio of thrust to power coefficients is a minimum. Minimum excursion of thrust and power will also be a consideration to provide the least rudder pedal motion with h/d. Knowledge of these critical heights is necessary to design tail rotor solidity and maximum blade incidence and to determine tail rotor power requirements.

6.1 DISCUSSION

As can be seen from Table 4-I of Guideline 4, the critical thrust azimuth is wind from the right front for most configurations. The lowest net thrust of any condition for the pusher configuration of bottom forward rotation occurred OGE at $\psi = 60°$, V = 20 knots (Figure 4-4). Since net thrust at $\psi = 60°$ was close to the minimum for all other conditions, it was selected as the azimuth at which h/d sweeps were run for each configuration to determine critical hover heights in the Boeing tests. Results of these tests are shown in Figures 6-1 through 6-8; while the critical IGE hover heights are presented in Table 6-I on page 77.

Both thrust and power critical heights are between h/d = 0.37 and 0.45 for most configurations at a 20-knot wind speed. This is due to the tail rotor's passing through the wing tip vortex as the vortex angle of deflection changes with increasing h/d (see Flow Environment section). At 35 knots the tail rotor remains within this vortex as h/d is varied, resulting in little change of thrust and power with h/d. At V = 0, no wing tip vortex is formed, so thrust also remains relatively constant above h/d = 0.45. Below this value of h/d, the main rotor wake spreads outward, resulting in more of the tail rotor disc's being immersed in main rotor wash. Thrust, therefore, is increased for bottom forward rotation and would be decreased for bottom aft rotation.

6.2 GUIDELINE

Given aircraft alternate gross weight and maneuver requirements, tail rotor solidity, maximum blade incidence, and power required should be selected for wind speed of 20 knots at the hover heights presented in Table 6-I. For bottom forward rotation with fin on, the critical thrust and power hover height is h/d = 0.45. However, since the critical thrust values are

67

Preceding page blank

nearly the same for both IGE and OGE, the average of the values at $h/d = 0.45$ and 1.0 may be used to simplify the design variables at $V = 20$ knots.
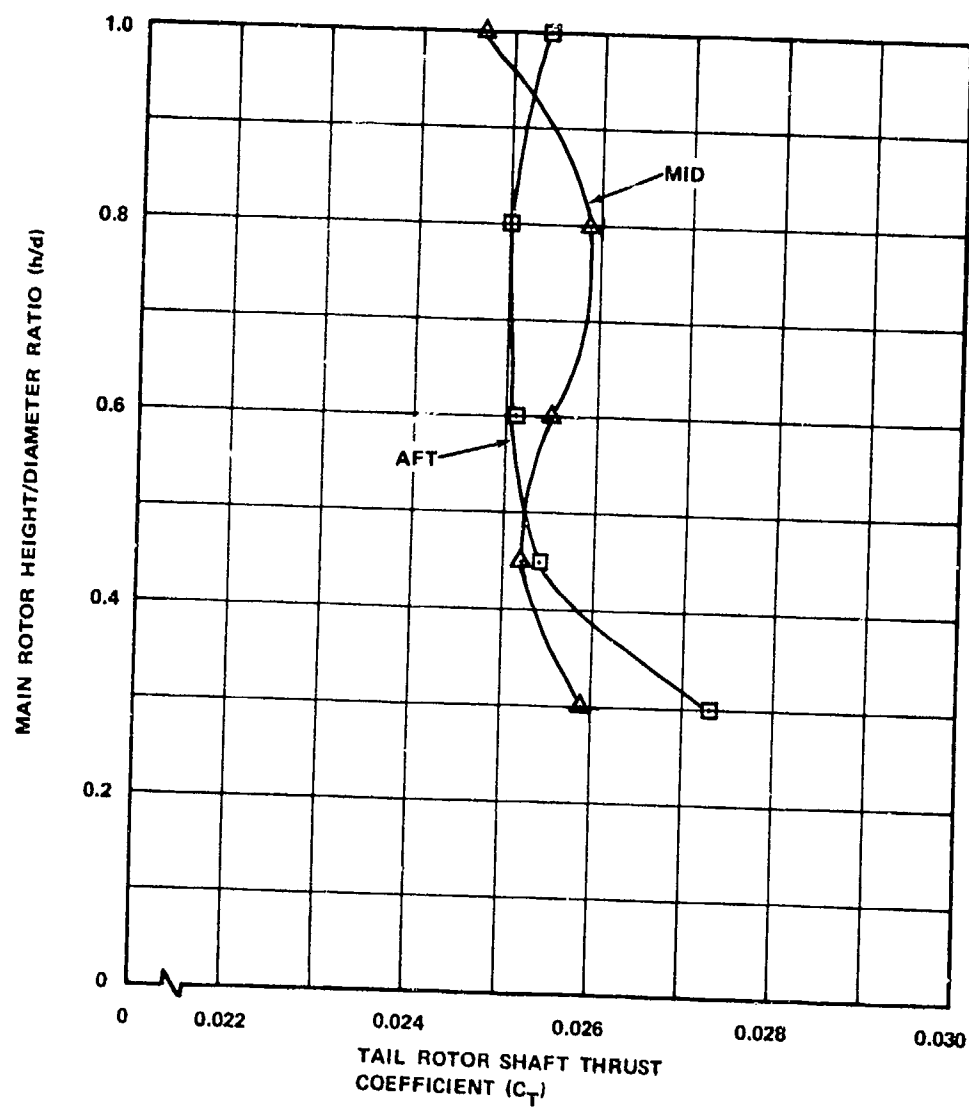
Figure 6-1. Effect of Tail Rotor Position on Variation of Tail Rotor Shaft Thrust With Main Rotor Height/ Diameter Ratio — V = 0 kn, ψ = 0°, θ = 20°, Fin = OFF, Rotation = BF.

69
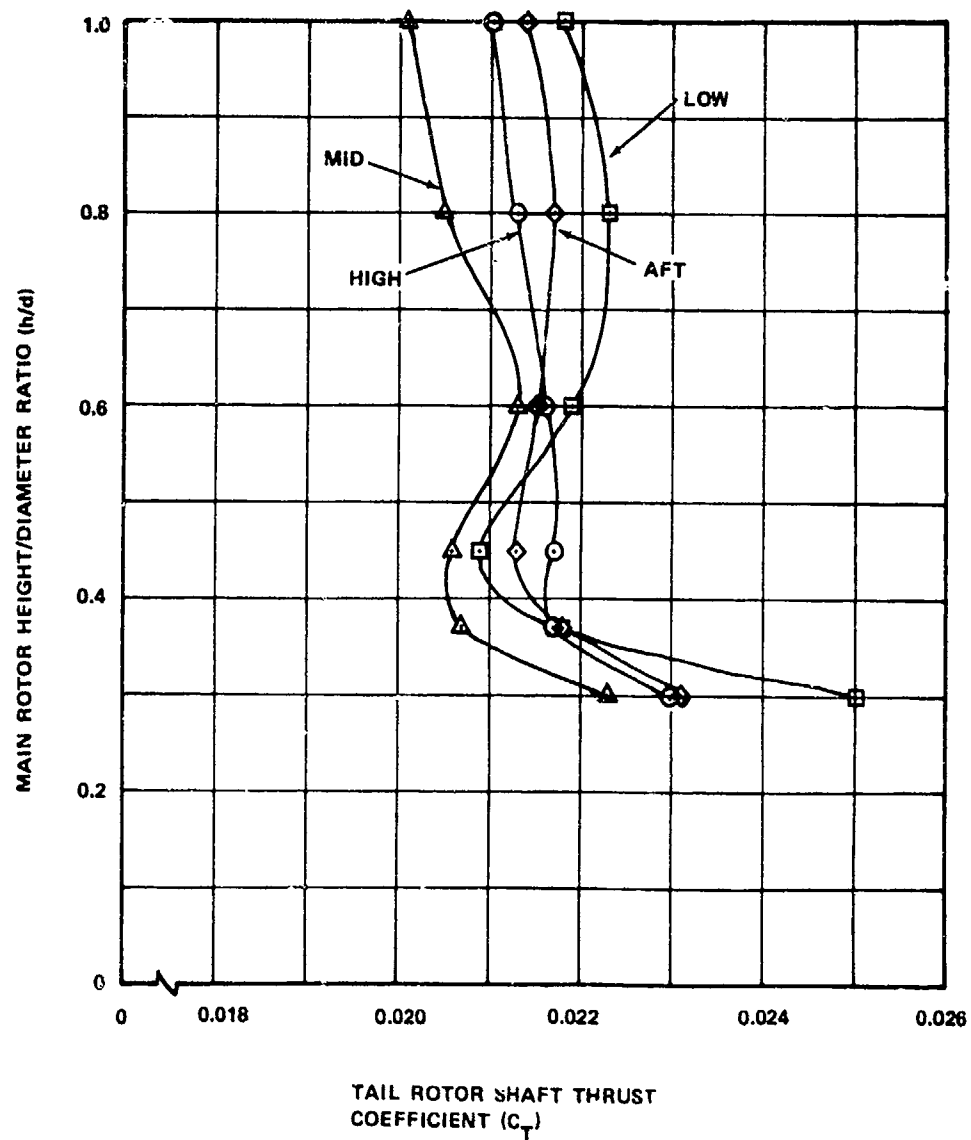
Figure 6—2. Effect of Tail Rotor Position on Variation of Tail Rotor Shaft Thrust With Main Rotor Height/ Diameter Ratio — V = 20 kn, ψ = 60°, θ = 20°, Fin = OFF, Rotation = BF.

70
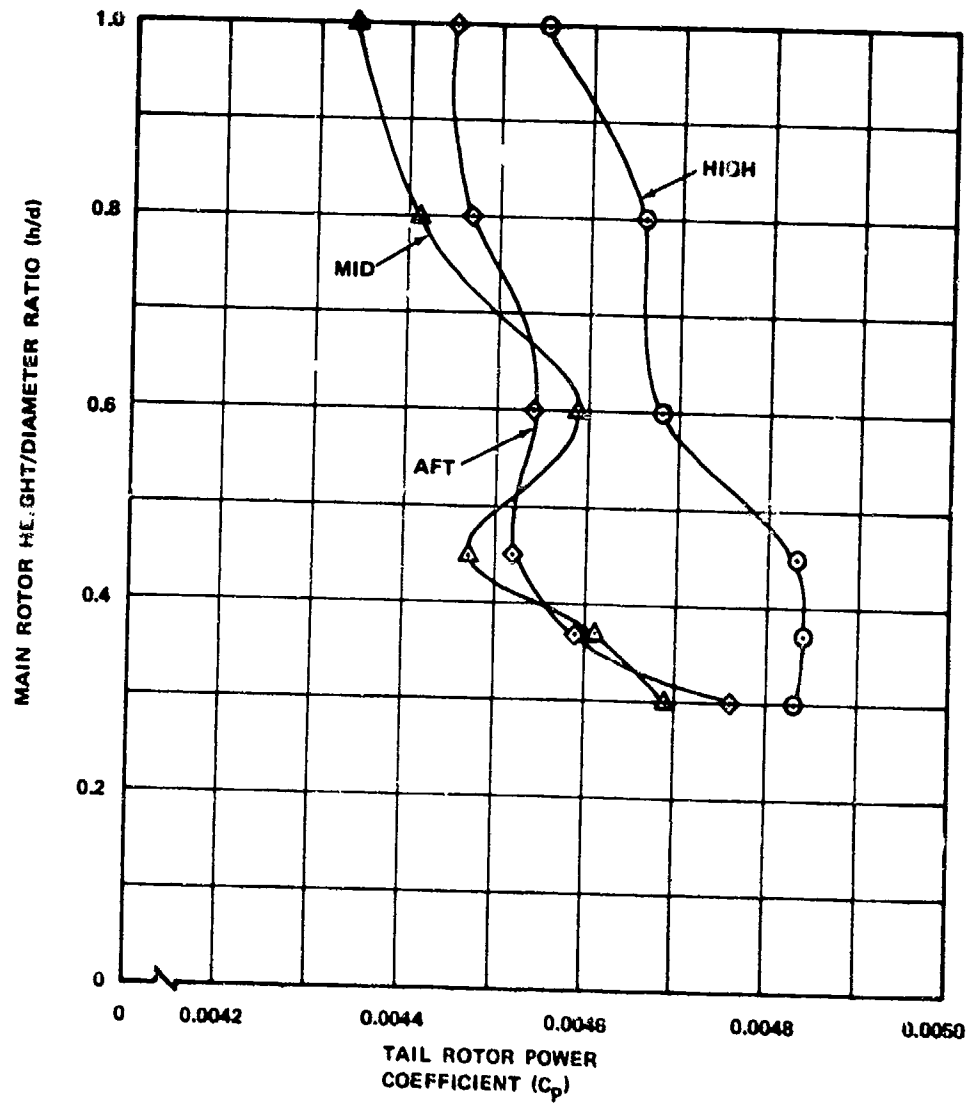
Figure 6—3. Effect of Tail Rotor Position on Variation of Tail Rotor Power With Main Rotor Height/Diameter Ratio — V = 20 kn, ψ = 60°, θ = 20°. Fin = OFF, Rotation = BF.

71
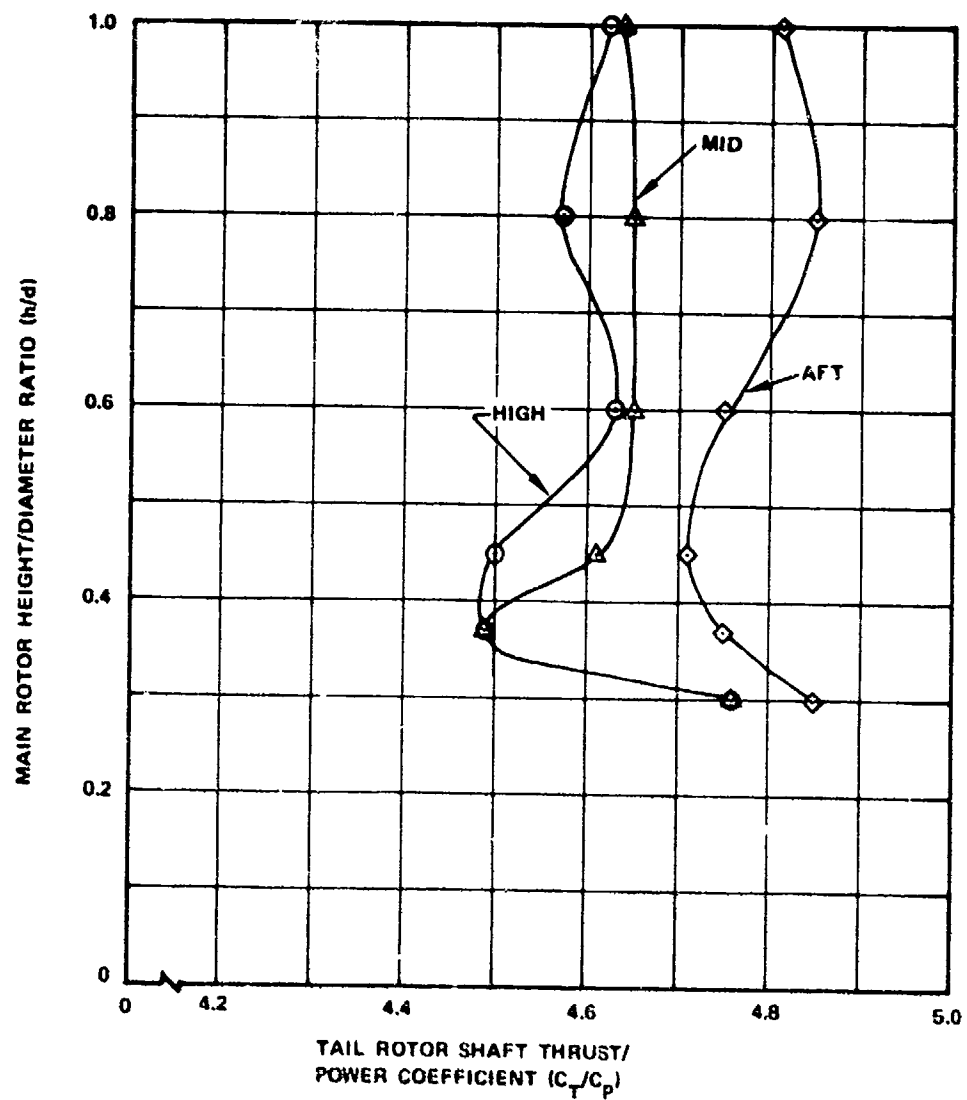
Figure 6—4. Effect of Tail Rotor Position on Variation of Tail Rotor Shaft Thrust/Power With Main Rotor Height/Diameter Ratio — V = 20 kn, ψ = 60°, θ = 20°, Fin = OFF, Rotation = BF.
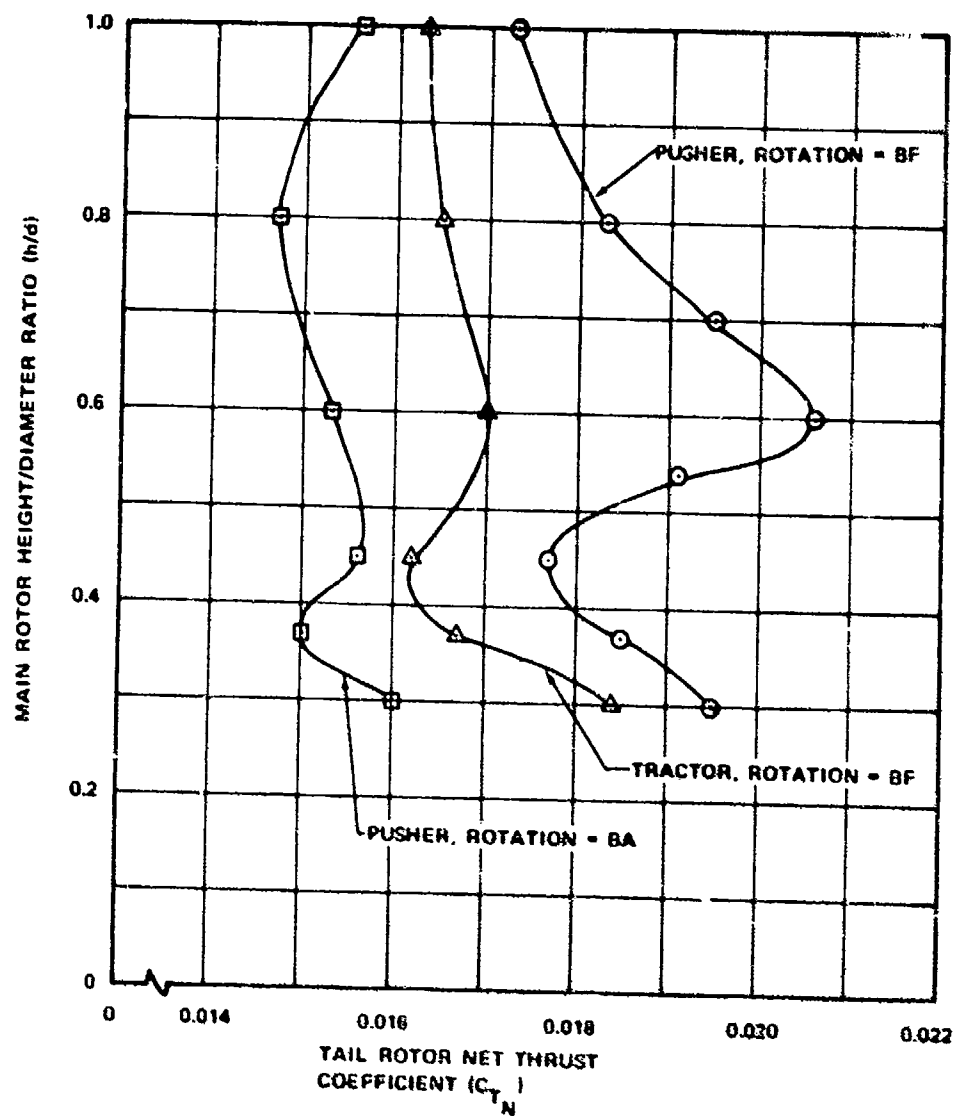
Figure 6-5. Effect of Fin Location and Direction of Rotation on Variation of Tail Rotor Net Thrust With Main Rotor Height/Diameter Ratio — V = 20 kn, ψ = 60°, θ = 20°, Position = MID, Fin = ON.

73

Figure 6—6. Effect of Fin Location and Direction of Rotation on Variation of Tail Rotor Net Thrust/Power With Main Rotor Height/Diameter Ratio — V = 20 kn, $\dot{\psi}$ = 60°, θ = 20°. Position = MRO, Fin = ON.

74
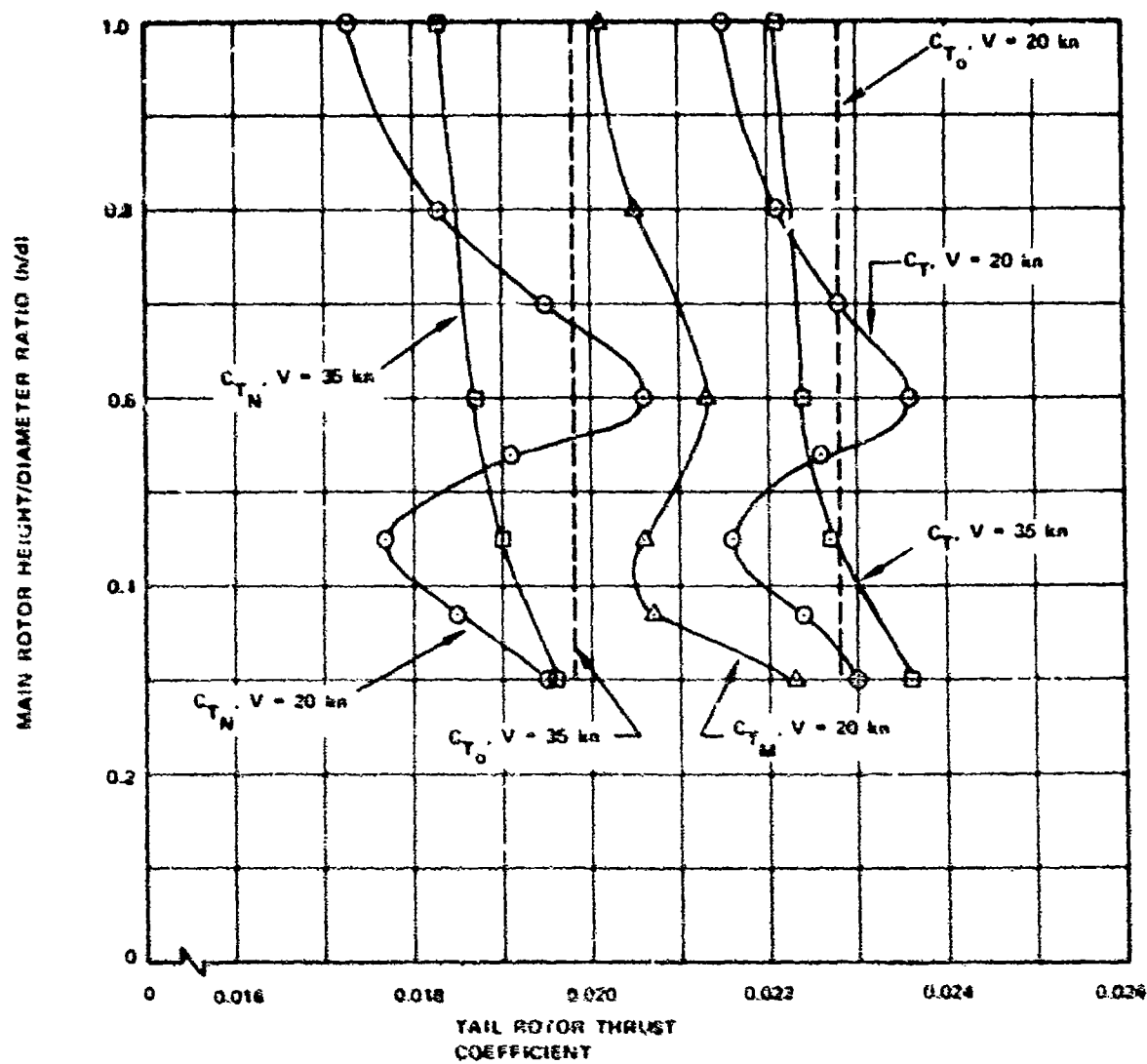
Figure 6-7. Effect of Wind Velocity on Variation of Tail Rotor Thrust With Main Rotor Height/Diameter Ratio — $\psi = 60^\circ$, $\theta = 20^\circ$, Position = MID, Rotation = BF.

75
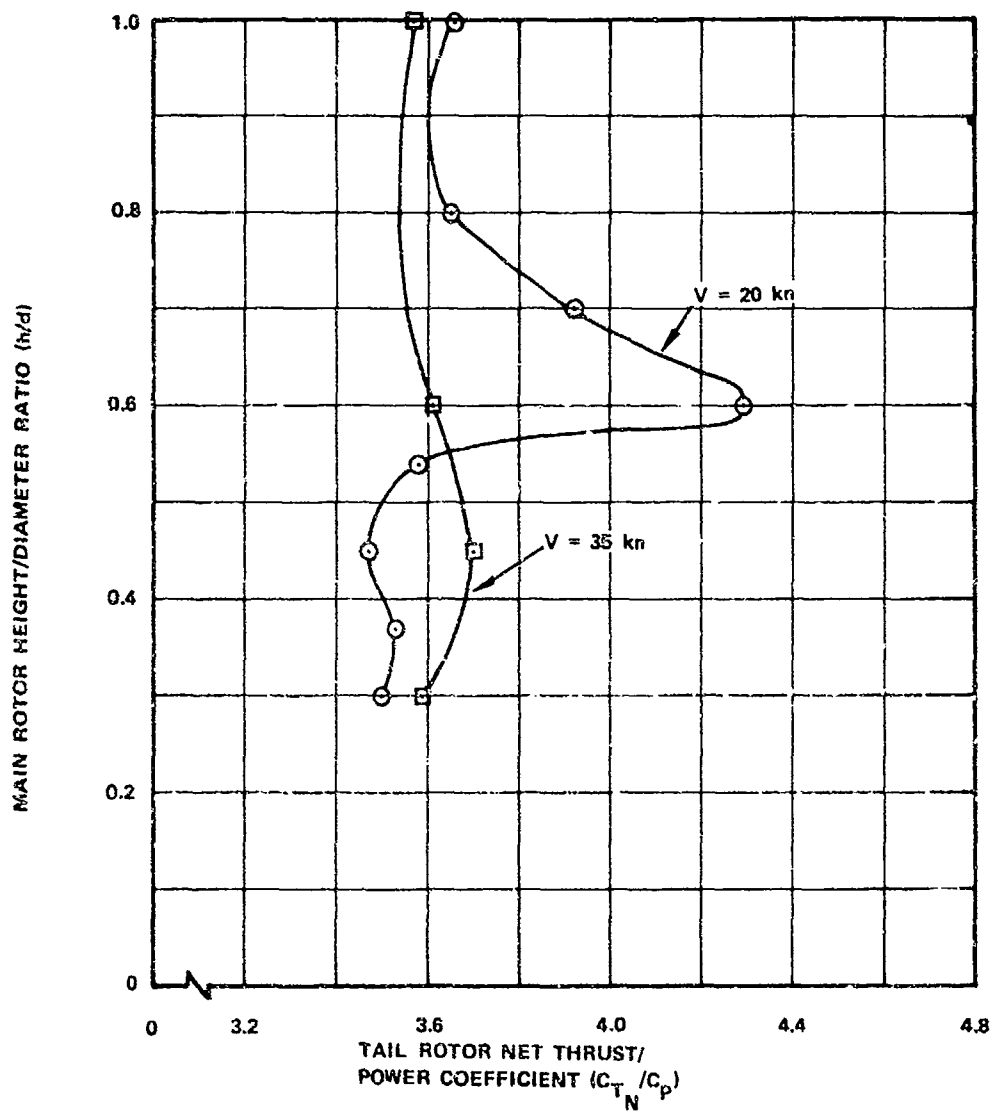
Figure 6–8. Effect of Wind Velocity on Variation of Tail Rotor Net Thrust/Power With Main Rotor Height/Diameter Ratio — $\psi = 60^\circ$, $\theta = 20^\circ$, Position = MID, Fin = ON, Rotation = BF.

TABLE 6-I. CRITICAL IGE HOVER HEIGHT, $(h/d)_{CRITICAL}$ - $\psi = 60$ AND $h/d \le 0.6$

Velocity (Kn)	0 Thrust Ranking	0 Power Ranking	20 Thrust Ranking	20 Power Ranking	35 Thrust Ranking	35 Power Ranking
High[1] (Reference Figure)			0.37 (6.2) 2	0.37 (6.4) 1		
Mid[1] (Reference Figure)	0.45 (6.1) 1	NA 1	0.45 (6.2) 3	0.37 (6.4) 3		
Low[1] (Reference Figure)	0.6 (6.1) 2	NA 2	0.45 (6.2) 4	NA NA		
Aft[1] (Reference Figure)			0.45 (6.2) 1	0.45 (6.4) 2		
Pusher Bottom Forward[2] (Reference Figure)			0.45 (6.5) 3	0.45 (6.6) 3	0.6 (6.7)	0.3 (6.8)
Tractor Bottom Forward[2] (Reference Figure)			0.45 (6.5) 2	0.45 (6.5) 1		
Pusher Bottom Aft[2] (Reference Figure)			0.37 (6.5) 1	0.6 (6.6) 2		

[1] Bottom forward rotation, fin off
[2] Mid position, fin on
NA indicates data not available
Ranking indicates relative excursion with h/d. 1 is for the least excursion; 4 is the largest excursion.

77

7.0 SELECTION OF OPTIMUM TAIL ROTOR DISC LOADING AND DIAMETER

This guideline presents a method to determine the optimum tail rotor disc loading, defined as that which requires minimum power and permits smooth, approximately linear pedal changes of minimum magnitude with changes of sideward flight velocity.

7.1 DISCUSSION

Tail rotor shaft thrust coefficient/solidity versus collective for left and right sideward flight is shown in Figures 7-1 and 7-2 for bottom forward rotation, and in Figures 7-3 and 7-4 for bottom aft rotation. This data has been cross-plotted to obtain collective pitch required versus sideward flight velocity for various disc loadings (Figures 7-5 and 7-6). (Transfer of C_T/σ to disc loading is given in Appendix III.) For bottom aft rotation in left sideward flight, the collective pitch increases as the rotor enters the vortex ring state. When the velocity for transition to the windmill brake state is reached, the collective pitch decreases due to elimination of flow recirculation.

For bottom forward rotation in left sideward flight, the development of the vortex ring state is retarded as discussed in the Flow Environment section. Thus the collective pitch required is approximately constant until the windmill brake state is reached, at which point the collective required decreases rapidly.

Figure 7-7 shows a plot of tail rotor disc loading versus the design left sidewind or flight velocity that can be reached for the two directions of rotation. The design velocity for linear pedal movement is selected as that velocity where the particular constant disc loading curve from Figures 7-5 and 7-6 breaks downward (i.e., where a right pedal excursion would start) from a reasonably straight line.

Also included in Figure 7-7 are curves of disc loading versus velocity for which 10 percent of right pedal remains (assuming that 10-percent right pedal remains at $\theta = 0$). Either set of curves can be used for initial selection of tail rotor disc loading, depending on whether smooth linear pedal movement is desired or merely sufficient pedal is desired to reach the design velocity.

Since the curves of Figures 7-5 and 7-6 are for collective pitch required to produce a constant tail rotor disc loading, they do not exactly correspond to actual pedal positions in flight. The disc loading required to balance main rotor

79

Preceding page blank

torque will vary with wind velocity. Disc loading required at hover can be determined from the disc loading selected from Figure 7-7 by multiplying by the ratio of main rotor power required at hover to power required at the design left sideward flight speed. Main rotor power ratios are available in Guideline 11.

Figure 7-8 shows a plot of the ratio of main rotor/tail rotor diameter ratio versus main rotor disc loading. The straight-line curve is a trend curve based on actual values of successful helicopters. The hyperbolic curves are based on what the trend would be if the tail rotor disc loading were held constant as developed by the theory in Appendix III. The conclusion is that larger helicopters with higher main rotor disc loadings optimize with a tail rotor loading that permits good left sideward flight qualities up to 35 knots. For smaller helicopters or those where minimum power to the tail rotor was the major consideration, left sideward flight to 35 knots is not possible without very large right pedal excursions. Figure 7-7 shows the speed at which the AG-1G required a very great increase in right pedal in left sideward flight (Reference 3). Such data substantiates the Boeing test data.

The tail rotor disc loading should be based on the tail rotor shaft thrust required to trim the helicopter plus the additional forces to balance fuselage aerodynamic moments and drag. Fin forces must be considered to determine the shaft thrust requirements (see Guideline 8).

7.2 GUIDELINE

Tail rotor diameter selection (disc loading) for a given helicopter is a compromise between minimum weight and power and the design sideward flight speed. For larger helicopters with main rotor disc loadings above 8 psf with tail rotor hubs positioned near the plane of the main rotor, select the disc loading from Figure 7-7 for the design left sideward flight speed and direction of rotation desired. For smooth linear pedal movement with sideward flight velocity, use the linear pedal curves. To obtain only 10-percent pedal remaining to reach the design velocity, use the 10-percent pedal remaining curves for selection of disc loading. The 10-percent pedal curves allow a lower tail rotor disc loading selection with the possibility of a better aircraft payload/gross weight ratio.

For smaller helicopters with main rotor disc loadings less than 6 psf, trade-offs of design left sideward speed with payload/gross weight ratio should be made to determine the best tail rotor disc loading.

In consideration of linear pedal thrust only, disc loading should be approximately 14 psf at design trim conditions for

a 35-knot design left sideward flight. For a 20-knot design left sideward flight, disc loading can approach 12 psf.

The diameter should be selected on the basis of tail rotor shaft thrust required at the design right sideward flight velocity and the selected disc loading.

Appendix III presents a more detailed discussion of tail rotor disc loading selection.
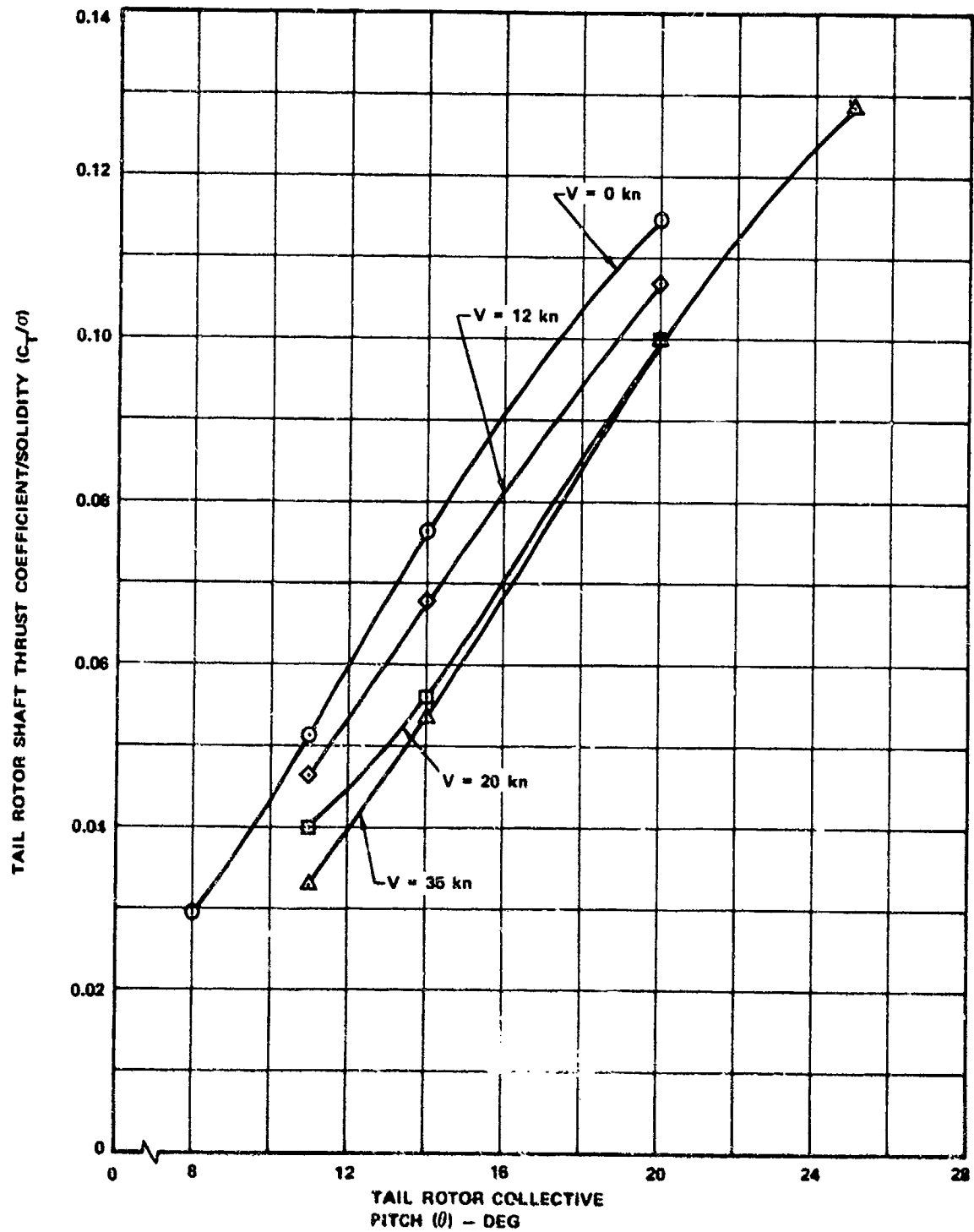
Figure 7—1. Effect of Wind Velocity on Variation of Tail Rotor Shaft Thrust/Solidity With Tail Rotor Collective Pitch — h/d = 0.3, ψ = 90°, Position = MID, Fin = ON, Rotation = BF.
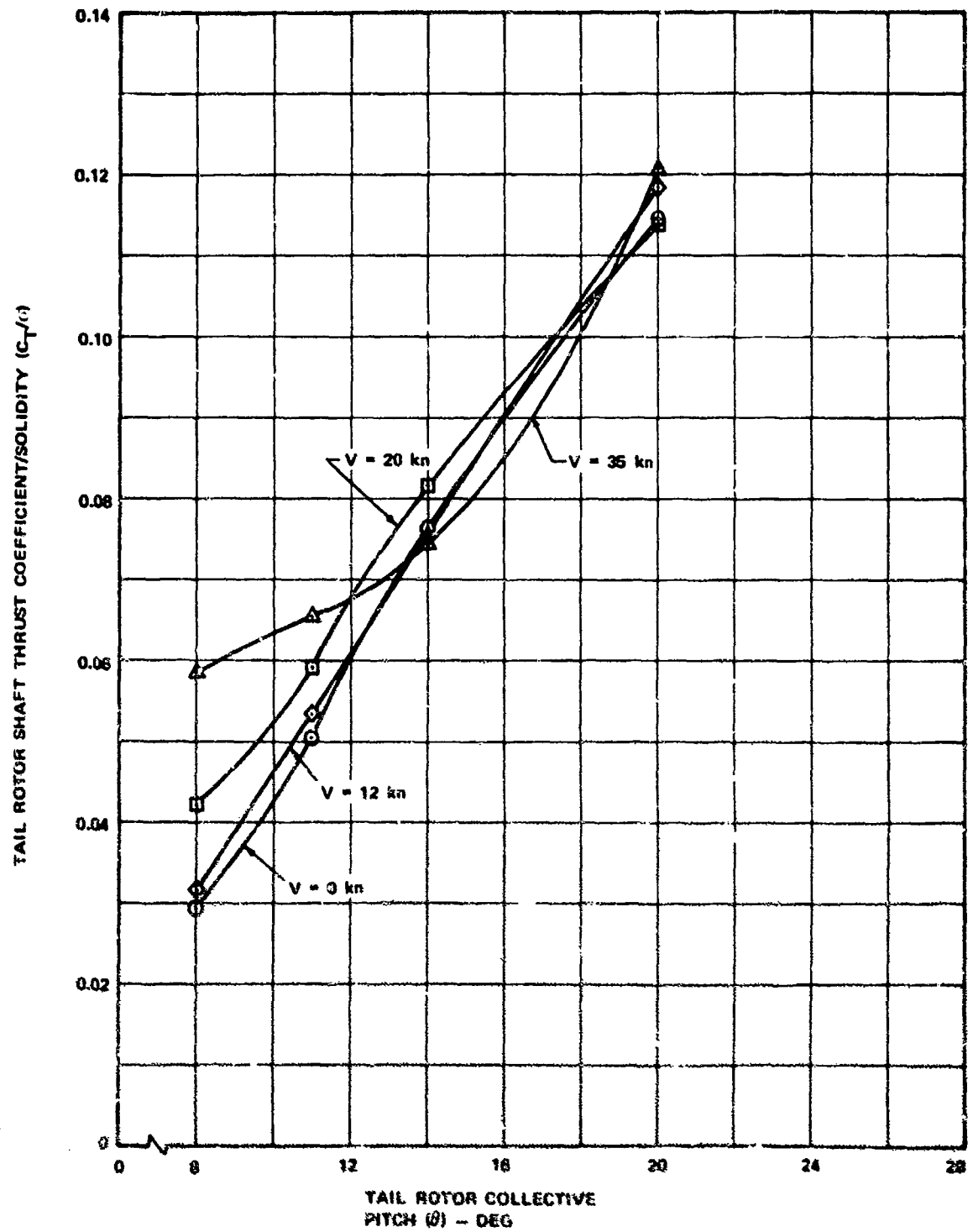
Figure 7–2. Effect of Wind Velocity on Variation of Tail Rotor Shaft Thrust/Solidity With Tail Rotor Collective Pitch – h/d = 0.3, ψ = 270°, Position = MID, Fin = ON, Rotation = BF.
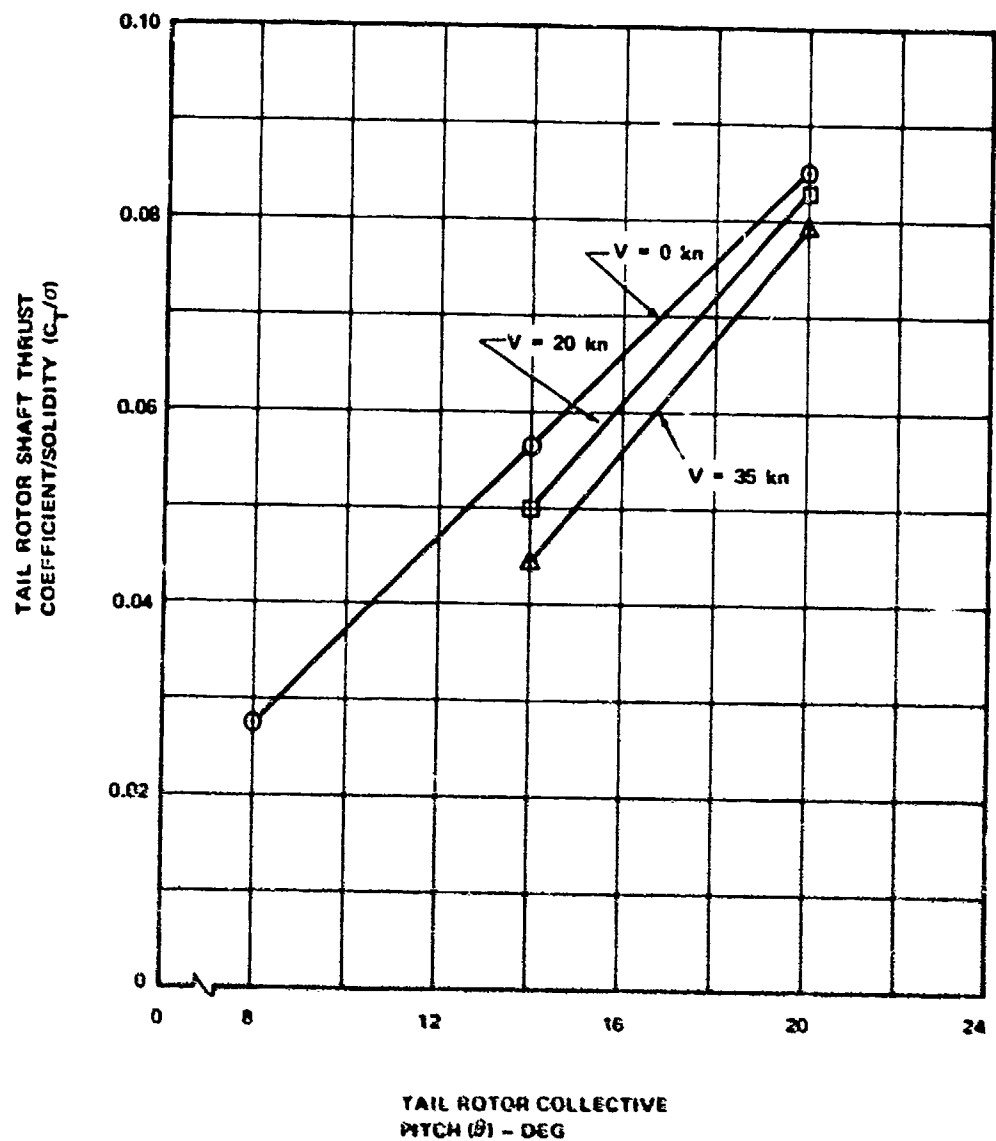
Figure 7-3. Effect of Wind Velocity on Variation of Tail Rotor Shaft Thrust/Solidity With Tail Rotor Collective Pitch — N/d = 0.3, $\dot{\psi}$ = 90°. Position = MID, Fin = ON, Rotation = BA.
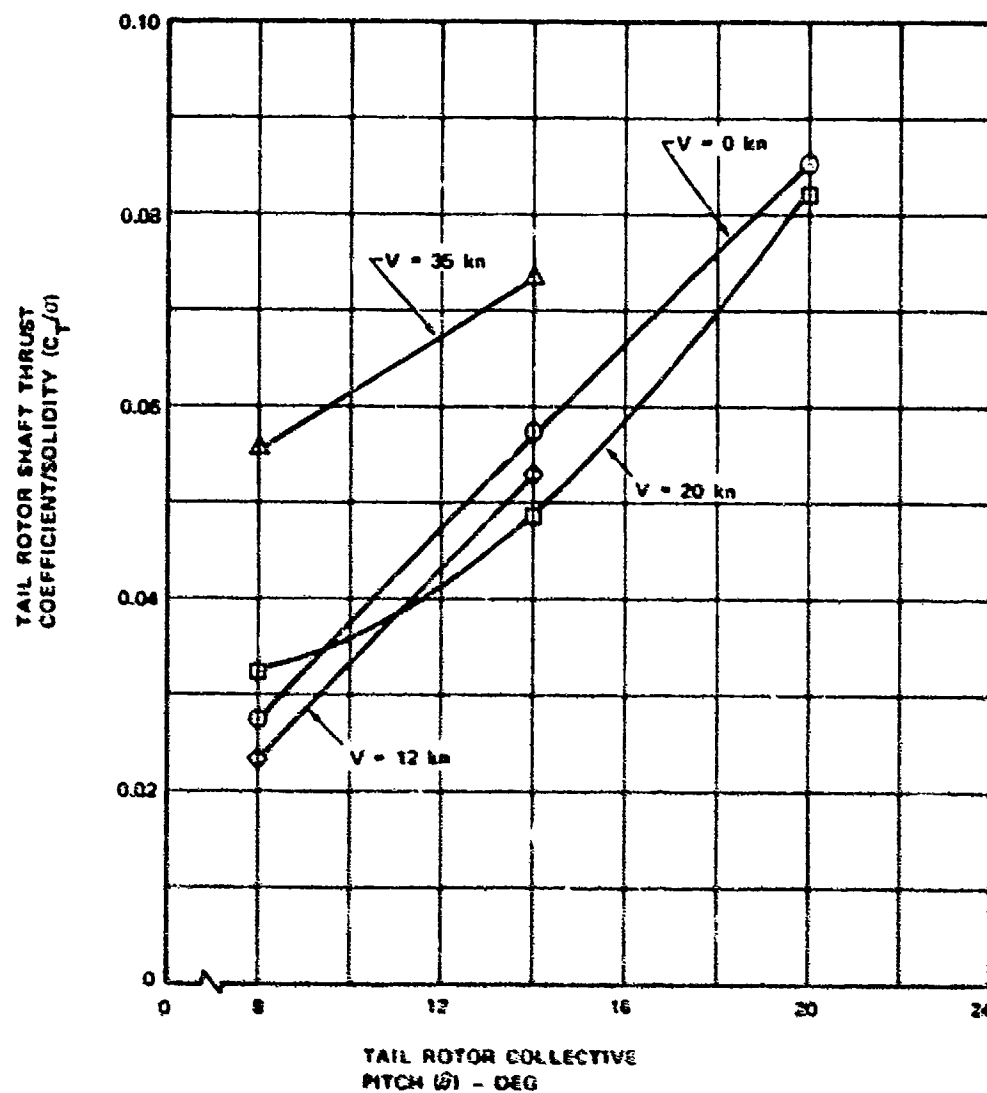
Figure 7-4. Effect of Wind Velocity on Variation of Tail Rotor Shaft Thrust/Solidity With Tail Rotor Collective Pitch – M/d = 0.3, ψ = 270°, Position = MID, Fin = ON, Rotation = BL.
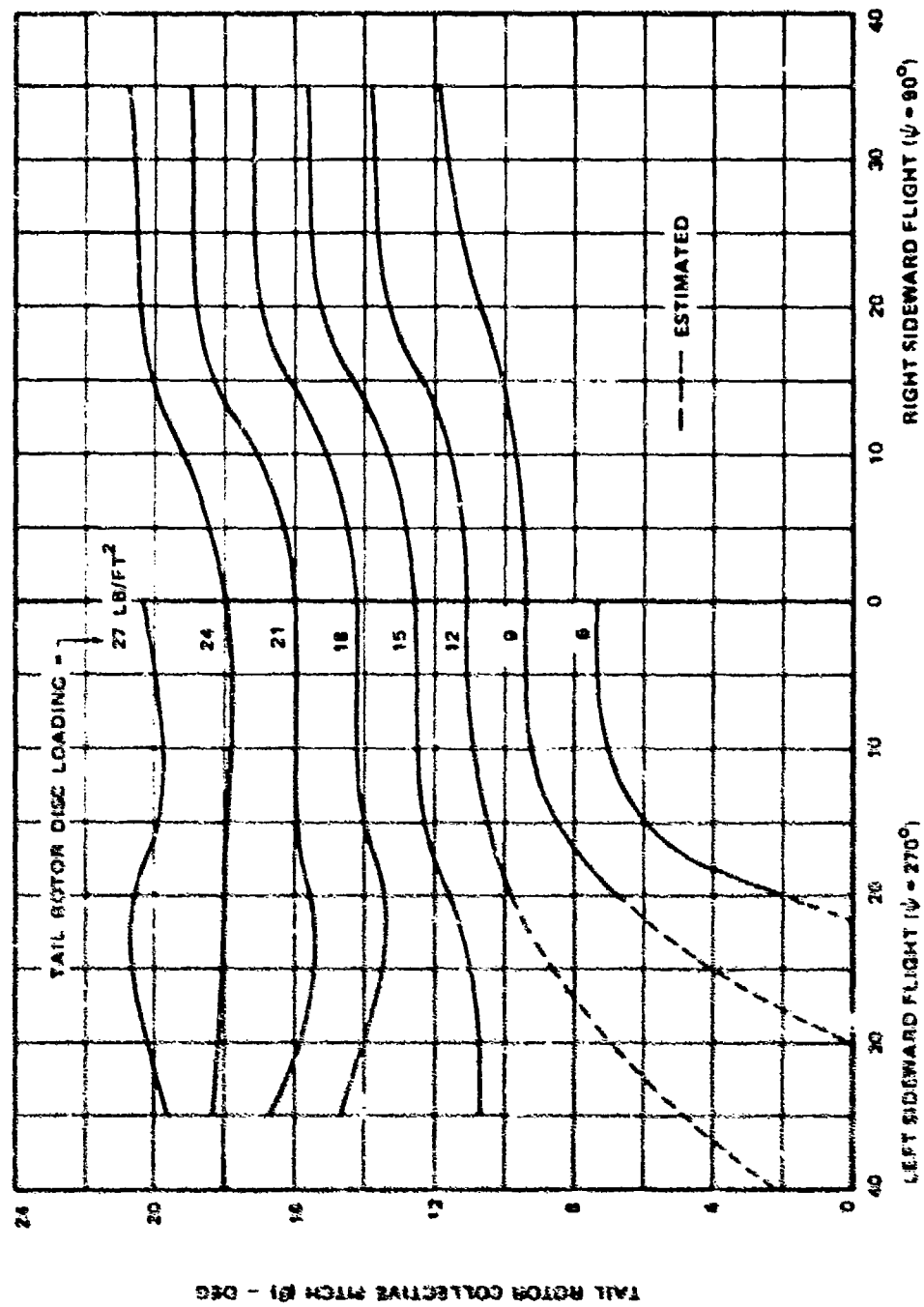
Figure 7–6. Effect of Tail Rotor Disc Loading on Tail Rotor Collective Pitch Required in Sideward Flight — h/s = 0.2, Position = MID, Rotation = BF, Fin = ON.
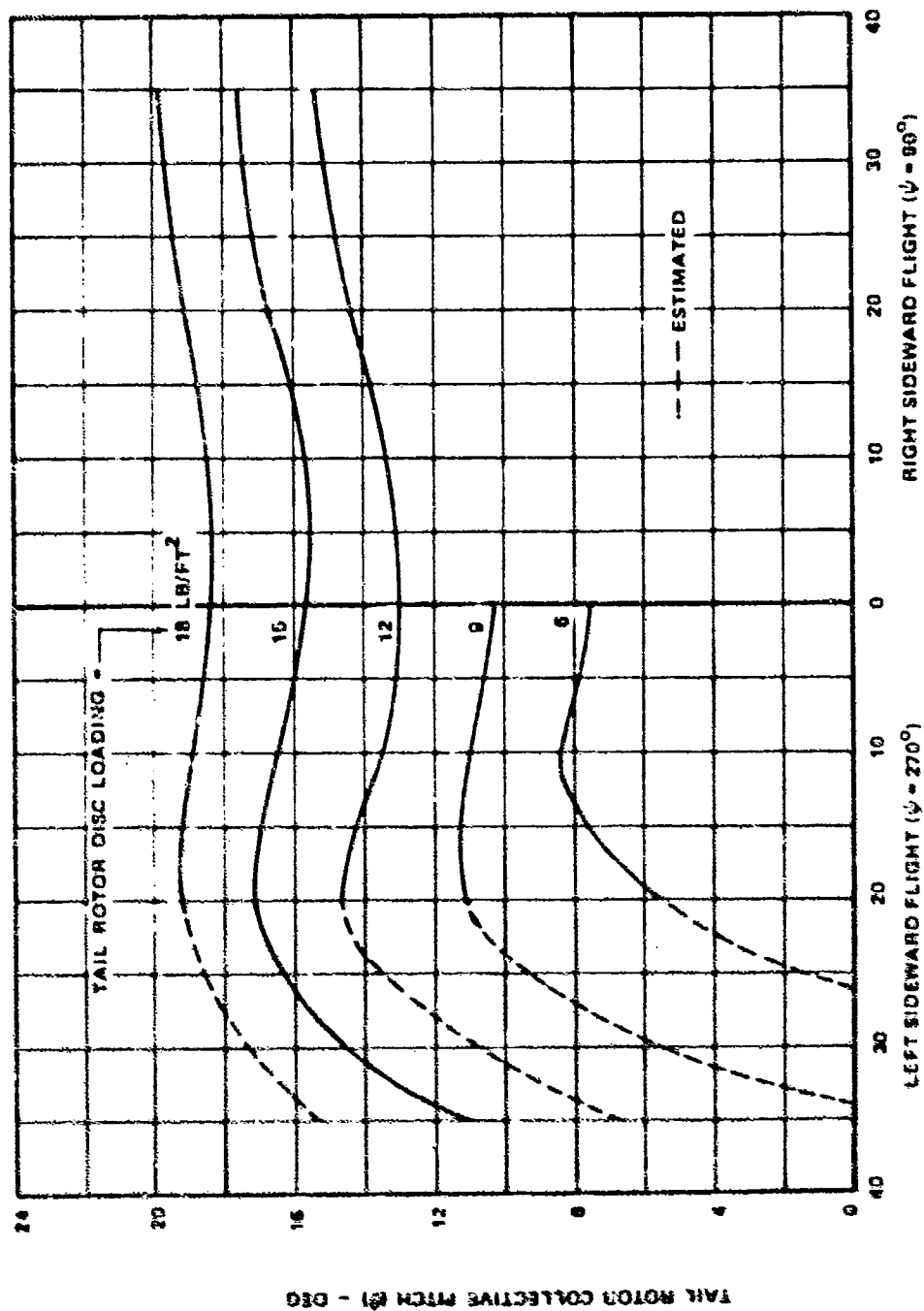
Figure 7—6. Effect of Tail Rotor Disc Loading on Tail Rotor Collective Pitch
Required in Sideward Flight — h/d = 0.3, Position = MID,
Rotation = BA, Fin = ON.

87
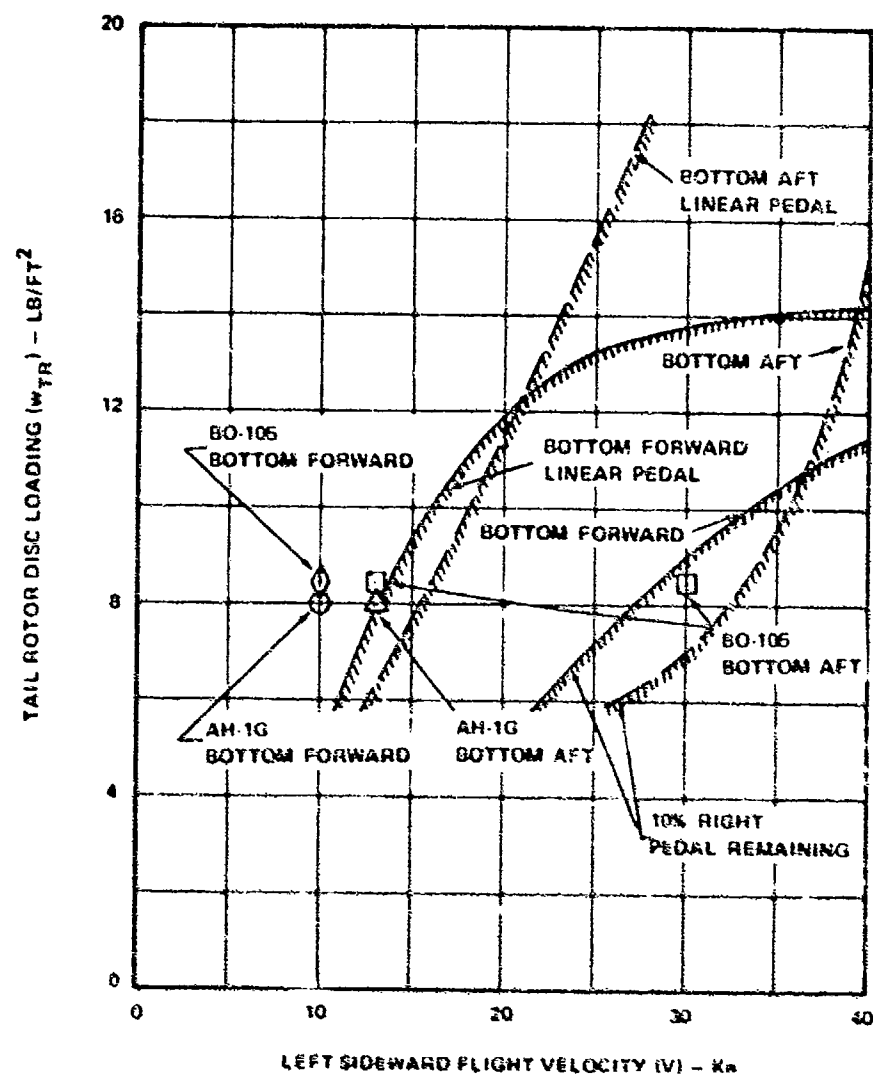
Figure 7-7. Selection of Tail Rotor Disc Loading.
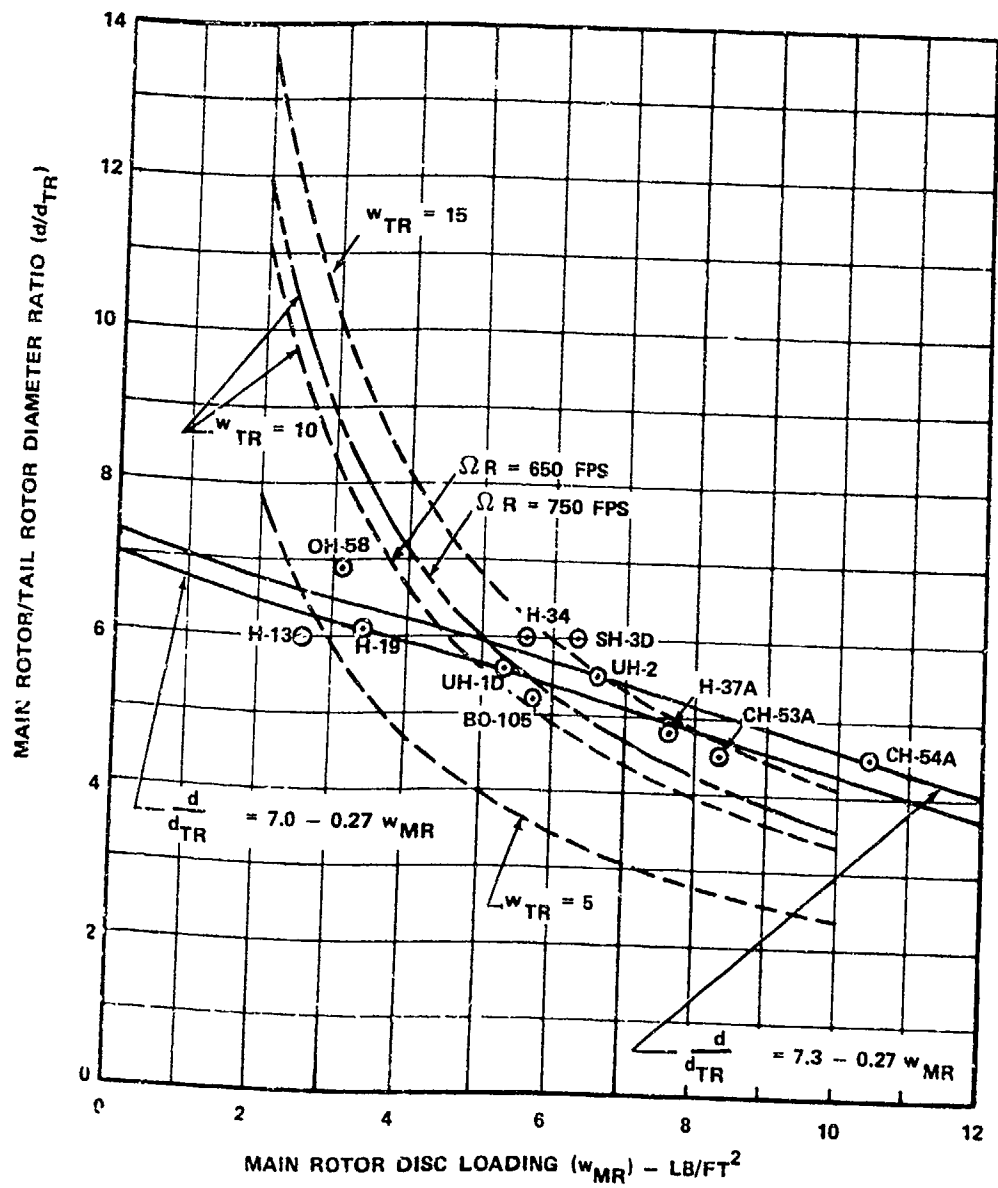
Figure 7–8. Disc Loading Comparison.

8.0 DETERMINATION OF SHAFT THRUST TO NET THRUST RATIO (FIN LOSS)

This guideline presents charts from which the ratio of shaft thrust to net thrust can be conveniently determined. This ratio, which is greatly dependent on fin size and position, is required in order to predict the shaft thrust. This, in turn, influences the design of tail rotor solidity and maximum blade incidence as well as the net thrust required to balance main rotor torque and to provide the desired yaw maneuver rate.

8.1 DISCUSSION

In Guideline 4, it was determined that $\psi = 60^\circ$ to 90° was the azimuth range at which the thrust level is lowest (i.e., the azimuth range where the tail rotor characteristics are determined). Therefore, a prediction method for the fin force at $\psi = 90^\circ$ was developed together with corrections for fin forces at $\psi = 60^\circ$. These predictions are presented in Appendix III.

A char　　for the determination of shaft thrust at $\psi = 90^\circ$ for various values of s/r, tail rotor advance ratio μ_{TR}, blockage ratio $\bar{A}$, and C_{T_N} is presented in Figure 8-1. To use Figure 8-1, enter the left at the appropriate s/r and ascend vertically to $\bar{A}$. Then go right horizontally to the $\bar{A}\mu_{TR} = 0$ line. From there, construct a C_{T_N} line parallel to the corresponding C_{T_N} line given. Follow the parallel line to the desired $\bar{A}\mu_{TR}$. Then go left horizontally to C_T/C_{T_N}.

Test results indicate that at the critical velocity of 20 knots (see Section 9), the fin force is greater at the critical azimuth $\psi = 60^\circ$ than at $\psi = 90^\circ$. The magnitude of the fin force at $\psi = 60^\circ$ is approximately constant from $V = 20$ knots to $V = 35$ knots and equal in magnitude to the fin force at $\psi = 90^\circ$, $V = 35$ knots (see, for example, Figure 5-3). Thus Figure 8-1 can also be used for determining the shaft thrust required at $\psi = 60^\circ$ between 20 and 35 knots by determining from the figure the C_T/C_{T_N} ratio at an $\bar{A}\mu_{TR}$ corresponding to 35 knots.

Comparisons of predictions to test data are given in Appendix III.

8.2 GUIDELINE

Given net tail rotor thrust required at the critical azimuth $\psi = 60^\circ$, fin-tail rotor separation distance s/r, blockage ratio $\bar{A}$, and tail rotor advance ratio μ_{TR} corresponding to velocities between 20 and 35 knots, the shaft thrust required is obtained from Figure 8-1.

91
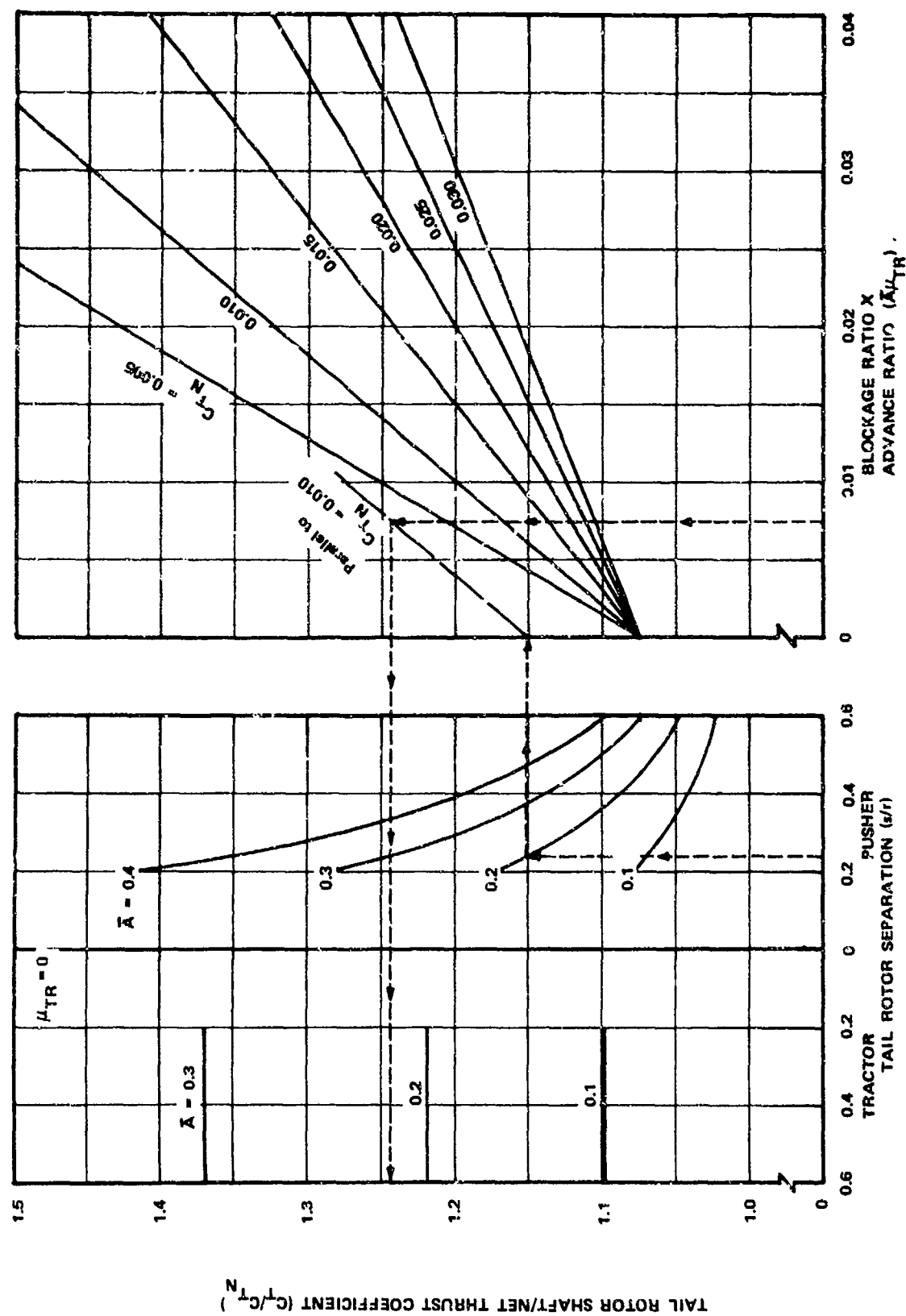
Figure 8–1. Determination of Shaft Thrust Coefficient.

9.0 AIRFOIL SELECTION

This guideline describes sectional characteristics desirable
on airfoils to be applied to tail rotors. In general, sec-
tional requirements are closely related to the overall perfor-
mance requirements of a tail rotor. Table 9-I summarizes such
requirements over the basic flight regimes of:

● Hover

● Low-speed flight and maneuver

● High-speed flight

Because of the complex nature of the flow environment in which
a tail rotor operates, optimizing the sectional requirements
separately for each of the three flight regimes listed would
lead to two or even three different and incompatible sets of
airfoil sections.

Therefore, the selection of the best section or sections for a
tail rotor will require a careful compromise of mutually ex-
clusive aerodynamic characteristics, and the final choice
should be made only after careful examination of both flight
requirements and structural constraints as discussed in the
following paragraphs.

9.1 DISCUSSION

The sectional characteristics of primary interest for tail
rotor applications are:

1. Maximum-lift coefficient

2. Pitching-moment coefficient (and center of pressure)

3. Type of stall

4. Profile drag

5. Compressibility effects on drag and pitching moment at
   Mach numbers above the critical Mach number.

Maximum Lift Coefficient

The NACA 0012 airfoil is the section most commonly used on hel-
icopter tail rotors. The Vertol section designated as V0012 is
an airfoil identical to the NACA 0012 except for the fairing of
a tab into the trailing edge. The characteristics of the V0012
will be used as the basis for comparison with other tail rotor
sections.

The maximum-lift capability of a section to be employed on a tail rotor is the single most important characteristic to be taken into account. This does not mean that airfoil selection should be based only on maximum-lift boundaries, but rather that an unsatisfactory maximum-lift envelope will disqualify a candidate section no matter how attractive the other sectional characteristics.

The first difficulty in comparing the lift capability of various sections is the lack of data at the necessary Mach number and Reynolds number ranges, as well as the usual problem of compatibility of data sources.

The maximum-lift and pitching-moment data shown in Figure 9-1 has been obtained from the same two-dimensional test section with comparable models and test techniques. Furthermore, the data has been corrected to the Reynolds number corresponding to a 1-foot chord.

From the point of view of maximum lift, the NACA 0012 (or V0012) section can be surpassed by any of a number of cambered airfoils. However, of all the sections examined, the VR-7 offers the most significant improvement, with an extension in maximum lift at $M = 0.5$ between 35 percent and 50 percent, depending on pitching-moment restrictions. By comparison, the V23010-1.58 (a modification of the NACA 23010) and the NACA 64A312 (a = 0.8 mod) (a typical propeller section) would improve the maximum lift at $M = 0.5$ by 12.5 percent. The NACA 64A312 would offer a much larger improvement at $M = 0.6$ (39 percent), but at the cost of unacceptable overall pitching moments (bottom of Figure 9-1).

The maximum-lift boundary of the VR-1 section is shown as representative of the few transonic sections with characteristics compatible with rotor requirements. The VR-1 airfoil does not significantly improve the thrust capability of the NACA 0012 section; but, as shown later, it does offer substantial advantages in drag.

The VR-8 airfoil section is related to the VR-7, with thickness and camber reduced to improve the high-Mach-number performance required at the tip of high-speed rotor blades. A VR-8 tip would be recommended for rotors with rotational tip velocities in excess of $M = 0.8$.

Some typical sectional lift requirements along a tail rotor are shown in Figure 9-2, together with the maximum-lift boundaries of the V0012, V23010-1.58, and VR-7 sections.

Pitching Moment Coefficient and Center of Pressure

The lower half of Figure 9-1 compares the variation of the

94

zero-lift pitching-moment coefficient with Mach number for selected airfoil sections.

The NACA 0012 airfoil has zero pitching-moment coefficient. Although this is desirable because of low control loads, a neutral pitching moment is not generally required as long as the sectional pitching moments are low. Vertol rotor sections have been designed with a pitching-moment level of less than $C_{m_0} = \pm0.04$ which can be shifted or reduced by means of trailing-edge tab reflex. A typical trailing-edge tab extending over 5 percent of the airfoil chord will correct the pitching moment by

$$\frac{d\ C_m}{d\delta_{TAB}} = -0.006/\text{degree of tab deflection}$$

at the cost of a moderate loss in lift, as shown in Figure 9-1 for the VR-7 with the trailing-edge tab deflected 0^0 and -6^0.

The effect of trailing-edge tab deflection on the location of the center of pressure is illustrated in Figure 9-3. The lower half of Figure 9-3 compares the center of pressure required to reduce the control loads of two main rotor configurations.

Type of Stall

The best sections for use at lift levels through stall (e.g., maneuver) are sections which display a small amount of stall hysteresis. The highest amount of hysteresis is associated with leading-edge stall, and airfoils with pure leading-edge stall should be avoided to reduce the occurrence of stall flutter. This restriction is not as significant on rigid rotors as it is on some of the new structurally soft rotor systems.

Blunt-nosed airfoils and thick sections generally display trailing-edge stall characteristics. D. E. Gault (Reference 6) compiled a vast amount of airfoil stall information and condensed it into a chart, taking into account a leading-edge geometry parameter (the y/c coordinate for the upper surface at x/c = 0.0125) and the Reynolds number. Although this chart is valid only for relatively low Mach numbers (M < 0.4), the correlation with test data is generally good. It should be noted that the only airfoil family which systematically does not follow the Gault correlation is the NACA 230XX series. Gault's chart is presented in Figure 9-4 with some comments on the characteristics desirable for tail rotor applications.

Profile Drag

Although drag does not play a major role in tail rotor

performance, some sections, like the VR-7, have the necessary maximum-lift characteristics along with low drag. Figure 9-5 compares the drag of various sections at the C_ℓ = 0.6 level and at zero lift. The zero-lift comparison shows the necessity of decambering and reducing the thickness of tip sections.

Compressibility Effects on Drag and Pitching Moment

The growth of control loads, which is one of the conditions which limit the range of usefulness of a rotor, is a function of either or both of the following:

1. Lift and pitching-moment stall boundaries for the subcritical Mach number range.

2. Drag divergence and pitching-moment break (sectional Mach tuck).

Drag divergence, characterized by a rapid growth of drag with increasing Mach number for a given incidence, is associated with the occurrence of supercritical flow conditions ($M_{LOCAL} \geq$ 1.0) at the crestline. Pitching-moment break is a function of the shift of the center of pressure toward the trailing edge with increasing freestream Mach number; it is also associated with supercritical flow (and shock location) behind the crest-line. Although the two boundaries are not identical, they are close enough for the types of airfoils of interest for tail rotor applications and for the purpose of this guideline.

Therefore, as a first approximation, a section satisfying drag-divergence requirements can be assumed to satisfy pitching-moment break requirements as well. The drag-divergence boundaries of several sections are compared in Figure 9-6. Figure 9-7 compares the maximum lift of various airfoil sections at M = 0.5 against the Mach number at which the zero-lift drag grows to a fixed level (C_d = 0.018) after drag divergence. The figure again points out the necessity of tapering the tip of a rotor when high thrust and high tip Mach numbers are required.

9.2 GUIDELINE

The airfoil to be selected for a tail rotor should have high lift, near-zero pitching moment, low drag, and trailing-edge stall characteristics similar to those of the VR-7. The coordinates of the VR-7 airfoil section are listed in Table 9-II on page 98.

96

TABLE 9-I. TAIL ROTOR FLOW ENVIRONMENT SUMMARY

Flight Condition	Mach No. Range	Dominant Sectional Requirements		
		Thrust	Power	Control Loads
Hover	$M_{TIP}=0.6\lozenge0.75$	• 100% of restoring torque • $C_{\ell MAX}$ at $0.4<M<0.6$ • No dynamic stall delay	• Low drag desirable, but not critical	• Low C_M • Gradual stall (minimized stall hysteresis)
Maneuver or Low Speed	$M_{TIP}=0.7\lozenge0.8$	• 80% to 100% of restoring torque • $C_{\ell MAX}$ at $0.4<M<0.7$ • Some dynamic stall delay at $M<0.6$	• Low drag • High M_{DD}	• Low C_M • Gradual stall (minimized stall hysteresis) • High M_{DD}
High Speed	$M_{TIP}=0.75\lozenge1.0$	• Low lift required in presence of other tail surfaces	• Overall low drag • High M_{DD}	• Low C_M • High M_{DD} • Delayed Mach tuck • Tip shapes for tip relief recommended in some cases

TABLE 9-II. COORDINATES OF THE VR-7 AIRFOIL
(IN THE NACA REFERENCE SYSTEM)

Leading-edge circle: $r/c = 0.0113$
Center at: $x/c = 0.01055$
     $y/c = 0.004$

Trailing-edge tab, from $x/c = 0.96$
to $x/c = 1.01$

x/c	(y/c) upp	(y/c) low	x/c	(y/c) upp	(y/c) low
0.	0.	0.			
0.005	0.0165	−0.00575	0.37	0.0905	−0.0290
0.01	0.0218	−0.0081	0.41	0.0885	−0.0285
0.02	0.0299	−0.0109	0.45	0.0856	−0.02735
0.03	0.03625	−0.0129	0.49	0.08165	−0.0258
0.04	0.04155	−0.01445	0.53	0.0767	−0.0240
0.05	0.04610	−0.0160	0.57	0.0710	−0.0220
0.06	0.05025	−0.01735	0.61	0.0646	−0.0199
0.07	0.0541	−0.0185	0.65	0.0580	−0.0179
0.085	0.05935	−0.020	0.69	0.0514	−0.0158
0.102	0.0645	−0.02145	0.73	0.0447	−0.0138
0.12	0.0691	−0.02285	0.77	0.0381	−0.0117
0.14	0.0737	−0.0241	0.81	0.0315	−0.0097
0.16	0.0775	−0.0251	0.845	0.0257	−0.00791
0.18	0.0808	−0.0260	0.88	0.0199	−0.00613
0.20	0.0838	−0.0266	0.91	0.0149	−0.00459
0.225	0.0867	−0.0273	0.935	0.01078	−0.00332
0.255	0.0892	−0.0280	0.955	0.00745	−0.00230
0.29	0.0909	−0.0285	0.98	0.00331	−0.00102
0.33	0.0914	−0.0289	1.00	0.	0.
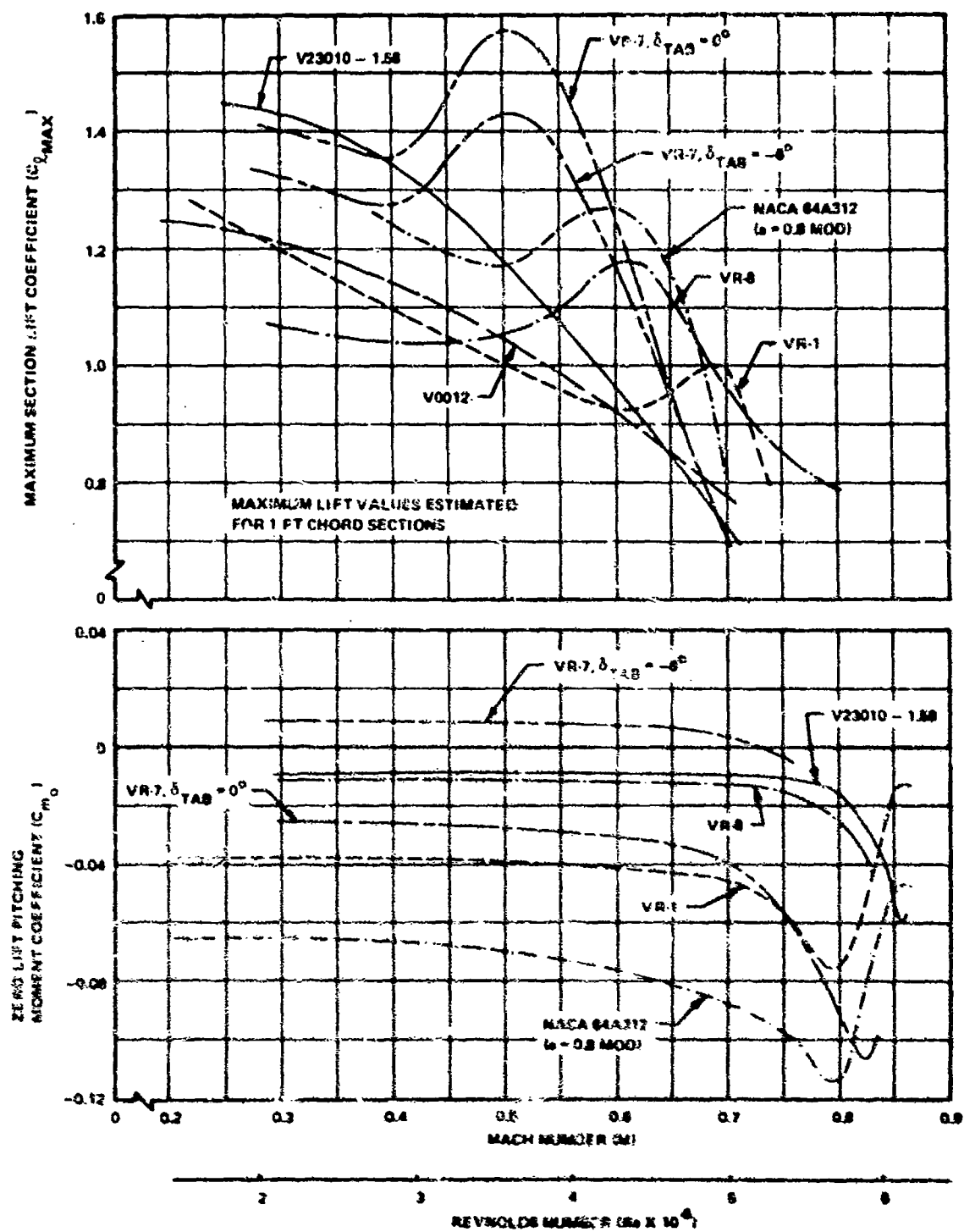
Figure 9-1. Comparison of Maximum Lift and Pitching-Moment Coefficients.
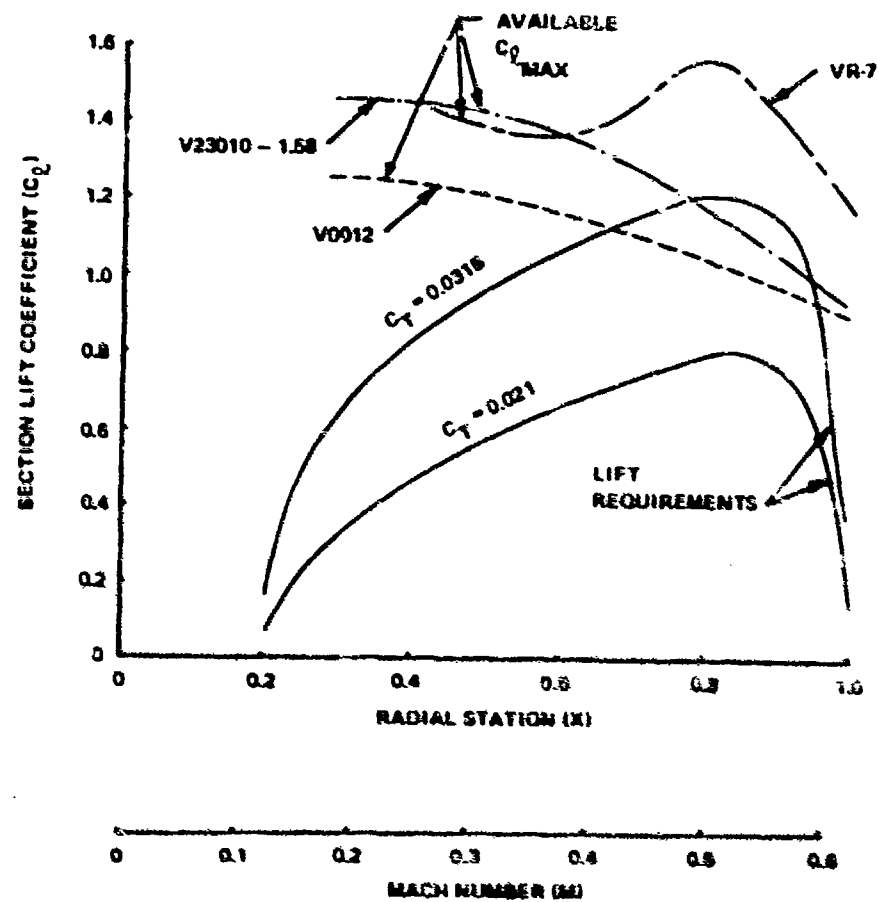
Figure 9—2. Comparison of Theoretical Tail Rotor Lift Requirements and Sectional Maximum-Lift Boundaries.

100
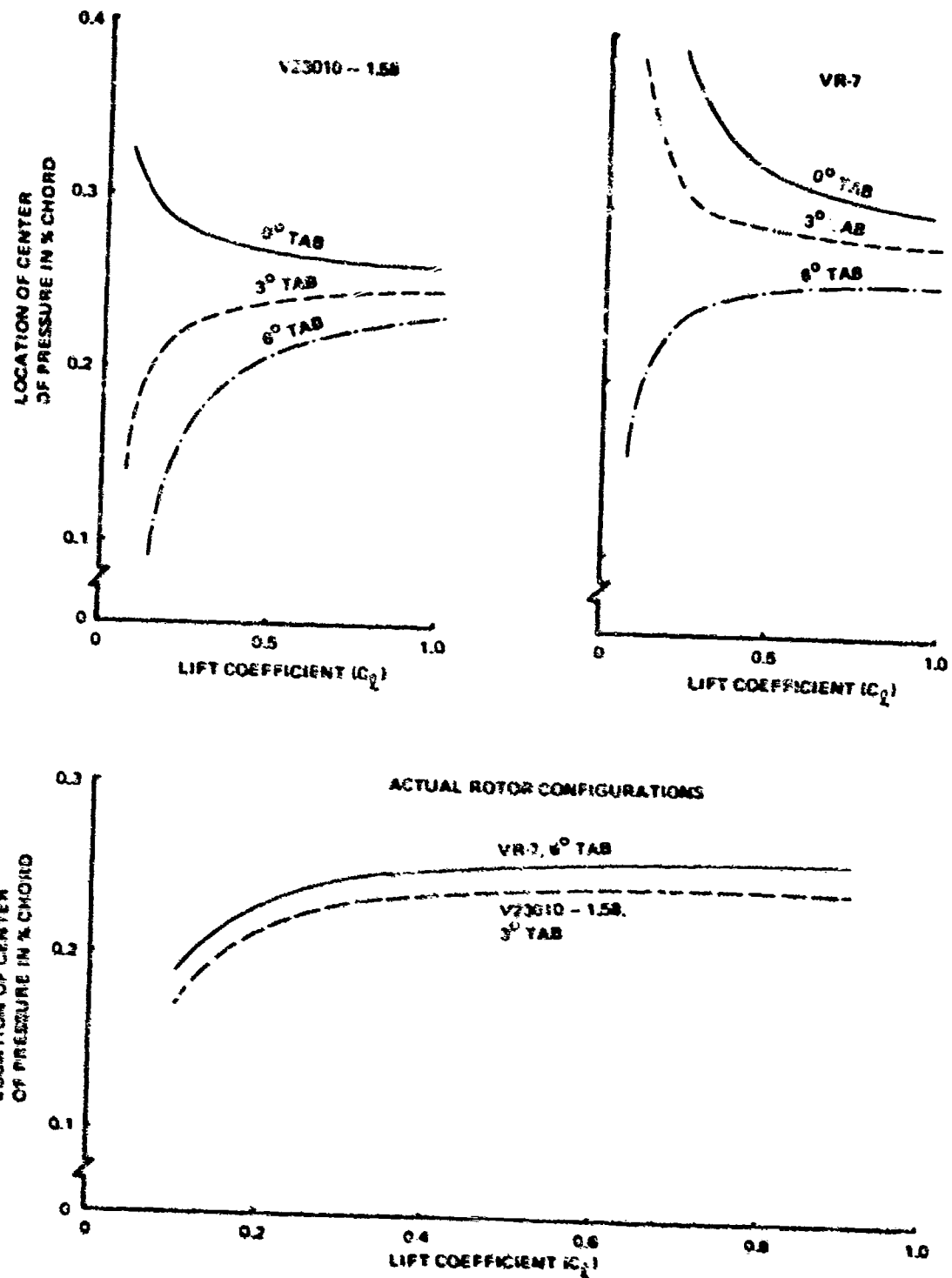
Figure 9—3. Effect of Trailing-Edge Tab Deflection Angle on the Location of the Center of Pressure of the V23010 — 1.58 and VR-7 Airfoils at M = 0.5.
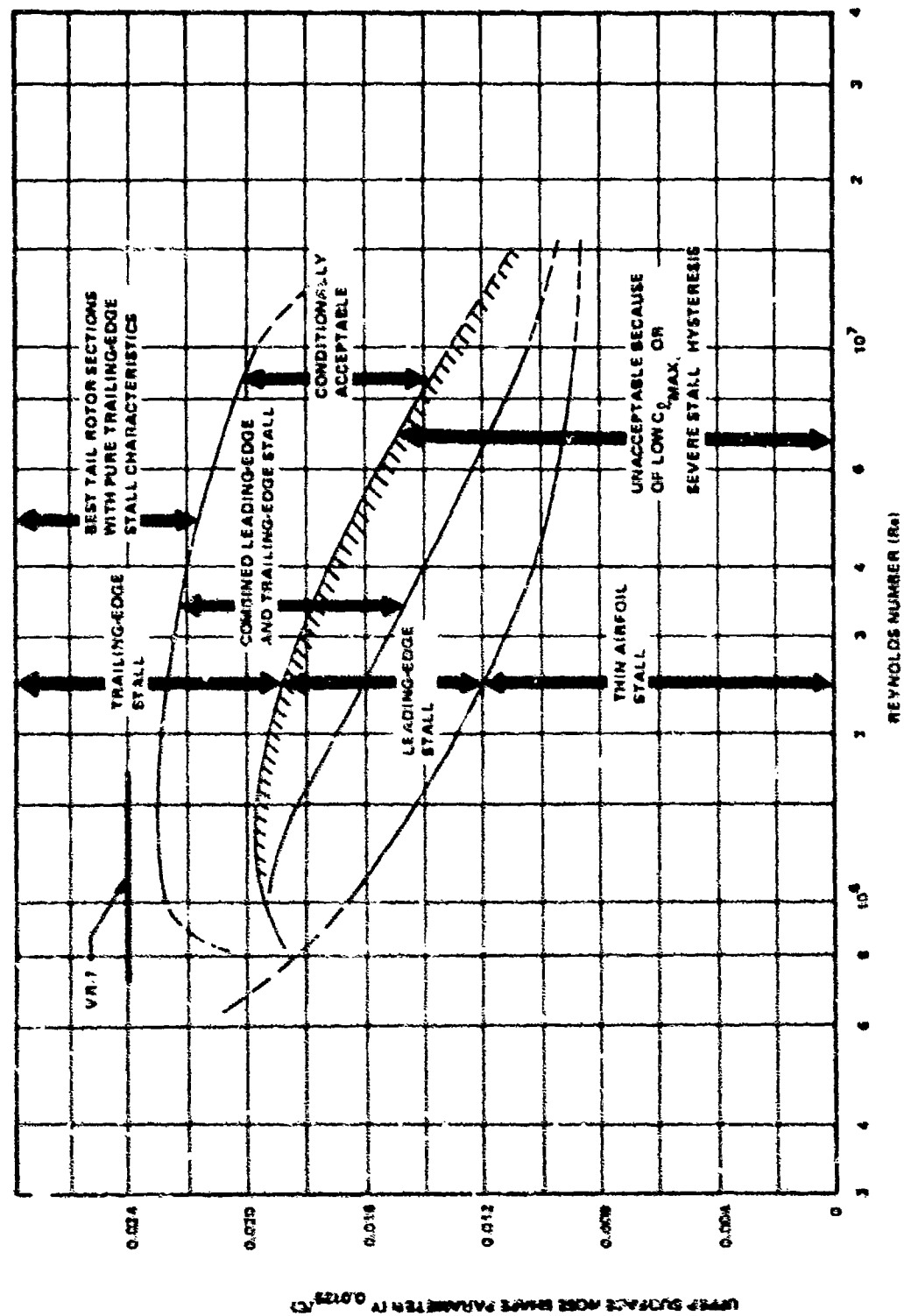
Figure 9-4. Dependence of Stall Characteristics on Leading-Edge Geometry From Reference 8.
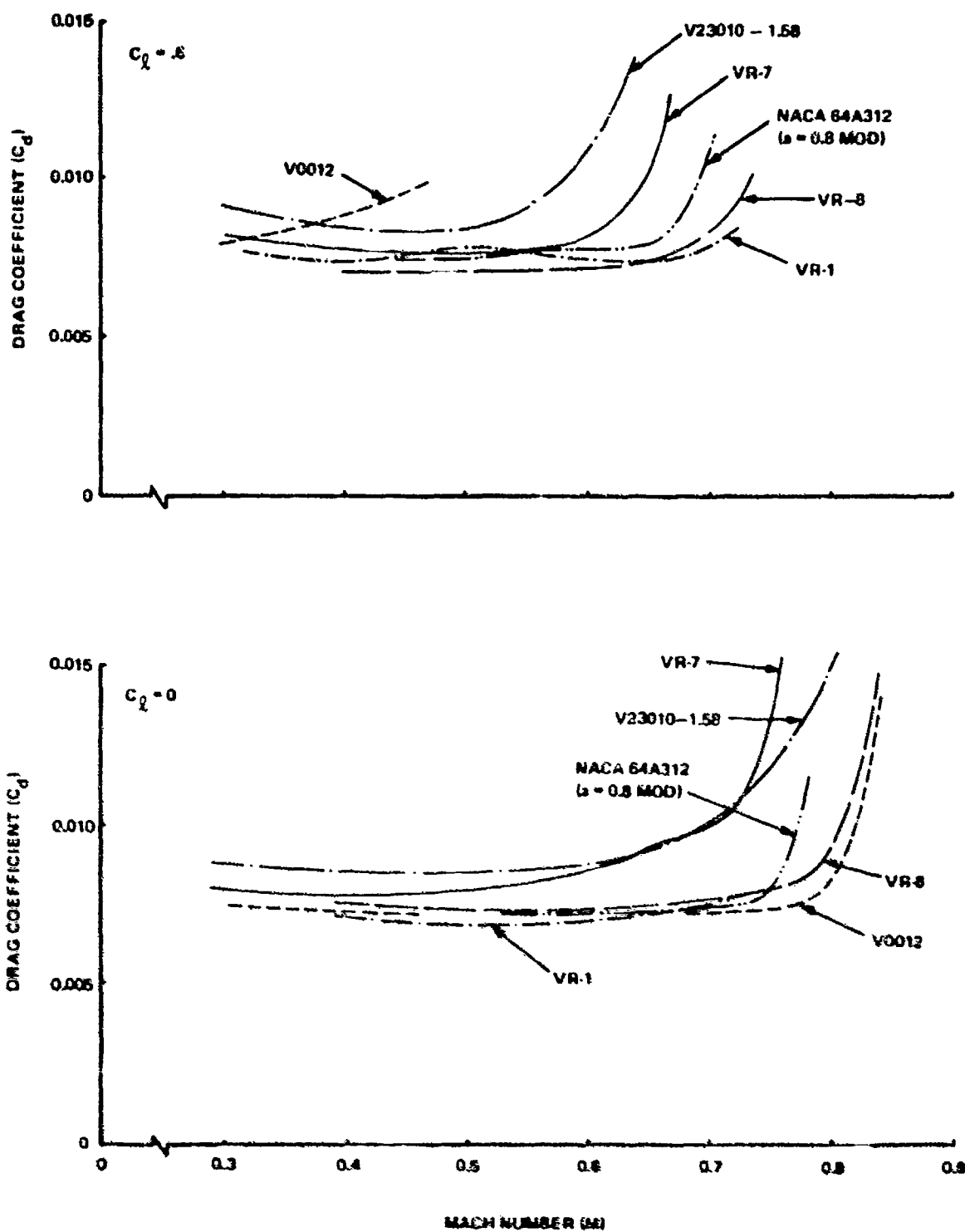
102

Figure 9-6. Drag Level Comparison.

103
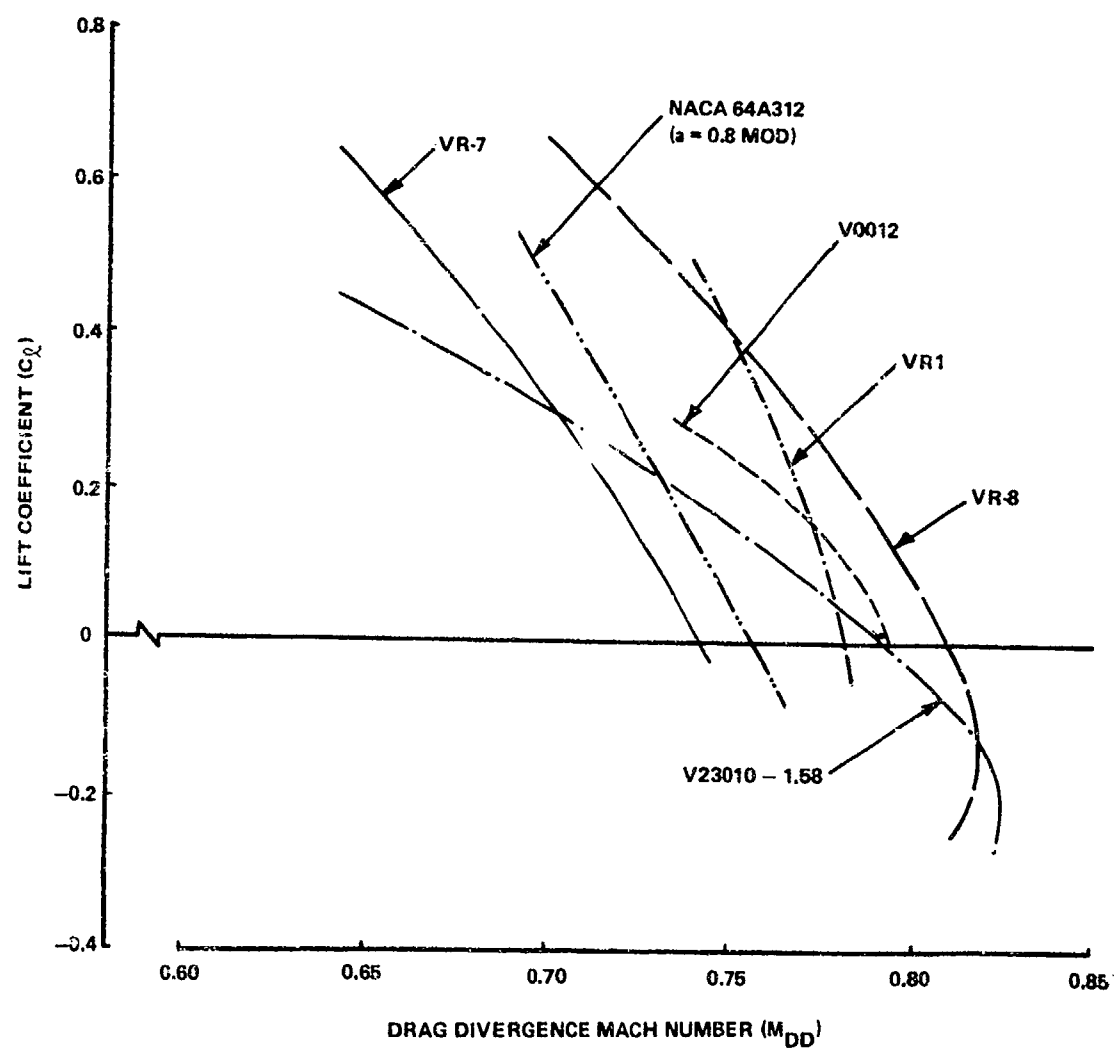
Figure 9—6. Comparison of Drag Divergence Boundaries.

104
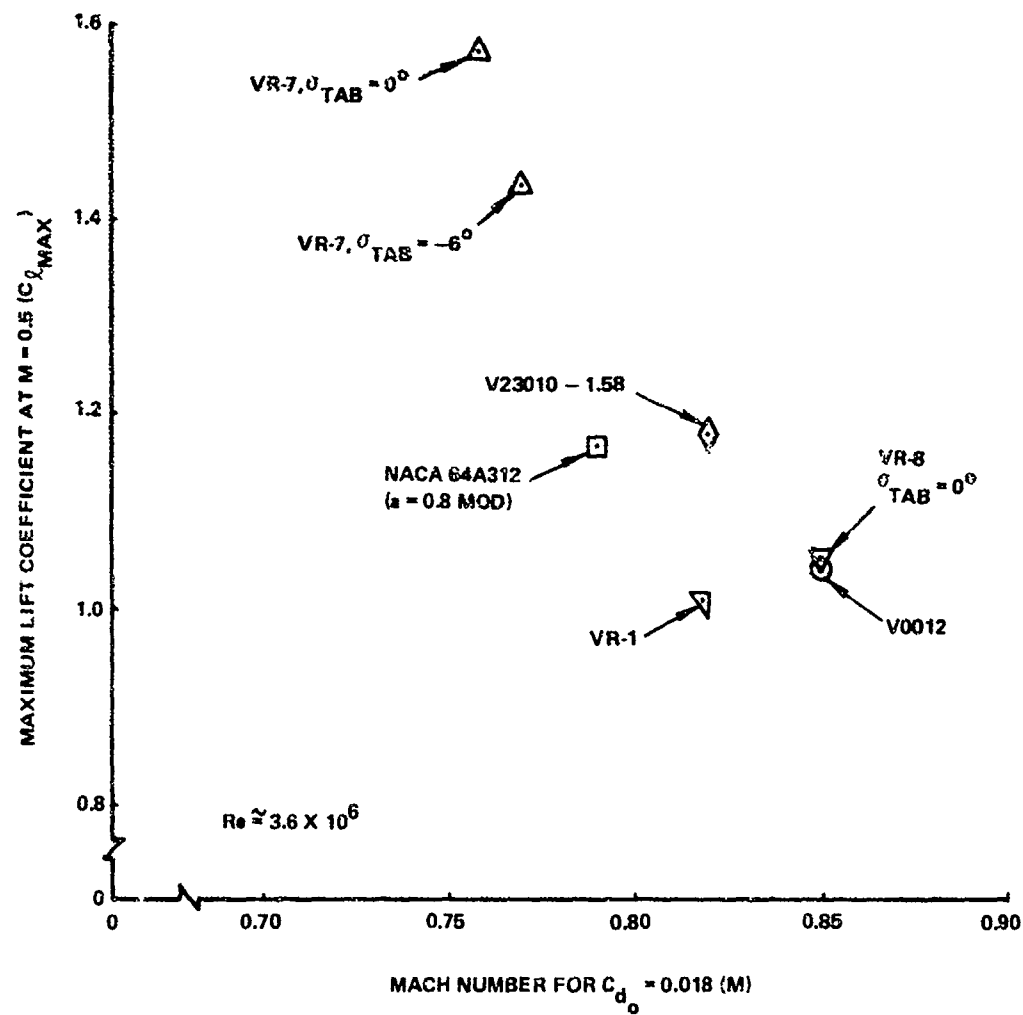
Figure 9—7. Summary of Stall and Drag Rise Characteristics of Several Tail Rotor Airfoils.

105

10.0 BLADE TWIST

The objective of this guideline is to aid in the selection of tail rotor blade twist. Because vehicle sensitivity to twist is small, the final decision will be based on a qualitative judgement. The important considerations are hovering efficiency, directional control capability, and blade loads.

10.1 DISCUSSION

The spanwise distributions of airload and induced velocity are improved in hover and low-speed forward flight regimes by negative values of blade twist. Ideally, the airload distribution is triangular and the induced velocity distribution is uniform for minimum power requirements and hence maximum hovering efficiency. However, many conventional tail rotor blades possess zero twist to compromise for the conditions which require a change in rotor inflow (i.e., negative thrust).

Negative blade twist increases the positive thrust capability and reduces the positive blade pitch requirement. However, it reduces the negative thrust capability and increases the negative blade pitch requirement. Since the maximum positive blade pitch and thrust exceed the maximum negative blade pitch and thrust by a factor of 2, a moderate amount of negative blade pitch is desirable. The beneficial effects of negative twist (-9°) with positive thrust are illustrated by the example tail rotor of Figure 10-1.

Analytical predictions indicate that blade bending moment increases 8.5 percent for each degree of negative blade twist. The increase in blade loads creates higher tail rotor system weight. However, the increased thrust or lift capability of the main rotor due to increased hovering efficiency more than offsets the tail rotor weight penalty, so an increase in payload capability equivalent to about 0.2 percent of gross weight results with -10 degrees of tail rotor blade twist.

10.2 GUIDELINE

Conduct a trade-off study of the effect of blade twist on payload capability. Select the blade twist for which maximum payload capability exists. Based on data from current helicopters, a value of -9 degrees of blade twist represents a good compromise.

Preceding page blank

107
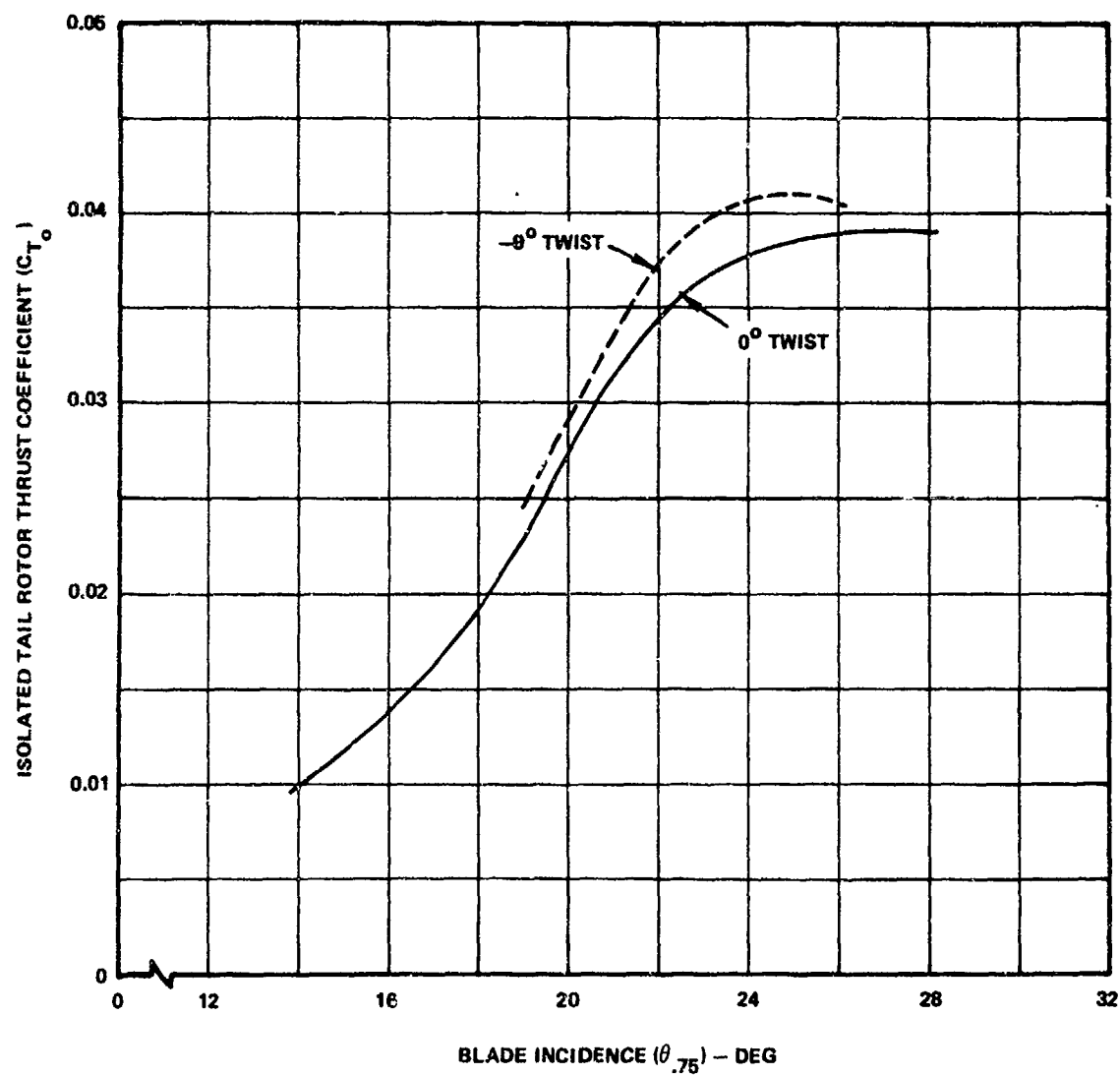
Figure 10--1. Effect of Twist on Theoretical Tail Rotor Thrust at $\mu_{TR} = 0.52$.

108

11.0 MAIN ROTOR POWER

The effects of the tail rotor on main rotor power required in low-speed flight as measured during the Boeing tests are presented in this guideline. Some NASA data of Reference 7 are also shown. The power values at $C_\sigma = 1$, when used in conjunction with fuselage moments, allow the designer to predict tail rotor trim thrust requirements in low-speed flight.

11.1 DISCUSSION

Power required by the main rotor to maintain constant thrust (i.e., for constant gross weight) in direct headwinds and tailwinds of varying velocity is illustrated in Figures 11-1 and 11-2. Values of the trim coefficient C_σ are above two for the Boeing data, indicating extreme yaw maneuver tail rotor thrust. The curves of these figures are presented as a ratio of power required in winds to power required by an isolated rotor at $V = 0$. The recirculation of tail rotor wash into the main rotor increases the main rotor power required in low-speed winds by a significant amount over that of an isolated main rotor; it even increases the main rotor power at zero wind velocity. The greatest increase occurs IGE in a tailwind of approximately 14.7 knots ($\mu = 0.033$), where the power required is approximately 21 percent greater for the tail rotor configuration than for the isolated main rotor. Since the ratio of isolated main rotor power OGE to IGE at $V = 0$ is 1.19, the maximum IGE power required is slightly more than that required OGE at $\mu = 0$. The maximum OGE power, 15 percent greater than hover, occurs at $\mu = 0.031$.

IGE data at $C_\sigma = 1$ from the NASA tests (Reference 7) is included in Figure 11-2. Here, the maximum increase of 8 percent occurs at $\mu = 0.022$. The NASA main rotor was operated at a disc loading of approximately 5.3 psf with the tail rotor installed. NASA's isolated rotor power has been adjusted to correspond to that value. The greater disc loading of the Boeing rotor, 7 psf, results, therefore, in an increase in the velocity at which maximum power is required as compared to the NASA rotor.

Similar data for left and right sideward flight is shown in Figures 11-3 (OGE) and 11-4 (IGE). The maximum increase in power required in left sideward flight is only slightly less than in a direct tailwind. The maximum increase of the Boeing rotor ($C_\sigma > 2$) is 18-percent IGE and 13-percent OGE.

The maximum rotor power increase (which occurs at $\psi = 180$ or

109

210 at most velocities) is shown in Table 11-I compared to
tail rotor power at the advance ratio for maximum main rotor
power increase (both referenced to main rotor power at $\mu = 0$).

TABLE 11-I.	MAXIMUM MAIN ROTOR POWER INCREASE IN IGE TAILWIND COMPARED TO TAIL ROTOR POWER		
Test	Maximum Main Rotor Power Increase $$\frac{P_{MR}}{P_{MR, \; \mu \; = \; 0}} -1$$	Tail Rotor Power $$\frac{P_{TR}}{P_{MR, \; \mu \; = \; 0}}$$	Critical Advance Ratio μ
Boeing	0.21	0.33	0.033
NASA	0.06	0.12	0.022

From Table 11-I, it can be concluded that in rearward flight,
the maximum increase in main rotor power is approximately half
of the tail rotor power required. This increase in main rotor
power should be used in the calculation of helicopter perform-
ance at low speeds. Since tail rotor thrust for trim is
directly proportional to main rotor power, these effects must
be included in determining maximum tail rotor thrust required.

11.2 GUIDELINE

Maximum tail rotor thrust is required to balance main rotor
torque in rearward flight ($\psi = 180$ to 210°). Tail rotor trim
thrust to balance main rotor torque should be obtained from
the main rotor power value obtained by

● Calculating main rotor power for an isolated rotor at zero
  airspeed

● Multiplying the calculated power by the percentage increase
  obtained from Figures 11-1 and 11-2. For large values of
  the trim coefficient ($C_\sigma \geq 2$) and for high disc loadings
  ($w \approx 7$), the Boeing curves may be used directly. For trim
  ($C_\sigma = 1$) and lower disc loadings ($w \approx 5$), the NASA curves
  may be used directly. For values of C_σ between 1 and 2,
  interpolation of the power increase is required; for inter-
  mediate values of disc loading, interpolation of the advance
  ratio for maximum power is required.
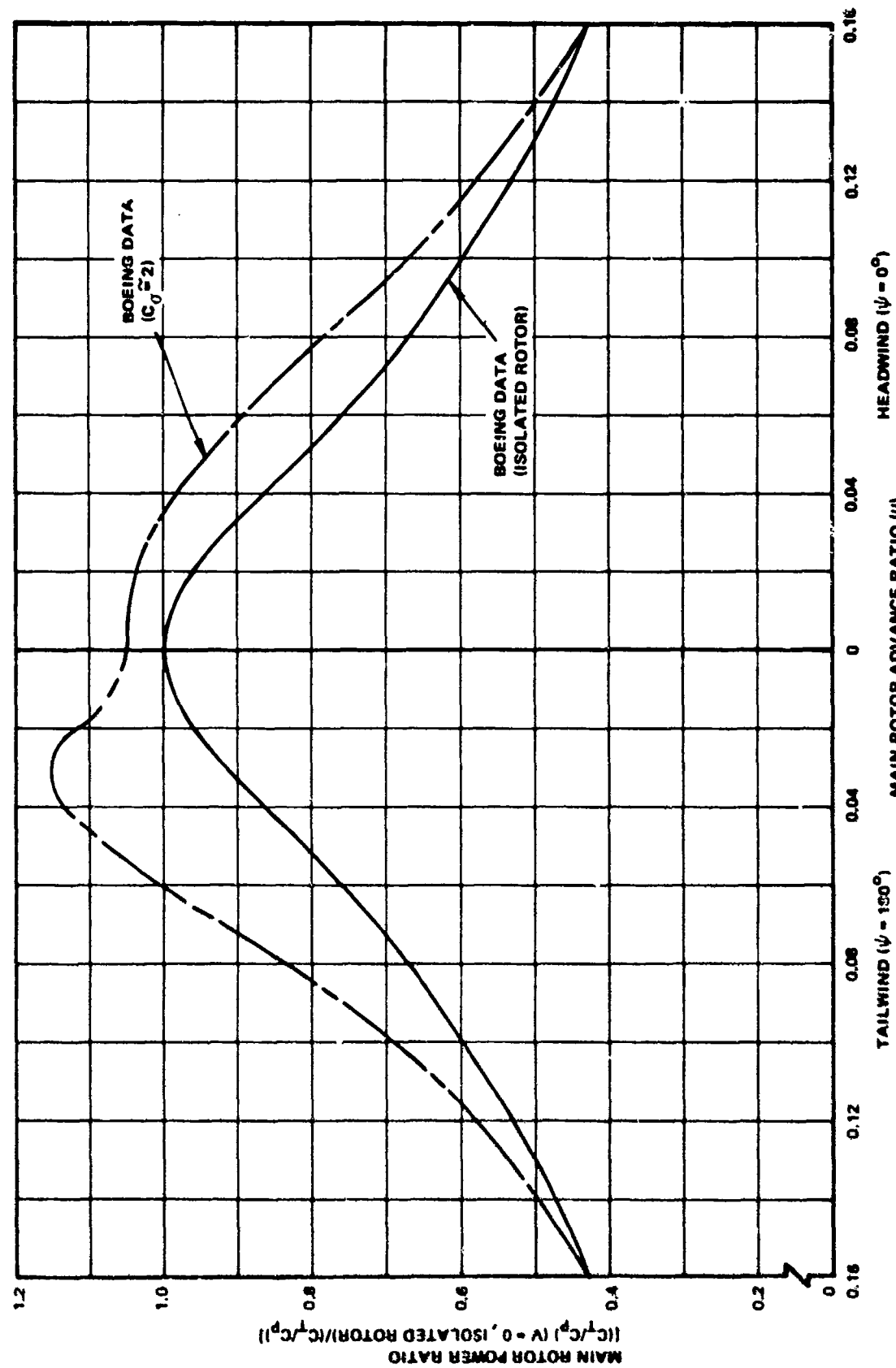
Figure 11–1. Effect of Tail Rotor on Main Power Required in Headwinds and Tailwinds — h/d = 1.0, Rotation = BF.

111
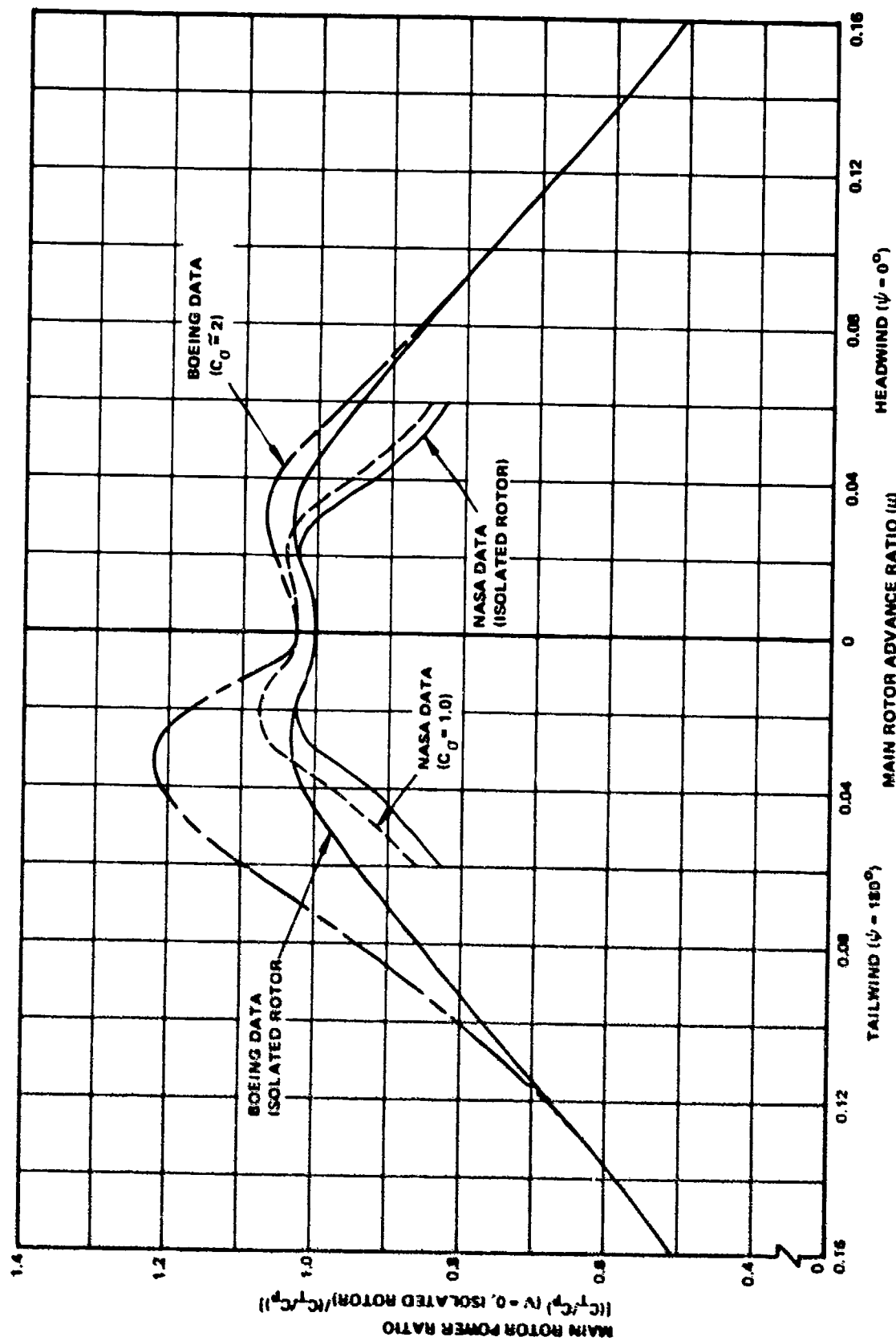
Figure 11–2. Effect of Tail Rotor on Main Rotor Power Required in Headwinds and Tailwinds — h/d = 0.3, Rotation = BF.

112
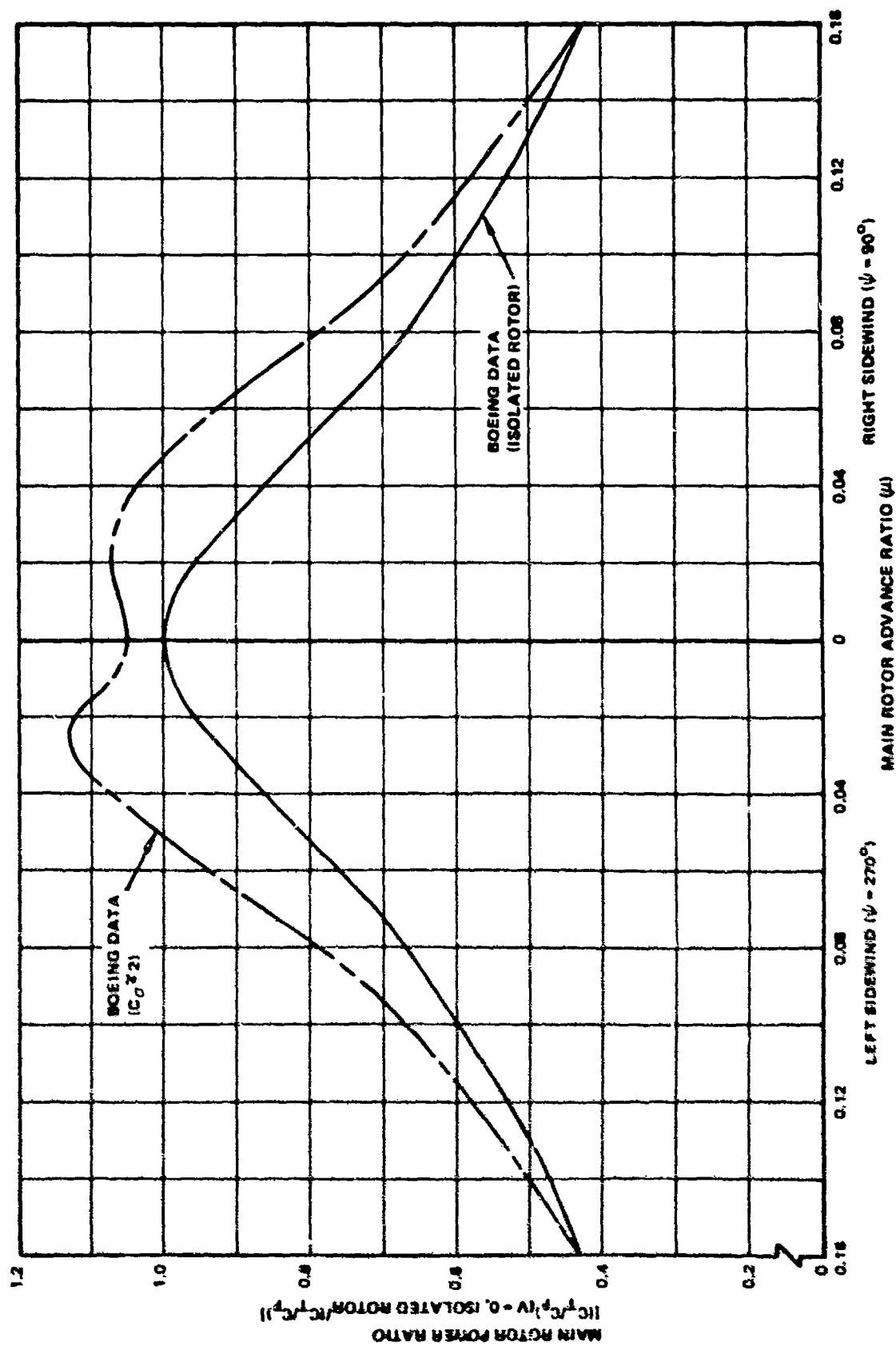
Figure 11—3. Effects of Tail Rotor on Main Rotor Power Required in Right and Left Sidewinds — h/d = 1.0, Rotation = BF.

113
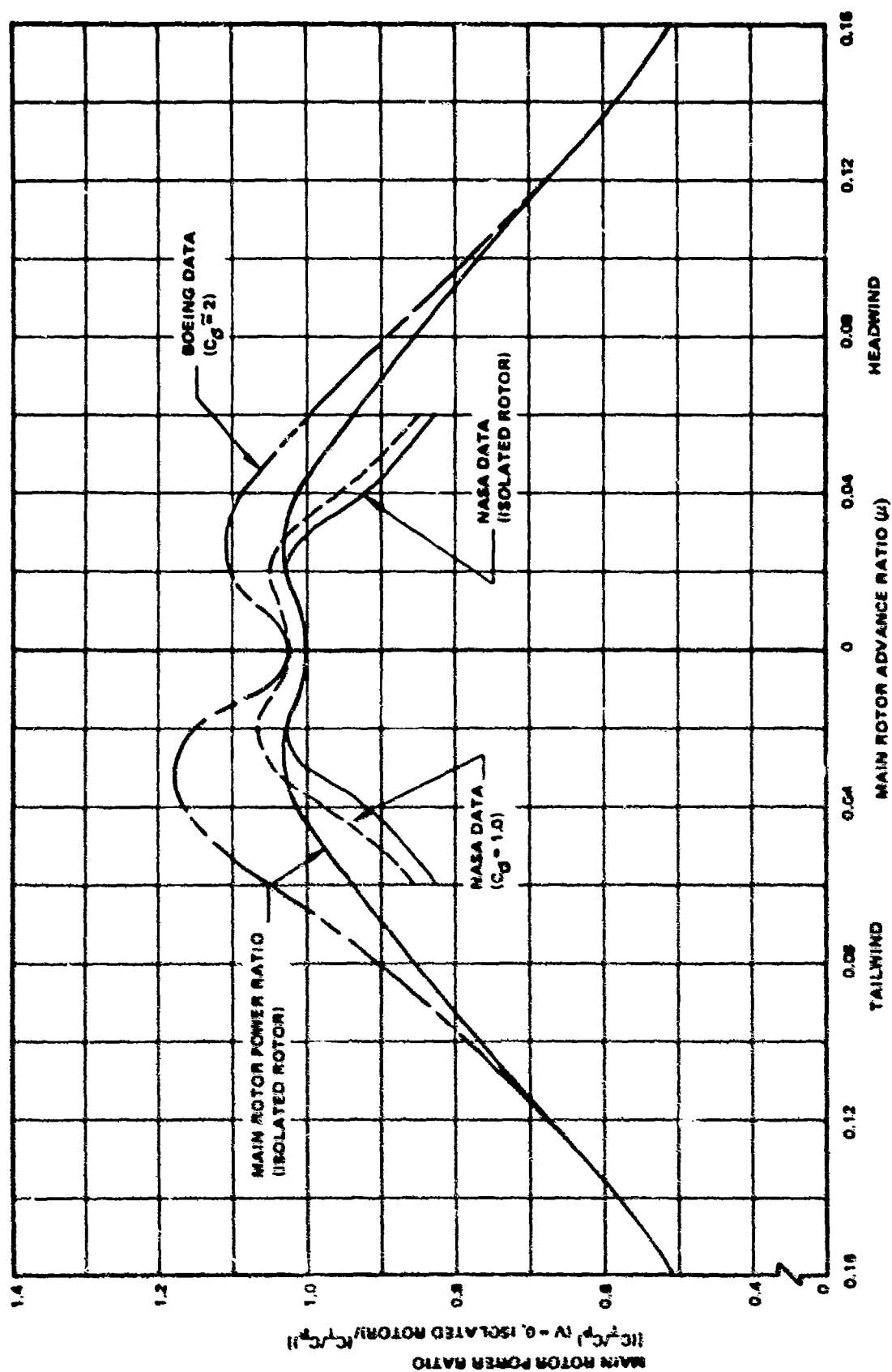
Figure 11—4. Effect of Tail Rotor on Main Rotor Power Required in Right and Left Sidewinds — h/d = 0.3, Rotation = BF.

12.0 SELECTION OF TIP SPEED AND NUMBER OF BLADES

The objective of this guideline is to present charts of detection distance for a hovering helicopter (in lieu of some fixed noise level criteria) for a given terrain and ambient noise level from which tip speed and number of blades can be selected.

12.1 DISCUSSION

Tail rotor rotational noise is a function of the total aerodynamic forces acting on the blades, the number of blades, and the tip speed.

Figures 12-1 through 12-3 show tail rotor and main rotor detection distance versus tip speed for various gross weight aircraft and number of tail rotor blades. These values are based on medium ambient noise level and sparse jungle ground attenuation conditions for the helicopter hovering in ground effect. Both isolated main rotor and tail rotor detection distances are presented for the purpose of showing which rotor is the most critical (i.e., greatest distance at which detection is possible). The method used to calculate the detection distances is discussed in Appendix III. Disc loadings assumed for the cases computed are as follows:

| | Disc Loading, lb/sq ft | |
Gross Weight, lb	Main Rotor	Tail Rotor
5000	6	10
15,000	8	15
45,000	12	20

Prior studies have shown that noise reduction produces survivability payoffs when the detection range is less than the maximum effective range of the weapon employed against the helicopter. Such range might typically be 2000 to 3000 feet. Taking the lower value as an example, it is seen from Figure 12-1 that small helicopters (5000 pounds gross weight class) are relatively insensitive to number of blades and tip speed for such ranges. Medium helicopters (15,000 pounds gross) should have four-bladed tail rotors (Figure 12-2) and possibly five- to six-bladed main rotors for tip speeds in the range of 700 to 750 fps. Large helicopters (45,000 pounds gross) will have to have five- or six-bladed tail rotors and eight-bladed main rotors to meet such detection distances for 700 to 750 fps tip speed.

115

Tip speeds should be kept in the range of 700 to 750 fps to keep the advance ratio at the lowest value possible in forward flight for lower structural bending loads. These tip speeds combined with the number of blades selected on the basis of the above noise considerations will produce the lowest control pitch link loads, since the centrifugal centering loads vary as the cube of the chord. Blade surface (leading edge) erosion doubles when tip speed is increased from 600 to 700 fps per Reference 8. Other reasons for keeping the tip speed as high as possible are:

● Less blade stall at high speed and during maneuver

● Lower tail rotor system weight

● Less gust sensitivity

As stated, the detection distance trends with tip speed shown in this guideline are based on a medium ambient noise condition as described further in Appendix III. Should the ambient noise condition approach that of low ambient, the detection distance will increase approximately four to five times the value for medium ambient as an average. Thus the surrounding noise level must be considered. Further, the noise attenuation has been based on a ground condition of sparse jungle. If applicable, consideration should be given to other conditions.

12.2 GUIDELINE

Select the required detection distance based on operational requirements. Then select blade number from Figures 12-1 through 12-3 for a tip speed near 700 fps for the gross weight class of the aircraft being considered. Consideration should also be given to erosion and ambient noise conditions.

116
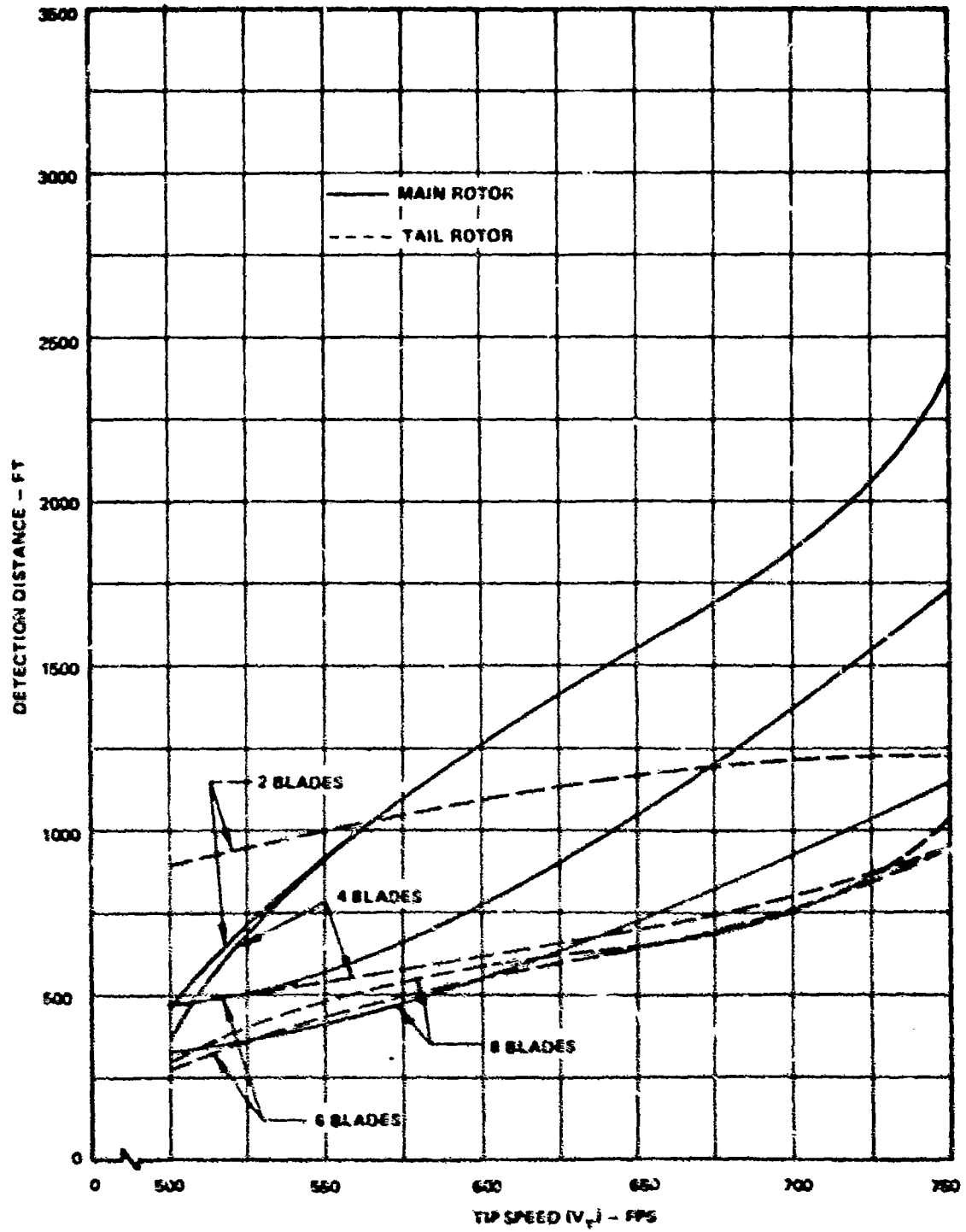
Figure 17-1. Effect of Number of Blades and Tip Speed on Main Rotor and Tail Rotor Detection Distance at a Gross Weight = 9300 Lb.

117
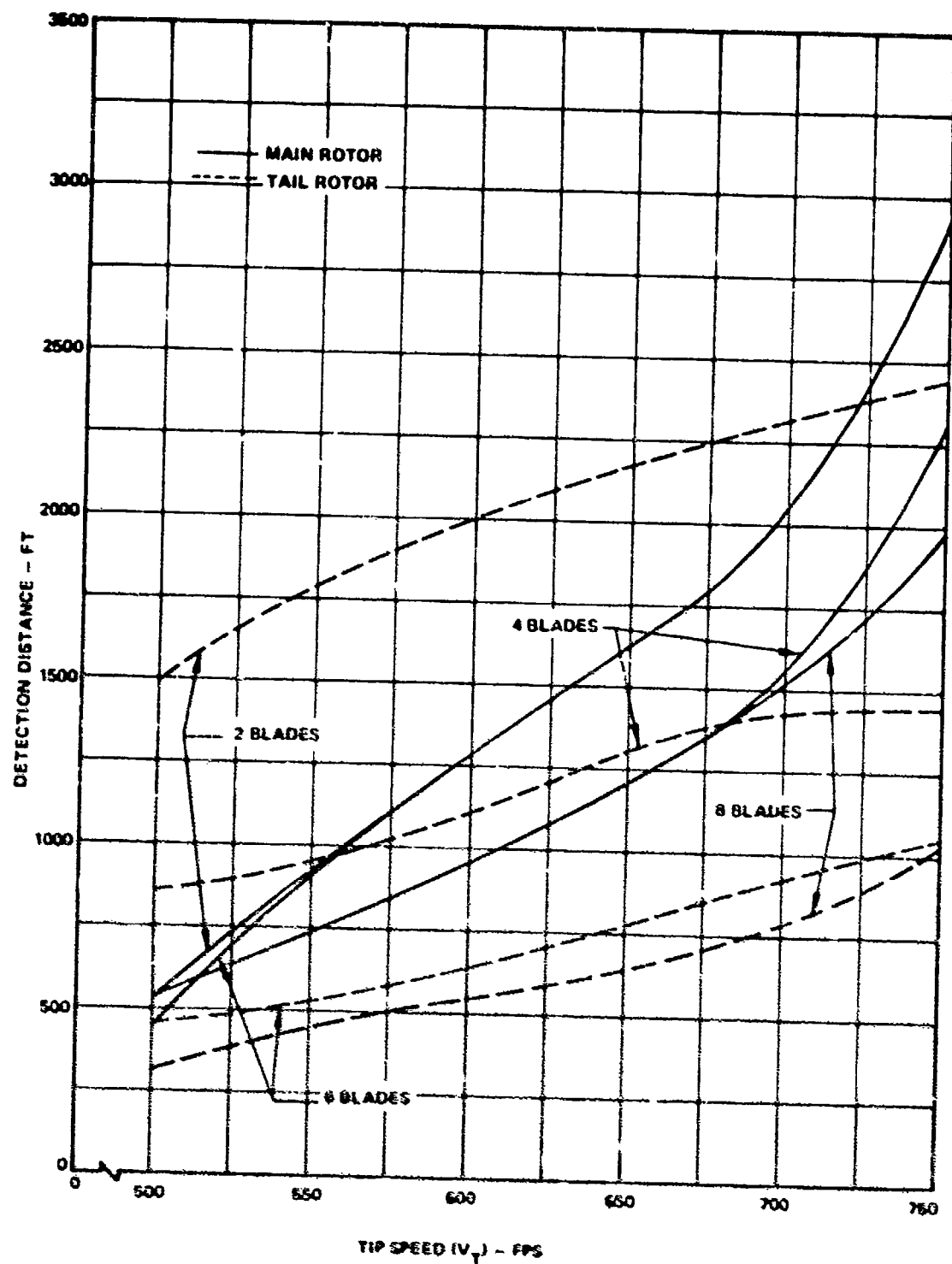
Figure 12-2. Effect of Number of Blades and Tip Speed on Main Rotor and Tail Rotor Detection Distance at a Gross Weight = 15,000 Lb.

118
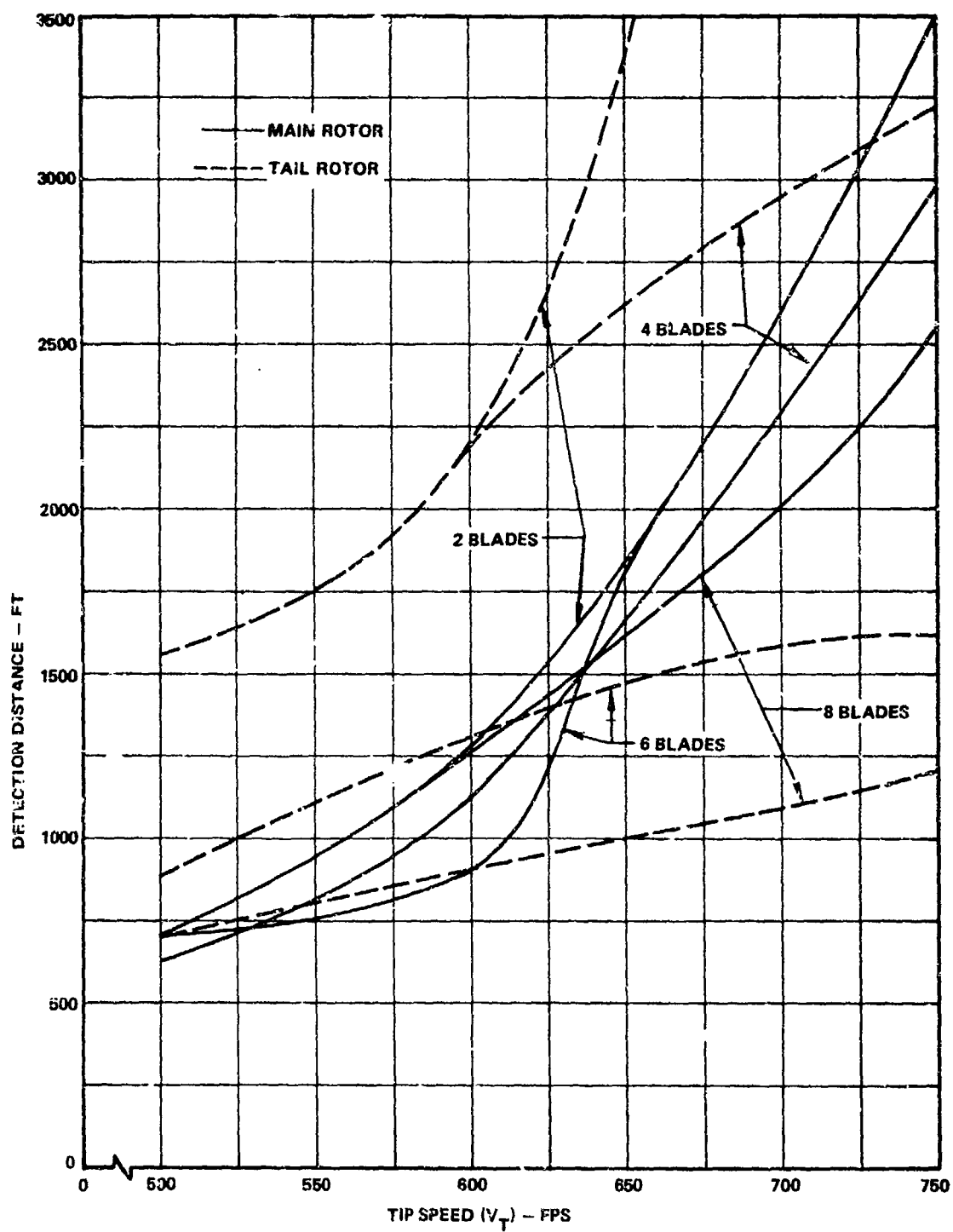
Figure 12–3. Effect of Number of Blades and Tip Speed on Main Rotor and Tail Rotor Detection Distance at a Gross Weight = 45,000 Lb.

119

13.0 DESIGN NET THRUST REQUIRED

The objective of this guideline is to outline a method for derivation of the maximum value of tail rotor net thrust for the critical maneuver or trim condition where maximum tail rotor thrust is required. This thrust is then converted into C_{T_N} at design altitude, and the tail rotor solidity and maximum left pedal blade incidence are then selected from Guideline 14. Derivation of method, formulae, and charts is given in Appendix III.

13.1 DISCUSSION

The three criteria that are most commonly used to design the tail rotor are:

- Trim the aircraft at a critical operating condition such as hover with 35-knot wind plus ±15-knot gust.

- Trim and provide yaw control ability for specified yaw maneuver in hover (refer to MIL-H-8501A) such as 15 deg/sec in 1.5 seconds with 10-percent control margin.

- Trim and provide a yaw deceleration such as 0.4 rad/sec, while rotating to the right with a yaw velocity of 0.75 rad/sec (criteria recommended in Reference 9).

While all three conditions should be investigated, it is believed that the second is the most critical. In these guidelines the second condition will be used, since with the 10-percent thrust margin it will require the highest solidity.

Therefore, for Condition No. 2, the tail rotor thrust required* is the sum of the following:

- Trim thrust required to balance main rotor torque ($\psi = 90^\circ$)

- Thrust increment required to perform the maneuver; i.e., to accelerate the aircraft to the specified angular yaw rate (start maneuver at $\psi = 90^\circ$)

- The simulated thrust increment to match the cyclic blade element angle of attack, providing aerodynamic moment to precess the tail rotor

---

*From Guideline 5, critical velocity is 20 knots; from Guideline 4, critical thrust azimuth is 60° to 90°. For convenience, therefore, the azimuth values of $\psi = 60^\circ$ and 90° are used interchangeably.

121

- The thrust required to balance the body moment ($\psi = 90^\circ$)

- Thrust to provide the desired thrust margin

13.2   GUIDELINE

1. For the alternate gross weight at the maximum IGE hover altitude and temperature, obtain the tail rotor trim thrust from Figure 13-1. Multiply the trim thrust by the ratio of main rotor power required with the tail rotor on to isolated main rotor power at $\psi = 90^\circ$ and $V = 20$ knots. The main rotor power ratio is obtained from the $C_\sigma = 1$ curve of Figure 11-4 for alternate gross weight IGE hover ceiling.

2. Select maneuver time and angular velocity from MIL-H-8501A or from a specified yaw maneuver such as 15 deg/sec required in 1.5 seconds. Select required yaw damping from flying qualities requirements from values determined by a simulator such as shown in Figure 13-2 or from MIL-H-8501A. Select yaw moment of inertia/tail length from Figure 13-3. Finally, select maneuver increment thrust from Figure 13-4.

3. Estimate "simulated" thrust required to precess tail rotor at an angular yaw rate of 30 percent of the final specified yaw rate from Figure 13-5.

4. Determine thrust required to balance body aerodynamic moment from Figure 13-6.

5. Total these thrusts and convert to (C_{T_N}), using density at design or gross weight hover ceiling, tail rotor radius from Guideline 6, and tip speed from Guideline 12.

6. Increase the C_{T_N} by the amount of thrust margin desired. For example, for a 10-percent thrust margin,

$$(C_{T_N})_d = (C_{T_N})/0.90$$

$$K_T = 1.2 \, (FM) \sqrt{2\rho\pi} \, \Omega R^2$$
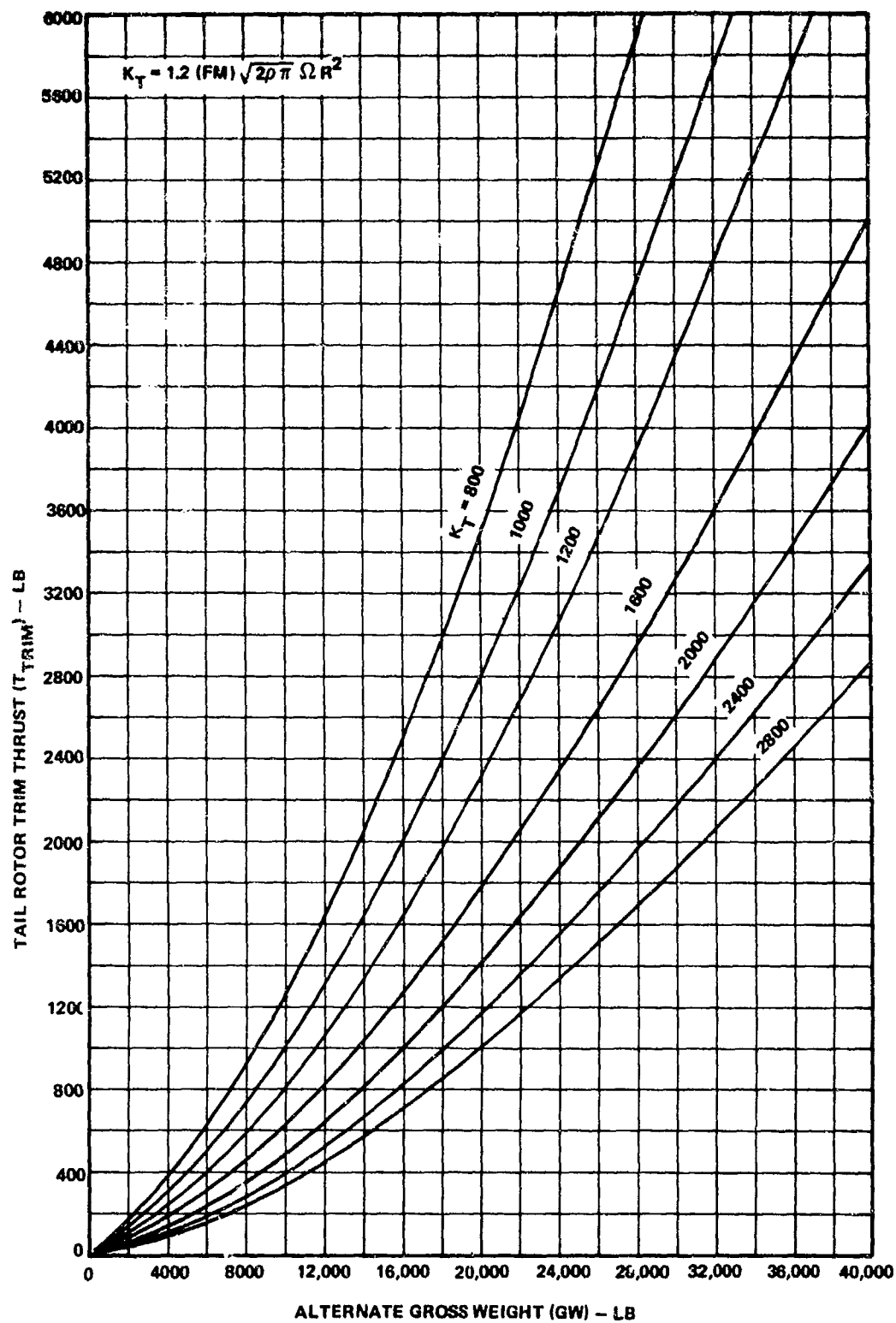
Figure 13–1. Determination of Tail Rotor Trim Thrust.

123
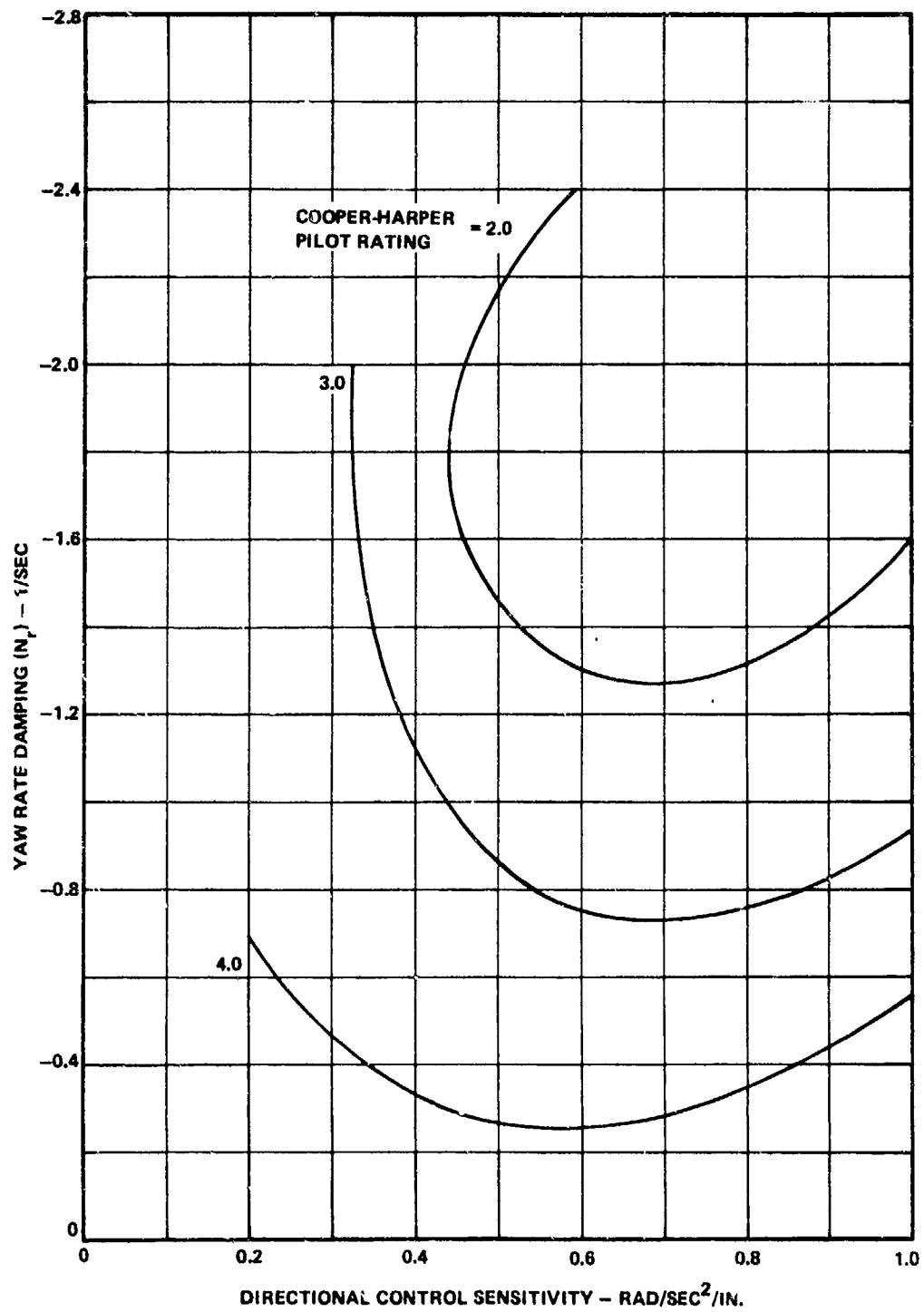
Figure 13–2. Determination of Yaw Rate Damping Required (Based on Boeing-Vertol Flight Simulator).
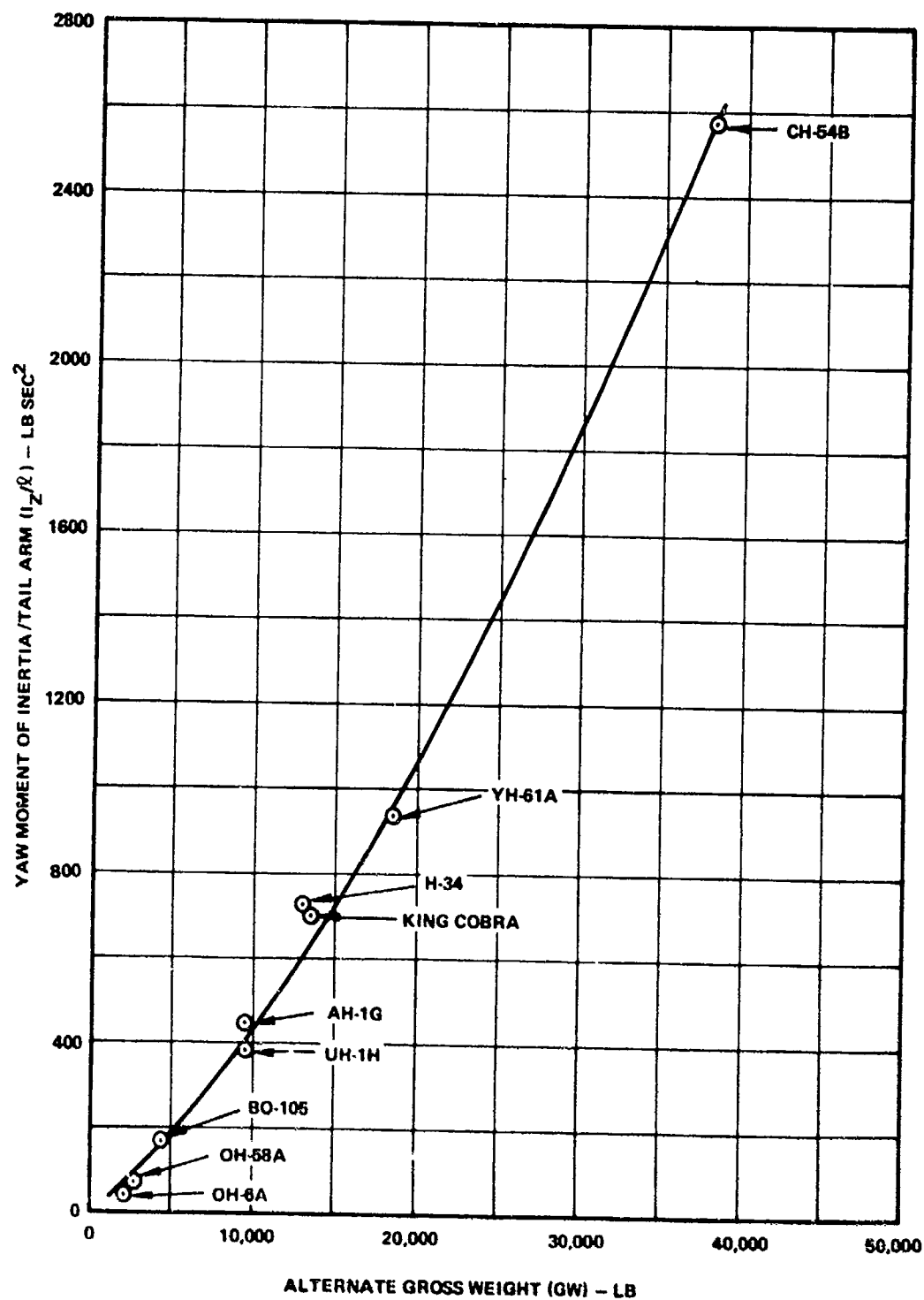
Figure 13-3. Determination of Yaw Moment of Inertia.

125
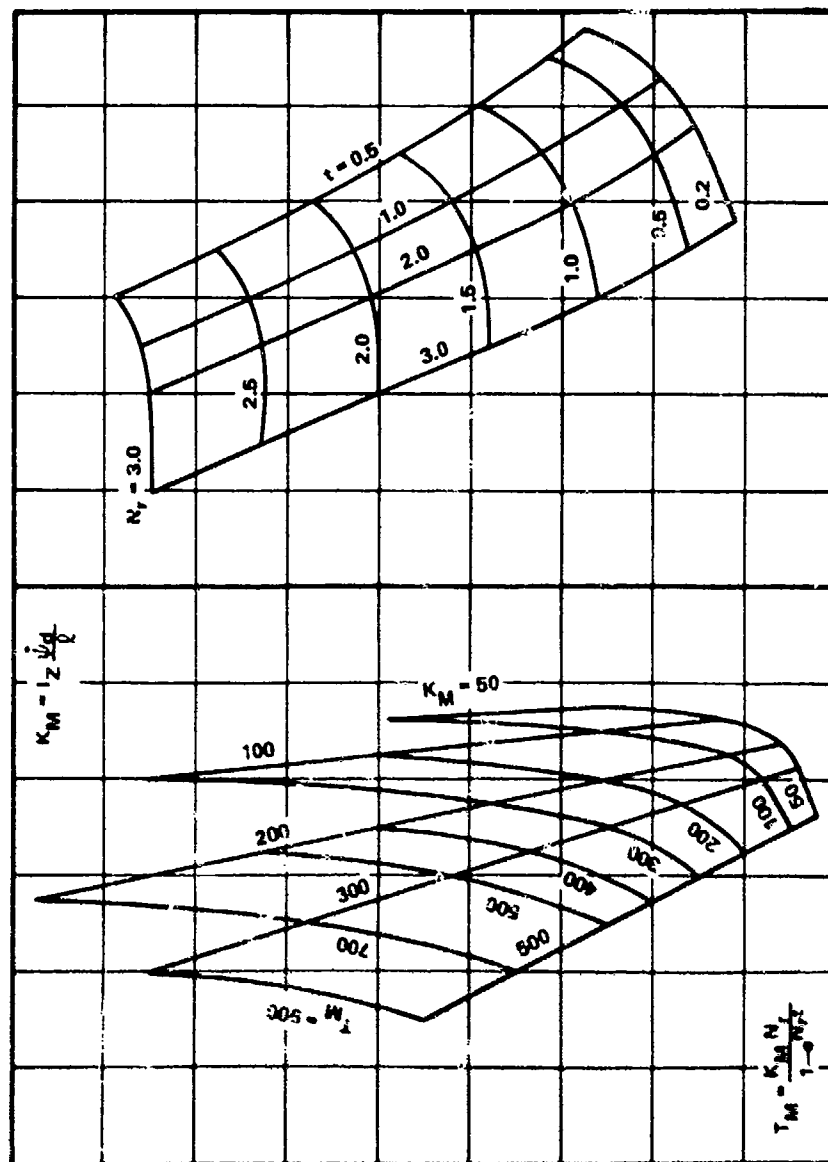
Figure 13—4. Determination of Maneuver Thrust Increment Required To Produce a Desired Yaw Rate.

126
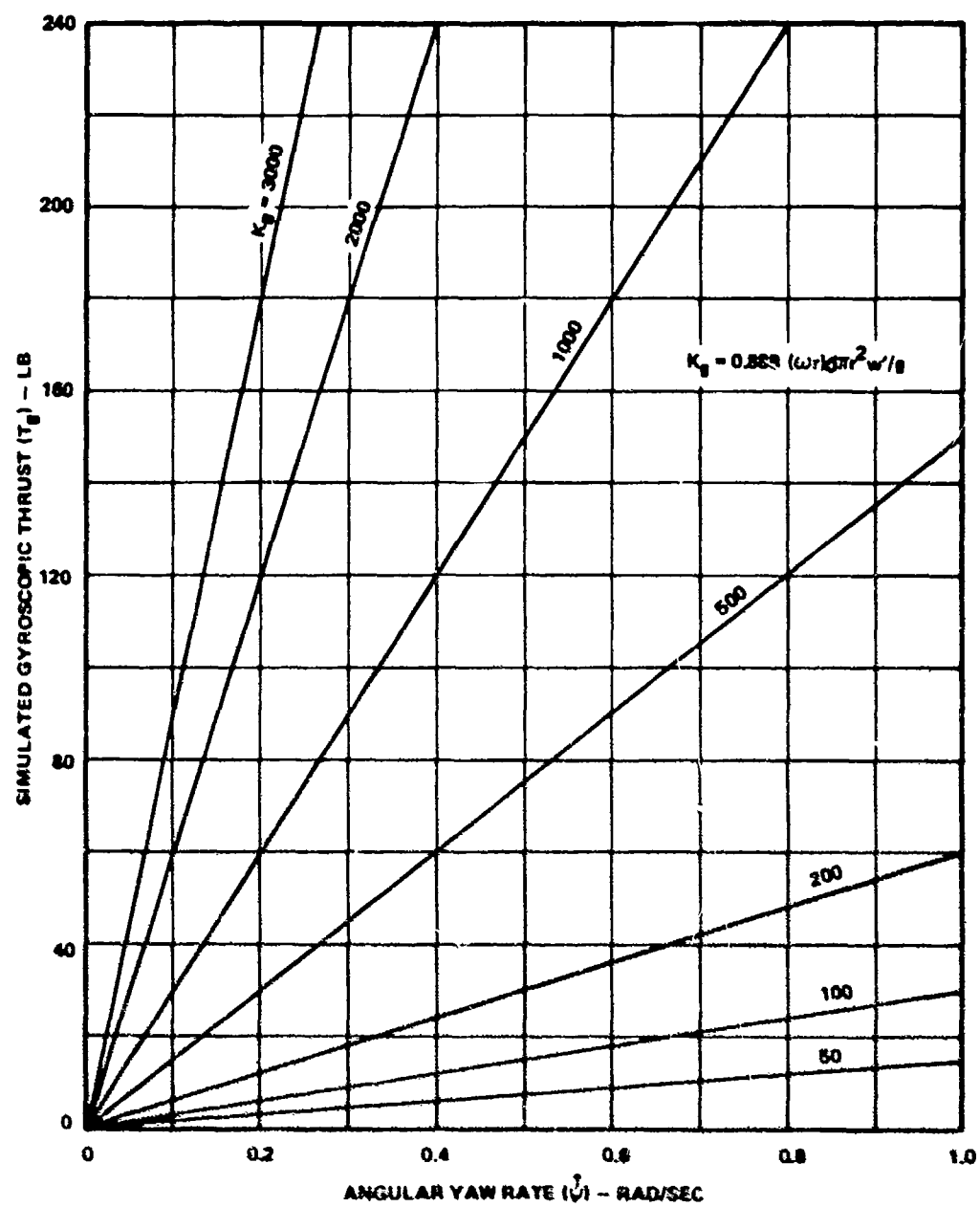
Figure 13–5. Determination of Simulated Gyroscopic Thrust.

127
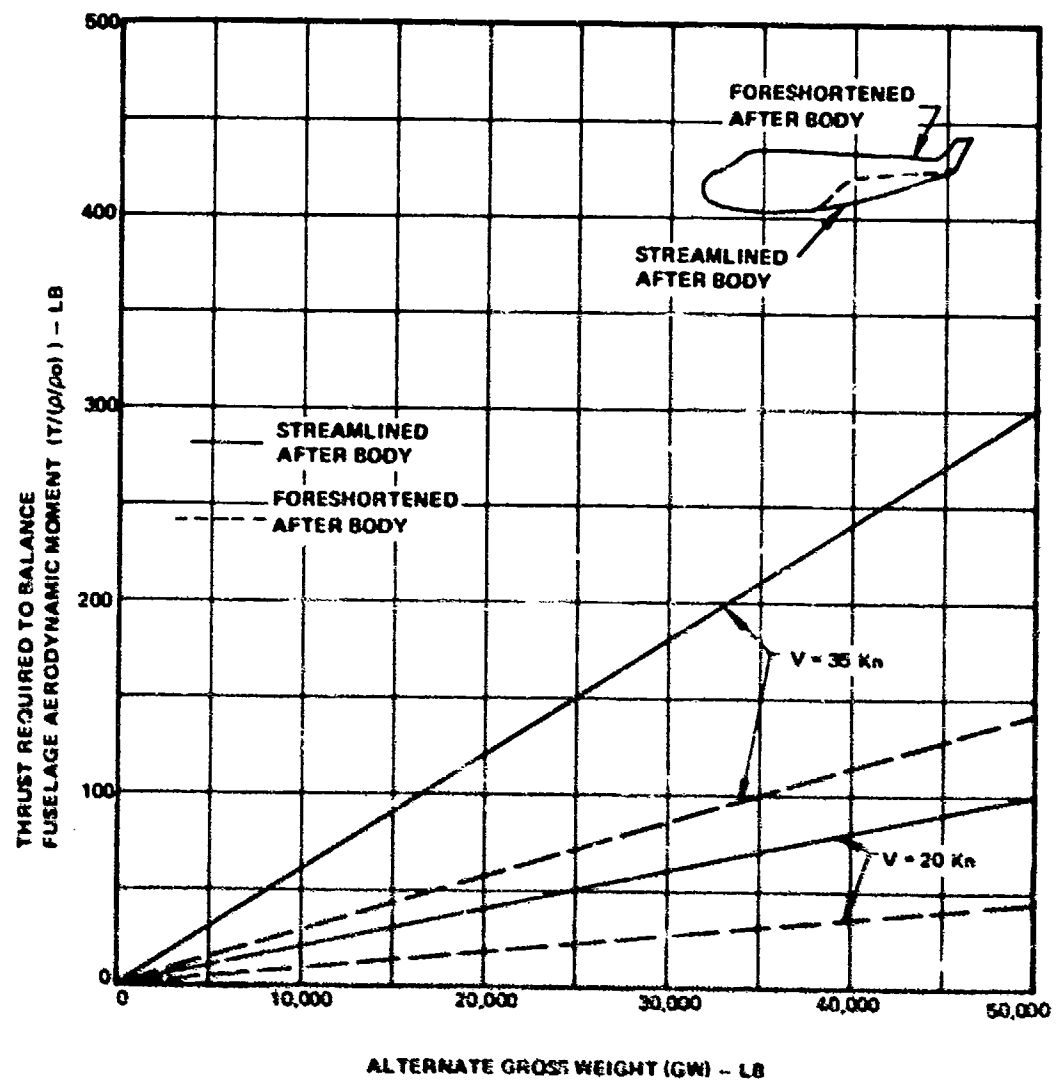
Figure 13-6. Determination of Thrust Required To Balance Fuselage Aerodynamic Moments.

128

14.0 SELECTION OF SOLIDITY AND MAXIMUM BLADE INCIDENCE

This guideline presents methods to enable the designer to se-
lect the proper solidity and maximum positive (left pedal)
blade incidence for adequate control margins under maneuvers
at maximum gross weight and altitude.

14.1 DISCUSSION

Guideline 11 shows that main rotor power required at 20 knots
is equal to or greater than the zero wind case; therefore,
tail rotor trim thrust required at 20 knots is not less than
the zero wind case.

From Guidelines 4 and 5, the critical thrust available con-
dition is $\psi = 60^\circ$ at $V = 20$ knots. Boeing-tested tail rotor
thrust data is presented at these conditions for various
values of h/d in Figure 14-1. Taking the average minimum
thrusts obtained at h/d = 0.45 and 1.0, the isolated tail
rotor thrust/net thrust for the 20-knot wind is

$$C_{T_O}/C_{T_N} = 1.11 + 0.777 \ (C_T/C_{T_N}-1) \qquad (14-1)$$

As a convenience for rapid determination, this relationship is
plotted in Figure 14-2. For derivation of this equation and
for corresponding equations at 0 and 35 knots, see Appendix
III.

Design thrust, $(C_{T_N})_d$, is defined as the net thrust required
to perform a specific yaw maneuver at the most critical com-
bination of gross weight and altitude. The determination of
$(C_{T_N})_d$ is given in Guideline 13.

With design net thrust known, the design C_{T_O} can be determined
from Figure 14-2. The blade incidence and solidity required
to produce that thrust without stall can be determined from
Figure 14-3, using the design C_{T_O} from Figure 14-2.

Figures 4-5, 4-6, and 14-6 show that net thrust is lower com-
pared to isolated tail rotor thrust at $\theta = 20^\circ$ than at the
lower collectives. The equations as plotted in Figure 14-2
obtained for $\theta = 20^\circ$ and $C_\sigma = 2.5$ are, therefore, conservative
when compared with what would be obtained at lower collectives
and trim coefficients.

The amount of stall margin when the tail rotor is developing
full left-pedal thrust in the static condition can be obtained
from Figure 14-4. The stall margin at an advance ratio of

129

0.084 (35-knot wind speed at ωr = 700 ft/sec) is obtained from Figure 14-5.

14.2 GUIDELINE

Using the required net thrust determined in Guideline 13 and the ratio of shaft to net thrust determined in Guideline 8, the equivalent isolated rotor thrust is obtained from Figure 14-2.

Solidity and maximum left-pedal blade incidence can then be determined from the critical 20-knot design chart, Figure 14-3, or from the designer's own isolated tail rotor charts. Determination of whether or not the tail rotor blade will stall in static full left-pedal condition can be determined from Figure 14-4.

A complete flow chart for determination of θ and σ is given in Figure 14-7.
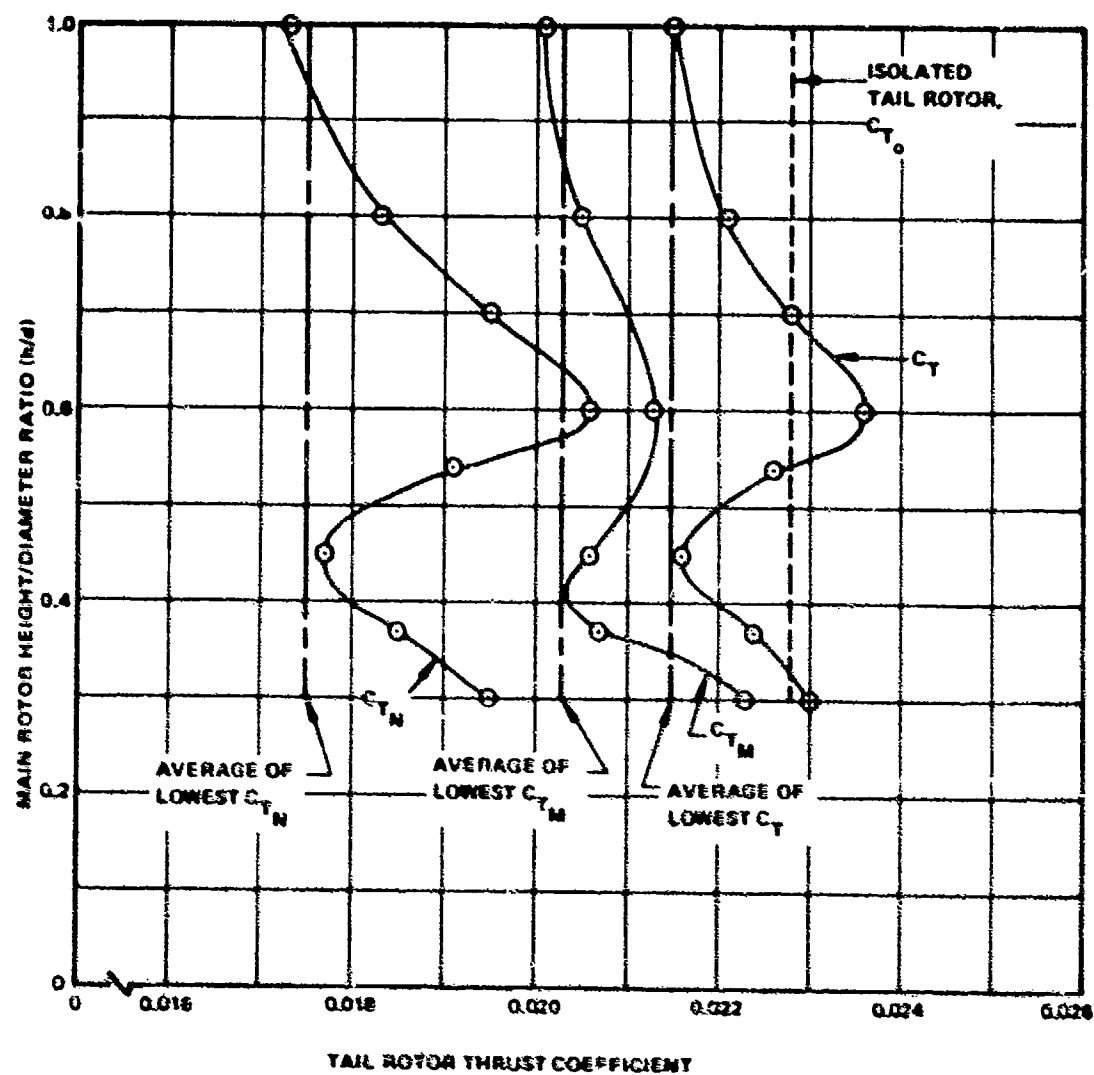
Figure 14-1. Variation of Tail Rotor Thrust With Main Rotor Height — V = 30 kn, ψ = 90°.
θ = 20°, Position = MID, Rotation = 87

131
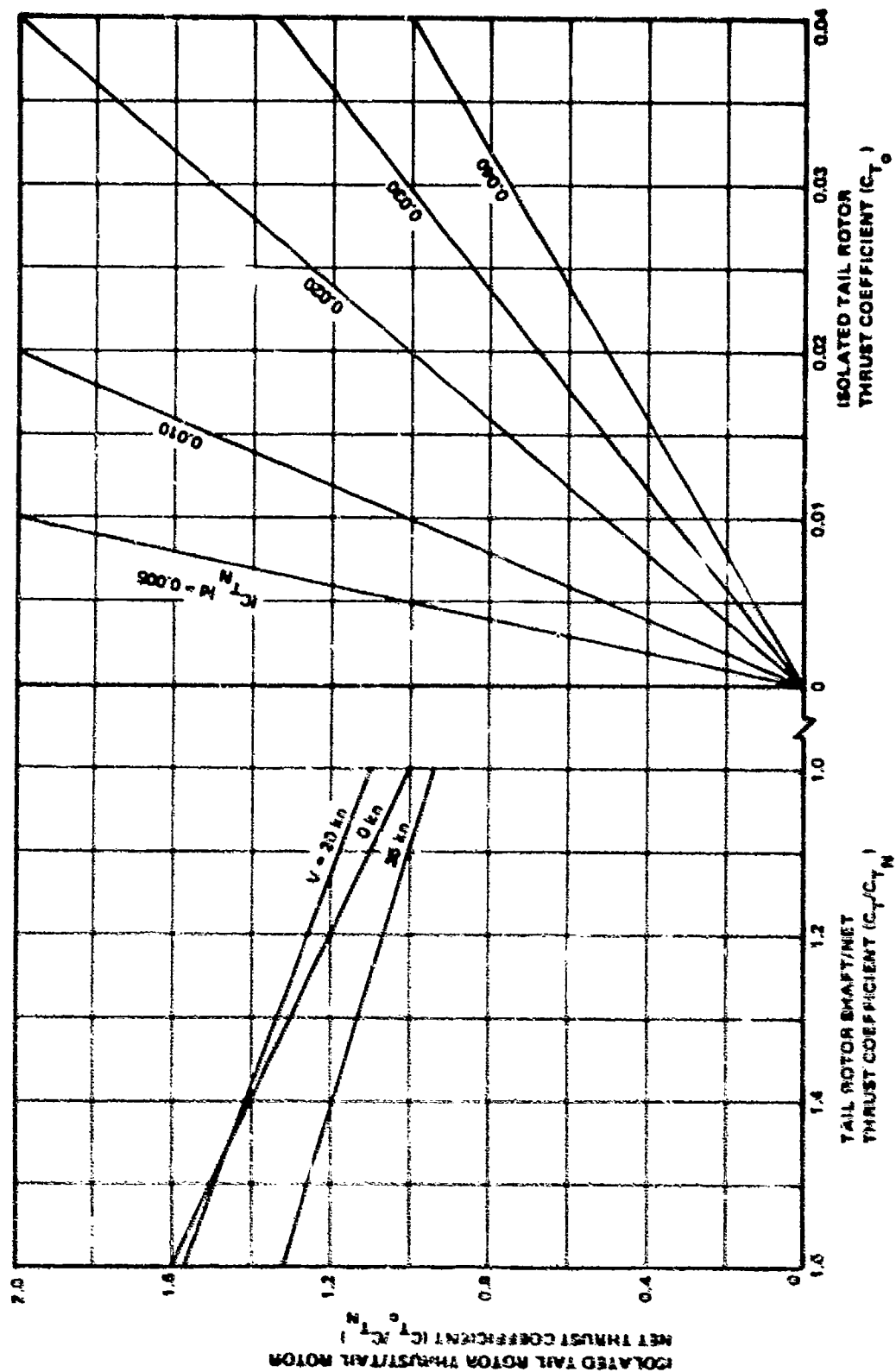
Figure 14–2. Determination of Isolated Tail Rotor Thrust.

132
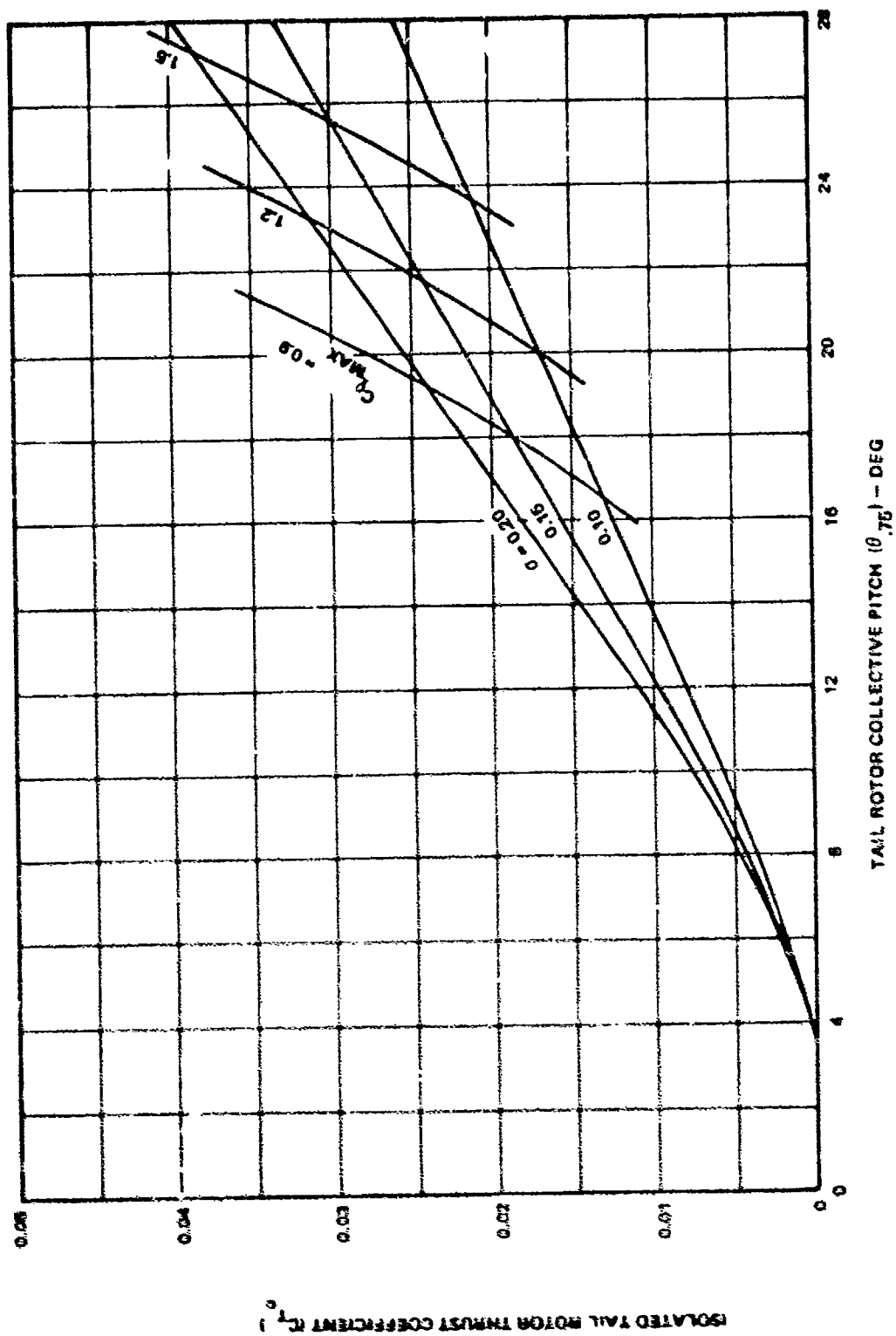
Figure 14—3. Solidity and Maximum Blade Incidence Design Chart at $\mu = 0.048$.
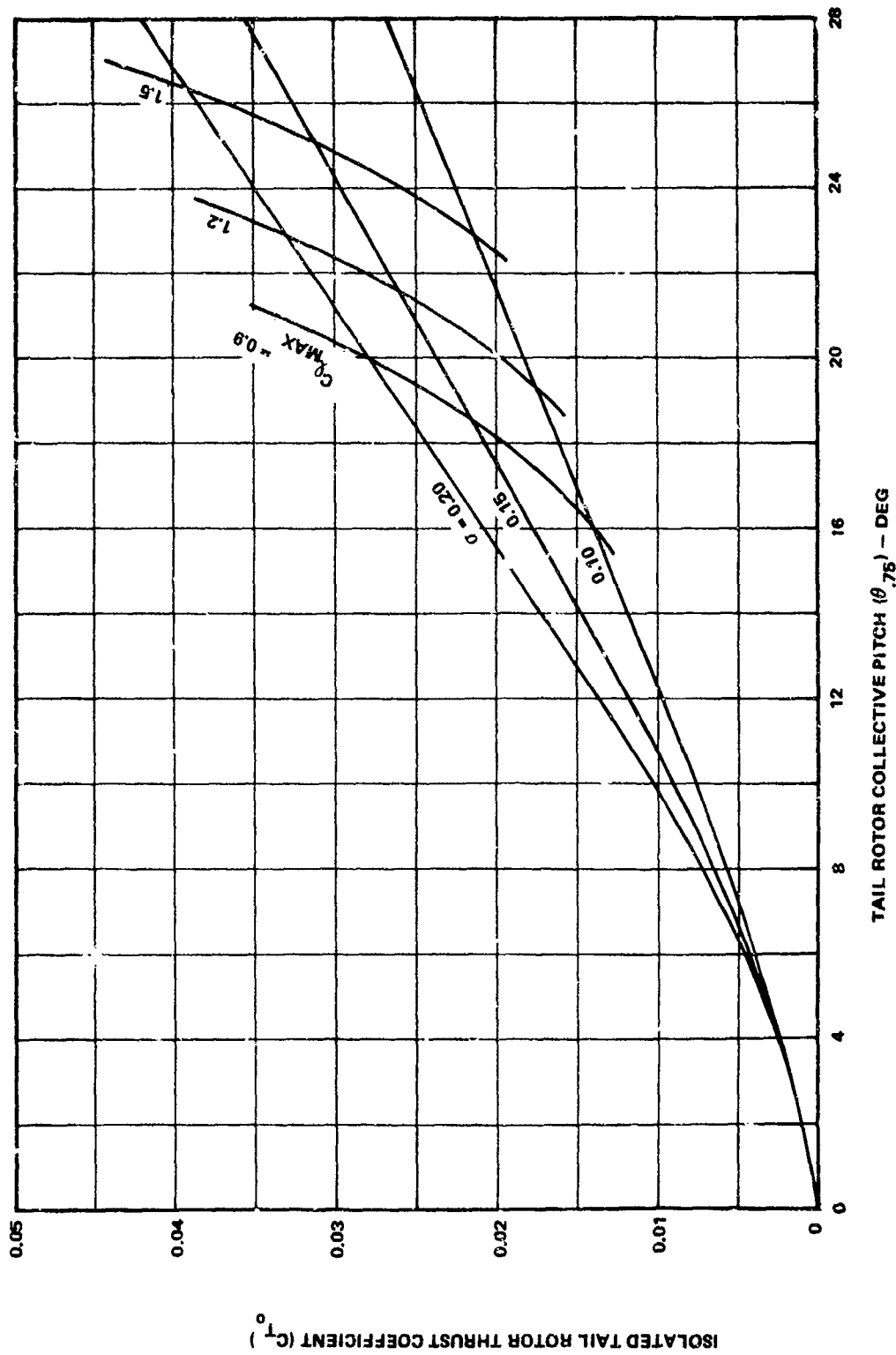
Figure 14-4. Solidity and Maximum Blade Incidence Design Chart at $\mu = 0$.
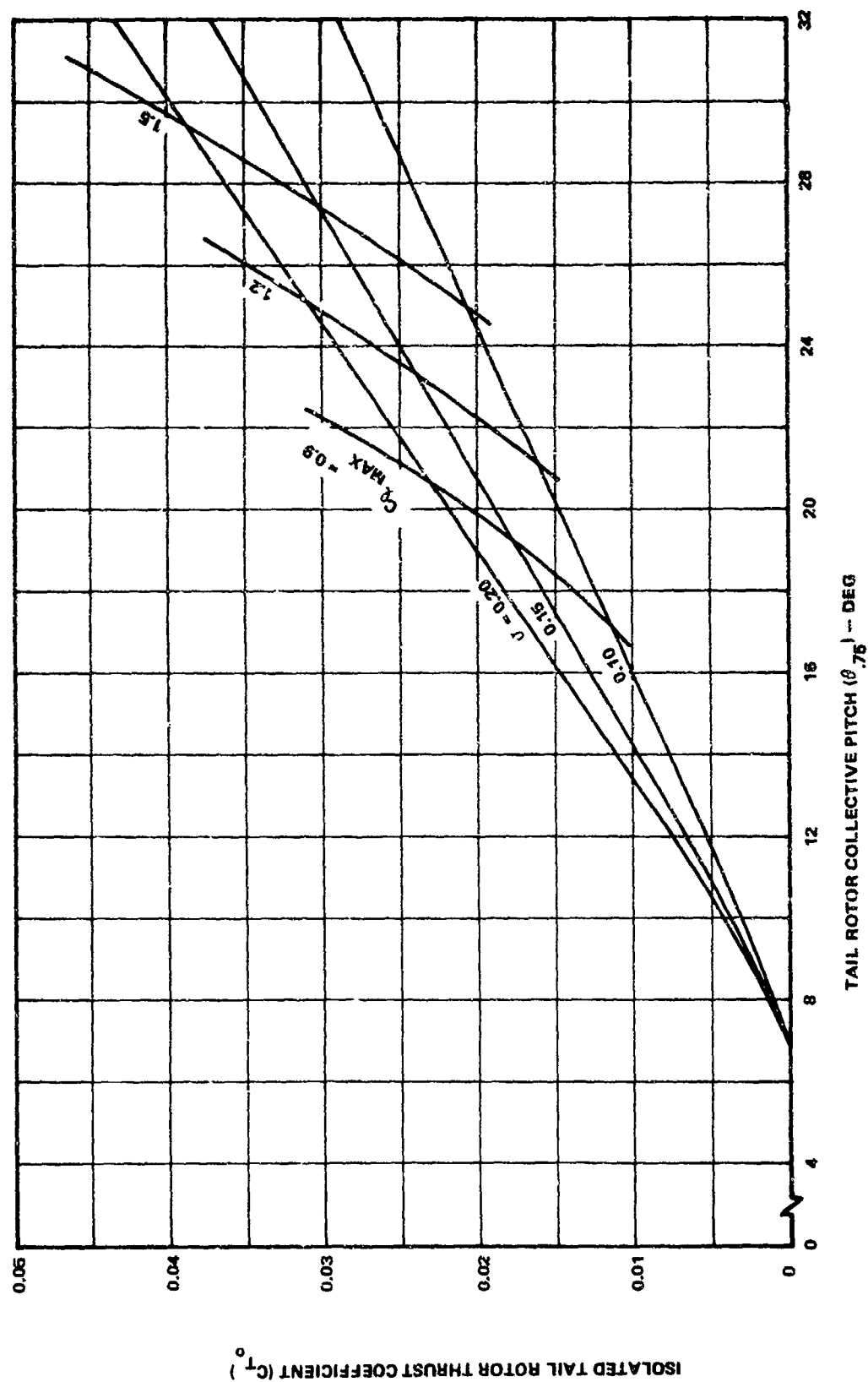
Figure 14—5. Solidity and Maximum Blade Incidence Design Chart at $\mu = 0.084$.

135
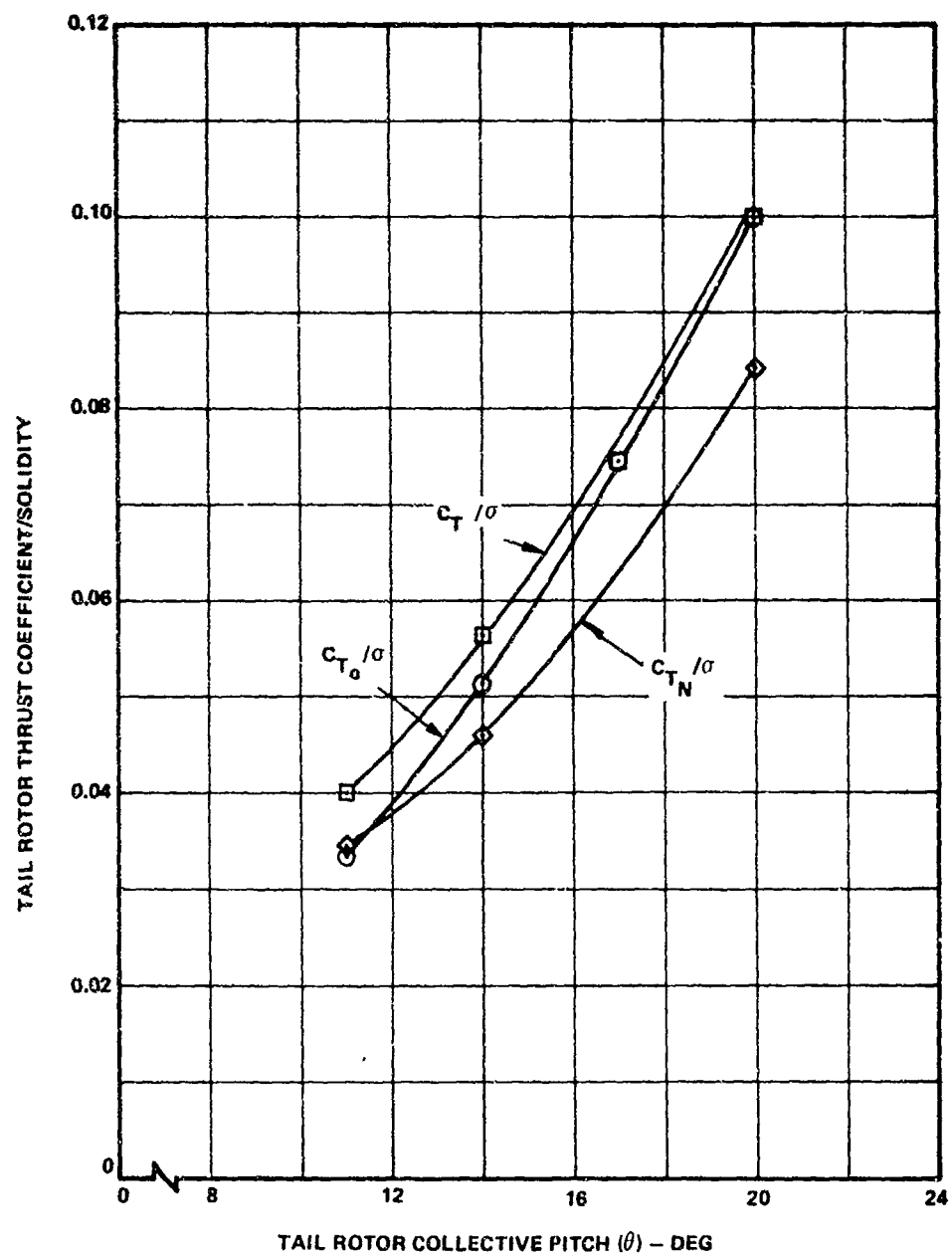
Figure 14–6. Variation of Tail Rotor Thrust/Solidity With Collective Pitch — V = 20 kn, h/d = .3, ψ = 90°, Position = MID, Rotation = BF.

136
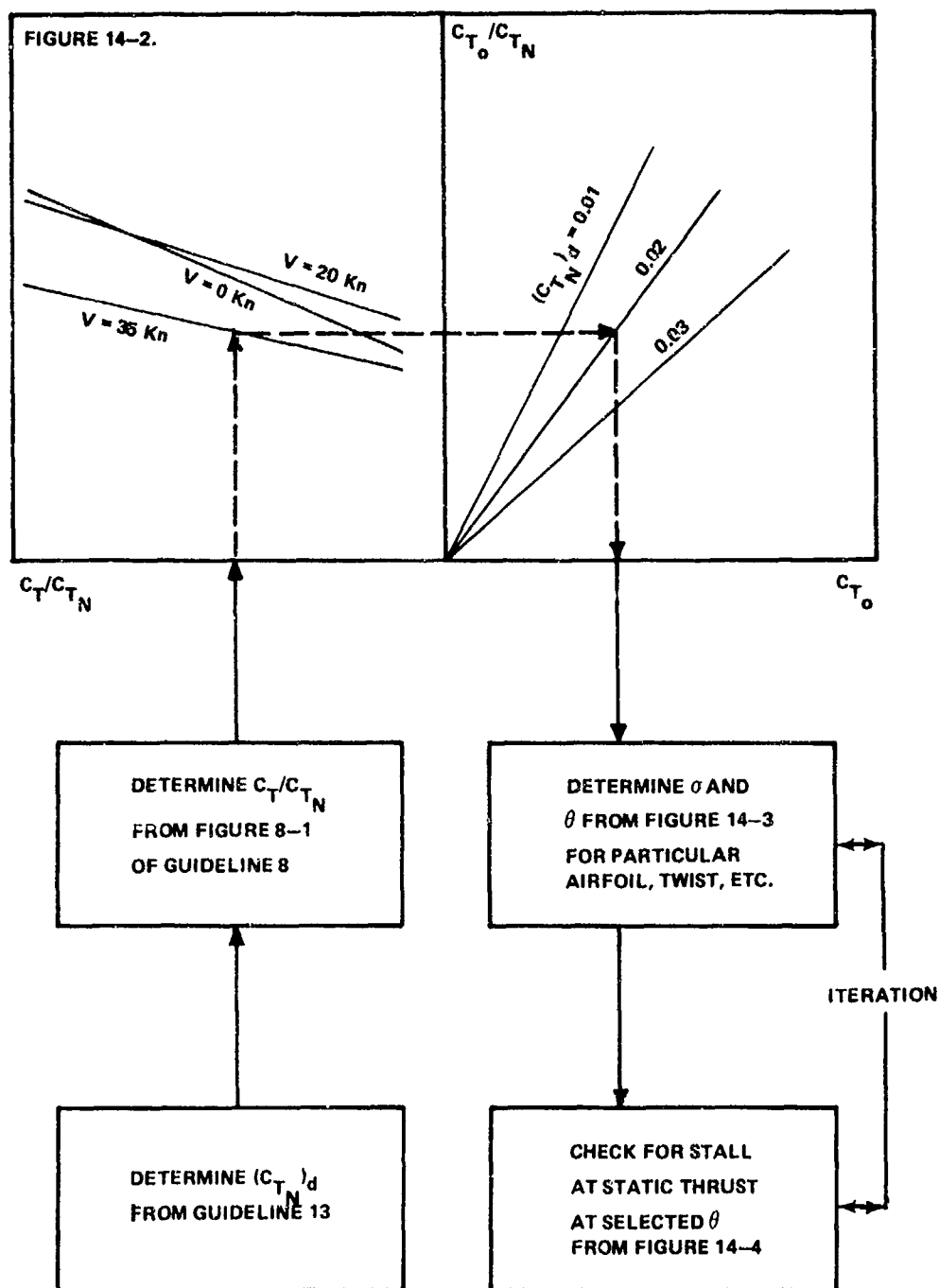
Figure 14-7. Flow Chart for Selection of Tail Rotor Collective Pitch and Solidity.

137

15.0 RIGHT PEDAL BLADE PITCH LIMIT

The objective of this guideline is to establish a method of selecting the maximum right pedal blade pitch limit. The critical operating conditions and methods of analysis are defined below.

15.1 DISCUSSION

The maximum right pedal blade pitch requirement is governed by the most stringent of the following criteria for good flying and ground handling qualities. The aircraft shall have sufficient directional control displacement and trim capability to achieve:

a. A specified yaw rate during autorotation in winds of a specified velocity from any azimuth

b. Ground taxi through 360° right turns by pivoting on one of the main landing gears in winds of a specified speed

c. A left sideslip envelope of required slideslip angles versus flight speed

When turning to the right or entering a left sideslip, the tail rotor produces thrust in the direction opposite to that for normal trim conditions. The reversed tail rotor slipstream effectively alters a pusher configuration to a tractor with greater fin loss (see Guideline 8).

Procedures similar to those used to determine maximum left pedal (Guideline 14) are used to determine the maximum right pedal required to satisfy a above.

From Boeing test results, it was determined that at $\psi = 60^{\circ}$, the relationship between C_T/C_{T_N} and C_{T_O}, given in Figure 14-2, applies to the tractor configuration as well as the pusher. The difference between the pusher and tractor configurations appears in the C_T/C_{T_N} ratio. Since from Guideline 4 the tractor with positive blade incidence produces minimum thrust at $\psi = 60^{\circ}$, it can be expected from symmetry that a pusher tail rotor with constant negative incidence will produce minimum thrust at $\psi = 300^{\circ}$. Thus for negative blade incidence, the relationship of Figure 14-2 will apply to the pusher at $\psi = 300^{\circ}$ if the C_T/C_{T_N} ratio is determined from the tractor curves of Figure 8-1.

Taxiing turns (b above) require tail rotor thrust to counteract the friction forces and moments that develop on all wheels. The most demanding right-turn case occurs when the main rotor

139

Preceding page blank

is near zero thrust and producing torque commensurate with minimum rotor profile power. The tail rotor thrust required in zero wind for such a condition can be expressed by

$$-T_{TR} = \frac{1}{\ell_g} \left\{ \mu_s \left(\frac{GW}{2}\right) \left[1 - \frac{\ell_m - x}{\ell_x} \right] \ell_{eff} \right.$$

$$+ \mu_r \, GW \left[a + (a - \ell_x) \, (\frac{\ell_m - x}{\ell_x}) \right]$$

$$\left. - \frac{\sigma_{MR} \, \delta}{8} \, \rho A V^2_{T_{MR}} \, R \right\} \tag{15-1}$$

where μ_s = static-steering friction coefficient, determined from Figure 15-3

μ_r = rolling friction coefficient, = 0.1 for medium hard soil
= 0.01 for concrete
= 0.3 for sand

ℓ_{eff} = effective torque arm

$\ell_{eff} = e^2 + f^2/8$

(e is kingpin offset, f is main gear tire width; see Figure 15-2)

ℓ_m = distance between main gear and main rotor centerline

x = distance from main rotor centerline to forward cg limit for tail wheel gear or aft cg limit for nose wheel gear

ℓ_x = distance between auxiliary gear wheels (station line)

a = distance between main gear wheels

ℓ_g = distance between tail rotor centerline and main gear (station line)

δ = main rotor average profile drag coefficient

The first term of this equation is wheel turning torque, the second is wheel rolling friction torque, and the third is main rotor torque. This equation is applicable for either conventional tricycle gear or nose gear with two aft main gears. The

140

moment developed on the particular main gear about which the ship is pivoting is caused by static-steering friction. This friction is a function of the gear geometry and can amount to 10 to 100 percent of total friction torque depending on ground conditions.

In addressing c above, minimum sideslip envelope, trim analyses that cannot be presented in this report are conducted along the limits of the sideslip envelope. These analyses encompass the most critical combination of sideslip and airspeed to determine the maximum negative thrust and blade pitch requirements. This requires a comprehensive technical description of the configuration under consideration, including the fuselage and vertical fin aerodynamic characteristics. It is noteworthy that designing the fin to unload the tail rotor during level forward-flight conditions will increase negative blade pitch requirements for trim during left sideslip flight.

15.2 GUIDELINE

To assure adequate directional control displacement and trim capability, the maximum right-pedal blade pitch should be established by the most critical of the following cases:

A. For a right yaw rate of, for example, 15 deg/sec in 1.5 seconds, during autorotation in winds up to 35 knots at any azimuth, the calculation procedure is:

1. Select the value of yaw rate damping from Figure 13-2.

2. Estimate the ratio of inertia to tail arm (I_z/ℓ) from Figure 13-3.

3. Calculate $K_m = (I_z/\ell)\ \dot{\psi}_d$ and determine the peak net tail rotor thrust to produce the desired yaw rate from Figure 13-4.

4. Determine the simulated gyroscopic thrust from Figure 13-5.

5. Determine thrust required to balance the fuselage aerodynamic moment from Figure 13-6.

6. Total the above thrusts and convert to C_{T_N}, using the density at alternate gross weight hover ceiling, tail rotor radius from Guideline 6, and tip speed from Guideline 12.

7. Increase the net thrust coefficient by the amount of thrust margin desired.

141

8. Determine C_T/C_{T_N} from Figure 8-1 using the curves for tractor if the tail rotor is normally a pusher.

9. Use Figure 14-2 to obtain the isolated tail rotor thrust, C_{T_O}, corresponding to the shaft thrust determined in the previous step.

10. Maximum right-pedal blade incidence is determined from Figure 14-3 for 20 knots, Figure 14-4 for 0 knots, or Figure 14-5 for 35 knots of wind using the solidity selected for maximum left pedal in Guideline 14. For cambered airfoils, the $C_{\ell_{MAX}}$ for negative blade incidence will be less than for positive incidence.

B. For a 360° taxiing right turn, pivoting on one of the main landing gears in winds of a specified speed, the calculation procedure is:

1. Use Equation 15-1 to establish net tail rotor thrust to overcome friction loads with no wind on the type of ground surface specified.

2. Determine from Figure 13-6 the thrust required to balance the fuselage aerodynamic moment for the wind speed desired. If the wind speed is greater than 35 knots, ratio the 35-knot value by the square of the velocities.

3. Total the above thrusts. If the result is less than the sum of the thrusts obtained in step 6 of part A, the autorotational maneuver is critical and designs the right pedal blade incidence. If the result is greater than that obtained for the autorotational maneuver, convert the total thrust to C_{T_N} and follow steps 7 through 10 of part A.

C. An example of a specified left sideslip envelope is given in Figure 15-1. The maximum tail rotor thrust and blade pitch must be determined by comparing the thrust and pitch required at various speeds along the sideslip envelope, using a theoretical forward-flight trim analysis.
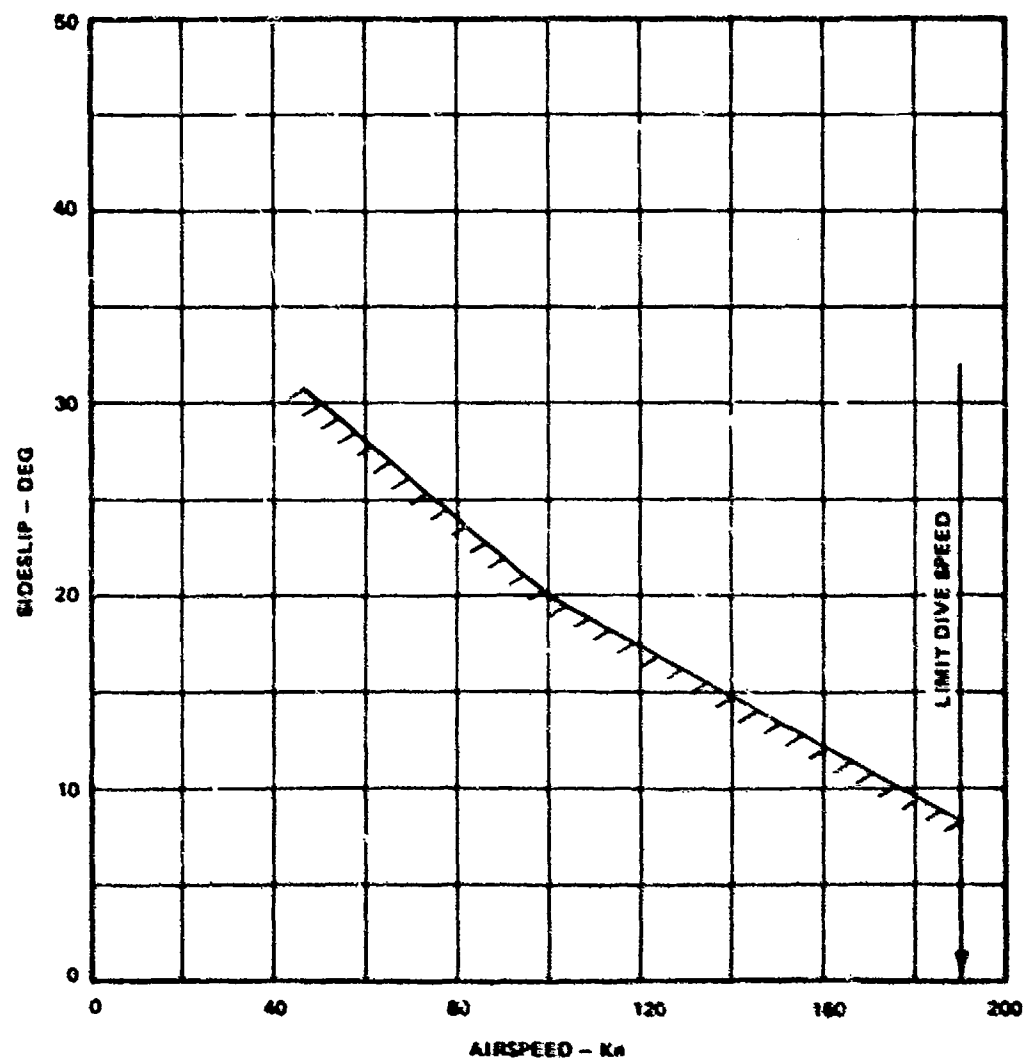
Figure 15-1. Example Sideslip Envelope.

143

RADIUS OF GYRATION

FOOTPRINT AREA

KINGPIN OFFSET

KINGPIN AXIS
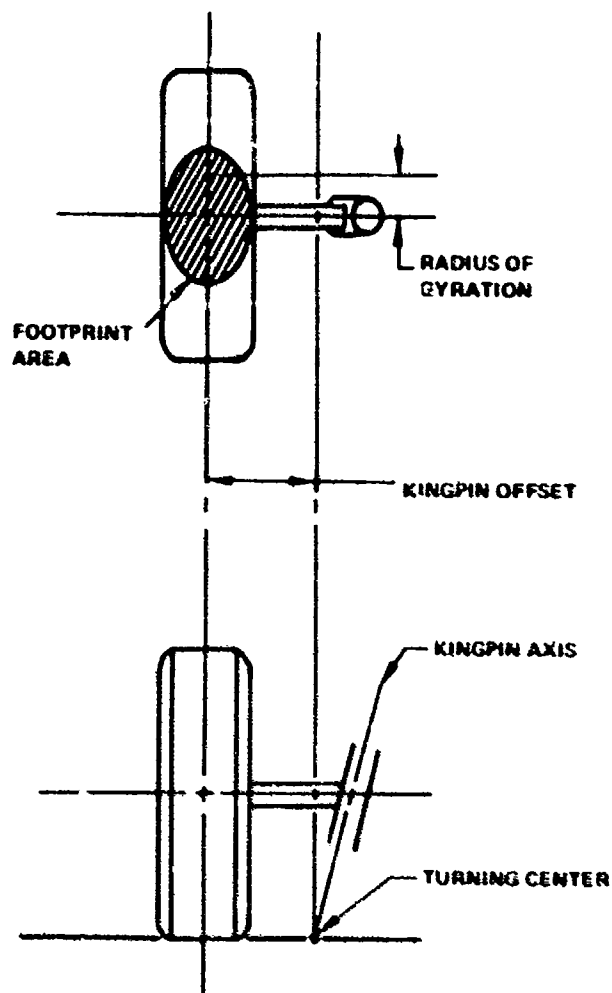
TURNING CENTER

NOTE: ACTUAL TURNING CENTER OF A STEERED WHEEL IS THE INTERSECTION OF THE KINGPIN AXIS WITH THE GROUND. STEERING MOTION OF THE WHEEL AROUND THIS POINT COMBINES WHEEL SLIDING AND ROTATION.

Figure 15-2. Landing Gear Characteristics.

144
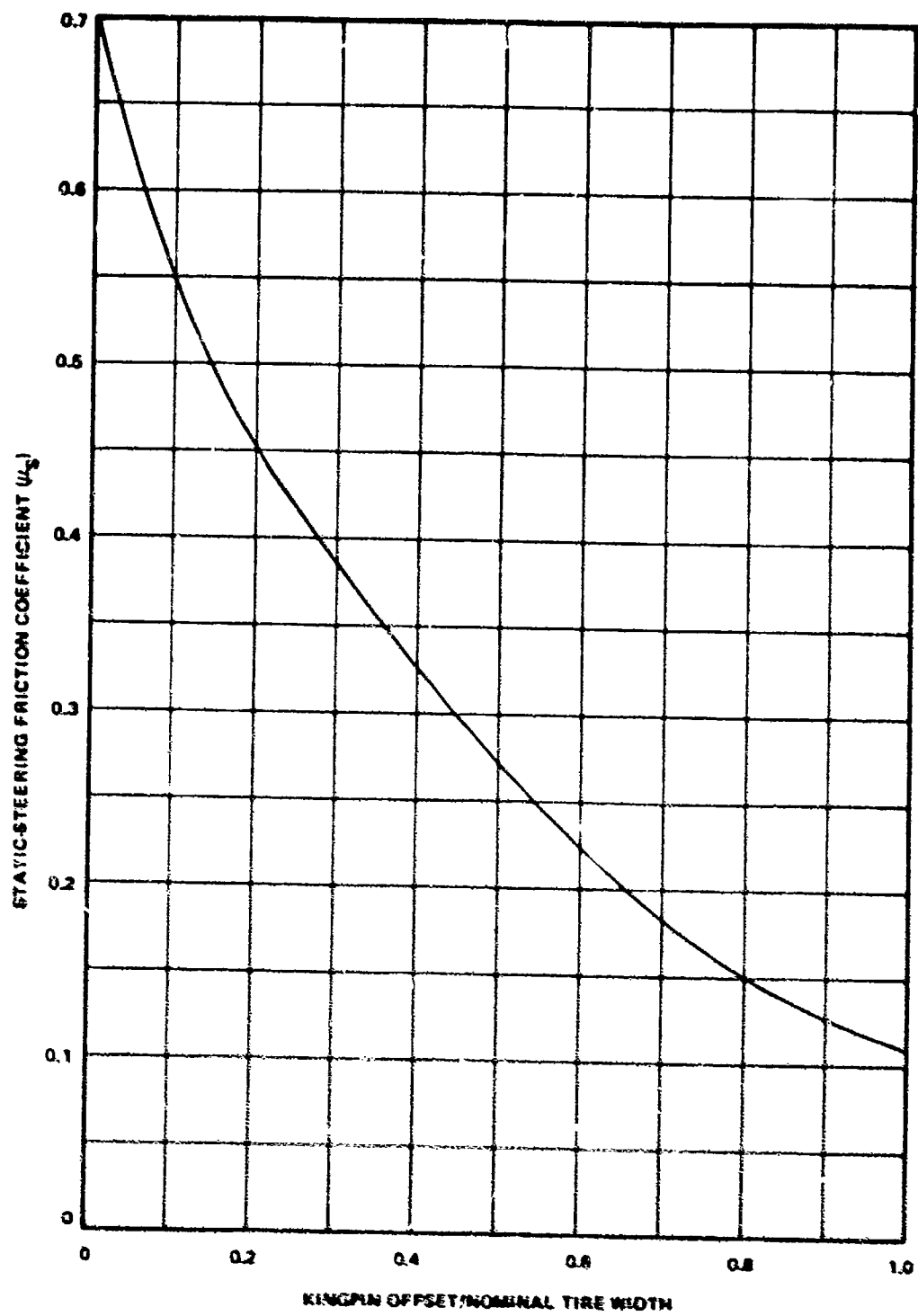
Figure 16-3. Static-Steering Friction Coefficient.

145

16.0 DESIGN POWER

This guideline presents data relative to the tail rotor power requirements for use in calculating (1) total helicopter performance such as hover ceiling in winds from zero to 35 knots and (2) the value of power that should be used to design the drive system.

16.1 DISCUSSION

Tail Rotor Power for Performance Calculations

Boeing test data was reduced to compare the power required by the tail rotor in the presence of the main rotor and fin to that required for the tail rotor alone. The reason for such comparison is that isolated tail rotor power can be calculated by the usual blade element theory, and then factors from Boeing tests can be applied to determine the actual power required in the presence of the main rotor and fin.

Figure 16-1 shows multiplying factors (derived in Appendix III) that should be applied to isolated tail rotor calculated power to give actual power in the presence of the main rotor and fin. It should be noted that for headwinds, the multiplying factors are near unity and, therefore, the usual power-required methods can be used; but for winds from the right front critical azimuth (see Guideline 4), considerably more power is required by the tail rotor to develop a given thrust. The power multiplying factors for fin blockage ratios other than the 0.207 in Boeing tests were obtained by assuming that the fin loss (and thus net thrust) varies directly with the fin blockage factor. The power multiplying factor will, therefore, vary as the fin blockage factor to the 1.5 power. Note that the values in Figure 16-1 are based on a C_d near 2.0 and therefore may be conservative; also, values are for $s/r \approx 0.45$.

Figure 16-2 shows a chart for $V = 20$ knots and $\psi = 90^\circ$ of isolated tail rotor C_{T_0} versus C_P for various solidities from which, for a given ωr, the value of $HP/\rho \pi r^2$ can be determined. The right side of Figure 16-2 was obtained by use of the rotor performance program described in Reference 10. Such figures should be prepared for the given airfoil selected to serve, together with Figure 16-1, as the basis for aircraft performance calculation.

Maximum Tail Rotor Power

To design the static strength of the tail rotor and drive system, the horsepower absorbed by the selected tail rotor under full left pedal at full rpm should be calculated. The

147

aircraft is assumed to be on the ground with the main rotor at zero collective pitch. Previous experiences have shown that horsepower required under such conditions exceeds the maximum that will be experienced in flight, since the aircraft will yaw in flight and reduce the power requirement under full left-pedal application. The flight maneuver that will approach this power value is rapid arrestment of a right turn in hover. Such a maneuver should be examined, but it is not considered in this guideline. Figure 16-3, also obtained by the methods of Reference 10, shows the design chart of isolated C_{T_0} versus Cp for V = 0 for various solidities and tip speeds from which maximum static thrust horsepower can be determined.

16.2 GUIDELINE

Construct the right side of the power charts (Figures 16-2 and 16-3) for the airfoil selected. To get actual power required by the tail rotor in the presence of fin and main rotor for performance estimation, apply the multiplying factor from Figure 16-1 to the isolated tail rotor power constructed from Figure 16-2. For static design strength, obtain the isolated static power under full left pedal from Figure 16-3.
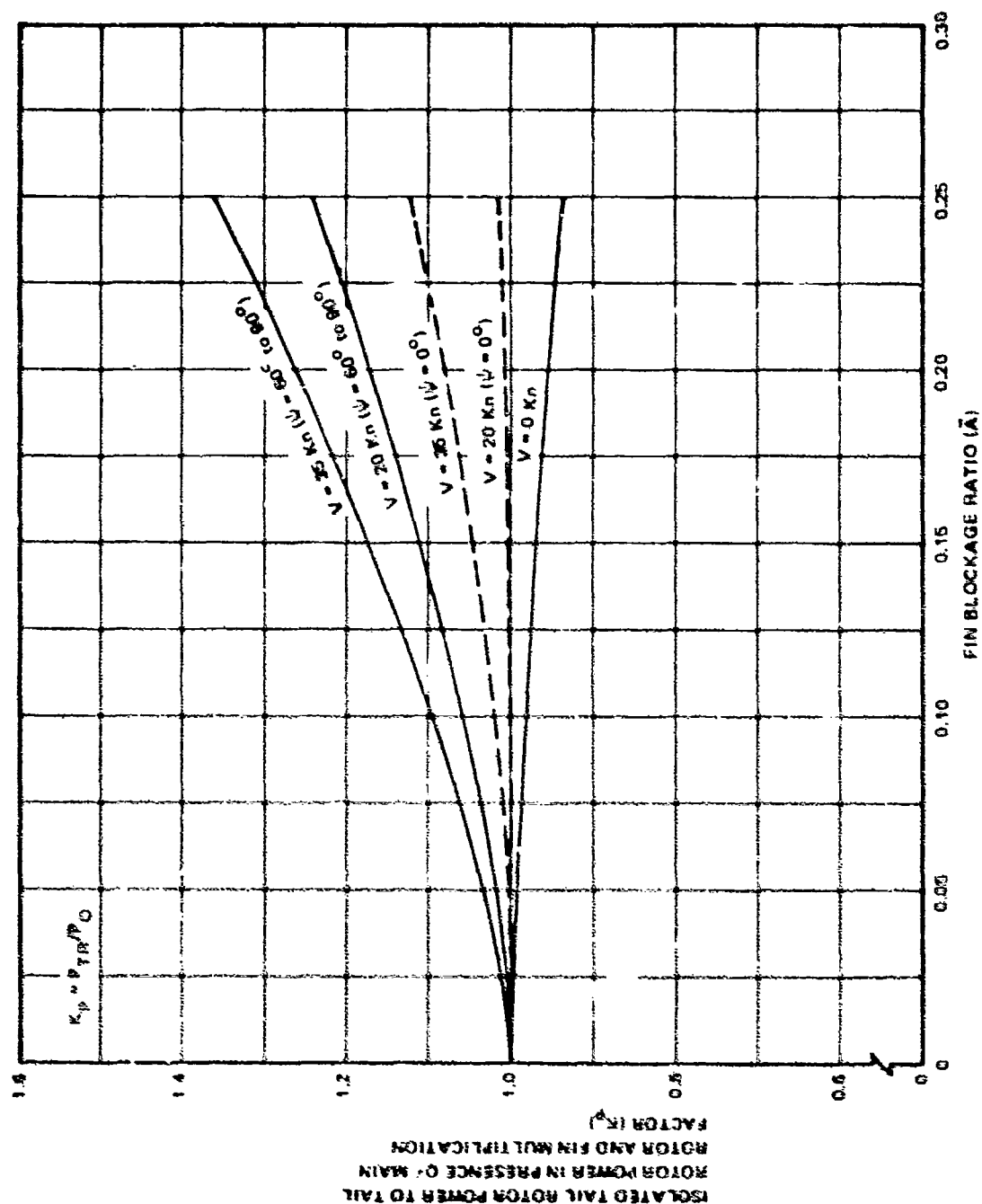
Figure 16—1. Determination of Tail Rotor Power in Presence of Main Rotor and Fin From Isolated Tail Rotor Power – $h/d = 0.3$, $\theta = 20^\circ$, Rotation = BF, $C_\sigma \cong 2.0$, $J/r = 0.45$.

149
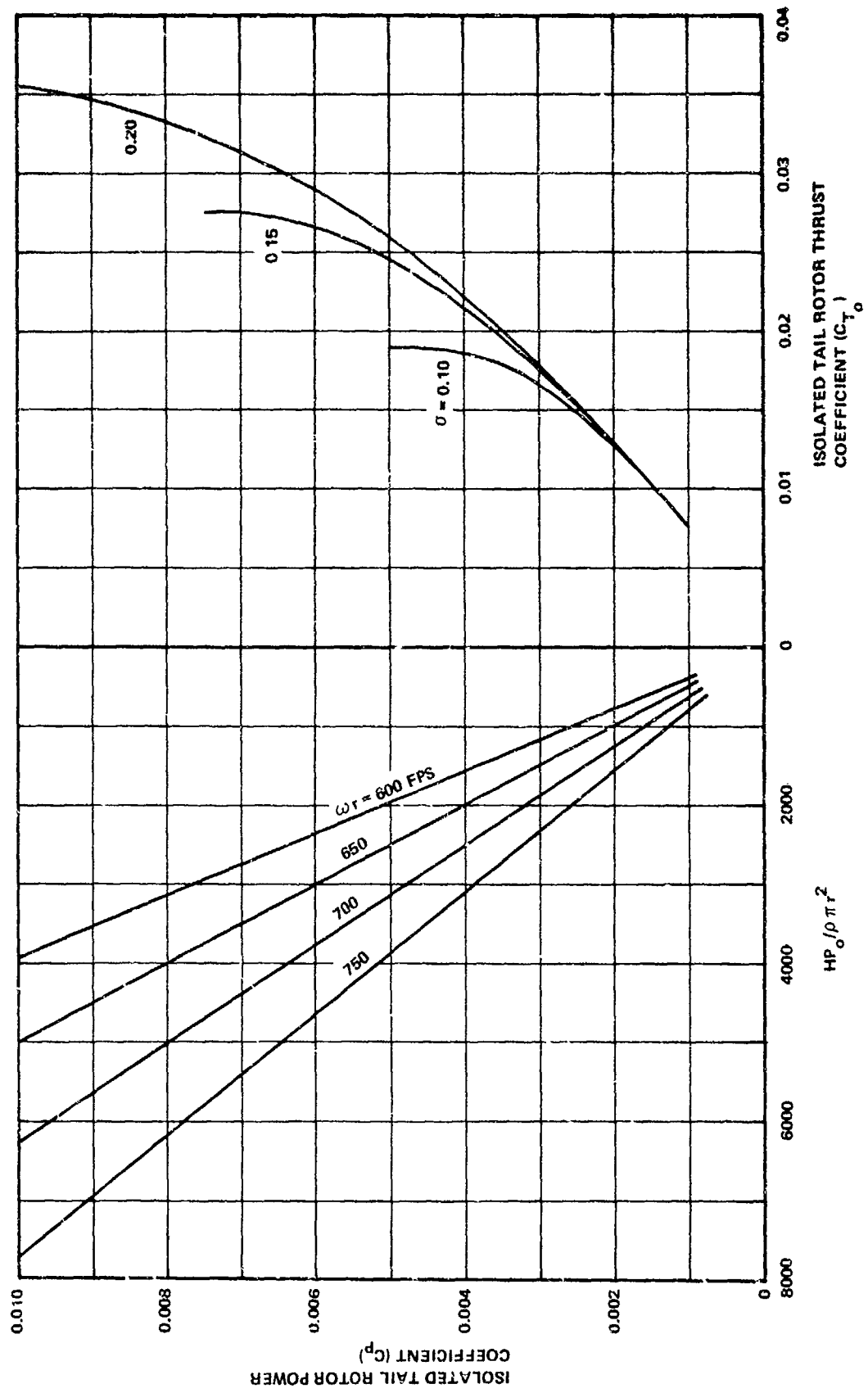
Figure 16–2. Determination of Maximum Static Thrust Horsepower at $\mu = .046$, $\psi = 90°$.

150
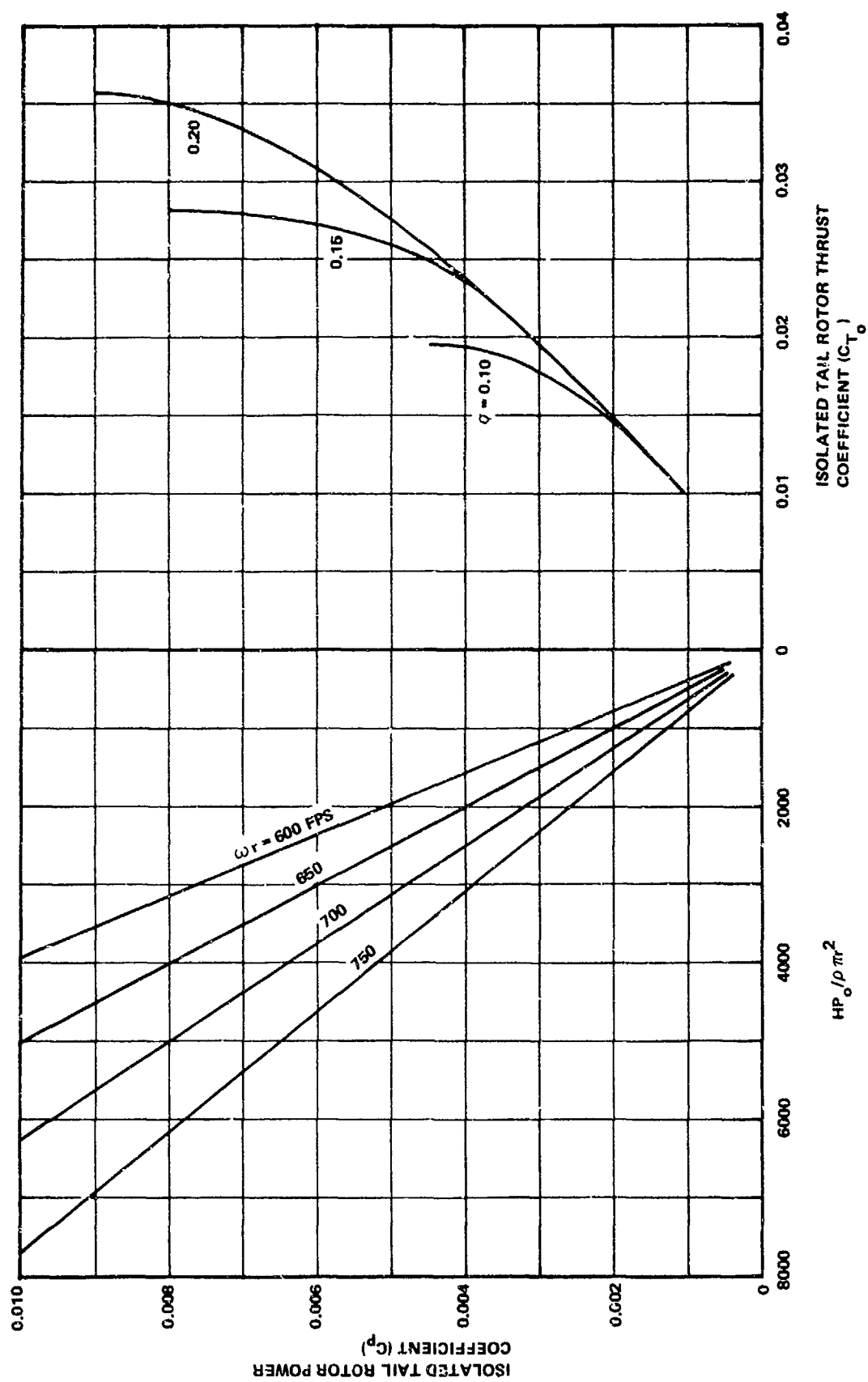
Figure 16–3. Determination of Maximum Static Thrust Horsepower at $\mu = 0$.

151

17.0 PITCH-FLAP COUPLING, δ_3

The objective of this section is to define a procedure for the selection of tail rotor pitch-flap coupling, δ_3, requirements. The primary benefit of tail rotor δ_3 is in the reduction of blade flapping relative to the shaft axis and the resulting decrease in blade and pitch link loads. Secondary factors that must be considered with tail rotor δ_3 include:

- Helicopter directional stability

- Rotor blade stability (in-plane and flap)

- Coupled tail boom - rotor aeroelastic instability

- Blade flutter

- Rotor-fin clearance

17.1 DISCUSSION

As typified in Figure 17-1, first harmonic blade flapping decreases with both negative (up flap - decrease blade angle) and positive (up flap - increase blade angle) δ_3. An increase in effective flap hinge offset will also decrease blade flapping for both $+\delta_3$ and $-\delta_3$. This reduction in blade flapping will tend to decrease blade and pitch link loads and increase blade-fin clearance.

Because $-\delta_3$ reduces the tail rotor thrust variation with shaft angle of attack at fixed collective, there is a reduction in the unaugmented helicopter directional static stability. With a conventional directional stability augmentation system this effect is generally small.

Generally, $-\delta_3$ will have a favorable effect on blade stability and blade flutter characteristics. Because $-\delta_3$ increases the effective flap natural frequencies as a function of advance ratio, some blade instability characteristics (such as the scissors mode) have been encountered. Although these instabilities may be eliminated by changing the value and/or sign of δ_3, this would represent a design compromise.

Coupled tail boom-rotor aeroelastic instabilities have also been encountered. This is the result of mismatching the tail boom lateral-torsional natural frequencies with the blade flap natural frequencies. Again, these instabilities may be corrected by varying the blade flap natural frequency by changing δ_3. Proper selection of the blade flap, chordwise and torsional

153

natural frequencies with the value of δ_3 based on the flapping criteria would minimize these design compromises.

With a pusher tail rotor configuration, blade-fin clearances are increased due to the reduced flapping resulting from a δ_3 hinge. With a tractor tail rotor configuration, this would not be a factor.

17.2   GUIDELINE

Tail rotor δ_3 angles of -45^0 (flap up - decrease blade angle) have proven to be successful on many existing helicopters, and for preliminary design purposes this represents a good baseline value. δ_3 can be used to separate first flap frequencies from in-plane natural frequencies. In such cases, positive δ_3 should be considered. When designing the tail boom and tail rotor aeroelastic characteristics, δ_3 should be included as a variable in the analysis to help eliminate frequency mismatches.
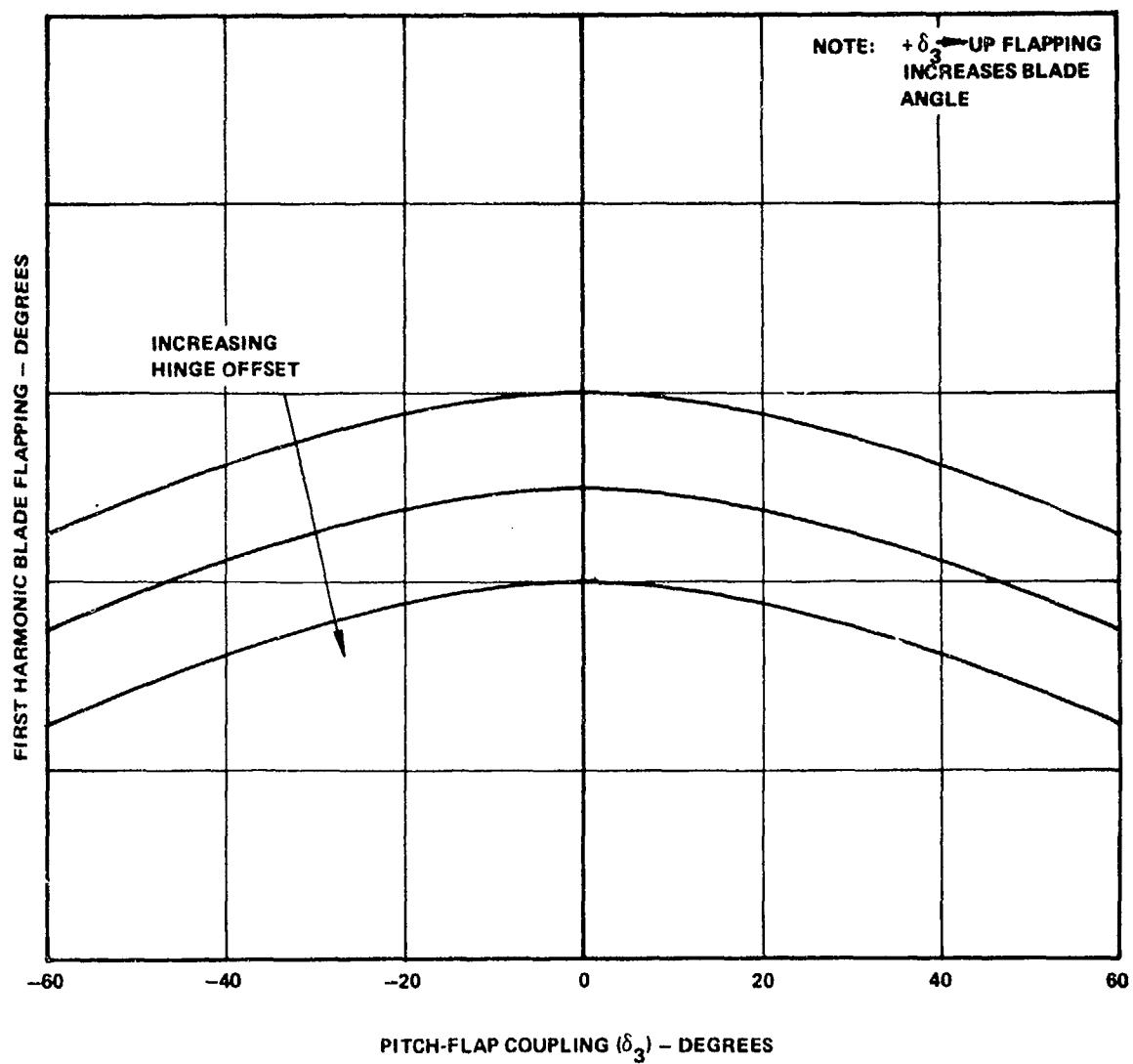
Figure 17−1. Effect of Pitch-Flap Coupling on First Harmonic Blade Flapping (High Speed).

155

18.0   TAIL ROTOR SHAFT SWEEP

The objective of this section is to outline a procedure to
determine a favorable amount of tail rotor shaft sweep (fore
and aft); i.e., a procedure which gives a minimum rudder pedal
travel difference between hover and high-speed forward flight.
The helicopter characteristics and considerations that should
be investigated when selecting a tail rotor shaft sweep
include:

- Tail rotor flapping relative to the shaft axis and the
  resulting blade and pitch link loads

- High-speed tail rotor collective (and thrust) required for
  trimmed flight

- Tail rotor blade-fin clearance

- Effect on sideslip envelope for a given amount of
  collective

- Power transmitted through the tail rotor drive system

18.1   DISCUSSION

Figure 18-1 shows that the effect of tail rotor shaft sweep on
blade flapping and the resulting blade and pitch link stresses
are significant at high advance ratios. This data, based upon
a zero sideslip condition and constant thrust, represents a
typical trend. This data indicates that for a pusher config-
uration, forward shaft sweep reduces the flapping and, there-
fore, blade stresses. The blade flapping resulting from shaft
sweep must be calculated for the particular configuration
under consideration to include the effect of the fin size,
camber, and incidence.

Figure 18-2 shows typical tail rotor collective requirements
as a function of airspeed and tail rotor shaft sweep. Depend-
ing upon the maximum speed requirements, a particular tail
rotor sweep angle can be selected to minimize the pedal trim
requirements with airspeed. For the example shown, aft shaft
sweep gives less pedal travel between hover and high speed
(160 knots). Vertical fin size and incidence effects on tail
rotor collective requirements at higher speed should be
evaluated.

Figure 18-3 indicates that the tail rotor shaft power required
for trim at high advance ratios can be reduced with a moderate
amount of forward shaft sweep. Vertical fin size and incidence
accomplish a similar effect.

157

Preceding page blank

18.2 GUIDELINE

It appears that a moderate amount of forward shaft tilt (5°)
could be beneficial for a conventional single-rotor helicopter.
This would tend to reduce the high-speed pedal and shaft power
required for trim. Because the design of the vertical tail
could accomplish a similar result, a trade-off study should be
conducted for the configuration under consideration. Forward
shaft sweep effects on blade stresses must be considered.
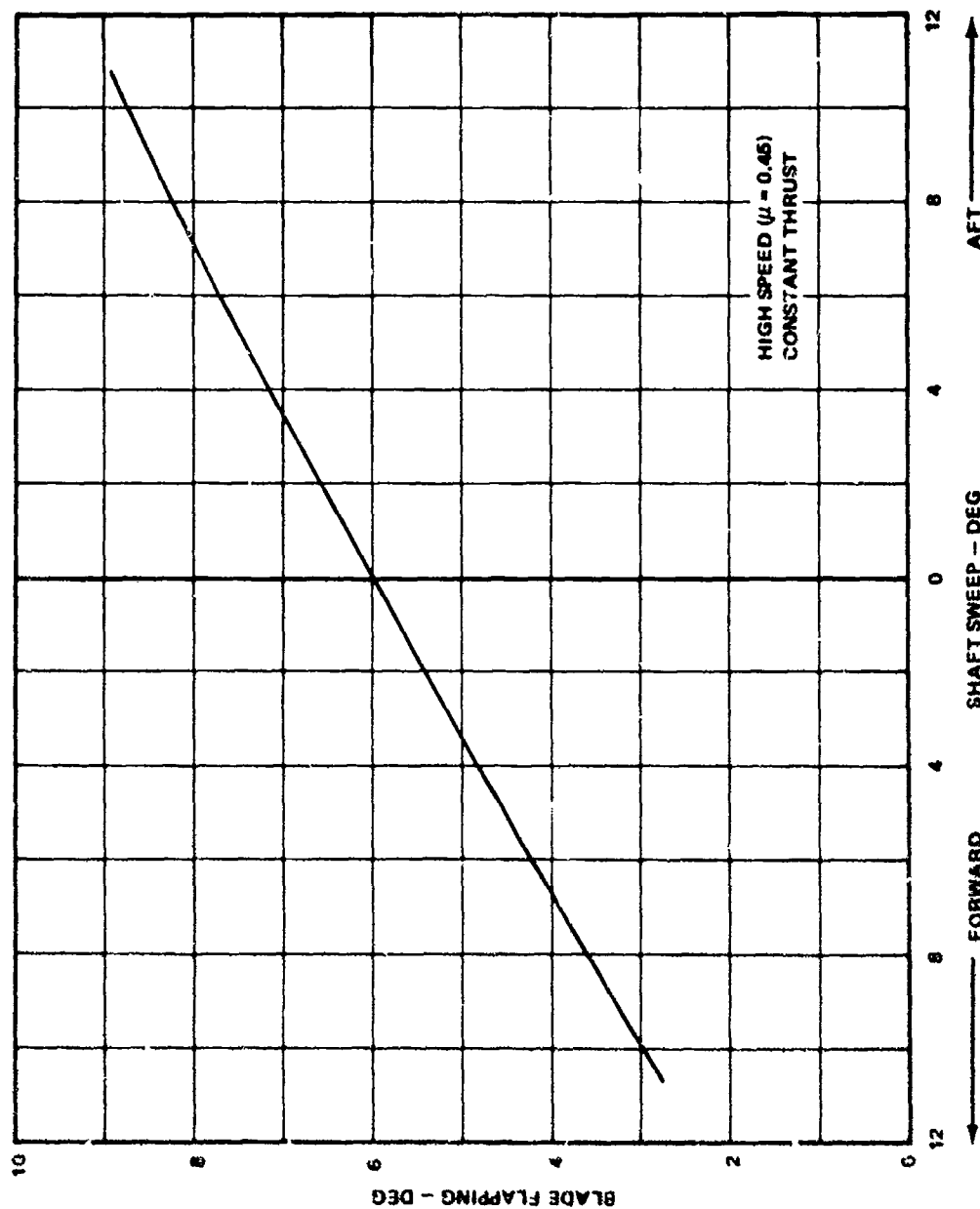
Figure 18—1. Effect of Tail Rotor Shaft Sweep on Blade Flapping (Typical Trend).

159
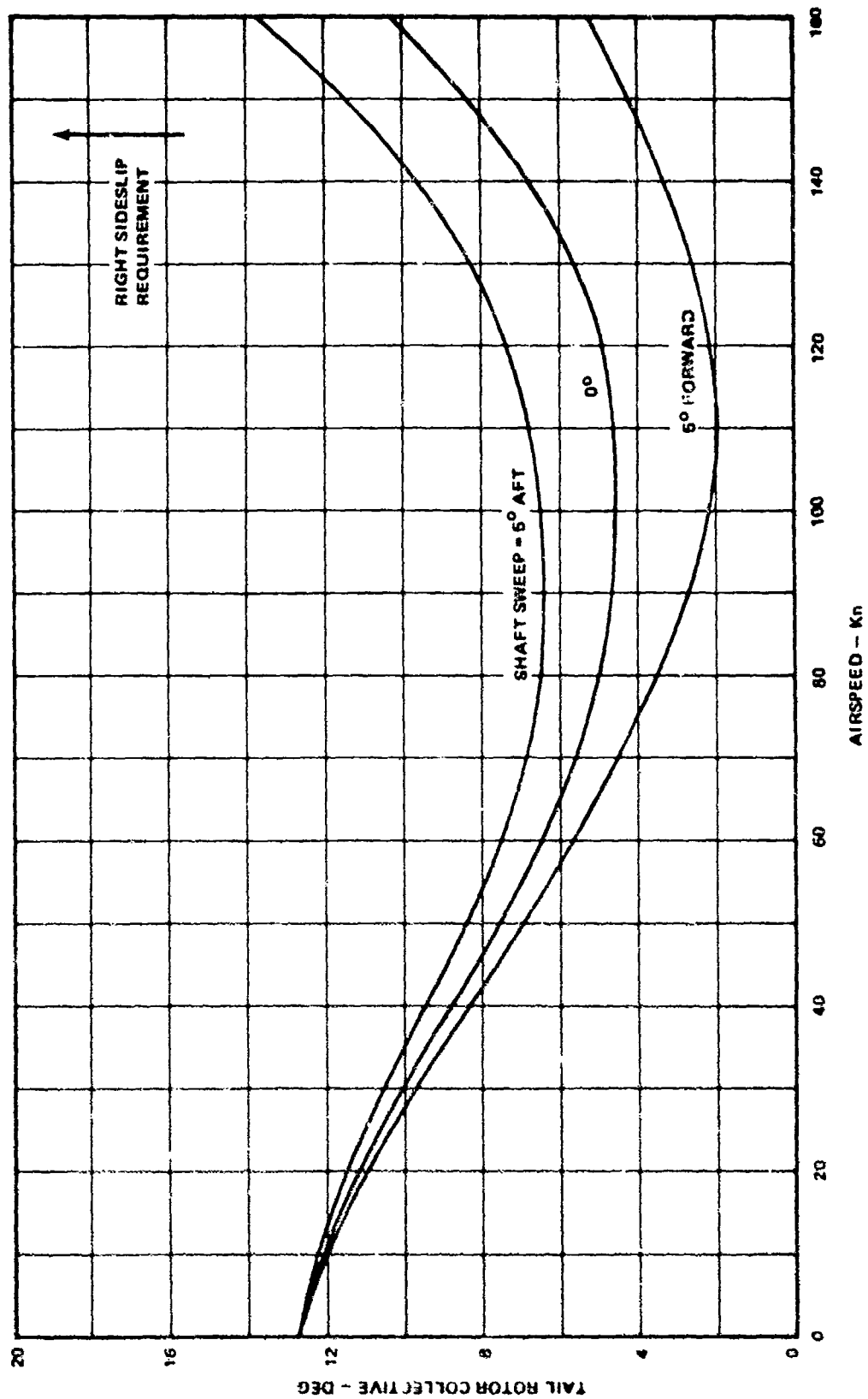
Figure 18–2. Effect of Tail Rotor Shaft Sweep on Tail Rotor Collective.
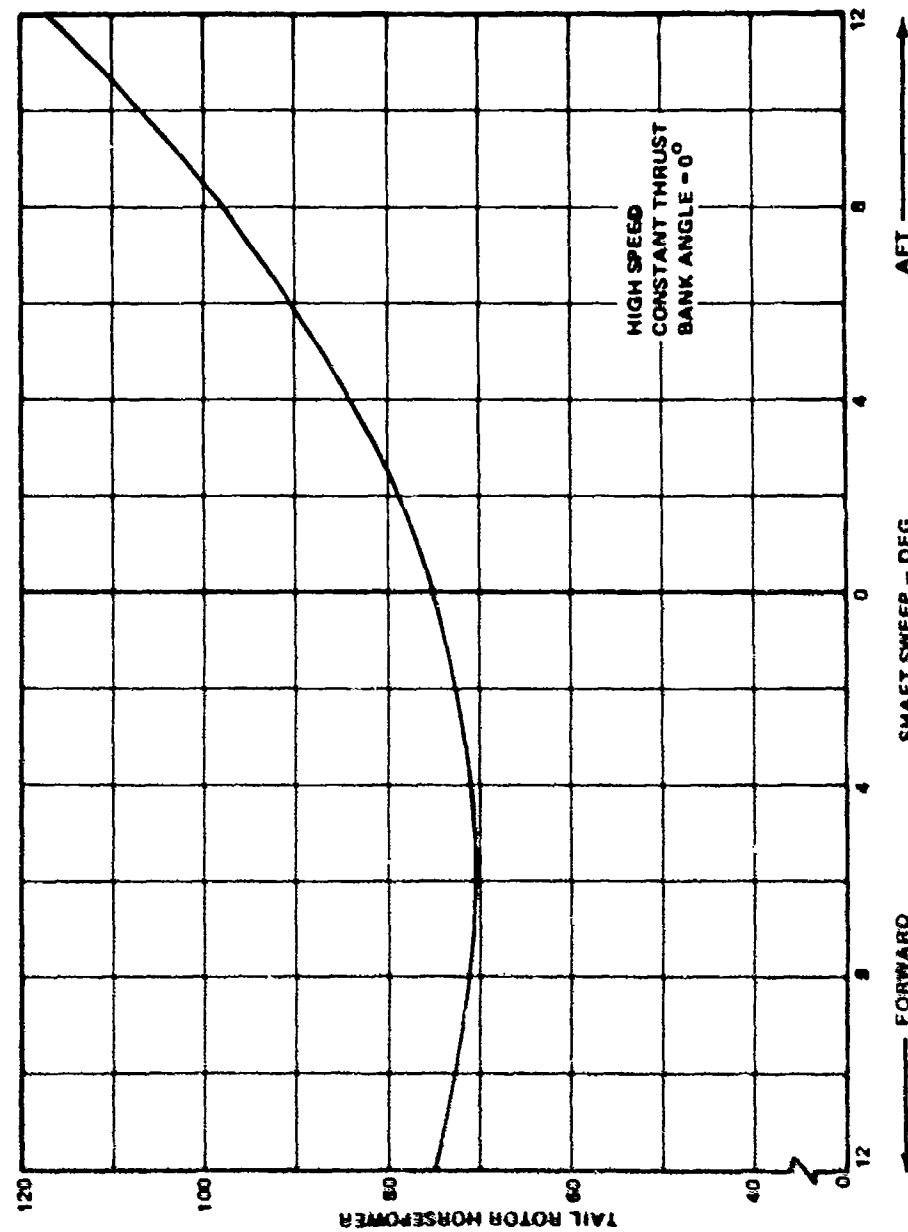
Figure 18—3. Effect of Tail Rotor Shaft Sweep on Tail Rotor Power Required (Typical Trend).

161

19.0   DIRECTIONAL CONTROL RATE LIMITING

The objective of this guideline is to outline a procedure for
selecting a directional control rate limit. The amount of
rate limiting must not inhibit the aircraft's ability to sat-
isfy the short-period maneuver requirements. The potential
benefits derived from directional control rate limiting
include:

- Reduction in peak transient blade flapping

- Reduction in peak blade, control linkage, and drive system
  loads

- Reduction in helicopter response to hardover directional
  control failure

19.1   DISCUSSION

As shown in Figure 19-1, a substantial limitation on direc-
tional control input rate capability will have a negligible
effect on airframe response. The amount of directional con-
trol rate limiting that can be tolerated without compromising
maneuver requirements is primarily dependent upon the aircraft
yaw-control sensitivity and yaw-rate damping.

A primary benefit to be attained from pedal rate limiting is a
reduction in transient blade flapping for high-speed maneuver-
ing. Typical blade flapping characteristics for pedal inputs
at high speeds are shown in Figure 19-2. Associated with this
flapping are high blade stresses and control-linkage loads.
With the conventional demand antitorque system, high drive
system loads can also be generated.

With a pure control rate limit, the control input envelope
will assume the contour of the dashed lines in Figure 19-3.
Further limiting can be imposed, as shown by the solid enve-
lope, that will not compromise the stability or maneuver re-
quirements. This further limiting will reduce peak transient
flapping and enhance flight safety characteristics in the
event of a hardover failure. The implementation of this con-
trol limiting will depend upon the control arrangement for the
configuration under consideration.

A major consideration in selection of control rate is the ef-
fect of control rate on transient power increase during an
arrestment of a right turn in hover. In Reference 3, a control
rate of 50 deg/sec produced large transient power increases
for this maneuver. It is suggested that values at least one-
third of 50 deg/sec would relieve such transient power
increases.

163

Preceding page blank

19.2 GUIDELINE

From a flying qualities point of view, the major benefit of
directional control rate limiting is the improvement in hard-
over failure response characteristics. An acceptable amount
of rate limiting will depend upon the maneuver requirements
and the particular configuration control sensitivity and rate
damping characteristics. For a helicopter with high maneuver-
ability requirements, a rate limit of approximately one-third
of full travel per second represents a good preliminary selec-
tion that should not adversely compromise maneuver require-
ments. This limiting should not result in excessive pedal
force characteristics for rapid pilot inputs and should be of
the right magnitude to relieve large transient power increases
during arrestment of right turns in hover.
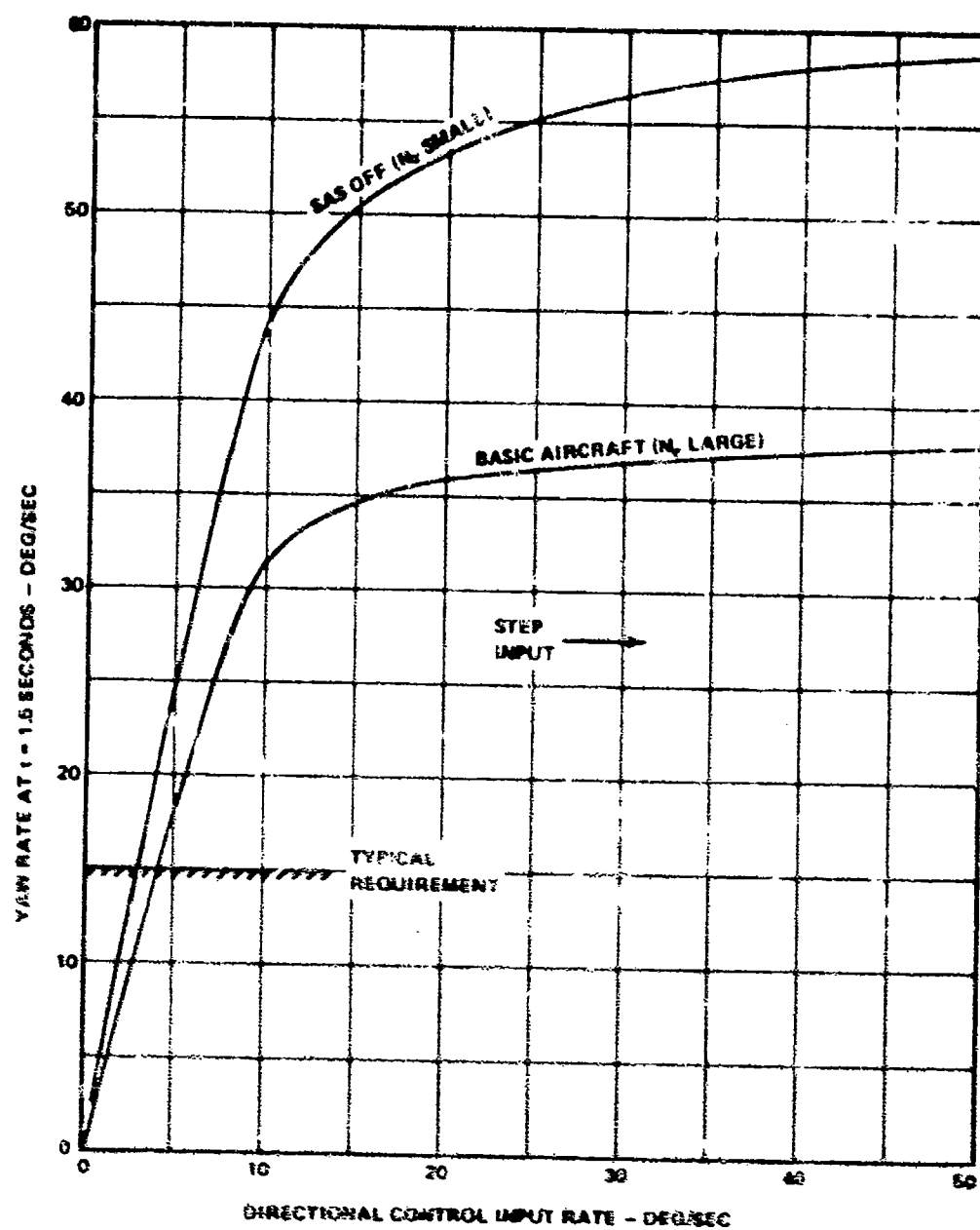
Figure 19-1. Effect of Directional Control Input Rate on Hover Maneuverability (Typical Trend).
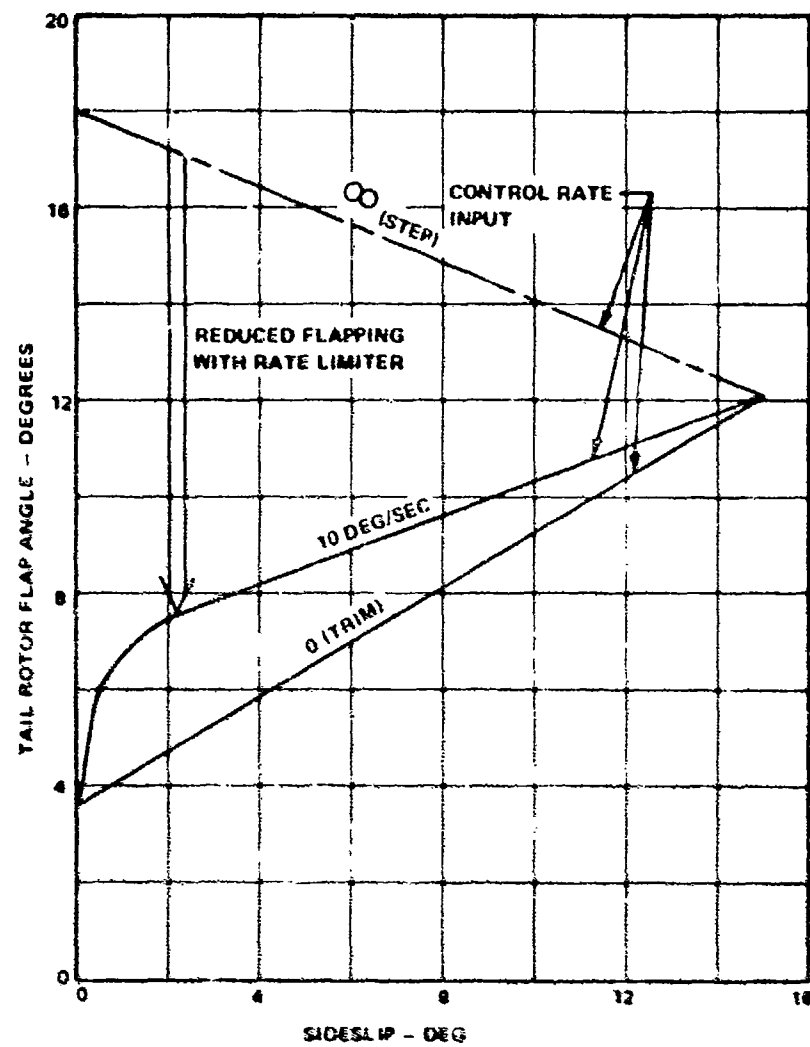
Figure 10-2. High-Speed Tail Rotor Flapping Response (Typical Trend).

166
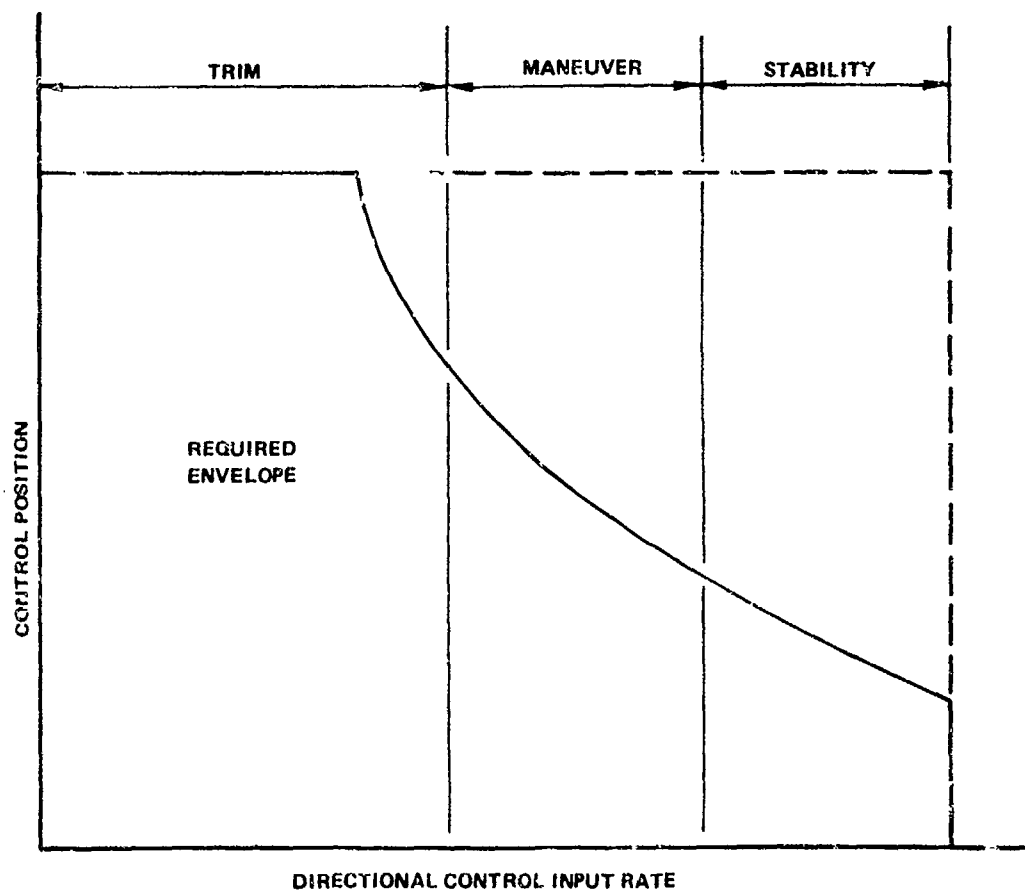
Figure 19–3. Required Directional Control Input Envelope (Typical Trend).

167

20.0 BLADE FLAPPING LIMIT

The objective of this guideline is to define a limit to tail
rotor blade flapping to prevent possible tail rotor-vertical
fin contact during maneuvers in flight. Design parameters
that affect the tail rotor flapping range include:

- Blade flapping stiffness

- δ_3

- Shaft sweep

- Fin-tail rotor placement

- Flight envelope (trim and maneuver)

20.1 DISCUSSION

To prevent possible tail rotor-fin contact in flight during
maneuvers, it is necessary to place the plane of the tail
rotor far enough away from the fin to prevent blade tip-fin
contact. Mechanical stops should be provided to limit rev-up
or down flapping motions which can be rather high, but such
stops should not be contacted in flight because of the pos-
sibility of high bending loads.

Because of the many factors affecting blade flapping and the
resulting loads and clearance characteristics, it would be
difficult to generalize a procedure for defining a flapping
stop limit; therefore, individual consideration should be given
for a particular configuration. It is believed that ±20 cos δ_3
degrees measured from the mean coning angle is a good value to
assure that stop contact is not made for a severe left-pedal
motion at maximum speed of the helicopter.

20.2 GUIDELINE

The mechanical flapping stops should be selected to allow a
flapping magnitude (with respect to the mean coning plane)
of ±20 cos δ_3 to occur without mechanical stop contact. The
plane of the tail rotor should be located such that when the
stops are contacted, the blade tips clear the fin surface
by 0.1r of the tail rotor. This will allow margin for blade
deflection and collective pitch effects.

21.0 CRITICAL LOADS AZIMUTH

For endurance (static tiedown) testing in winds, the critical wind azimuth will be selected where the average total moment on the tail rotor divided by thrust is the greatest. The rationale for this selection is that at such azimuth the tail rotor will be subjected to the largest change in blade load as it rotates; therefore, the blade bending fatigue stresses are the highest.

In order to conduct flight vibratory tests at the critical azimuth, the critical azimuth for flight will be that at which the greatest variation in tail rotor in-plane vertical force and rolling moment divided by mean thrust occurs. The reason is that the greatest vibrations and therefore fatigue stresses in the tail rotor and drive system will occur at such azimuth in flight.

NOTE: The variation in tail rotor thrust should also be considered. This could not be done for the Boeing test because it was determined during data reduction that the first blade bending natural frequency was exactly two per rev at operating rpm, producing a very high two-per-rev thrust variation.

21.1 DISCUSSION

Figures 21-1, 21-2, 21-3 show total moment (vector sum of yaw and roll moments) for V = 20 and 30 knots. Examination shows that the steady moment is highest near $\psi = 0^{\circ}$ and 180°. Figure 21-4 shows that for the V = 35 knots case, the steady moment/thrust is still highest near $\psi = 0^{\circ}$ and 180°. Therefore, the critical static test azimuth should be selected near $\psi = 0^{\circ}$ or 180°.

Figures 21-5 and 21-6 show alternating, in-plane vertical force and alternating rolling moment (only variation recorded on Boeing's recording oscillograph) divided by thrust for V = 20 and 35 knots at a constant collective tail rotor blade pitch of 14° (near the trim thrust value) for isolated tail rotor. These figures show that the vortex ring state azimuth (240°) is the critical azimuth for flight.

21.2 GUIDELINE

The critical wind azimuths at high blade incidence where the highest structural loads may occur when conducting ground tests are near $\psi = 0^{\circ}$ or 180°.

The critical wind azimuth where highest structural loads may occur in flight, especially higher harmonic loads, is near $\psi = 240^\circ$ (vortex ring state).
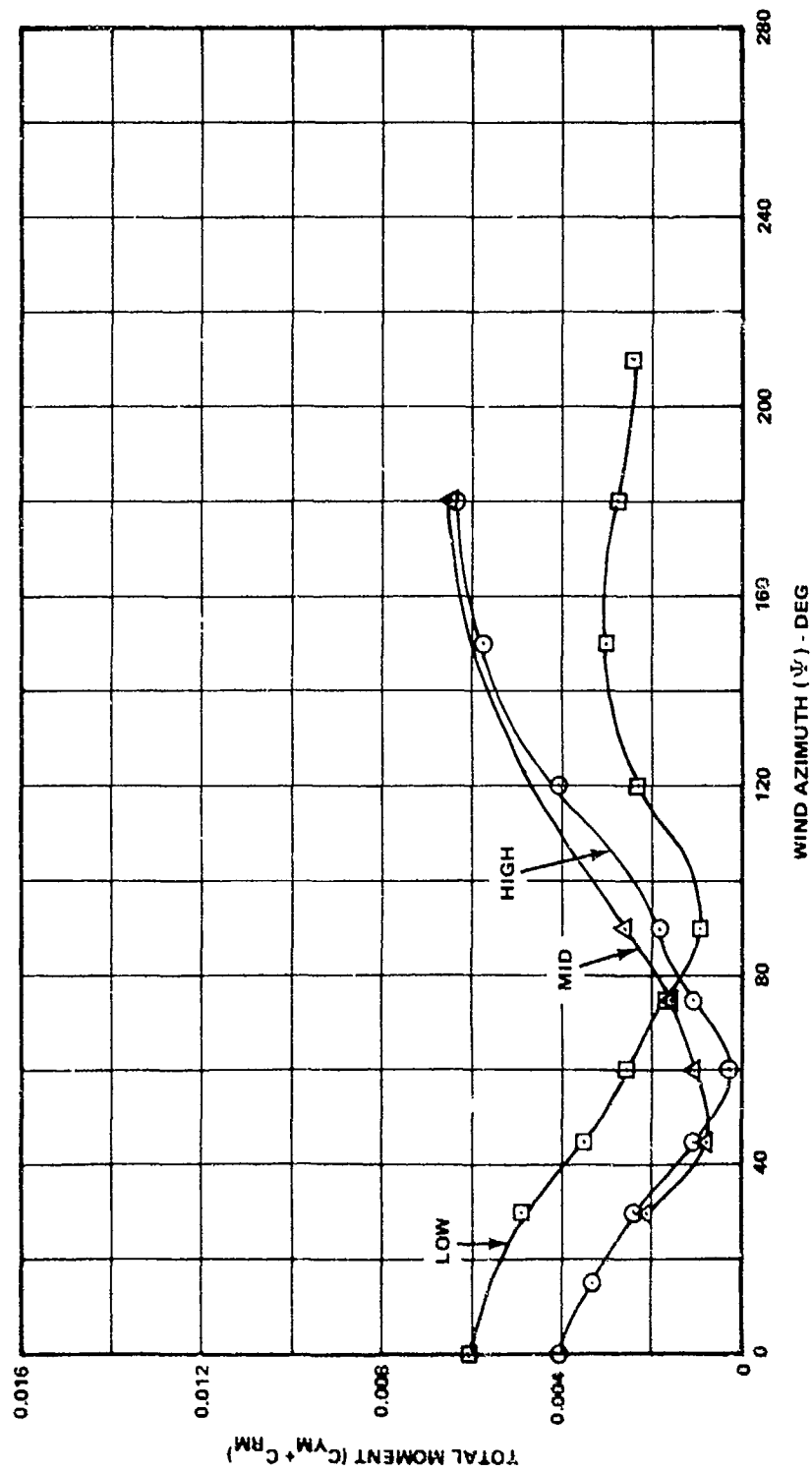
Figure 21–1. Effect of Tail Rotor Position on Total Moment – V = 20 kn, h/d = 0.3, θ = 20°, Fin = OFF, Rotation = BF.

173
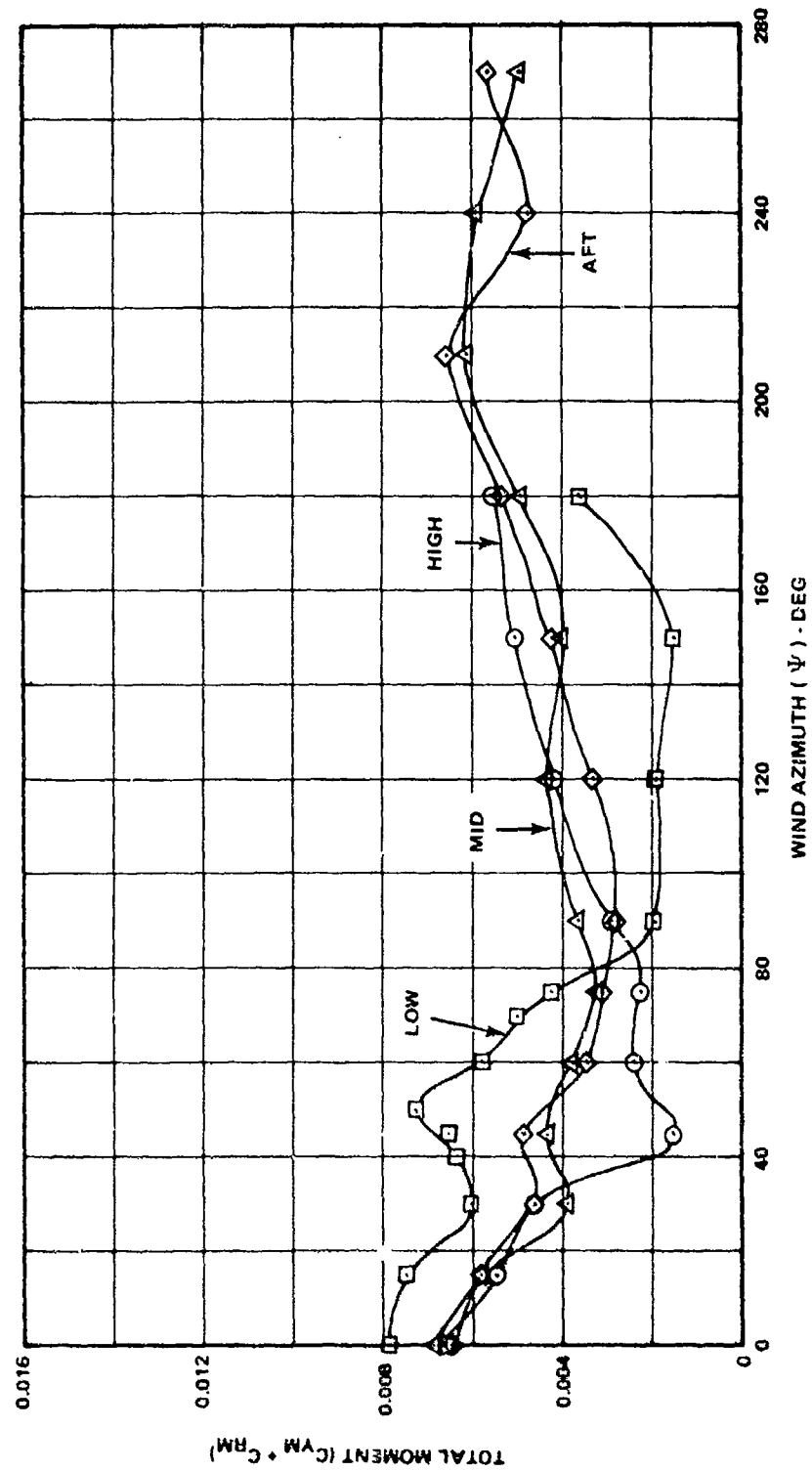
Figure 21—2. Effect of Tail Rotor Position on Total Moment — V = 35 kn, h/d = 0.3, θ = 20°, Fin = OFF, Rotation = BF.

174
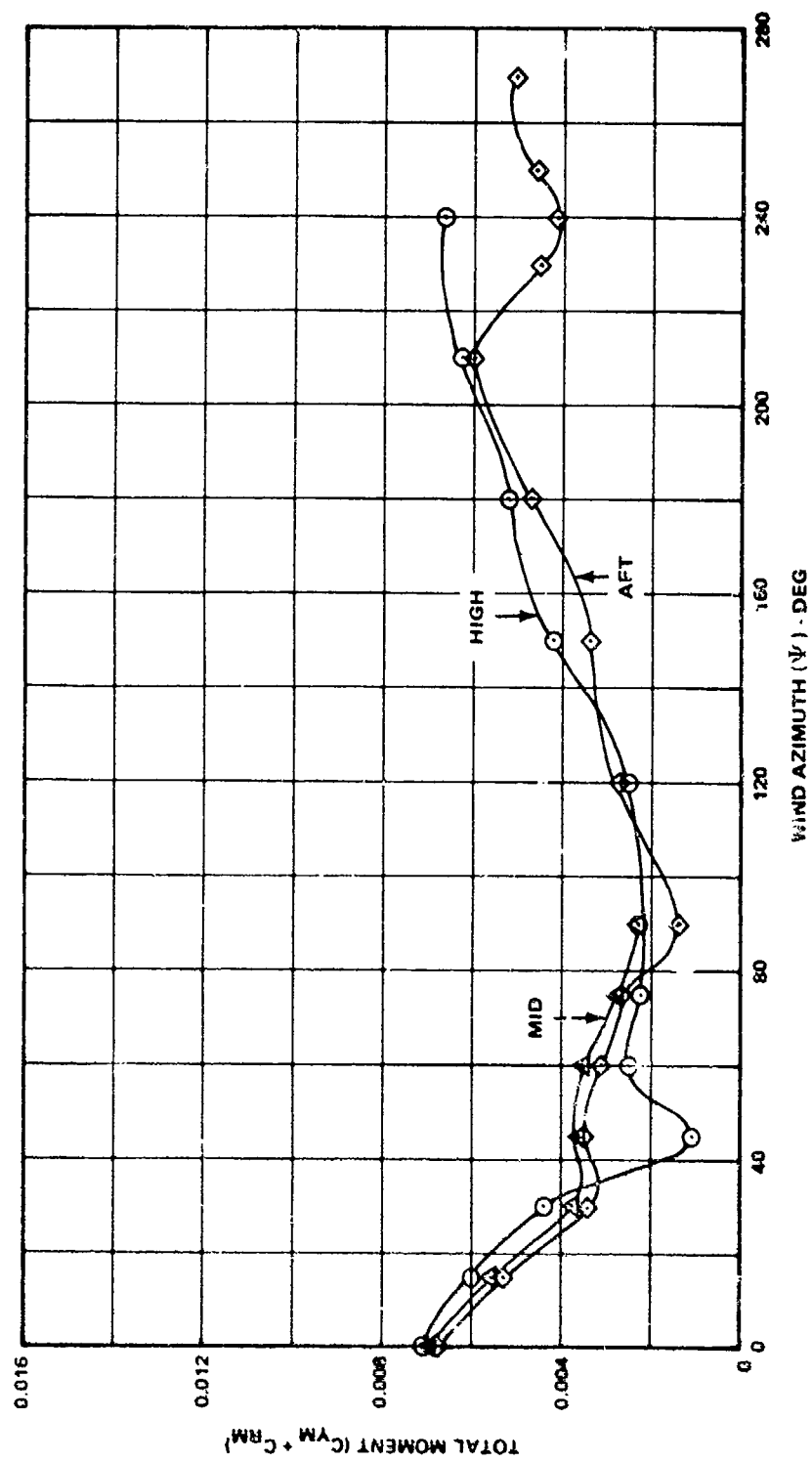
Figure 21-3. Effect of Tail Rotor Position on Total Moment — V = 35 kn, h/d = 1.0, θ = 20°, Fin = OFF, Rotation = BF.

175
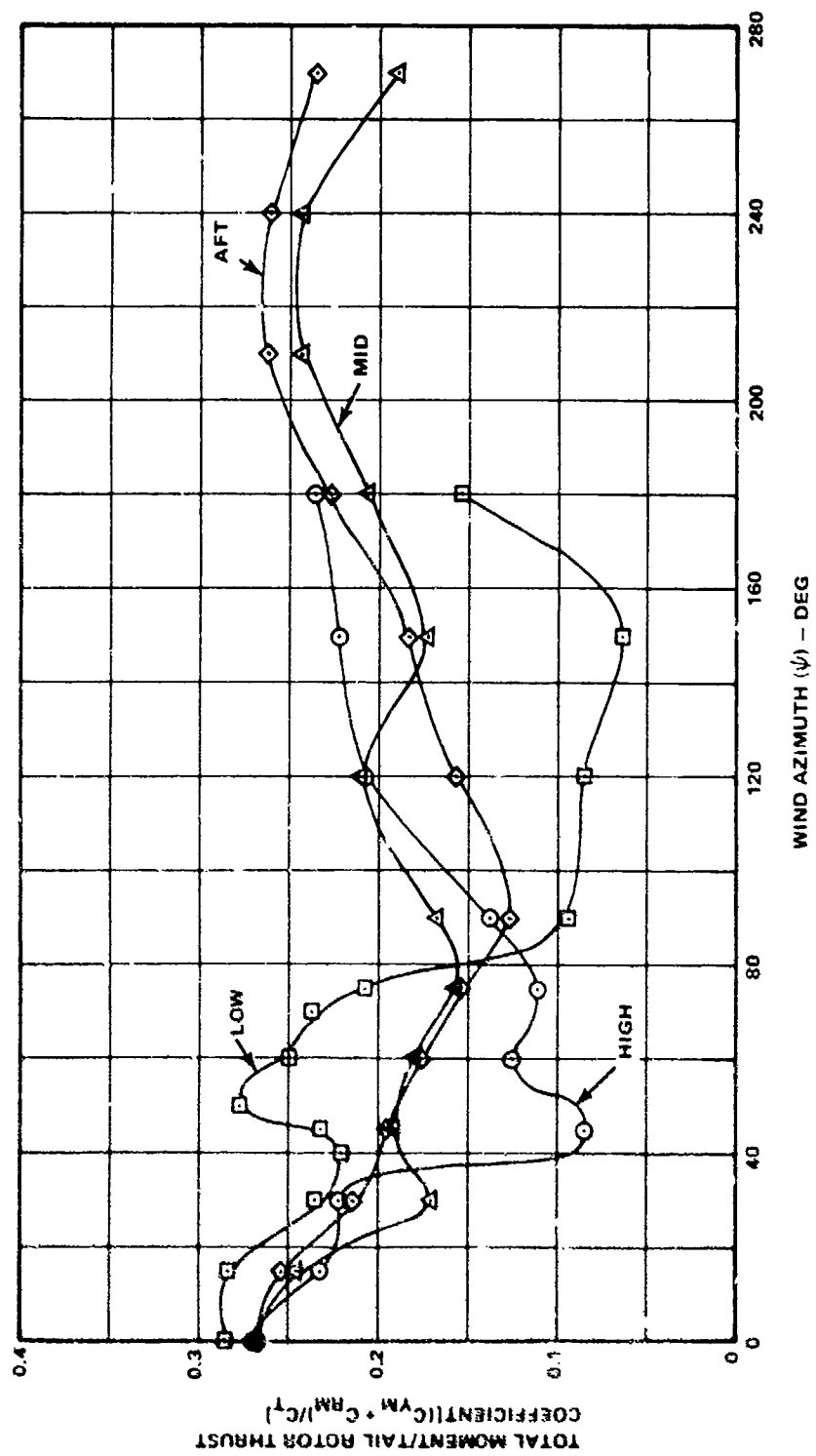
Figure 21—4. Effect of Tail Rotor Position on Total Moment/Tail Rotor Thrust — V = 35 kn, h/d = 0.3, ℓ = 20°, Fin = OFF, Rotation = BF.

176
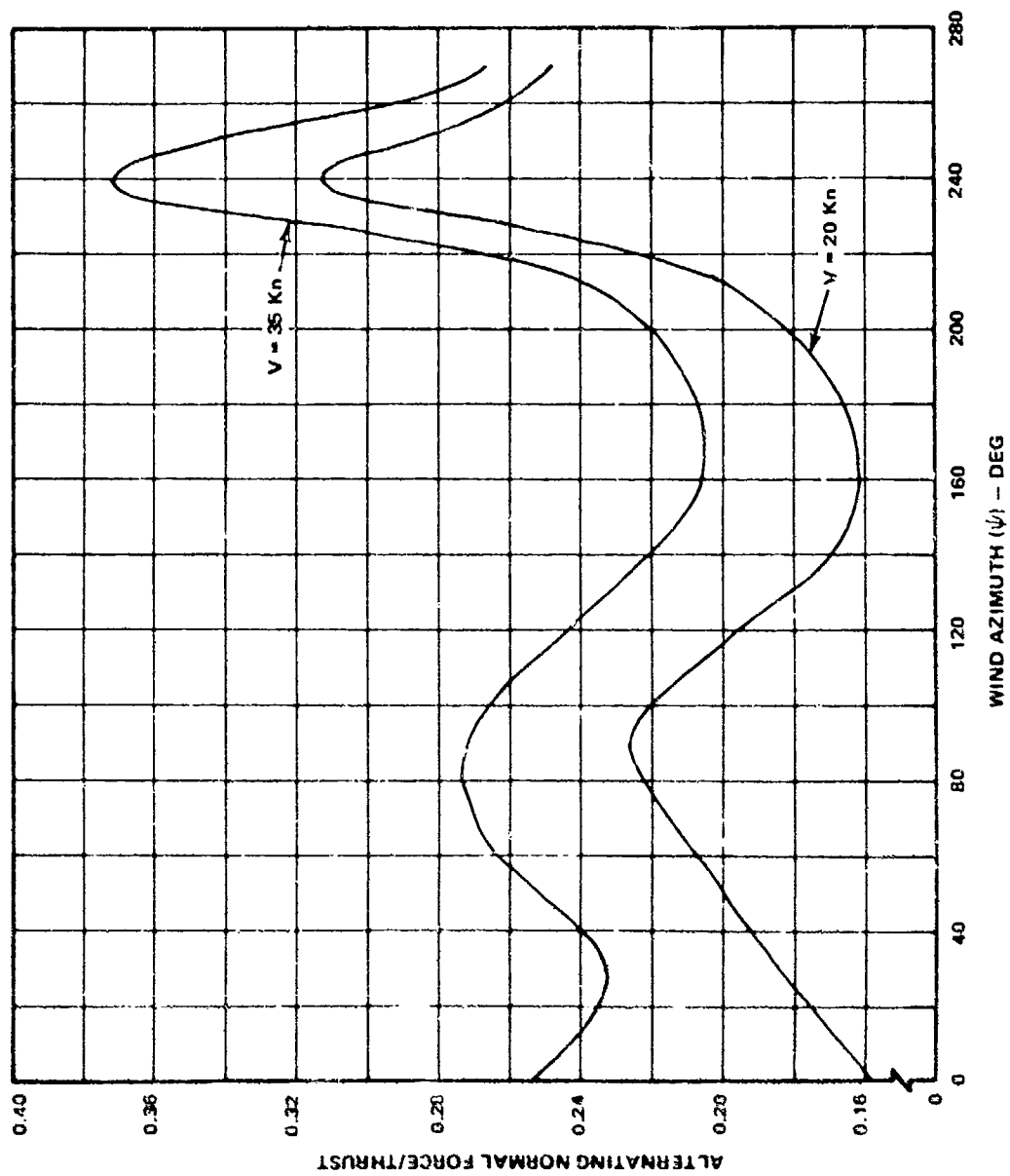
Figure 21—5. Effect of Wind Velocity on the Alternating Normal Force of an Isolated Tail Rotor — $\theta = 14°$.

177
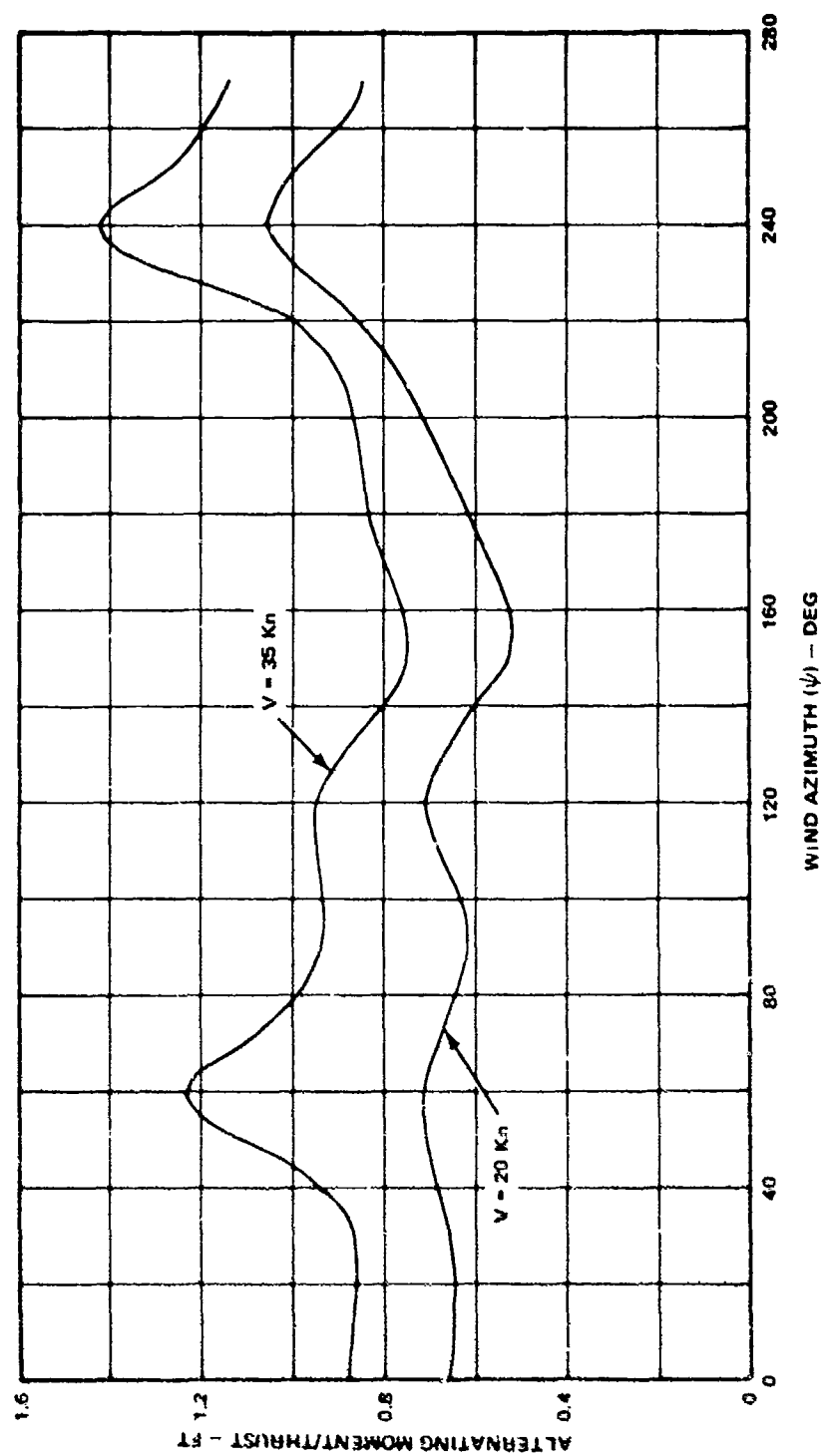
Figure 21-6. Effect of Wind Velocity on the Alternating Moment of an Isolated Tail Rotor — $\theta = 14^\circ$.

178

22.0 FULL-SCALE DESIGN THRUST VERSUS BLADE INCIDENCE

This guideline suggests a method wherein model test data can be used to establish the thrust performance of a full-scale tail rotor.

22.1 DISCUSSION

The performance results of model tail rotor tests normally apply only to the limited range of values of solidity, twist, and airfoils tested. In addition, model results must be adjusted for Reynolds number differences. The following guideline shows how model test data, in conjunction with theoretical predictions, can be used to predict full-scale performance at other values of these parameters.

22.2 GUIDELINE

Model data can be used to establish the level of thrust for a full-scale tail rotor by use of the following procedure:

- Plot the isolated model tail rotor data (C_T/σ versus θ) for the desired wind speed and azimuth. An example is given in Figure 22-1 for $\psi = 90^\circ$ and $V = 0$.

- Compute the tail rotor performance by use of theoretical analysis for the same parameters (but full-scale) and operating conditions as in the model tests.

- Determine the distance that the theoretical curve must be shifted to obtain exact correspondence with the test data at low thrust values (before the slopes diverge due to Reynolds number effects). This correction, designated B in Figure 22-1, provides adjustment for effects such as hub drag not accounted for in the computer simulation.

- Compute the full-scale thrust for other desired values of solidity, twist, and different airfoils.

- Determine the shift, designated A in Figure 22-1, to adjust for differences in solidity, twist, and airfoil.

- The shift A can then be applied to other test data taken at the same wind speed and azimuth at which A was determined.

179
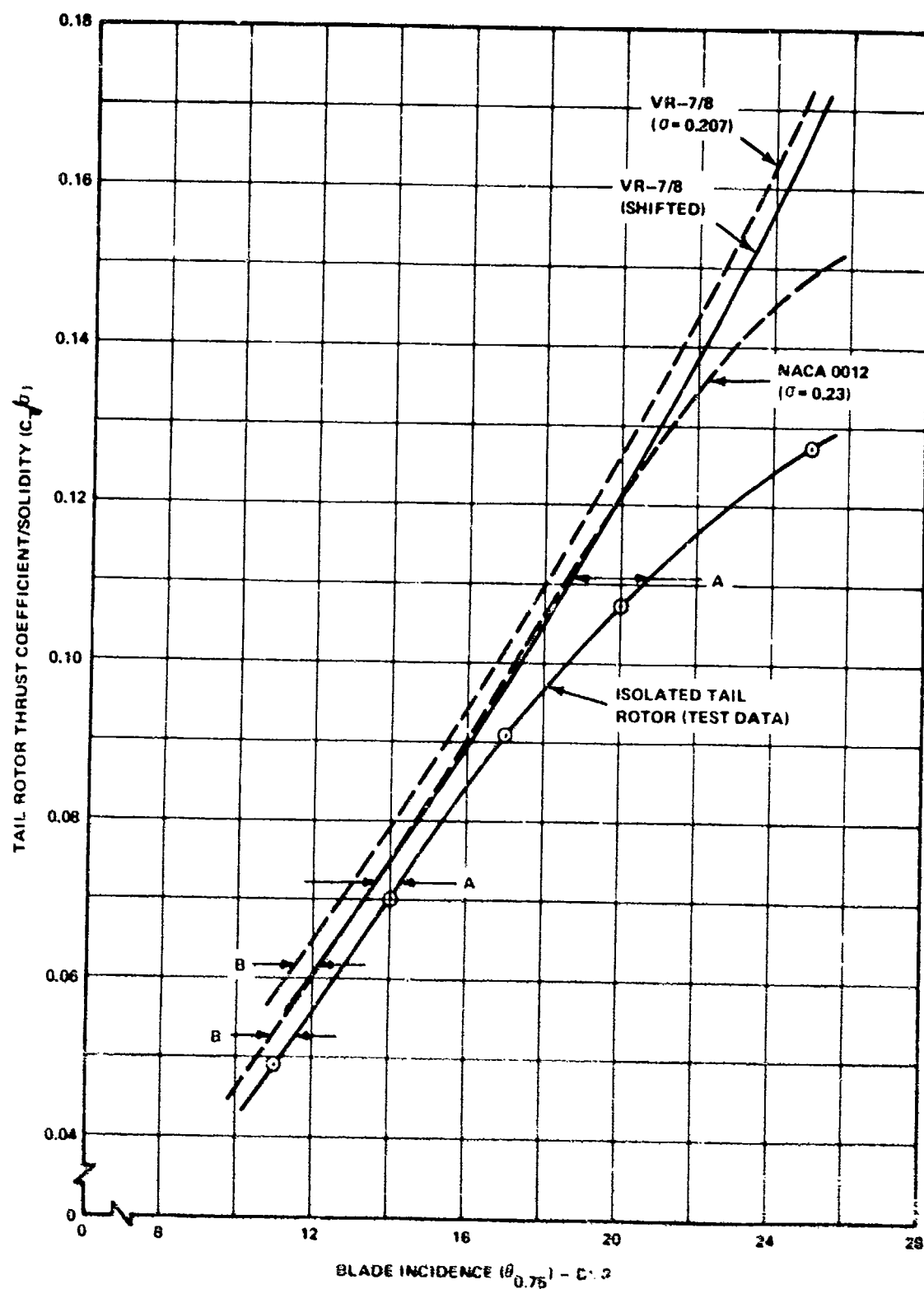
Figure 22-1. Determination of Theoretical Full-Scale Tail Rotor Thrust From Model Test Data at V = 0 Kn.

23.0 HORIZONTAL STABILIZER LOADS

Aerodynamic loadings of horizontal stabilizers located approximately one-quarter main rotor radius below the main rotor blade tips are presented in this section. Estimates of stabilizer loadings are required to determine the effect of the stabilizer on cyclic control trim.

23.1 DISCUSSION

A diagram of the horizontal stabilizer used in the Boeing tests is shown in Figure 13, Appendix II. Stabilizer loads in low-speed forward flight are presented as fractions of the main rotor disc loading in Figure 23-1. Maximum loads, approaching a magnitude of three times the main rotor disc loading OGE and twice the main rotor disc loading IGE, occur at approximately $V/u_0 = 1.6$ due to impingement of the main rotor downwash. The stabilizer loading is decreased at lower speeds because the main rotor wake contracts ahead of the stabilizer. At speeds above $V/u_0 = 1.6$, the main rotor becomes more nearly parallel to the stabilizer and the product of angle of attack and dynamic pressure is reduced, thus decreasing the download.

In IGE rearward flight (Figure 23-2), the stabilizer encounters a large upward load, approaching the magnitude of the main rotor disc loading, at approximately $V/u_0 = 1.0$. This is caused by the ground vortex acting on the stabilizer.

The location of the ground vortex for varying wind velocity is shown in Figures 23-3 and 23-4 for h/d = 0.3 and 0.45, respectively. For h/d = 0.3 and V = 23 knots ($V/u_0 = 1.0$), note that the ground vortex coincides with the location of the horizontal stabilizer in rearward flight, causing maximum loads as described earlier.

23.2 GUIDELINE

To determine the effect of horizontal stabilizer loads on cyclic control trim, the loads given in Table 23-I should be used. These values are applicable for stabilizers located approximately one-quarter main rotor radius below the main rotor blade tips.

181
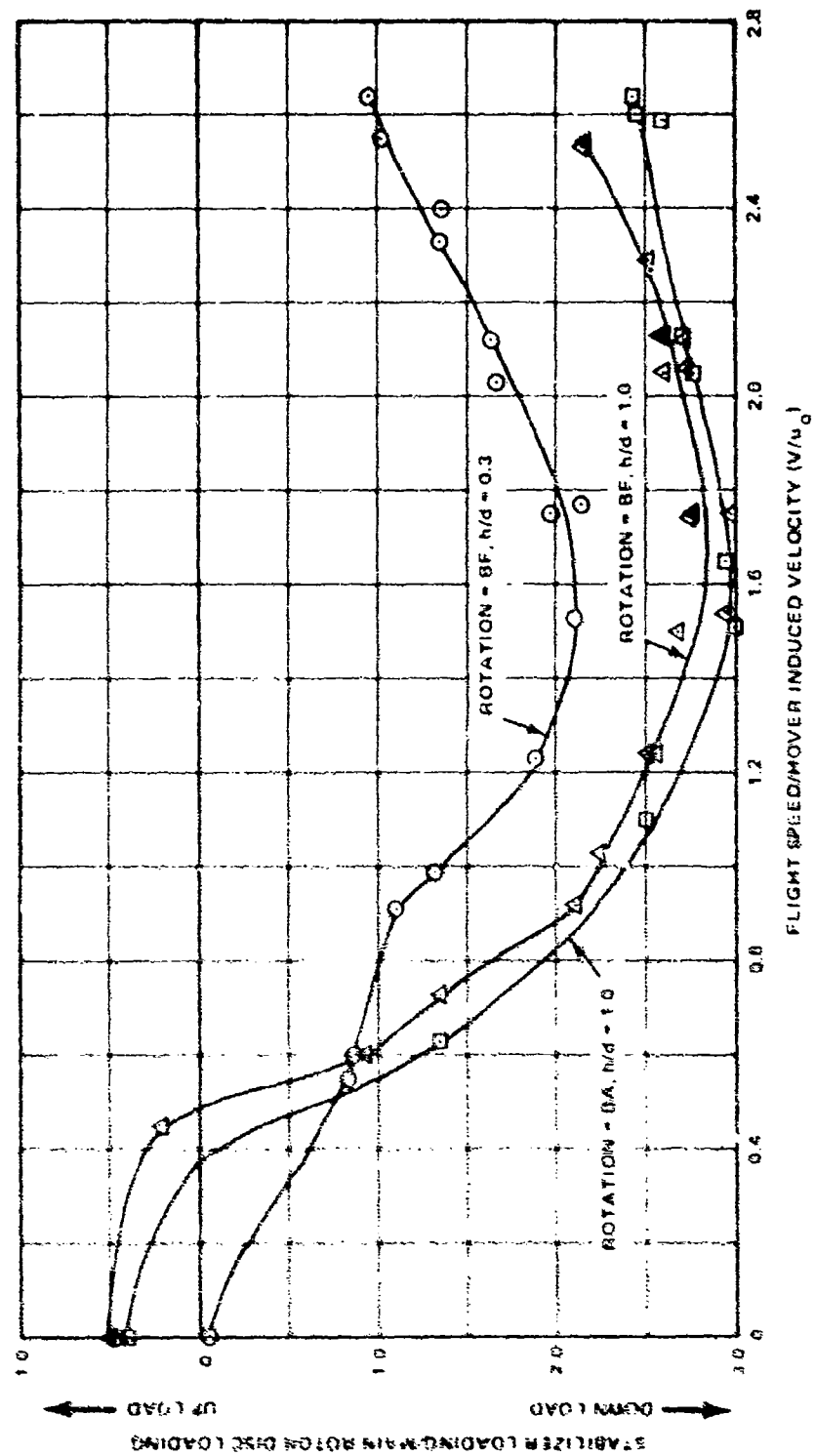
Figure 23—1. Horizontal Stabilizer Loading in Forward Flight.
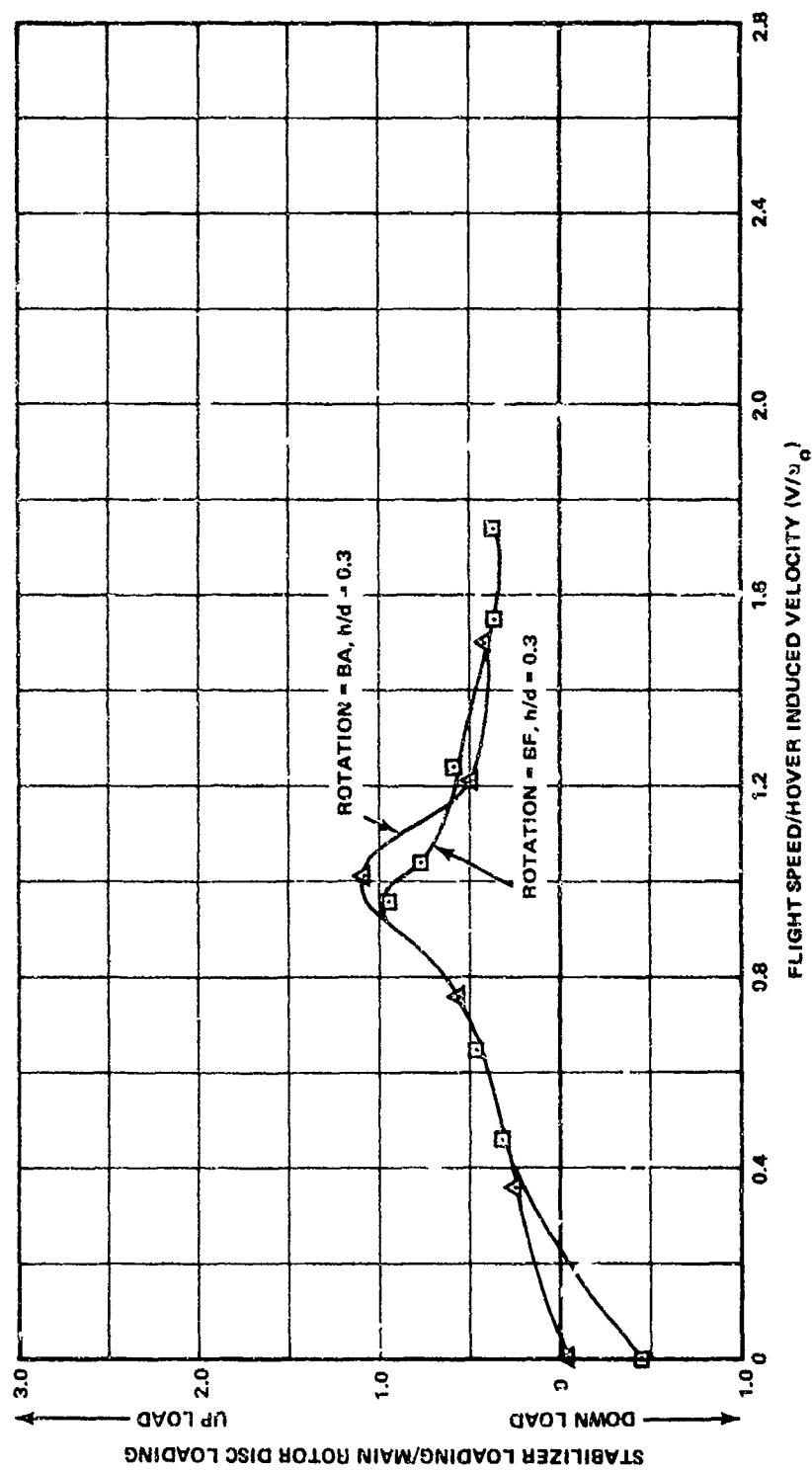
Figure 23–2. Horizontal Stabilizer Loading in Rearward Flight.

183
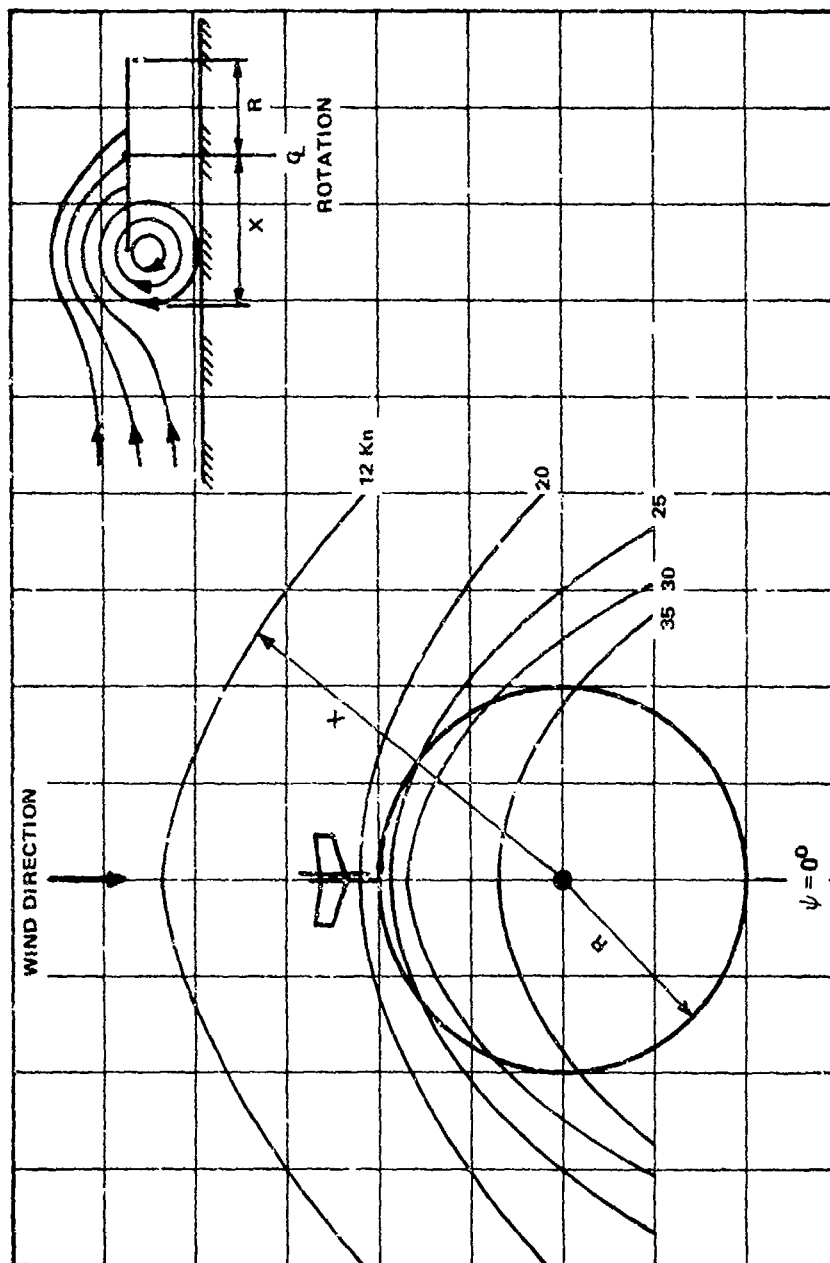
Figure 23–3. Effect of Wind or Ground Vortex Location — h/d ≈ 0.3.

184
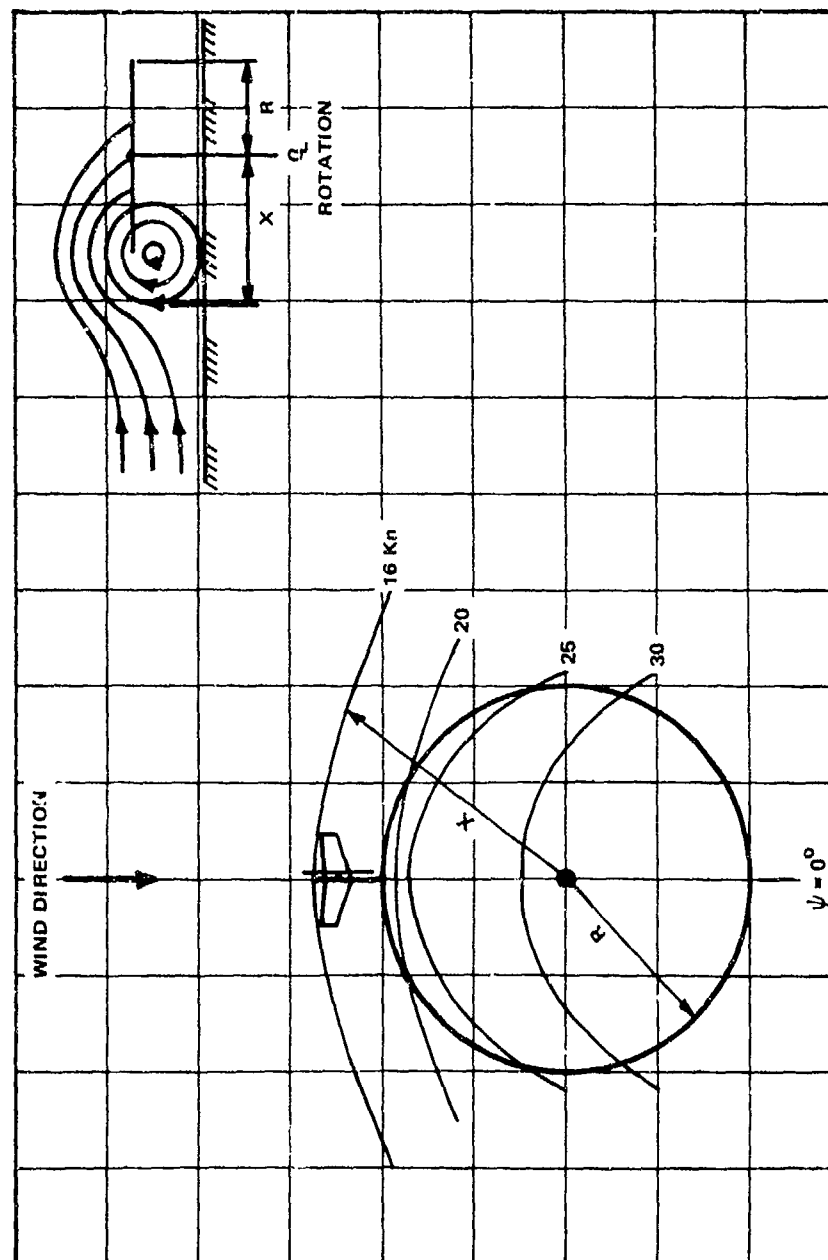
Figure 23–4. Effect of Wind on Ground Vortex Location — h/d = 0.45.

185

Table 23-I.	HORIZONTAL STABILIZER LOADINGS IN REARWARD AND FORWARD LOW-SPEED FLIGHT		
Direction of Flight	h/d	Velocity for Maximum Load, V/u_0	Maximum Load Magnitude
Rearward	0.3	1.0	1.0 w
Forward	0.3	1.6	2.0 w
	1.0	1.6	3.0 w

EXAMPLE USE OF GUIDELINES

Guidelines presented in this report can be used to select tail rotor parameters and characteristics. An example of tail rotor design procedure is given in this section using the aircraft characteristics listed in Table I.

Item	Characteristic	Sample Value
	TABLE I. HELICOPTER CHARACTERISTICS REQUIRED FOR DETERMINATION OF TAIL ROTOR CHARACTERISTICS	
1	Gross weight, lb	15,000
2	Design altitude, ft	8000
3	Main rotor diameter, ft	49
4	Main rotor solidity	0.10
5	Main rotor tip speed, fps	750
6	Meet hover performance to wind of, kn	35
7	Rudder pedal travel required for left sideward flight up to 35 knots at alternate gross weight	Linear
8	Installed SHP	2800
9	Alternate gross weight, lb	18,000
10	Fin area, sq ft	30
11	Fin aspect ratio	3
12	Fin incidence (produces right force)	3°
13	Type of aircraft	Cargo
14	Maximum detection distance for medium ambient, sparse jungle condition, ft	1500
15	Yaw rate at end of 1.5-second maneuver, deg/sec	15
16	Direction of rotation of main rotor	Right blade forward

187

Item	Characteristic	Sample Value
	TABLE I. Continued	
17	Yaw rate damping, 1/sec	-1.7
18	Afterbody shape	Streamlined
19	Fin blockage ratio	0.25
20	Fin separation ratio, s/r	0.45
21	Airfoil stall C_ℓ	1.2
22	Thrust margin during maneuver	10 percent
23	Main rotor figure of merit IGE, FM	0.70

1. Position of Tail Rotor With Respect to Main Rotor

From Guideline 1, select the tail rotor shaft axis
position in line with the plane of the main rotor for a
normal aircraft center-of-gravity location. The reason
for such selection is that Guideline 1 shows that the
tail rotor in this position will produce the highest
level of thrust for a given collective pitch and require
the least solidity and, therefore, weight without stall
of the blade airfoil. The clearance between the tips of
the tail and main rotor blades should be determined from
the possible structural deflection. The usual clearance
is about 6 inches.

Very little solidity and weight penalty will exist, even
though the placement is selected up to one-half of the
tail rotor radius below the recommended position. Larger
pedal excursion may, however, be experienced in making
hover turns in winds.

2. Placement of Tail Rotor With Respect to Fin

From statements and data in Guideline 2, place the tail
rotor on the left side of the fin (pusher). To obtain
minimum fin force loss without a great weight penalty due
to tail rotor "overhang" and to allow adequate clearance
between fin and blade tip when blade is on stop, the
plane of rotation of the tail rotor should be between
0.40 and 0.50 (select 0.45 for this example) tail rotor
radius from chordline of fin. The penalty for an equiv-
alent installation on the right side of the fin with a
blockage ratio of 0.21, for example, will be a tail rotor

188

of 12-percent higher solidity, 6-percent higher system weight, and 18-percent higher static thrust power. Guideline 18 discusses the effects of tail rotor shaft sweep. For this sample problem, the selected shaft sweep will be zero, which is a good trade-off between pedal travel, blade and pitch link loads, and high-speed power required by the tail rotor. Since the vertical fin is set at 3^0 right incidence (produces force to right in forward flight), it will reduce the collective pitch of the tail rotor required for high-speed flight.

3. Direction of Rotation of Tail Rotor

For beneficial effects on solidity, weight, and power as shown in Guideline 3, bottom forward rotation is selected. Smaller helicopters with unprotected tail rotors close to the ground have been designed with bottom aft rotation. This is justified because if the tail rotor strikes the ground during a flared landing, the blade parts will be thrown aft, away from the cabin. If such a design criterion is used, the penalties could be as high as a 50-percent increase in solidity, which, for a given maximum blade incidence, would increase static thrust by 50 percent, static power by 80 percent, and weight of tail rotor system by 20 percent.

4. Critical Thrust and Power Azimuths

Guideline 4 shows that for most velocities up to 35 knots, the thrust delivered by the tail rotor at a given blade incidence is minimal in the azimuth range of 60^0 to 90^0. This is the azimuth where the main rotor trailing vortex and/or the ground vortex has a great effect on the flow characteristics entering the tail rotor. The Ames Directorate, AMRDL, hydrogen bubble tests clearly show the ground vortex entering the tail rotor at a wind azimuth of 90^0 and wind magnitudes of 20 to 25 knots (Reference 17). Boeing tests showed a strong influence of the wing tip vortex at 35 knots.

The importance of selecting the critical thrust azimuth (60^0 selected for the sample case) is to assure that thrust variation with h/d is made at the critical azimuth. Note that h/d thrust data at 60^0 azimuth is presented in Guideline 5, and that data forms the basis for converting Boeing tail rotor test data into conventional isolated tail rotor data in Guideline 14. The critical power azimuths for maneuver will be selected at $\psi = 60^c$ to correspond to the critical thrust azimuth.

This critical thrust azimuth will design the physical characteristics of the tail rotor; but other azimuths in

189

the rear flight hemisphere may be more critical with regard to pedal movement required by the pilot to maintain a given heading. If the azimuth and winds permit fin stall or vortex ring formation on the tail rotor, pedal motions to maintain heading may be high enough to contact the stops, even though the mean pedal position is further from the stops than at the critical design azimuth of 60°. Bottom forward rotation of the tail rotor (see Guideline 6) will diminish vortex ring formation, while a rounded trailing edge applied to the fin airfoil could smooth the effects of reverse stall (from the trailing edge) of the fin and its subsequent alternating flow effects on tail rotor thrust and fin force.

5. **Critical Wind Velocity**

Guideline 5 shows that for the pusher configuration with bottom forward rotation, the critical wind velocity is 20 to 25 knots at wind azimuth = 60° as determined in the Boeing tests. The 20-knot velocity is selected for this sample. It should be noted that the critical wind velocity will be affected by main rotor disc loadings. Boeing tests which form the basis for Guideline 5 were conducted at a main rotor disc-loading value of 7.0 lb/ft².

6. **Critical Hover Height**

Guideline 6 shows that the critical hover height at the critical wind velocity of 20 knots for a pusher configuration with bottom forward rotation (selected configuration) is either h/d = 0.45 or 1.0. As a result, the conversion curve (Figure 14-2) of Guideline 14 for V = 20 knots is based on the average of thrust developed at h/d = 0.45 and 1.0. Critical hover height for 0- and 35-knot winds is h/d = 1.0.

7. **Tail Rotor Disc Loading and Diameter**

The specified pedal control in left-side flight (Item 7, Table I) is linear at the prescribed 35-knot side velocity. Figure 7-7 of Guideline 7 shows that a hover disc loading of 13 psf will satisfy these specified conditions.

In selection of diameter based on these conditions, calculate the hover trim thrust required at alternate gross weight at the design altitude as follows:

$$K_{TRIM} = 1.2 \sqrt{2\rho\pi} \; R^2 \; \Omega \; (FM) \qquad \text{(see Appendix III)}$$

$\rho = 0.00197$ at 8000 feet, standard temp.

190

$R = 24.5$ feet

$FM = 0.70$

$\Omega = 750/24.5 = 30.6$ rad/sec

Thus $K_{TRIM} = 1672$.

Then from Figure 13-1, the hover trim thrust at 18,000 pounds gross weight is 1440 pounds. From Figure 11-4 of Guideline 11. the main rotor power in 35-knot left-sideward flight ($\mu = 0.078$) is 0.78 of that at hover (IGE); therefore, the trim thrust at a 35-knot left-sideward flight ($\psi = 270°$) is $(1440)(0.78) = 1123$ pounds.

From this must be subtracted the force to balance the body moment of Figure 13-6. This value is 120 pounds times $\rho/\rho_o = 93$ pounds. Thus, total net thrust required in a 35-knot left-side flight is $1123 - 93 = 1030$ pounds.

Make a first-round assumption that the tail rotor shaft thrust is 1.20 greater than this value; thus the tail rotor shaft thrust that is used to determine diameter is $(1030)(1.20) = 1236$ pounds.

Thus $d = \left[\left(\frac{1236}{13}\right)\left(\frac{4}{\pi}\right) \right]^{1/2} = 11.0$ feet.

Select 11 feet for the initial diameter.

Many factors affect the final selection of disc loading, such as:

a. Optimum Diameter To Produce the Greatest Payload. Such a diameter can be established only after the usual payload trade-off studies are made as the design progresses.

b. Overall Geometric Layout of the Aircraft. The previously mentioned diameter may be too large to provide ground or stabilizer clearance. Thus, the final diameter may be smaller to provide a more compact aircraft. Note that a smaller diameter which gives higher disc loading will also provide left-sideward flight linear pedal characteristics.

8. Tip Speed and Number of Blades

Figure 12-2 of Guideline 12 shows that for a design 15,000-pound gross weight and for tail rotor disc loadings near 15 psf, the tail rotor tip speed should be 700 fps

with four blades to meet the 1500-foot maximum detection
distance described in Table I. Figure 12-2 shows that
for the prescribed 750-ft/sec main rotor tip speed, the
main rotor will be noisier than the tail rotor and,
therefore, the main rotor tip speed should be lowered.
However, for this sample, no further consideration of the
main rotor will be made. The tip speed selected for the
tail rotor will be 700 ft/sec and there will be 4 blades.

9. Determination of Shaft to Net Thrust Ratio (Fin Loss)

To determine the effect of the fin on thrust output, the
fin blockage ratio must be determined. For this sample
problem, that ratio is 0.25 (Table I). Such ratio will
vary, depending on the spanwise location of the fin at
which the tail rotor is supported, on the aspect ratio
of the fin, and the diameter of the tail rotor.

The ratio of C_T/C_{T_N} can be determined from Figure 8-1 of
Guideline 8, using the tip speed selected from Guideline
12 to calculate the appropriate value of μ_{TR}.

10. Selection of Airfoil

The airfoil selected will be cambered and shaped such
that the two-dimensional maximum C_ℓ is 1.2 at a Mach
number of 0.6 and with trailing edge shaped such that the
aerodynamic pitching moment is zero. This selection fol-
lows from the discussion in Guideline 9.

11. Blade Twist

Guideline 10 shows that a payload increase equivalent to
0.2 percent of the gross weight can be realized with a
blade twist of -10° with some increase in blade struc-
tural loading. Twist also produces a slightly higher
C_T/σ allowable at full left pedal for a given airfoil.
Select -10° blade twist for this sample.

12. Main Rotor Power Requirements

Values of main rotor power versus velocity for several
wind azimuths for OGE and IGE are given in Guideline 11.
Such values are used to determine tail rotor trim thrust
for any desired condition. The procedure used will be to
calculate hover power and trim and then determine tail
rotor trim force required in a manner similar to that
shown in Part 7 of this section (Example Use of Guidelines).

As pointed out in Guideline 11, the wash of the tail
rotor greatly influences the power required by the main
rotor. Such an influence must be considered not only in

192

tail rotor design but in predicting overall performance
of the helicopter, especially hover ceiling at various
wind azimuths and magnitudes.

13. **Design Net Thrust Required**

The design net thrust required for selection of solidity
and left pedal blade incidence is selected by use of the
procedure given in Guideline 13. The critical conditions
are $V = 20$ knots, $\psi = 60^{\circ}$ to 90°, $W = 18{,}000$ pounds
(alternate gross), altitude = 8000 feet (standard), and
yaw maneuver = 15°/second at the end of 1.5 seconds.

a. Trim thrust in hover previously calculated is 1440
   pounds (part 7 of this example).

b. Ratio of power at 20 knots and $\psi = 90^{\circ}$ to power at
   $V = 0$ is 0.96, from Figure 11-4 for $\mu = 0.045$.

c. Trim thrust = $1440 \times 0.96 = 1382$ pounds at 20 knots.

d. Select yaw rate damping of $N_r = -1.7$ as prescribed in
   Table I determined from flight simulation data,
   Figure 13-2, or from experience.

e. Select $I_z/\ell = 900$ from Figure 13-3 for gross weight =
   18,000 pounds.

f. Compute $K_M = (I_z/\ell) \, \dot{\psi} = 900 \times \dfrac{15}{57.3} = 235$.

g. Determine maximum thrust increment for maneuver from
   Figure 13-4 for $N_r = -1.7$, $\psi = 15$ deg/sec, $t = 1.5$
   seconds, and $K_M = 235$. The value is 460 pounds.

h. Assume weight of blade = 1.7 psf.

i. Estimate tail rotor solidity = 0.20.

j. Compute $K_g = 0.888 \, (r\omega) \, (\sigma \pi r^2) \, w'/g$ (see Guideline 13)

   $(r\omega) = 700$ fps

   $\sigma \pi r^2 = (0.20)(\pi)(5.5)^2 = 19$ ft^2

   $w = 1.7$ psf

   $g = 32.2$ fps^2

   $K_g = 0.888 \, (700)(19)(1.7)/32.2 = 623$

k. For an angular yaw rate of one-third of the final yaw
    rate of 15 deg/sec, read gyroscopic thrust increment =
    60 pounds from Figure 13-5. Note that since the max-
    imum peak maneuver thrust occurs approximately one-
    third of the time through the maneuver, the gyroscopic
    thrust increment is calculated at that time also.

l. From Figure 13-6 for streamlined afterbody, read 40
    pounds for 18,000 pounds gross weight and 20 knots
    for fuselage moment balance.

m. Total net thrust required for the 15 deg/sec yaw
    maneuver = 1382 + 460 + 60 + 40 = 1942 pounds.

n. Compute $C_{T_N} = T/\rho \pi r^2 \ (\omega r)^2$

    $= 1942/ \ (0.00187) \ (\pi)(5.5)^2(700)^2 \ = 0.0220$

o. For the specified 10 percent thrust margin, the
    design C_{T_N} is $(C_{T_N})_d = 0.0220/0.90 = 0.0244$.

14. Selection of Solidity and Maximum Left Pedal Incidence

A summation of the critical conditions and characteristics
from which the solidity and left pedal incidence will be
selected is:

Item	Reference Part of Example
V = 20 knots	5
s/r = 0.45	2
$\bar{A}$ = 0.25	Table I
Pusher configuration	2
$(C_{T_N})_d$ = 0.0244	13
Rotation = BF	3
Critical ψ = 60°	4

a. Determination of C_T/C_{T_N}. In Guideline 8, it is stated
    that the fin force is the same at 20 knots as at 35
    knots if the wind azimuth is 60°. Therefore, for 20
    knots at ψ = 60° case, ψ_{TR} should be calculated at
    35 knots:

$$\mu_{TR} = \frac{(35)(1.69)}{700} = 0.0845$$

$$\overline{A}\mu = (0.25)(0.0845) = 0.021$$

Then from conditions above and for $\overline{A} = 0.021$, read

$(C_T/C_{T_N}) = 1.195$ from Figure 8-1 of Guideline 8.

b. From Figure 14-2 of Guideline 14 for

$(C_T/C_{T_N}) = 1.195$

$V = 20$ knots

$(C_{T_N})_d = 0.0244$

read $C_{T_O} = 0.031$ or calculate from Equation 14-1 in Guideline 14.

c. Read first iteration solidity and blade incidence from Figure 14-3, Guideline 14, at $V = 20$ knots ($\mu = 0.048$) for $C_{T_O} = 0.031$ and for airfoil maximum $C_\ell = 1.2$. The values are $\sigma = 0.20$, $\theta_{max} = 23.2^\circ$.

d. Check to see if these values stall the tail rotor when full left pedal is applied "on the ground" at $V = 0$ ($\mu = 0$) from Figure 14-4. Such check shows that at the first iteration values of σ and θ, the airfoil is only 0.01 C_ℓ beyond stall. Therefore, no second iteration at $V = 20$ knots is required, and these values are the required values for the solidity and maximum left pedal. Note that for the twisted blade the selected θ should be referenced to the incidence at 0.75 of blade radius.

15. Maximum Right Pedal Blade Incidence

The maximum right pedal blade incidence must be calculated for each of conditions a, b, and c which are described in Guideline 15.

a. Autorotational Maneuver. The specified yaw maneuver rate of 15 degrees/second in 1.5 seconds to the right is required in 35-knot winds at 8000 feet altitude at alternate gross weight (see Table I).

i. The components of net tail rotor previously calculated for the left-pedal blade pitch for such a maneuver are, from part 14 of this section, peak maneuver thrust, 460 pounds and simulated gyroscopic thrust, 60 pounds.

195

2. The thrust required to balance body moments is obtained from Figure 13-6 as 86 pounds.

3. Total net thrust required to perform the maneuver is

$$
\begin{array}{r}
460 \text{ pounds} \\
60 \text{ pounds} \\
\underline{86 \text{ pounds}} \\
606 \text{ pounds}
\end{array}
$$

4. For the 10-percent thrust margin,

$$\frac{606}{0.9} = 673 \text{ pounds}$$

5. Compute the thrust coefficient:

$$C_{T_N} = \frac{673}{(0.001868)\ \pi\ (5.5)^2\ (700)^2} = 0.00775$$

6. The shaft thrust to net thrust ratio is obtained from Figure 8-1 using the tractor curves to simulate the reverse thrust condition. At $V = 35$ knots, $\overline{A}\ \mu_{TR} = 0.021$, $C_T/C_{T_N} = 1.6$.

7. Equivalent isolated rotor thrust is obtained from Figure 14-2. For $C_T/C_{T_N} = 1.6$, $V = 35$, and $C_{T_N} = 0.00775$,

$$C_{T_O} = 0.010$$

8. Establish the maximum right pedal blade incidence required at $V = 35$ knots from Figure 14-5. For an airfoil with a negative $C\ell_{MAX}$ of -1.1, the combination of $C_{T_O} = 0.010$ and $\sigma = 0.20$ gives θ_{max} right pedal $= 13.8^\circ$. This value does not exceed the $C\ell_{MAX}$ of -1.1.

b. Taxiing right turn. Assuming that a 360° taxiing right turn is required on medium hard soil in winds of 45 knots at alternate gross weight, aircraft characteristics needed in addition to those listed in Table I are:

$\ell_m = 62.7$ in.	$\delta\ = 0.008$
$\ell_x = 188$ in.	$x_{cg} = 12$ in.
$\ell_g = 289$ in.	$a\ = 102.8$ in.
$f = 8.5$ in.	$e = 0$

196

Calculation procedure is to

1. Select friction coefficients

    μ_s = 0.7 from Figure 15-3

    μ_r = 0.1 for medium hard soil

2. Calculate net tail rotor thrust required with zero wind from Equation 15-1:

$$T = \frac{1}{289} \left\{ 0.7 \left(\frac{1800}{2} \right) \left(1 - \frac{62.7 - 12}{188} \right) \frac{8.5^2}{8} \right.$$

$$+ 0.1 \left[102.8 + (102.8 - 188) \left(\frac{62 - 12}{188} \right) \right]$$

$$- \frac{(0.1)(0.008)}{8} (0.001868) \; \pi \; (24.5)^2 \; (750)^2$$

$$\left. (24.5) \right\} = 439 \text{ pounds}$$

3. For a streamlined afterbody, the thrust required to balance fuselage moment at 8000 feet in 35-knot winds is 86 pounds as obtained from Figure 13-6. At 45 knots, the thrust required

$$= 86 \; \frac{(45)^2}{(35)^2} = 142 \text{ pounds}$$

4. The total thrust required is

    $$\begin{array}{r} 439 \text{ pounds} \\ + \; 142 \text{ pounds} \\ \hline 581 \text{ pounds} \end{array}$$

    Thus the autorotational yaw maneuver is more critical (606 pounds) and, therefore, requires more negative blade incidence. If the aircraft were required to perform the right taxi turn in soft sand (μ_r = 0.3), the taxi turn would be critical compared to the autorotational maneuver.

c. Left Sideslip Envelope. The trim analysis required to determine the maximum right pedal for a specified left sideslip envelope is not presented in this example.

197

16. **Design Tail Rotor Power**

Guideline 16 outlines methods for obtaining tail rotor power for use in aircraft performance calculations and for obtaining design power for tail rotor drive-strength design.

Trim Power in Hover

To obtain sea-level trim power is hover at alternate gross weight, calculate K_T (from Guideline 13):

$$K_T = 1.2 \sqrt{2\rho\pi}\ R^2\ FM\ \Omega$$

$$= 1.2 \sqrt{2(0.002378)\ \pi}\ (24.5)^2\ (0.70)\ (30.6) = 1886$$

From Figure 13-1, $T_{TRIM} = \dfrac{W^{3/2}}{K_T} = \dfrac{18000^{3/2}}{1886} = 1280$

Converting to C_{T_N},

$$C_{T_N} = \frac{1280}{(0.002378)(\pi)(5.5)^2(700)^2} = 0.0116$$

For zero wind speed and $s/r = 0.45$,

$C_T/C_{T_N} = 1.1$ from Figure 8-1

Use Figure 14-2 to obtain $C_{T_O} = 0.012$.

From Figure 16-3,

$$hp/\rho\pi\ r^2 = 900$$

$$hp = (900)(0.002378)\pi(5.5)^2 = 203.4$$

Static Strength Power Determination

a. For $\sigma = 0.20$ and $\upsilon = 23.2°$ as selected in part 14 of this example, the isolated C_{T_O} at $V = 0$ knots is 0.0316 from Figure 14-4 of Guideline 14.

b. From Figure 16-3 for $\sigma = 0.20$, $\omega r = 700$ fps, and $C_{T_O} = 0.0316$, the isolated static value of $hp_O/(\rho\pi\ r^2) = 3700$.

c. The static horsepower will be maximum at sea level; thus hp_O (at sea level standard) $= 3700\ (0.00237)(\pi)(5.5)^2 = 833$.

This is the horsepower on which the static strength of the drive system should be based.

Maximum horsepower required during critical maneuver at 20 knots at alternate gross weight (18,000 pounds) and 8000 feet altitude (standard).

a. The actual C_{T_N} from the critical 15 deg/sec yaw maneuver is 0.0220 from part 13 n.

b. For $C_{T_N} = 0.00220$, $\overline{A} = 0.25$. $\overline{A}\mu = 0.021$ (part 14 a) and $s/r = 0.45$ for pusher, read

$$C_T/C_{T_N} = 1.2 \text{ from Figure 8-1}$$

c. From Figure 14-2 of Guideline 14 for

$$C_T/C_{T_N} = 1.2$$

$$V = 20 \text{ knots}$$

$$C_{T_N} = 0.0220$$

$$\text{read } C_{T_O} = 0.0282$$

d. From Figure 16-2 (Guideline 16) for $\sigma = 0.20$ and $\omega r = 700$ fps, read

$$hp/(\rho\pi\ r^2) = 3700$$

Thus $hp = 37000\ (0.00187)(\pi)(5.5)^2 = 657$ hp

This is the peak horsepower during the given maneuver for isolated tail rotor.

e. When tail rotor is in presence of main rotor and fin for $V = 20$ knots, the 657 horsepower must be multiplied by the factor from Figure 16-1 (Guideline 16) which is 1.24 for $\overline{A} = 0.25$. Thus, the actual peak power in presence of main rotor and fin is

$$(657)(1.24) = 815 \text{ hp}$$

17. Pitch Flap Coupling

From Guideline 17, select a δ_3 of -45°; therefore, the maximum tip path plane travel will be in the order of $\pm(20^\circ)(\cos\delta_3) = \pm14^\circ$.

199

18. Tail Rotor Shaft Sweep

Guideline 18 discusses the effects of tail rotor shaft sweep. For this sample problem, the selected shaft sweep will be zero, which is a good trade-off between pedal travel, blade and pitch link loads, and high-speed power required by the tail rotor. Since the vertical fin is set at 3^0 right incidence (produces force to right in forward flight), it will reduce the collective pitch of the tail rotor required for high-speed flight.

19. Control Rate Damping

The total blade incidence travel is the sum of lett pedal plus right pedal incidence or $23.2 + 13.8 = 37.0^0$. Guideline 19 recommends that the control rate limiting be one-third of this value; therefore, select $37.0/3 = 12.3$ deg/sec as the maximum value for rate of change of tail rotor blade incidence.

20. Mechanical Flapping Stops

As recommended in Guideline 20, the mechanical flapping stops should be placed at $\pm 20^0 \cos \delta_3$ or at $\pm (20)(0.707) = 14^0$. In some installations a soft stop is provided at values lower than the $\pm 14^0$. Consideration should be given to the mean coning angle.

CONCLUSIONS AND RECOMMENDATIONS

Conclusions

1. Design guidelines have been formulated which quantify data in such a manner that tail rotor systems evolved from such guidelines should show good performance and control characteristics and should have sufficient strength to meet severe operating conditions.

2. A new consideration (rudder pedal motion in side flight) for selection of tail rotor disc loading has been developed.

3. Thrust requirements are as important as thrust output. Considerable emphasis has been placed on a convenient and accurate method which considers the several critical variables and conditions upon which the total required design thrust depends.

4. Variations in main rotor trim cyclic (tip path plane position) caused by changing the helicopter's longitudinal center of gravity have the same effect as raising or lowering the tail rotor position.

5. The effects of the tail-rotor induced flow velocity on the main rotor power required are shown to increase the main rotor power, especially in the rear flight quadrants. This will increase the trim thrust required by the tail rotor and, as usually calculated, reduce aircraft hover ceiling performance.

6. A method has been developed to conveniently transfer critical tail rotor test data into isolated tail rotor data, permitting parameter selection from design data developed on the basis of an isolated tail rotor.

7. A convenient method to select tail rotor tip speed and number of blades, based on detection distance, has been prepared and documented.

8. A new design chart has been developed to permit rapid determination of fin losses for several variables such as conditions of flow, fin size, and fin position with respect to the tail rotor.

9. The fin increases the power required by the tail rotor. Such effects have been included by showing a power multiplying factor variation with fin blockage ratio.

10. Horizontal stabilizer loads can approach the magnitude of the main rotor disc loading in rearward flight and three times that disc loading in forward flight. These loads are the major cause of ground skittishness in rearward flight and stick reversal in forward flight transition.

Recommendations

1. Due to the geometry of the Boeing test rig, fin loads were measured for only one position of the tail rotor (mid). Future tests should be conducted to determine if the same fin loss characteristics, as presented in this report, apply to other locations of the tail rotor.

2. During the Boeing tests, the effect of the tail rotor flow on main rotor power requirements was not expected; therefore, tests were not conducted in enough variations such as main rotor alone and in different attitudes and several tail rotor loadings which would have given assurance that such results shown were completely quantified. It is recommended that future tests be made to cover many more main rotor attitudes, loadings with more combinations of fin areas, and tail rotor loadings.

3. The majority of the guidelines related to the thrust output and power required of a tail rotor are based on Boeing test conditions, which are believed to be critical; however, such conditions are based on one specific main rotor disc loading. Such disc loading governs the position and strength of the ground and main rotor trailing vortices. In the future, the effect of main rotor disc loading should be further investigated.

4. Fin effects on the tail rotor shaft and net thrust have been empirically calculated on the basis of test data taken for one size and shape of fin. Although the method used to calculate the effect of other sizes of fins is believed justified, future tests should be conducted to verify fin size effects shown in this report.

5. The detection distance versus tip speed curves have been prepared on the basis of one sound attenuation condition and one ambient noise condition. Future expansion of these guidelines should be made, considering other variants of these conditions.

6. The critical design condition has been selected as a left yaw maneuver initiated in a 20-knot right sidewind with no tail rotor airfoil stall allowed for this condition or for the condition of full left pedal on the ground. These conditions are severe, but are sufficiently straightforward

202

to allow for computation of thrust requirements. Rapid arrestment of a right turn yaw maneuver, however, may be even more severe in initiating stall of the tail rotor. Future in-flight tests should be conducted to determine the maneuver where the greatest thrust is required.

7. Boeing tests show a great effect of wind, h/d, and wind azimuth on the main rotor flow field. Because of the many combinations of these variables, it is suggested that eventually a theory should be developed to describe such a flow field and that tail rotor performance in such a field should be predicted and checked with test results.

8. The method for selection of solidity and maximum blade incidence depends on: What are the rotor limits of the tail rotor? That is: what is the maximum thrust a given tail rotor can produce? Is such thrust limited by power, pitch link loads, stall flutter, or thrust drop-off as determined by airfoil characteristics? Tests should be conducted to determine the rotor limits of full-scale tail rotors so that the upper limits of thrust can be more clearly defined for tail rotor design.

9. In the future, the guidelines should be expanded to include guidelines for good dynamical behavior of tail rotors.

10. In Guideline 13, the condition of a specified rate of yaw at the end of a given time period, together with a selected thrust margin, was chosen as the critical condition to be used in selection of the design thrust of the tail rotor. This condition was selected because it has most recently been specified by various agencies. For future application, conditions such as the three stated in Guideline 13 should be reexamined. Particular attention should be given to the selection of parameters that are completely based on holding the aircraft in trim under the most extreme conditions of wind, gusts, gross weight, and altitude. Fixed-wing aircraft designed on such a basis meet all the maneuver requirements for normal operation.

11. Considerable power can be required by the tail rotor in certain maneuvers as shown in the example design. If the sum of the tail rotor power and the main rotor power exceeds that available from the powerplant, the tail rotor will take energy from the main rotor and, as a result, the main rotor rpm will drop. Reference 11 suggests that an acceptable value of main rotor rpm drop is 2 percent in 1 second. This criterion is not considered in this report, but it should be considered in future use.

203

12. The effect of fin blockage ratio on tail rotor power
    required has been quantified for one blockage ratio and
    for the pusher condition at a fixed distance from the
    fin. This effect on power should be expanded for other
    fin distances, for blockage ratios, and for both pusher
    and tractor positions.

13. The effect of tail rotor blade incidence rate of change
    on flapping has been discussed, but its effect on thrust
    and power required has not been quantified for a maneu-
    ver. It is recommended that transient tests be conducted
    so that the effect of blade incidence change rate on
    power and thrust can be quantified for various grades of
    maneuver.

14. Tail rotor power required in hover trim was 203 horse-
    power for the example tail rotor design shown in this
    report. In full left pedal incidence on the ground at
    sea level, the power required was 833 horsepower. In the
    future, methods should be investigated so that such a
    large increase in power above trim power required can be
    reduced to allow for lighter weight tail rotor drive
    systems.

15. The airfoil characteristics recommended in this report
    require a section that stalls from the trailing edge, but
    still retains high-lift characteristics. It is recom-
    mended that further research be conducted on full-scale
    tail rotors to determine the airfoil section that pro-
    duces the most stable characteristics in and near stall.

16. A velocity of 20 knots was suggested as the critical
    velocity for tail rotor thrust output. Some velocity
    less than 20 knots will, however, be critical with regard
    to maximum main rotor power and, in turn, maximum tail
    rotor trim thrust required. Thus, velocity lower than
    20 knots may be more critical in the selection of solid-
    ity and blade incidence. It is suggested that further
    tests and analyses be conducted to more clearly define
    the critical design velocity.

LITERATURE CITED

1. Huston, R. J., and Morris, C. E. K., Jr., A WIND TUNNEL INVESTIGATION OF HELICOPTER DIRECTIONAL CONTROL IN REARWARD FLIGHT IN GROUND EFFECT, NASA TN D-6118, National Aeronautics and Space Administration, Washington, DC, March 1971.

2. Wiesner, W., and Kohler, G., TAIL ROTOR PERFORMANCE IN PRESENCE OF MAIN ROTOR, GROUND, AND WINDS, AHS Preprint 764, American Helicopter Society, New York, NY, May 1973.

3. Nagata, J. T., and Bass, M. W., ARMY PRELIMINARY EVALUATION OF THE AH-1G TRACTOR TAIL ROTOR MODIFICATION, Final Report, USAASTA Project No. 68-37, United States Army Aviation Systems Test Activity, Edwards Air Force Base, CA, June 1969.

4. Lehman, A. F., MODEL STUDIES OF HELICOPTER TAIL ROTOR FLOW PATTERNS IN AND OUT OF GROUND EFFECT, Oceanics, Inc., USAAVLABS TR 71-12, U.S. Army Air Mobility Research and Development Laboratory, Ft. Eustis, VA, April 1971.

5. Melton, J. R., and Hall, G. C., ENGINEERING FLIGHT TEST OF THE AH-1G HELICOPTER TO DETERMINE THE AREA OF INADEQUATE DIRECTIONAL CONTROL POWER AT 8100 POUNDS GROSS WEIGHT, Final Report, USAAVNTA Project No. 66-06, U.S. Army Aviation Test Activity, Edwards Air Force Base, CA, February 1968.

6. Gault, D. E., A CORRELATION OF LOW-SPEED, AIRFOIL-SECTION STALLING CHARACTERISTICS WITH REYNOLDS NUMBER AND AIRFOIL GEOMETRY, NACA TN 3963, National Aeronautics and Space Administration, Washington, DC, March 1957.

7. Yeager, W. Jr., Young, W. Jr., and Mantay, W., A WIND TUNNEL INVESTIGATION OF PARAMETERS AFFECTING HELICOPTER DIRECTIONAL CONTROL IN LOW-SPEED FLIGHT IN GROUND EFFECT, Langley Directorate, U.S. Army Air Mobility Research and Development Laboratory, Langley, VA (to be published).

8. Robinson, F., INCREASING TAIL ROTOR THRUST AND COMMENTS OTHER YAW CONTROL DEVICES, Journal of the American Helicopter Society, Vol. 15 (4), New York, NY, October 1970.

9. Lynn, R. R., Robinson, F. D., Batra, N. N., and Duhon, J. M., TAIL ROTOR DESIGN, PART I - AERODYNAMICS, Journal of the American Helicopter Society, New York, NY, Vol. 15 (4), October 1970.

10. Davenport, F. J., ANALYSIS OF PROPELLER AND ROTOR PERFORMANCE IN STATIC AND AXIAL FLIGHT BY AN EXPLICIT VORTEX INFLUENCE TECHNIQUE, Boeing Vertol Report R-372, Boeing Vertol Company, Philadelphia, PA, February 1965.

11. Grumm, A. W., and Herrick, G. E., ADVANCED ANTITORQUE CONCEPTS STUDY, Sikorsky Aircraft, USAAMRDL TR 71-23, Eustis Directorate, U.S. Army Air Mobility Research and Development Laboratory, Ft. Eustis, VA, July 1971.

12. Gessow, A., and Myers G. C., Jr., AERODYNAMICS OF THE HELICOPTER, New York, NY, Ungar Publishing Co., 1967.

13. Heyson, H. H., and Katzoff, S., NORMAL COMPONENT OF INDUCED VELOCITY IN THE VICINITY OF A LIFTING ROTOR WITH A NON-UNIFORM DISK LOADING, NACA TN 3690, National Aeronautics and Space Administration, Washington, DC, April 1956.

14. Sternfeld, H., Bobo, C., Carmichael, D., Fukushima, T., and Spencer, R., AN INVESTIGATION OF NOISE GENERATION ON A HOVERING ROTOR, PART II, Boeing Vertol Company, Contract DAHC 04-69-C-0089, Army Research Office, Durham, NC, November 1972.

15. Lowson, M. V., and Ollerhead, J. B., STUDIES OF HELICOPTER ROTOR NOISE, Wyle Laboratories, USAAVLABS TR 68-60, Eustis Directorate, U.S. Army Air Mobility Research and Development Laboratory, Ft. Eustis, VA, January 1969.

16. Ollerhead, J. B., HELICOPTER AURAL DETECTIBILITY, Wyle Laboratories, USAAMRDL TR 71-33, Eustis Directorate, U.S. Army Air Mobility Research and Development Laboratory, Ft. Eustis, VA, July 1971.

17. Ormiston, R., SURVEY WITH HYDROGEN BUBBLES OF AIR FLOW IN VICINITY OF MAIN ROTOR AND TAIL ROTOR, paper to be presented at the 30th Annual National Forum of the American Helicopter Society, Washington, DC, May 1974.

APPENDIX I

SUMMARY OF TAIL ROTOR SERVICE EXPERIENCE

This section presents samples of problems which have been encountered with tail-rotor helicopters as reported from several sources. This listing is far from complete, but it is thought to contain some of the problems that may be eliminated if careful consideration is given to the use of the guidelines formulated in this report. It should be noted that many of the listed problems were solved by the very means recommended by these guidelines. Such experience has been extremely useful in formulation of the guidelines.

1. Conner, William J., "The Huey Cobra in Vietnam", 1968
    Report to the Aerospace Profession, Tech. Rev., Vol. 9,
    No. 2, Society of Experimental Test Pilots, 1968.

    The Huey Cobra was found to have inadequate directional
    control at high gross weight or with a left quartering
    tailwind. The first attempted correction was an increase
    of maximum blade pitch to 23°. This resulted in over-
    torque to the tail rotor drive train. The original
    pusher tail rotor was then replaced by a tractor.

    Another problem was that excessive pilot compensation was
    required to maintain coordinated flight during gunnery
    runs. To obtain zero sideslip, right pedal had to be
    continuously applied which required excessive pilot
    attention.

2. Johnston, J.F., and Cook, J.R., AH-56A Vehicle
    Development, AHS Preprint No. 574, May 1971.

    Inadequate directional control was encountered at high
    gross weights and in left sideward flight (which was
    limited to 15 knots). In left sideward flight, the pedal
    required changed rapidly between 10 and 15 knots. This
    effect was described by the pilots as "stepping into a
    hole" and is illustrated in Figure 8, which is taken from
    a preliminary version of the reference.

    The causes of these problems are tail rotor operation in
    the main rotor wake, close to the pusher propeller, and
    close to the ground. In full-scale tests, the main rotor
    was found to have the greatest effect.

    The fin had no effect in the pusher configuration. With
    the pusher configuration, the fin loss was approximately
    the same as the loss from the main rotor wake.

207
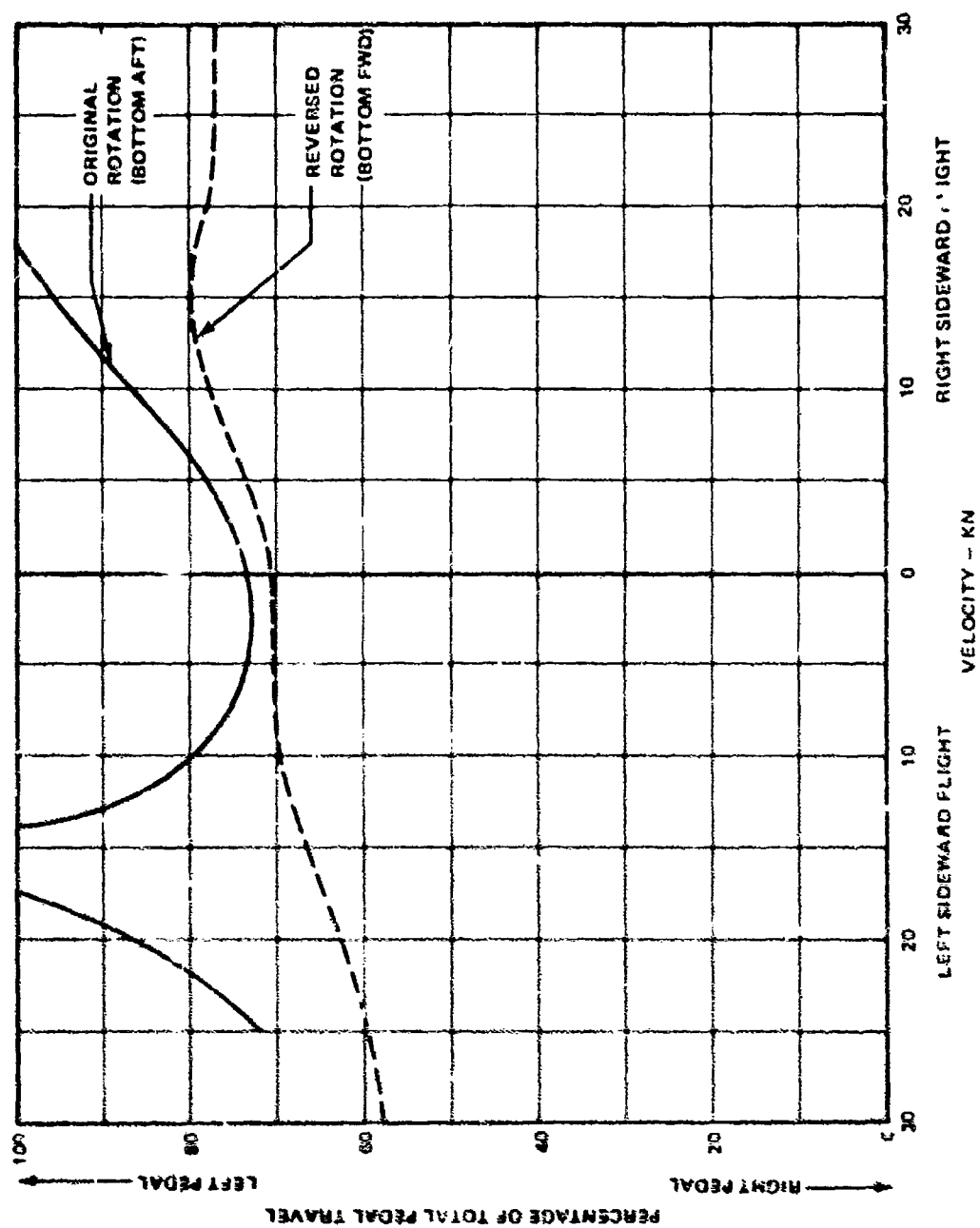
Figure B. Typical Pedal Requirements for AH-56A in Right and Left Sideward Flight (Reference 2, Appendix I).

208

Bottom forward rotation increased thrust IGE, but not OGE. The sideward flight problem was eliminated with bottom forward rotation.

3. Westphal, J.F., and Colvin, G.L., "YUH-1B Stability and Control Tests", Tech. Documentation Report Number 62-13, August 1962, AFFTC Edward Air Force Base, California.

Precision hovering was more easily accomplished in the YUH-1B than in the earlier HU-1/H-40 helicopters. The oscillations about all axes, criticized in the previous HU-1, were nearly eliminated in pitch and roll. A random yawing oscillation remained which required continuous pedal applications to control. This oscillation decreased above a 30-foot skid height.

4. Army Preliminary Evaluation of the AH-1G Tractor Tail Rotor Modification, USAASTA Project No. 68-37 Final Report, June 1969.

The standard (pusher) configuration (bottom aft rotation) was unstable at most crosswind and tailwind headings at 12 to 14 knots, resulting in marginal or inadequate directional control.

The tractor (bottom forward rotation) tail rotor was more stable and easier to control than the pusher. However, the problem of inadequate control was not eliminated. Adequate control was not available in many right wind conditions. Figure 9 is a typical plot of pedal position versus wind azimuth at 31 knots wind speed. There is insufficient left pedal to stabilize the heading from 60° through 110° of azimuth.

The results indicate that rapid arrestment of hover turn rates greater than 30 deg/sec produces very high power loads in the tail rotor drive system. Large pedal inputs (more than 1 inch) must be avoided, regardless of the initial turn rate, to prevent excessive power loading of the tail rotor shaft or to at least minimize the period of time that the tail rotor shaft horsepower limit is exceeded.

5. Vertical Replenishment Mission Evaluation (RH-3A Helicopter) Naval Air Test Center Tech. Report FT-62R-68, 5 September 1968.

Directional control power was found to be inadequate for normal maneuvering for $\psi = 60^\circ$ to 140° at high gross weights. At maximum gross weight (19,000 pounds) and $\psi = 90^\circ$, the maximum acceptable wind was 15 knots. In a 30-knot wind at $\psi = 90^\circ$, the gross weight must be reduced to 17,000 pounds.
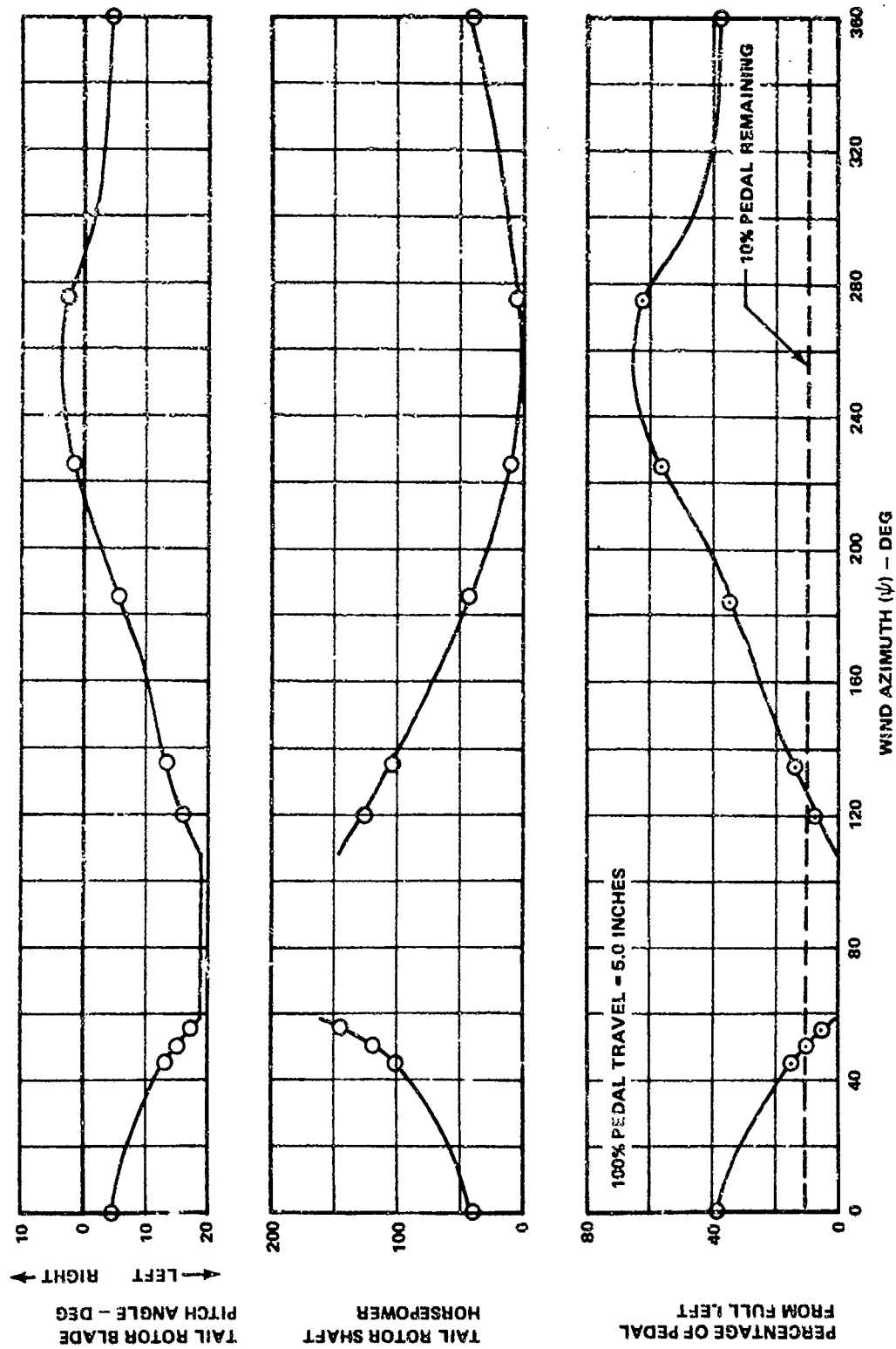
Figure 9. Directional Control of AH-1G Tractor Tail Rotor (Reference 3) — V = 31 kn, W = 8620 lb, Density Altitude = 6140 ft.

210

6. Vertical Replenishment Mission Evaluation (UH-2C
    Helicopter) Naval Air Test Center Tech. Report FT-61R-68,
    30 August 1968.

    The UH-2C, in IGE hover, suffered from lack of adequate
    directional control power and control effectiveness (see
    Figure 10). In winds between 75° and 125° and in excess
    of 12 to 15 knots, left directional control was insuffi-
    cient at gross weights greater than 11,000 pounds (see
    Figure 11). Left pedal stops were contacted often, while
    the pilot attempted to stabilize the aircraft for the
    steady-state conditions shown in Figure 11. There was
    insufficient control margin to counteract disruptions to
    stabilized flight in the preceding wind conditions.

    Directional instability was also experienced in winds at
    270° at 25 knots for gross weights greater than 10,000
    pounds.

7. BO-105 Tech. Translation No. 7556-10/71, "MBB's Response
    to Boeing Questions", October 1971.

    The BO-105, with bottom aft rotation, encountered a dis-
    tinct shudder of the tail resulting in increased pilot's
    pedal movement during left side flight between 8 and 18
    knots. Changing the direction of rotation eliminated the
    problem.

8. Vertical Replenishment Mission Evaluation (RH-3A
    Helicopter), Naval Air Test Center Tech. Report FT-62R-68,
    5 September 1968.

    Directional control power was not adequate for the
    VERTREP mission. The critical condition was reached in
    right sideward flight (wind from 60° to 140°, relative).
    Increased gross weight in this wind condition further de-
    creased left directional control power. During shipboard
    operations, the left directional control stop was reached
    on several occasions with the relative wind near 90°.
    This usually occurred when an increase in collective
    pitch or some other factor developed a slight right yaw
    rate. Full left pedal was then required to arrest the
    yaw rate.

211
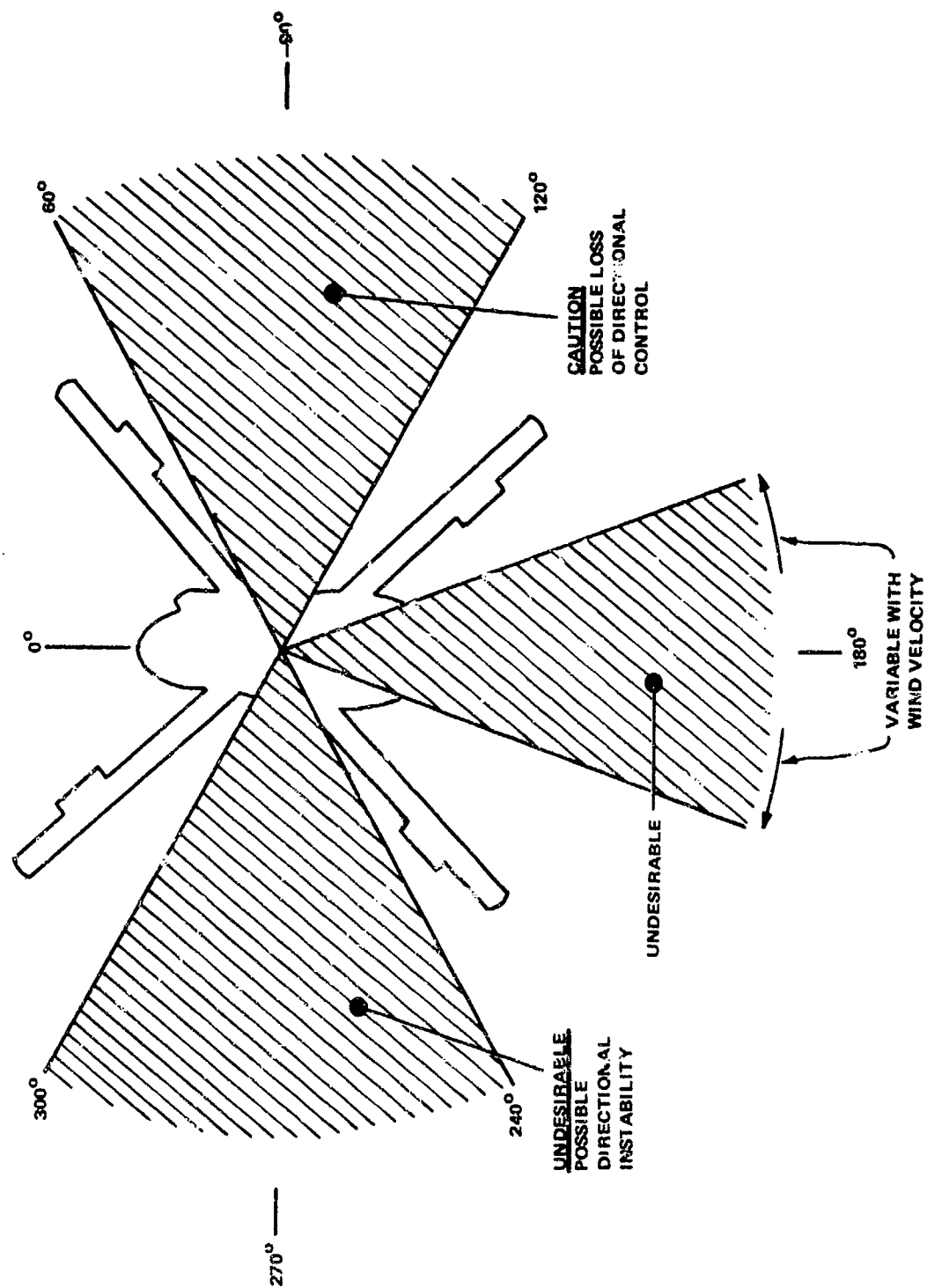
Figure 10. Effects of Wind Relative to Helicopter (Reference 6, Appendix I).
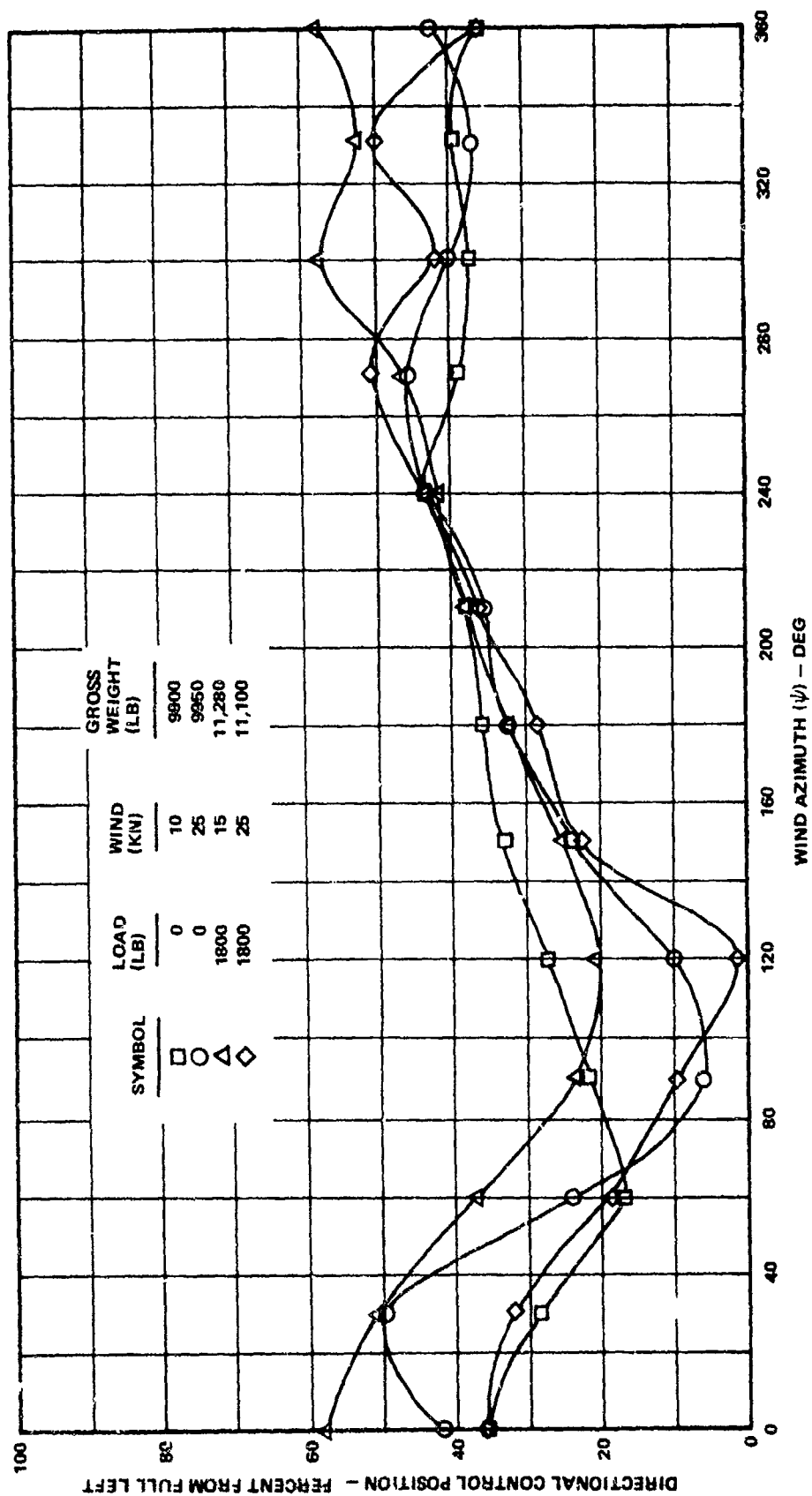
Figure 11. Directional Control of the UH-2C Helicopter (Reference 6, Appendix I).

213

APPENDIX II

BOEING WIND TUNNEL TEST - MODEL
DESCRIPTION AND TEST CONDITIONS

The test rig used in the Boeing wind tunnel tests, Reference 2, consisted of a fully articulated model CH-47C main rotor with a rigid tail rotor boom-mounted to the main rotor test stand. The model installed in the Boeing Vertol V/STOL wind tunnel is shown in Figure 12. Rotor characteristics and normal operating conditions are given in Table II.

TABLE II. ROTOR CHARACTERISTICS		
	Main Rotor	Tail Rotor
Number of Blades	3	4
Diameter, ft	8.0	1.57
Chord, in.	3.37	1.70
Solidity	0.067	0.23
Taper	None	None
Twist	-9° Linear	None
Cutout, % Radius	20	20
Airfoil	V23010-1.58	NACA 0012
Tip speed, ft/sec	750	650
RPM	1790	7990

The dimensions of the wind tunnel test section are 20 by 20 feet with the test section walls and ceiling removed. The main rotor test stand was pedestal-mounted to the centerline of the floor insert yaw table, providing 360° of remote control yaw angle variation. A hydraulic floor lift provided variable model height from $h/d = 0.3$ to 1.0 above the stationary floor.

The main rotor was equipped with remote collective and cyclic pitch controls, and its disc loading was held constant at approximately 7 pounds/foot^2.
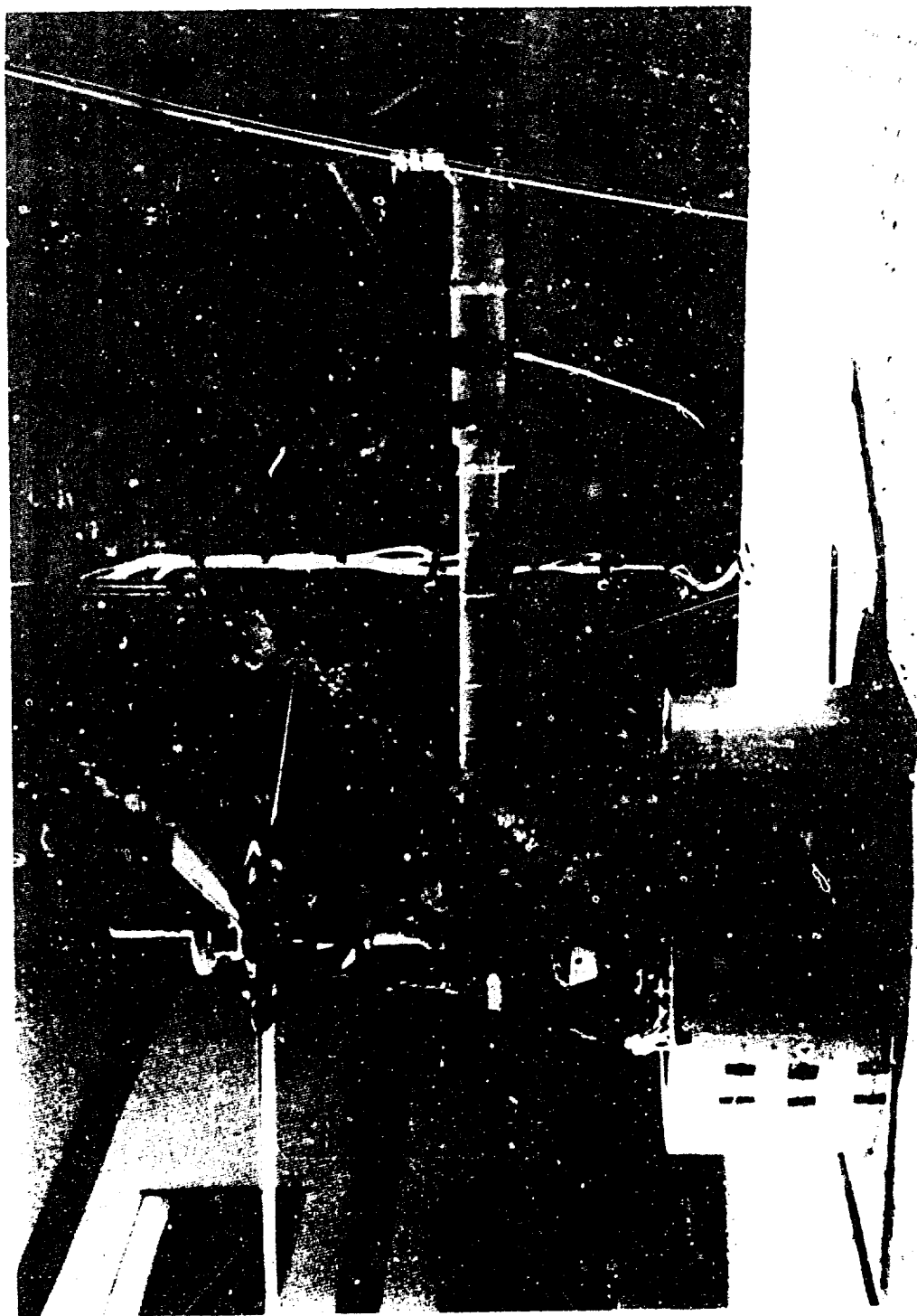
Figure 12. Fully Instrumented Rotor Test Stand With Tail Rotor Boom.

215

All runs were conducted with constant tail rotor collective
pitch, the majority at $\theta = 20^\circ$. The tail rotor was driven by
an air motor with a 52.5 foot-pound torque limit which re-
quired approximately 19 horsepower at 7900 rpm. An exhaust
pipe carried the air motor exhaust away from the vicinity of
both rotors.

The tail rotor could be located in four different positions
(see Figure 1-1). The fin and horizontal stabilizer, however,
could be mounted only in the mid position. Fin-tail rotor
separation in the mid position was variable. Diagrams of the
fin and stabilizer are shown in Figure 13. The tail rotor
could also be installed to operate in either the pusher or the
tractor configuration and with either direction of rotation.

The main rotor, tail rotor, and vertical fin were each mounted
on six-component balances with on-line steady and dynamic data
reduction. All steady data was averaged over a 1-second time
interval, and tail rotor dynamic data was averaged over three
tail rotor revolutions. The data acquisition system is ac-
curate to ±1 percent for all thrusts, moments, and torques.
Since the test section walls and ceiling were removed, no
tunnel boundary corrections were applied. Oscillograph time
history traces of tail rotor thrust, in-plane force, and rotor
moments were also taken.

Tufts were placed on the floor to locate the path of the ground
vortex and the general flow pattern. Smoke sources were placed
upstream of the model. Both still and motion picture cameras
were installed to photograph the tufts and smoke.

TEST CONDITIONS

Boeing wind tunnel test conditions are summarized in Table
III. Tail rotor collective pitch was held constant throughout
each run. Main rotor disc loading was held approximately
constant at 7 pounds/feet^2 throughout the test.

FIN BLOCKAGE
RATIO = 0.207

1.25r

0.80r

FIN AND STABILIZER USE
NACA 0018 AIRFOIL SECTIONS

0.48r

r = 0.755 FT

0.47r

1.05r

0.95r
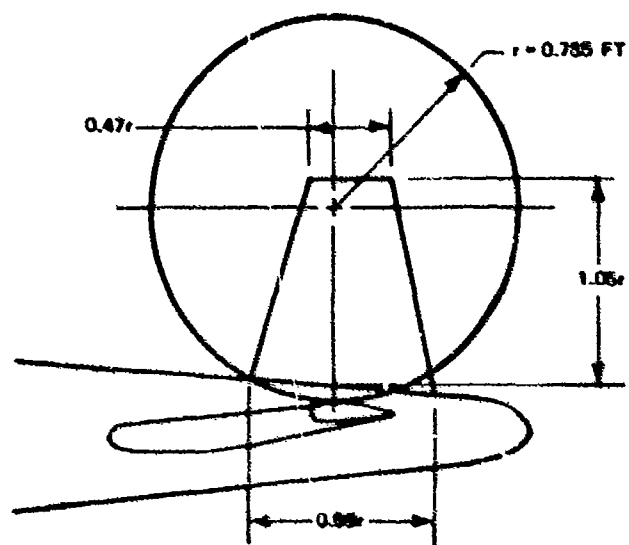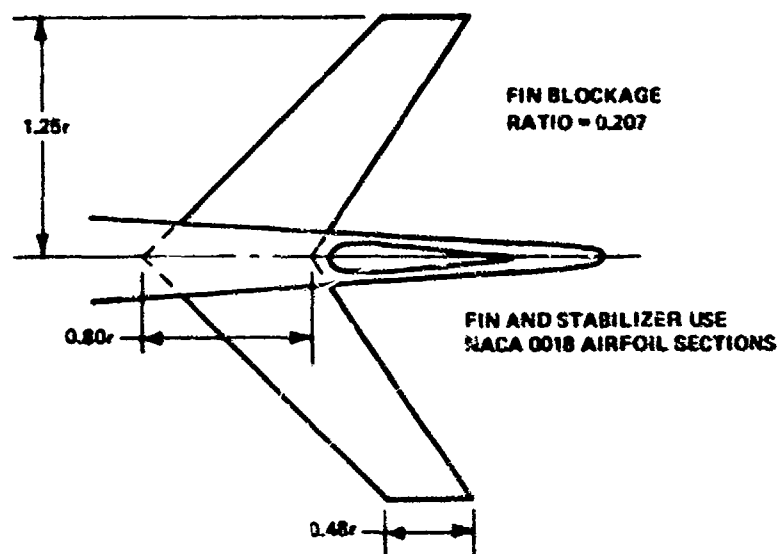
Figure 13. Horizontal Stabilizer and Vertical Fin Geometry With Tail Rotor in
MID Position.

217

TABLE III.   SUMMARY OF TEST CONDITIONS

Unless noted, V_T = 650 fps
s/r = 0.45

TAIL ROTOR POSITION	TUNNEL VELOC. (kn)	WIND AZIMUTH (deg)	θ (deg)	FIN STAB.	FIN LOC	BOT. ROT.	h/d	RUN NO.	NOTES
MID	0,12, 20,35	Sweep	11	Off/Off	Push/Fwd		0.3	1-4	Test of Tail
	0,20,35		14					5-7	Rotor Alone
			17					8-10	
			20					11-13	
	0,35		25					14,15	
MID	0	0	20	ON/ON	Push/Fwd		0.3,1.0	26,78	Test of Mid
	12,20,35	Sweep					0.3	17,20,62	Position
	20,35						1.0	21,22	
	35,50		25				1.0	81,82	
							0.3	83,84	
	35		11				0.3	85	
	20,35	60	20				Sweep	23,24	
	Sweep	180	14				0.3	35	Rear Flight
		90	14,11					34,86	Right Side Flt
		270	8,11,14					36,37,87	Left Side Flt
	0	0	20				1.0	38	Fin-T/R Sep s/r = 0.22
	0,20,35	Sweep					0.3	38,39	
	0	0					0.3,1.0	79	s/r = 0.60
	35	Sweep					1.0	80	
	0,35	Sweep	20	Off/On	N/A/Fwd		0.3/Fwd	32,33	Effect of Fin
	0,35			On/Off	Push/Fwd		0.3	27,28	Effect of Stab
	0	0		Off/Off	N/A /Fwd		Sweep	30	Effect of Fin+Stab
	20,35	Sweep					0.3	53,51	
	35						1.0	52	
	20	60					Sweep	57	
LOW	0	0	20	Off/Off	N/A /Fwd		Sweep	40	Test of Low Position
	20,35	Sweep					0.3	44,43	
	20,35						0.45	45,46	
	20	60					Sweep	41,42	
HIGH	20	60					Sweep	47	Test of High Position
	20,35	Sweep					0.3	48,49	
	35						1.0	50	
AFT	20	60					Sweep	54	Test of Aft Position
	35	Sweep					0.3	55	
	35						1.0	56	
MID	0	0	20	On/On	Trac/Fwd		0.3	59	Test of Tractor
	20	60					Sweep	59	
	35	Sweep					0.3	61	
MID	Sweep	90	14	On/On	Push/Aft		0.3	71	Effect of Dir of Rot on Side Flt
		270	8					74	
			14					72	
	0	0	20				0.3	63	Effect of Dir of Rot on Control Margin
	20	60					Sweep	64	
	20,35	Sweep					0.3	65,66	
	35						1.0	67	
	Sweep	0	20	Off/On			1.0	69	Horiz Stab Loads
					Push/Fwd		0.3	76	
							1.0	77	
		180			Push/Aft		0.3	70	
					Push/Fwd		0.3	75	
		0			N/A/N/A		0.3,1.0	91,92	Horiz Stab Loads
		180			N/A/N/A		0.3,1.0	93,94	Rotors Off
	0	–	20	On/On	Push/Aft		1.0	68	q=0,M/R On and Off
	20	0		Off/Off	N/A/Fwd		0.3	58	Effect of Cyclic, B=0,6,12
	20,35	270	N/A	On/On	N/A/N/A		1.0	73	T/R Off, Wind Fin Loads
LOW (2 Blades)	30	0 180	16	Off/Off	Push/Aft		0.4	88	Cobra Config V_T = 700 fps
	22	180 270						89	
	17.5	0 90						90	

APPENDIX III

GUIDELINE SUBSTANTIATING DATA

This appendix presents assumptions, equation derivation, and methods used to convert Boeing test data into the design charts and expressions given in the guidelines. The sections of this appendix are numbered to correspond to the appropriate guidelines. Section numbers are therefore not consecutive because many guidelines do not require substantiation in the appendix.

1.0 PLACEMENT OF TAIL ROTOR WITH RESPECT TO MAIN ROTOR

In Guidelines 1 through 4, thrust to power ratio curves are shown for constant reference thrust. C_T/C_p values for constant thrust were derived as follows:

From momentum theory (Reference 12),

$$\frac{C_T^{3/2}}{C_p} = \text{constant for small variations of } C_T.$$

Thus

$$\frac{C_{T_{Ref}}^{3/2}}{C_{p_{Ref}}} = \frac{C_{T_{Test}}^{3/2}}{C_{p_{Test}}}$$

$$\frac{C_{T_{Ref}}}{C_{p_{Ref}}} = \frac{C_{T_{Test}}^{3/2}}{C_{p_{Test}} C_{T_{Ref}}^{1/2}} = \frac{C_{T_{Test}}}{C_{p_{Test}}} \frac{C_{T_{Test}}^{1/2}}{C_{T_{Ref}}^{1/2}}$$

where the subscript Ref indicates the constant reference thrust coefficient. This correction accounts for change of induced power only.

The reference thrust was selected for each plot in Guidelines 1, 2, and 4 near the maximum thrust obtained in the $\psi = 0$ to $180°$ region. In Guideline 3, the reference was selected as the average maximum of the two curves. For example, for Figure 1-5, the constant reference thrust was selected as $C_{T_{Ref}} = 0.023$ from Figure 1-3. For the mid position at $\psi=90°$,

the test C_T is 0.0219 as obtained from Figure 1-3 and the test C_T/C_P is 4.75 as obtained from Figure 1-4. The induced power correction to obtain $C_{T_{ref}}/C_{P_{Ref}}$ at $C_T = 0.023$ is then

$$\frac{C_{T_{Ref}}}{C_{P_{Ref}}} = (4.75) \ \frac{0.0219^{1/2}}{0.0230^{1/2}} = 4.63$$

7.0 SELECTION OF OPTIMUM DISC LOADING AND DIAMETER

This section presents the methods used in Guideline 7 for conversion of C_T/σ to disc loading, the derivation of the theoretical relationship between main and tail rotor sizes, and a more thorough discussion of main and tail rotor disc loadings.

7.1 Conversion of C_T/σ to Disc Loading

To convert C_T/σ to disc loading, w, as was done to obtain Figures 7-5 and 7-6,

$$T = \frac{C_T}{\sigma} \rho \pi r^2 \ (\omega r)^2 \ \sigma$$

$$w = \frac{T}{\pi r^2} = \frac{C_T}{\sigma} \rho (\omega r)^2 \ \sigma$$

For the Boeing test,

$$w = \frac{C_T}{\sigma} \rho \ (650)^2 (0.23)$$

For $C_T/\sigma = 0.07$ and $\rho = 0.002378$ sl/ft^2,

$$w = 16.2$$

or

$$w = 231 \ \frac{C_T}{\sigma}$$

7.2 Relationship Between Main Rotor Size and Tail Rotor Size

The relationship between the size of the main rotor and the

220

size of the tail rotor can be determined using momentum theory.
The basic power equations are

$$HP_{MR} = \frac{W\ u_0}{FM(550)}$$

$$HP_{MR} = \frac{Q\ \Omega}{550}$$

where HP_{MR} = main rotor horsepower in hover

W = gross weight

u_0 = average flow velocity through the rotor

For most helicopters, the distance between centers of rotation
of the main and tail rotors is approximately $\ell = 1.2\ R$. (The
main rotor shaft is assumed to be the longitudinal cg.)

For trim

$$Q = \ell\ T_{TR} = 1.2\ T_{TR}\ R$$

Equating the above power expressions and substituting for Q.

$$\frac{W\ u_0}{FM(550)} = \frac{1.2\ T_{TR}\ \Omega R}{550}$$

from which

$$T_{TR} = \frac{W\ u_0}{1.2\ \Omega R\ FM}$$

Using

$$u_0 = \sqrt{\frac{w_{MR}}{2\rho}} = \frac{1}{R}\sqrt{\frac{W}{2\rho\pi}}$$

$$T_{TR} = \frac{W}{1.2(\Omega R)(FM)}\ \frac{1}{R}\sqrt{\frac{W}{2\rho\pi}}$$

$$= \frac{w^{3/2}}{1.2\sqrt{2\rho\pi}\ \Omega R^2\ (FM)}$$

221

Substituting $T_{TR} = w_{TR} \pi r^2$ and rearranging gives

$$\frac{R}{r} = \sqrt{K_T \frac{w_{TR}}{w_{MR}^{3/2}}}$$

where $K_T = 1.2 \sqrt{2\rho\pi} \, \Omega R^2$ (FM)

The preceding expression shows the following for given main and tail rotor disc loadings:

- Lower main rotor tip speed decreases the size of the main rotor with respect to the tail rotor (i.e., a larger tail rotor is required).

- A higher figure of merit reduces the size of the tail rotor with respect to the main rotor.

- A higher design density altitude requires a larger tail rotor with respect to the main rotor.

7.3 Main and Tail Rotor Disc Loadings

Disc loadings of the main and tail rotor are generally determined as follows:

1. The main rotor disc loading is selected as that which produces the largest payload to gross weight ratio. When all the variables such as weight, power, deflection, and downwash velocities are considered, the historical trend with gross weight is as shown in Figure 14. This chart shows that for single-rotor helicopters in the 15,000-pound weight class, the main rotor disc loading optimizes at about 8 lb/ft^2.

2. Tail rotor disc loadings are generally selected on the basis of the largest tail rotor (to minimize tail rotor power requirements and fin losses) that can be installed in the helicopter and still provide the necessary geometrical main rotor and ground clearances. Historical trends of tail rotors designed to this criterion are shown in Figure 15. There is a further consideration as discussed in Guideline 7, relating to good pedal characteristics in sideward flight. Boeing test results in Figures 7-5 and 7-6 show that the tail rotor disc loadings (with bottom forward rotation) near 14 lb/ft^2 give a good slope to the blade incidence trend with sideward flight up to 35 knots and that disc loadings as low as 10 lb/ft^2 can give satisfactory slope to 20 knots. In Figure 7-8 the trend of main/tail rotor diameter ratio with main rotor disc

222
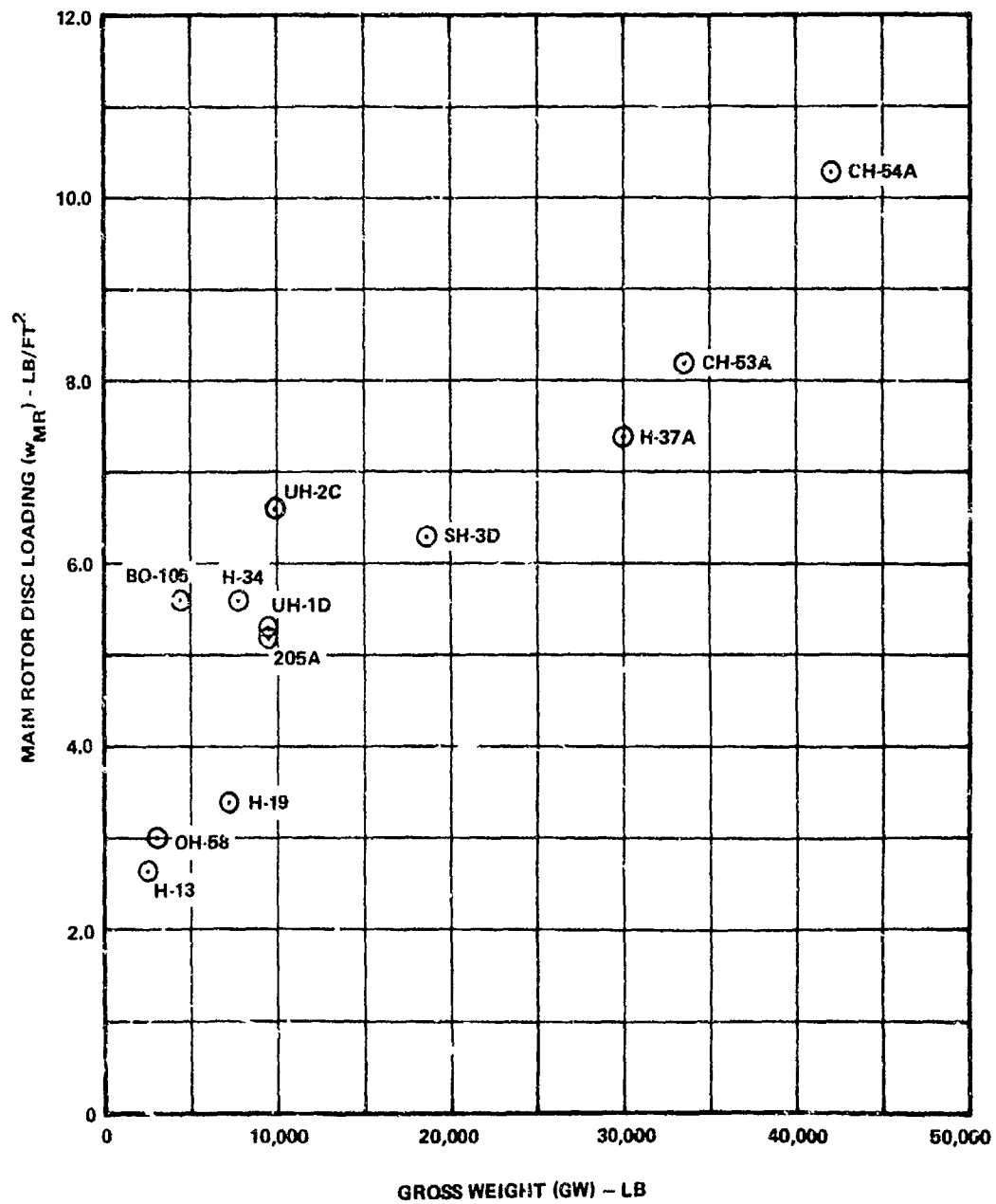
Figure 14. Main Rotor Disc Loading for Various Helicopters.
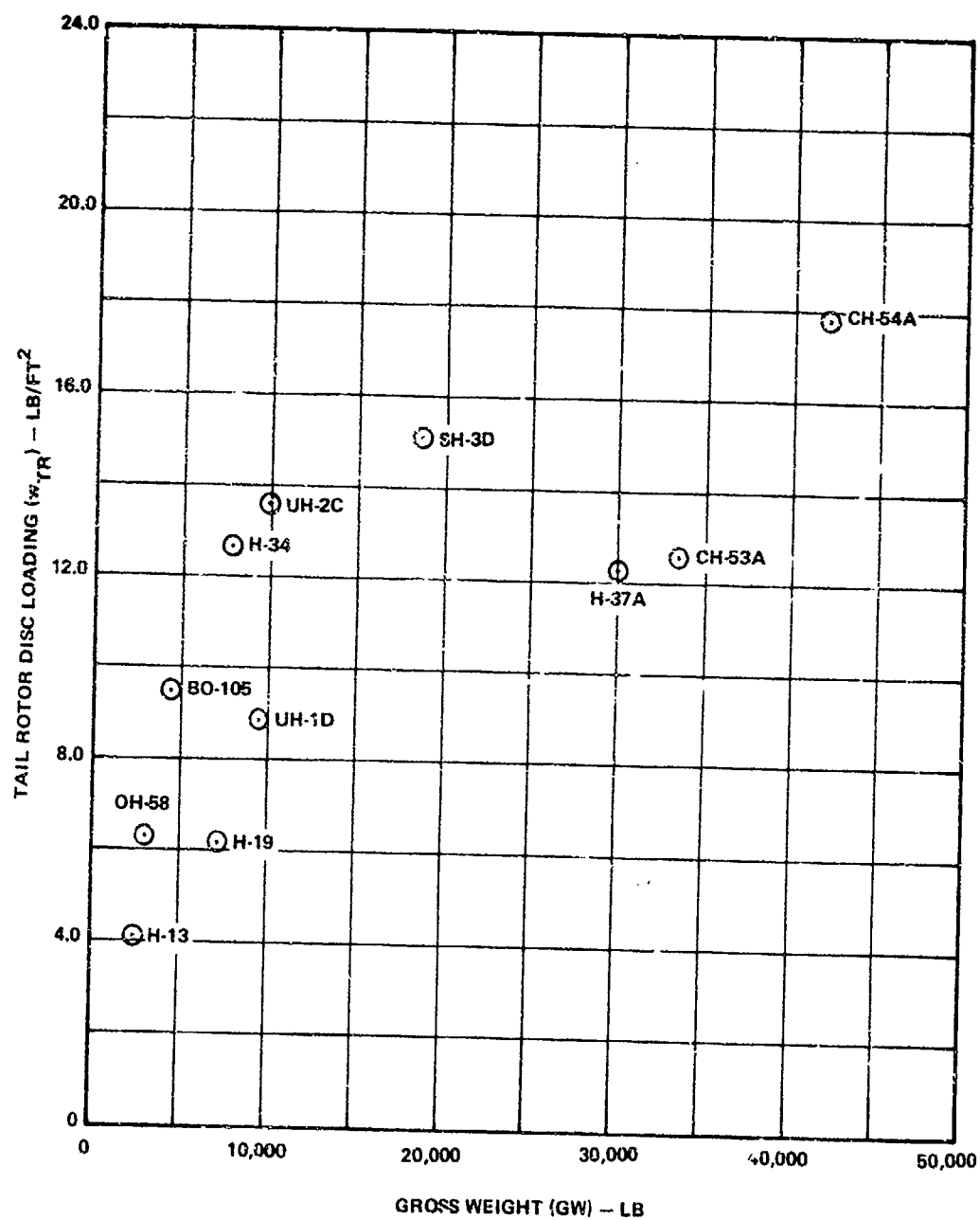
Figure 15. Tail Rotor Disc Loading for Various Helicopters.

224

loading is shown, using the equation derived above for tail rotor disc loadings of 5, 10, and 15 lb/ft^2. Comparing the historical trend with the theoretical curve shows that the modern helicopter with main rotor disc loadings of 7 and higher has a tail rotor of the correct size (disc loading) to produce good pedal travel characteristics in sideward flight up to 35 knots. Those below 7 lb/ft^2 are probably restricted to lower left sideward flight speeds. These comments assume that the tail rotor blade loading is sufficient to prevent stall of the tail rotor blade section and that the rotation is bottom forward.

Concluding Remarks

Tail rotor diameter selection (disc loading) for a given helicopter is a compromise between minimum weight and power and the design sideward flight velocity.

Disc loading should be approximately 14 lb/ft^2 at design trim conditions for a 35-knot design left sideward flight. For a 20-knot design left sideward flight, disc loading can be near 10 lb/ft^2. Figure 7-7 presents a curve for selection of disc loading, using the sideward flight criterion.

Because bottom forward rotation delays vortex ring formation, this rotation allows lower disc loadings for a given sideward flight velocity criterion.

8.0 DETERMINATION OF SHAFT THRUST TO NET THRUST RATIO (FIN LOSS)

This section presents a method to predict fin force and shaft/ ~t thrust ratio, using momentum theory and test results and ᴜᵣeating the fin as a flat plate. The method applies to the $\psi = 90^\circ$ azimuth with corrections applied for the critical azimuth of $\psi = 60^\circ$ (see Guideline 4).

8.1 Fin Force Prediction, $\psi = 90^\circ$

From momentum theory,

$$T = 2 \rho A u_0^2 = \rho A (V + u_i) 2 u_i$$

$$u_0^2 = (V + u_i) u_i$$

$$u_i = -V + \sqrt{\frac{V^2 + 4u_0^2}{2}} \text{ , where } u_0 = \omega r \sqrt{\frac{C_T}{2}}$$

225

For the tractor configuration:

$$(V) \qquad (V + u_i) \qquad \text{Fin} \qquad (V + 2u_i)$$
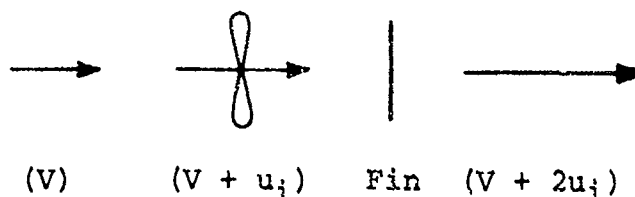
The velocity at the fin, v, is taken as the slipstream velocity at the fin position. The induced velocity ratio, C, of local to far downstream induced velocity for the proper s/r and C_T is obtained from Figure 16 (from Reference 10). Then

$$v = V + C\,(2u_i) \qquad\qquad \text{(C from Figure 16)}$$

For the pusher configuration:

$$(V) \qquad \text{Fin} \qquad (V + u_i) \qquad (V + 2u_i)$$
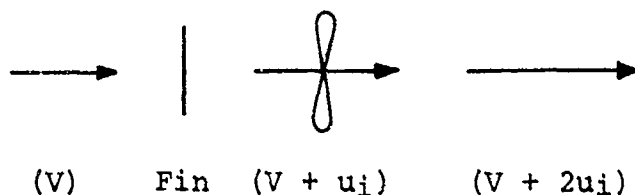
The induced velocity upstream of the disc is obtained from Figure 17 for the proper s/r. Figure 17 was obtained from the average velocity ratios across the disc as presented in Reference 13. The values of Reference 13 were calculated for no upstream obstruction. In Figure 17, these values were doubled to obtain correlation with test data with fin upstream of the rotor.

$$v = V + C\,(2u_i) \qquad\qquad \text{(C from Figure 17)}$$

Define the fin force coefficient as

$$C_f = \frac{\text{fin force}}{\rho(\omega r)^2\ \pi\ r^2}$$

For axial flow through the tail rotor, the flat plate drag coefficient is used for the fin force

$$C_f = \frac{C_D\ \rho/2\ v^2\ A_{Fin}}{\rho\ (\omega r)^2\ \pi\ r^2} = \frac{C_D}{2}\ \frac{v^2}{(\omega r)^2}\ \bar{A}$$

Using the momentum relation for induced velocity at $V = 0$ gives

$$(C_f)_{V=0} = C_D\ C^2\ \bar{A}\ C_T$$

For typical fin Reynolds numbers, $C_D = 1.4$. The fin force coefficient for the pusher is carpet plotted in Figure 18 for

226
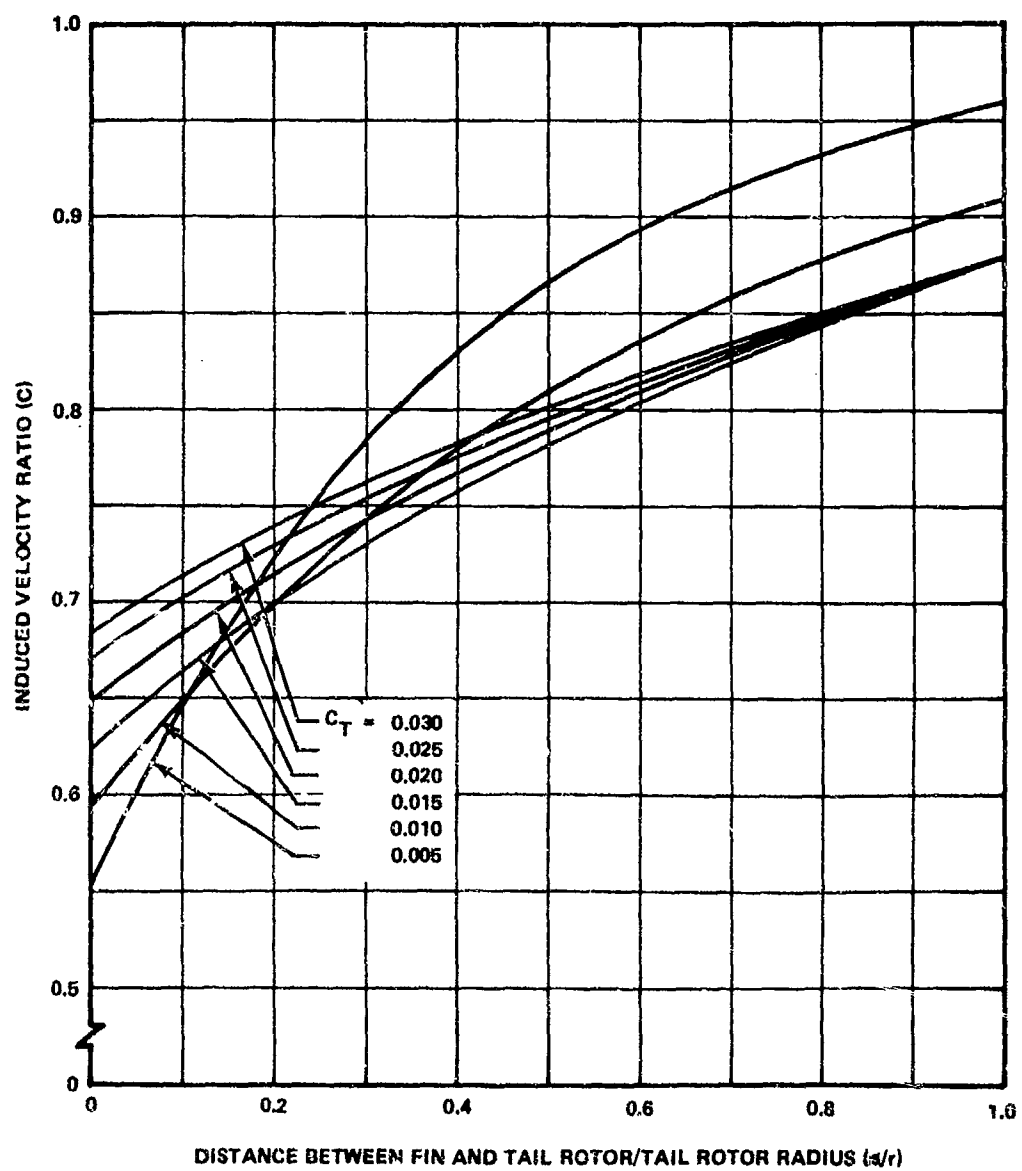
Figure 16. Induced Velocity Ratio for Tractor Tail Rotor.
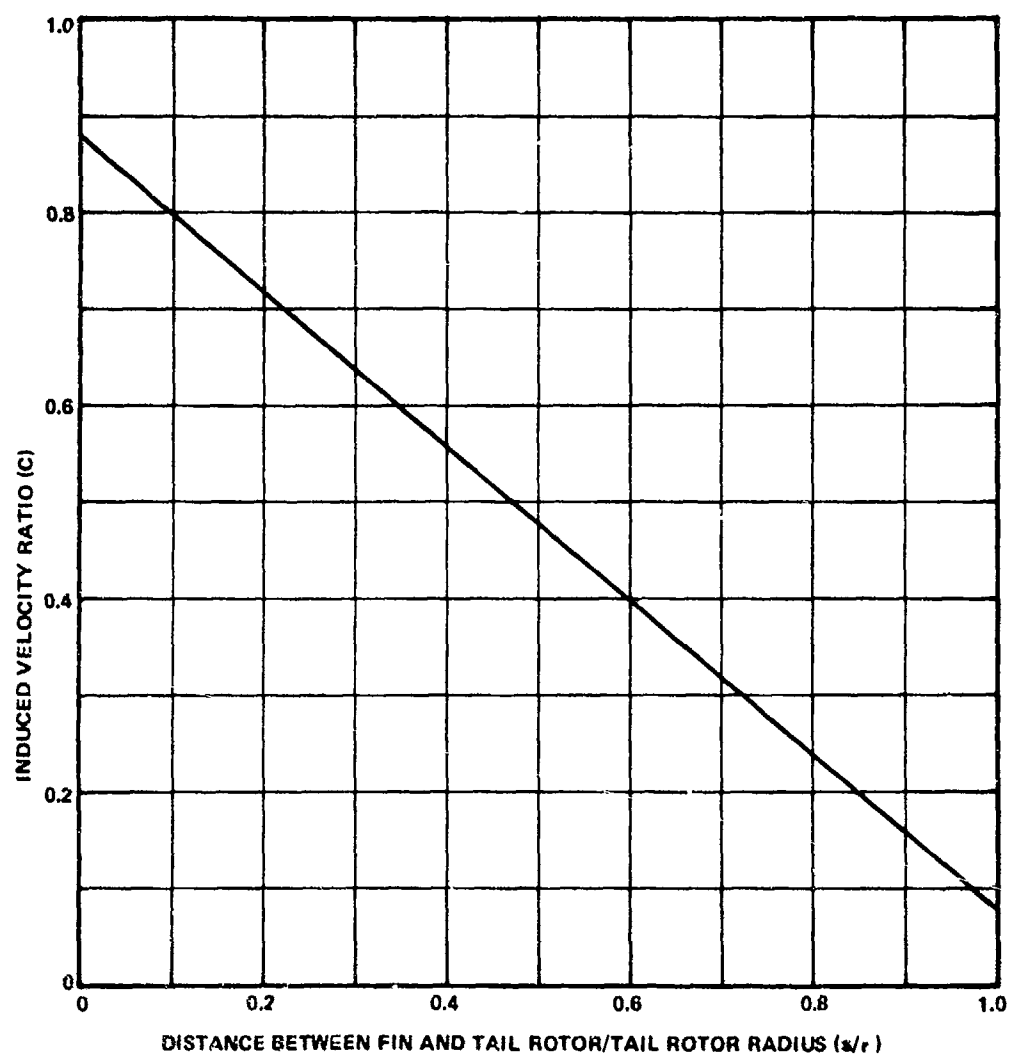
Figure 17. Induced Velocity Ratio for Pusher Tail Rotor.

228
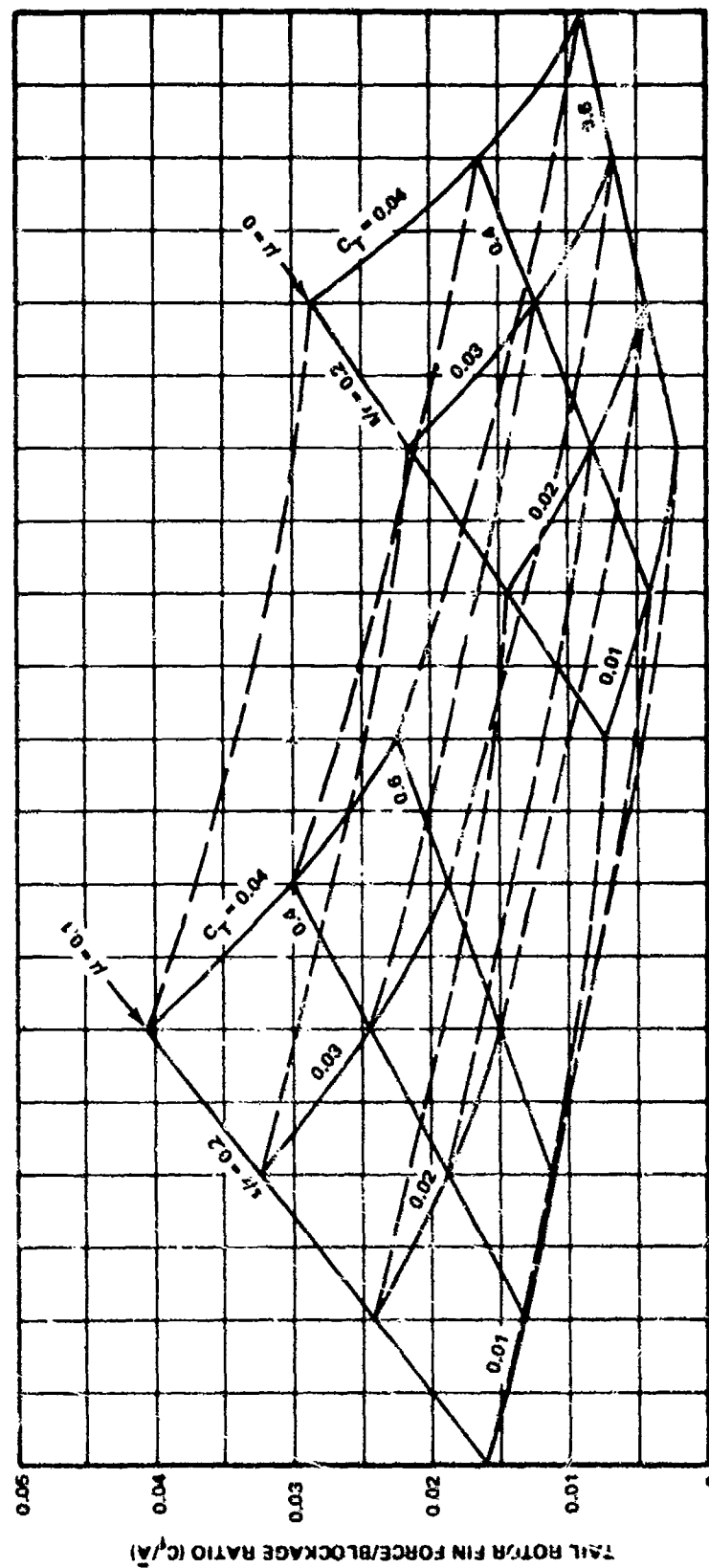
Figure 18. Determination of Fin Force Coefficient et $\psi = 90°$.

TAIL ROTOR FIN FORCE/BLOCKAGE RATIO (c_t/A)

229

various values of C_T, s/r and wind velocity referenced to tail rotor tip speed, μ_{TR}. Computed C_f is compared to test data in Tables IV and V.

8.2 Prediction of Shaft Thrust Net Thrust Ratio

To simplify the fin force prediction, let

$$C_f = (C_f)_{V=0} + \left(\frac{\Delta(C_f/\overline{A})}{\Delta \mu_{TR}}\right)_{AVE} \overline{A} \, \mu_{TR}$$

where $\dfrac{\Delta(C_f/\overline{A})}{\Delta \mu_{TR}}$ is the average slope of the velocity lines of the carpet plot (Figure 18). The average slope will vary with C_T level. Then

$$C_T = C_{T_N} + C_f$$

$$= C_{T_N} + C_D \, \overline{A} \, C^2 \, C_T + \left(\frac{\Delta(C_f/\overline{A})}{\Delta \mu_{TR}}\right)_{AVE} \overline{A} \, \mu_{TR}$$

where C is the induced velocity ratio obtained from Figure 16 for a pusher. Since the slope of $C_f/\overline{A}$ will be approximately the same for the tractor, this expression may be used if C is obtained from Figure 17.

The ratio of shaft to net thrust is

$$\frac{C_T}{C_{T_N}} = \frac{C_{T_N} + \left(\dfrac{\Delta(C_f/\overline{A})}{\Delta \mu_{TR}}\right)_{AVE} \overline{A} \, \mu_{TR}}{(1 - C_D \, \overline{A} \, C^2) \, C_{T_N}}$$

$$= \left(\frac{C_T}{C_{T_N}}\right)_{V=0} \left[1 + \left(\frac{\Delta(C_f/\overline{A})}{\Delta \mu_{TR}}\right)_{AVE} \overline{A} \, \mu_{TR}\right]$$

This equation has been plotted as a nomograph in Figure 8-1 for $C_D = 1.4$. The tractor portion of the figure was calculated

230

for an average induced velocity ratio of 0.8. For use of the nomograph, see Guideline 8. Table VI compares some predicted shaft thrust values with test data.

Test results (Figure 9-3) indicate that at the critical velocity of 20 knots (see Section 9), the fin force is greater at the critical azimuth $\psi = 60^{\circ}$ than at $\psi = 90^{\circ}$. The magnitude of the fin force at $\psi = 60^{\circ}$ is approximately constant from $V = 20$ knots to $V = 35$ knots and equal in magnitude to the fin force at $\psi = 90^{\circ}$, $V = 35$ knots. Thus, Figure 8-1 can also be used to determine shaft thrust required at $\psi = 60^{\circ}$ between 20 and 35 knots by determining from Figure 8-1 the C_T/C_{T_N} ratio at a μ_{TR} corresponding to 35 knots.

TABLE IV.	COMPARISON OF PREDICTED AND TEST FIN FORCE COEFFICIENTS, BOEING TEST DATA				
V (kn)	ψ (deg)	s/r /fin loc.	C_T	c_f calc.	c_f test
0	N/A	0.22/pusher	0.0264	0.00375	0.00453
			0.0274	0.00389	0.00436
			0.0270	0.00383	0.00467
		0.45/pusher	0.0264	0.00191	0.00255
			0.0248	0.00180	0.00190
			0.0254	0.00184	0.00230
			0.0176	0.00128	0.00170
			0.0118	0.00086	0.00110
			0.0234	0.00170	0.00190
			0.0242	0.00175	0.00170
		0.45/tractor	0.0281	0.00521	0.00620
			0.0268	0.00497	0.00620
		0.60/pusher	0.0243	0.00113	0.00120
12	90	0.45/pusher	0.0246	0.00236	0.00254
			0.0156	0.00160	0.00126
			0.0107	0.00118	0.00096
20			0.0231	0.00270	0.00255
			0.0129	0.00177	0.00227
			0.0092	0.00141	0.00110
		0.45/tractor	0.0242	0.00530	0.00591
35		0.45/pusher	0.0214	0.00364	0.00360
			0.0224	0.00374	0.00412
			0.0230	0.00268	0.00296
			0.0123	0.00380	0.00399
			0.0076	0.00216	0.00240
			0.0076	0.00216	0.00240
		0.45/tractor	0.0228	0.00602	0.00632
		0.60/pusher	0.0214	0.00304	0.00360

231

TABLE V. COMPARISON OF PREDICTED AND TEST FIN FORCE COEFFICIENTS, NASA DATA (REFERENCE 10)					
V (kn)	ψ (deg)	s/r /fin loc.	C_T	C_f calc.	C_f test
0	90	0.20/tractor	0.00300	0.00179	0.00166
		0.20/pusher	0.00800	0.00145	0.00138
		0.20/tractor	0.00850	0.00190	0.00208
10		0.20/pusher	0.00844	0.00180	0.00201
		0.20/pusher	0.00868	0.00185	0.00209
20		0.20/pusher	0.00850	0.00221	0.00240
		0.20/pusher	0.00860	0.00223	0.00248
25		0.20/pusher	0.00902	0.00245	0.00288
		0.20/pusher	0.00930	0.00251	0.00298

TABLE VI. COMPARISON OF PREDICTED AND TEST SHAFT THRUST COEFFICIENTS						
Model	Configuration	s/r	V (kn)	C_{T_N}	Predicted C_T	Test C_T
Boeing	Pusher, bottom forward	0.45	35	0.0176	0.0214	0.0214
	Tractor, bottom forward	0.45	35	0.0165	0.0230	0.0228
	Pusher, bottom forward	0.45	20	0.0206	0.0235	0.0231
	Pusher, bottom forward	0.45	0	0.0238	0.0257	0.0264
	Pusher, bottom forward	0.60	0	0.0237	0.0249	0.0255
	Pusher bottom forward	0.22	0	0.0219	0.0255	0.0264
	Pusher, bottom forward	0.45	12	0.0221	0.0246	0.0246
NASA	Pusher, bottom forward	0.2	10	0.00643	0.00846	0.00844
	Pusher, bottom forward		20	0.00610	0.00854	0.00850
	Pusher, bottom forward		25	0.00614	0.00889	0.00902
	Pusher, bottom aft		25	0.00632	0.00909	0.00930

11.0 MAIN ROTOR POWER

Main rotor power ratioed to hover power is presented in
Figures 11-1 through 11-4. The Boeing test curves were ob-
tained as follows.

A velocity sweep was conducted OGE and IGE at $\psi=0$. The power
to thrust coefficient ratio for such sweeps is shown in
Figures 19 and 20, respectively, along with data cross plotted
from azimuth sweeps. To correct for thrust drift of the main
rotor balance due to temperature effects, the C_T/C_P values for
each azimuth sweep run were ratioed such that the $\psi=0$ values
matched the headwind velocity sweep run at the corresponding
velocity.

Several test points from this data were not run at a constant
main rotor thrust. For these cases, an induced power correc-
tion was applied, ratioing the power by $T^{3/2}$. Profile power
corrections were not considered necessary, as the largest
thrust variation was 7 percent.

The main rotor power required is greatest at an azimuth of
$\psi=180^\circ$ as determined from Figures 19 and 20. The C_T/C_P values
for this azimuth are then divided into the C_T/C_P of the corre-
sponding hover isolated rotor curve to obtain the left side of
Figures 11-1 and 11-2. For comparison, main rotor power ratios
were also computed for $\psi=0^\circ$, 90° and 270° and plotted in
Figures 11-1 through 11-4.

Values of the trim coefficient C_g are noted on the figures.
C_g values above 2 correspond to a high maneuver thrust
condition.

The NASA curves (Ref 7) were obtained using the same pro-
cedure as for the Boeing curves, including induced power
corrections for non-constant isolated main rotor thrust. At
some advance ratios the maximum main rotor power occurs at
$\psi=210^\circ$, so the NASA curve on the left of Figure 11-2 is a
composite of the $\psi=180^\circ$ and 210° azimuths.

The main rotor power data of this section should be considered
as an indication of trends only. Since the main rotor data
was of secondary interest during the test, the main rotor rpm,
and in some cases thrust, was not always held constant in
order to expedite tail rotor testing. Absolute values of
power ratios may, therefore, not be exact; however, the gen-
eral order of magnitude of the effects of the tail rotor on
the main rotor are believed to be correct.
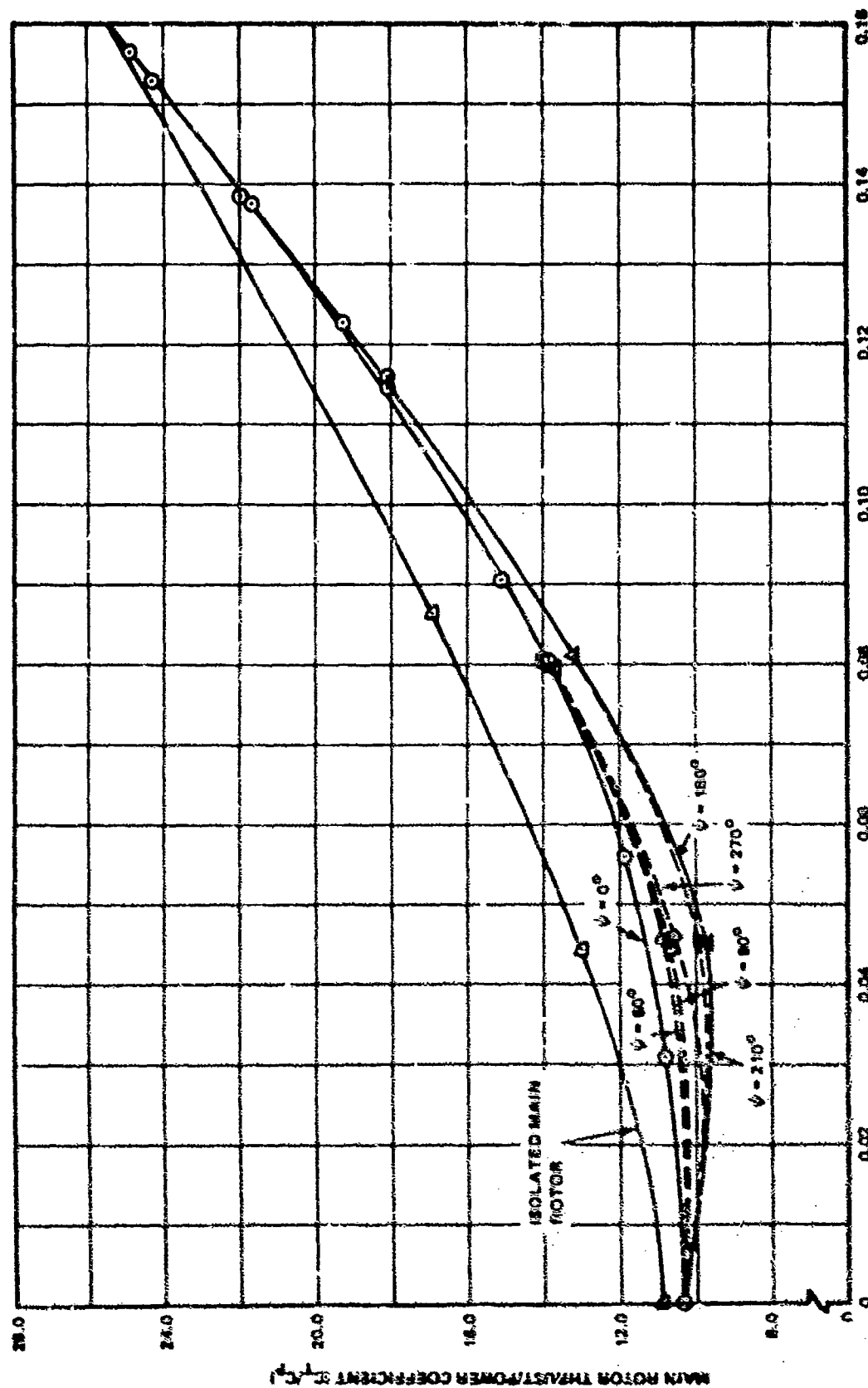
233

Figure 19. Effect of Tail Rotor and Wind Azimuth on Main Rotor Thrust/Power — $h/d = 1.2$, $\theta = 20°$, Position C MBD, Ramsden < BF. $C_Q = 2$.
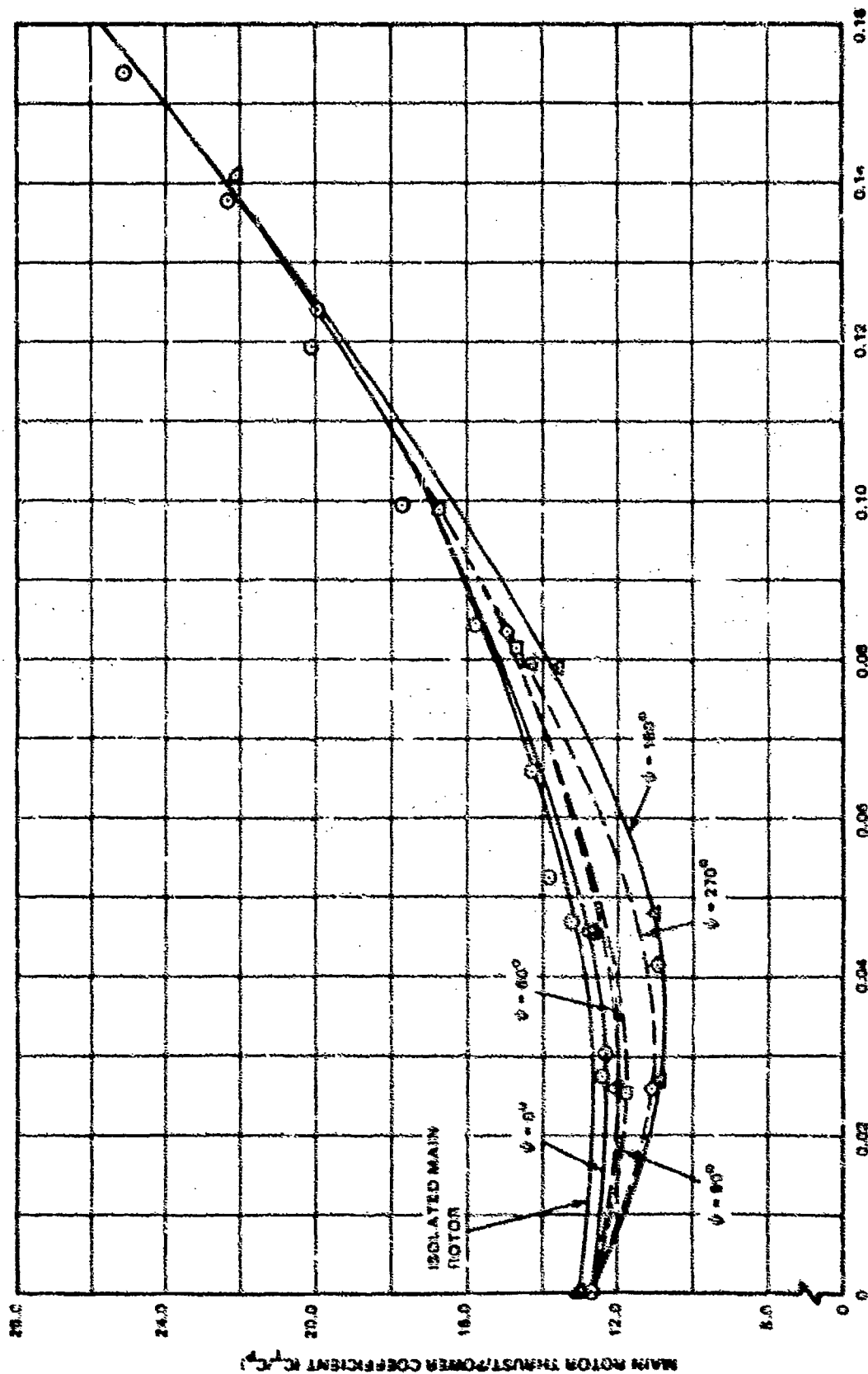
234

MAIN ROTOR ADVANCE RATIO (μ)

Figure 20. Effect of Tail Rotor and Wind Azimuth on Main Rotor, Thrust/Power –
h/d = 0.3, θ = 20°, Position = MID, Rotation = BF, C_{t_0} = 2.

12.0 SELECTION OF TIP SPEED AND NUMBER OF BLADES

The objective of Guideline 12 was to calculate tail rotor detection range as a function of tip speed and number of blades. The calculations were based on the assumption of a helicopter in hover at very low altitude. A variety of assumptions had to be made regarding the performance characteristics and the interrelationship of the two rotors. In particular, it was assumed that both rotors would have the same tip speed and that tail rotor thrust could be related to main rotor thrust (aircraft gross weight) according to the following relationship:

$$T_{TR} = \frac{W^{3/2}}{1.2 \sqrt{2} \pi \rho \ (\Omega R) \ (R) \ (FM)}$$

Main and tail rotor diameters were calculated on the basis of the gross weights and disc loadings in Guideline 12. Detection distances were calculated for tip speeds of 500, 600, 675, and 750 fps; two, four, six, and eight blades; and plotted in Figures 12-1 through 12-3.

Since helicopter aural detection may first occur from either main rotor noise or tail rotor noise, detection ranges were calculated for both rotors at each of the conditions investigated. First, it was necessary to calculate noise levels for each rotor at a position fairly close to the aircraft (300 feet). The noise prediction method was one that was developed by Boeing under Army contract (Ref 14), using the basic equations of Lowson and Ollerhead (Ref 15). The method uses a computer to perform the same functions as the Heron II method of Lowson and Ollerhead, except that somewhat different blade loading assumptions are used to give better correlation with test data.

For the detection calculations, the method of Ollerhead was used (Ref 16). This method relates aural detection range to the sound emitted by the aircraft, the attenuation of the sound with distance, the threshold of hearing, and the ambient masking noise at the observer position. For these calculations, the conditions assumed were sparse jungle terrain absorption and a moderate ambient noise level. Calculations were done on a 1/3-octave basis, with each noise harmonic entered at its correct frequency and the detection range being set by the harmonic that could be heard at the greatest distance. It was assumed that no other noise sources were present.

13.0 DESIGN THRUST REQUIRED

This section presents the derivation of the expressions used in Guideline 13 to determine the values of the components of the required tail rotor thrust. These components include trim thrust, maneuver thrust, and simulated gyroscopic thrust.

13.1 Trim Thrust

In Section 7-2, Appendix III, the trim thrust was calculated as

$$T_{Trim} = \frac{W^{3/2}}{1.2(FM) \sqrt{2\rho\pi} \ \Omega R^2}$$

if

$$K_T = 1.2(FM) \sqrt{2\rho\pi} \ \Omega R^2$$

Then

$$T_{Trim} = \frac{W^{3/2}}{K_T}$$

This expression is plotted in Figure 13-1 for various values of K_T.

13.2 Maneuver Thrust

$$\dot{\psi} = \frac{T_M \ \ell}{N_r I_z} \left[1 - e^{N_r t} \right]$$

where $\dot{\psi}$ = yaw rate in response to step control input

T_M = tail rotor thrust increment for maneuver

ℓ = longitudinal distance between aircraft cg and tail rotor shaft

I_z = aircraft yaw moment of inertia

N_r = yaw rate damping, $\frac{\partial N}{\partial r} \ \frac{1}{I_z}$

t = time from control input.

237

The maneuver thrust increment required to produce a desired yaw rate, $\dot{\psi}_d$, in a desired time t_d is then

$$T_M = -\frac{N_r I_z \dot{\psi}_d}{\ell(1-e^{N_r t_d})}$$

$$= -\frac{K_M N_r}{1-e^{N_r t_d}} \text{ , where } K_M = \frac{I_z \dot{\psi}_d}{\ell}$$

This equation is plotted in Figure 13-4.

Yaw rate damping is obtained from aircraft stability derivative data and includes any applicable SCAS augmentation contribution. Typical values of I_z/ℓ are plotted in Figure 13-3 for various categories of helicopters.

$\dot{\psi}_d$ and t_d are obtained from the aircraft specification requirement stated, for example, as 15 deg/sec yaw rate required in 1.5 seconds.

13.3 Simulated Gyroscopic Thrust

The "simulated" thrust required to precess the tail rotor is (from Ref 9)

$$\Delta C_L = \Delta \frac{6C_T}{\sigma} = \frac{16 \text{ Ip } \dot{\psi}}{\rho \text{ cr}^4 \omega}$$

where I_p is the polar moment of inertia per blade. For a blade of constant chord,

$$I_p = \int_o^r \xi^2 \text{ dm}, \ \xi = 0 \text{ at root, r at tip}$$

$$= \frac{1}{g} \int_o^r \xi^2 \text{ w' } c_{dr}, \text{ w' = weight of blade per square foot}$$

$$= \frac{c}{g} \text{ w' } \frac{r^3}{3}$$

Substituting this expression for I_p,

238

$$\Delta \frac{6C_T}{\sigma} = \frac{16}{3} \frac{w' \dot{\psi}}{g\rho \; \omega r}$$

Replacing ΔC_T by $T_g/\rho \; (\omega r)^2 \; \pi \; r^2$ and rearranging,

$$T_g = \frac{16}{18g} \; (\omega r) \quad \sigma \pi \; r^2 \; w' \; \dot{\psi}$$

Due to damping, the peak maneuver thrust occurs approximately 10 to 20 percent of the way through the maneuver; therefore, the gyroscopic thrust is calculated at that time also. Conservatively, 30 percent ψ_d can be used, giving

$$T_g = 0.3 K_g \; \dot{\psi}$$

where

$$K_g = 0.888 \; (\omega r) \; \sigma \; \pi \; r^2 \; w'/g$$

This equation is plotted in Figure 13-5 for various values of the constant K_g.

13.4 Thrust Required To Balance Fuselage Moment

The approximate thrust required to balance fuselage aerodynamic moments is shown in Figure 13-6. The curves were obtained by analyzing several aircraft of two basic fuselage shapes. The streamlined afterbody, as shown in Figure 13-6, is similar to a UH-2, while the foreshortened afterbody is similar to that of a BO-105 or CH-53.

14.0 ISOLATED TAIL ROTOR THRUST/NET THRUST RATIO

The ratio of isolated tail rotor thrust, C_{T_O}, to net thrust, C_{T_N}, for the Boeing test with bottom forward pusher configuration is determined as follows:

At 20 knots, the average minimum thrust coefficients for all values of h/d are designated in Figure 14-1. The thrust coefficient with main rotor on, but fin off, C_{T_M}, can be expressed in terms of C_T and C_{T_N} as:

$$C_{T_M} = C_{T_N} + 0.70 \, (C_T - C_{T_N})$$

239

Also from Figure 14-1,

$$C_{T_M} = 0.90 \; C_{T_O}$$

Combining the two equations to eliminate C_{T_M} gives

$$C_{T_O}/C_{T_N} = 1.11 + 0.777(C_T/C_{T_N} - 1)$$

This equation is plotted on the left side of Figure 14-2.

At V = 35 knots, from Figure 21, the minimum thrust values occur at h/d = 1. Thus,

$$C_{T_M} = C_{T_N} + 0.66 \; (C_T - C_{T_N})$$

$$C_{T_M} = 1.05 \; C_{T_O}$$

Combining,

$$C_{T_O}/C_{T_N} = 0.95 + 0.63 \; (C_T/C_{T_N} - 1)$$

This equation is also plotted in Figure 14-2.

At V = 0, from Figure 22 using the minimum thrust which occurs at h/d = 1,

$$C_{T_M} = C_{T_N} + 1.0 \; (C_T - C_{T_N})$$

$$C_{T_M} = C_{T_O} \qquad .$$

Eliminating C_{T_M},

$$C_{T_O}/C_{T_N} = C_T/C_{T_N}$$

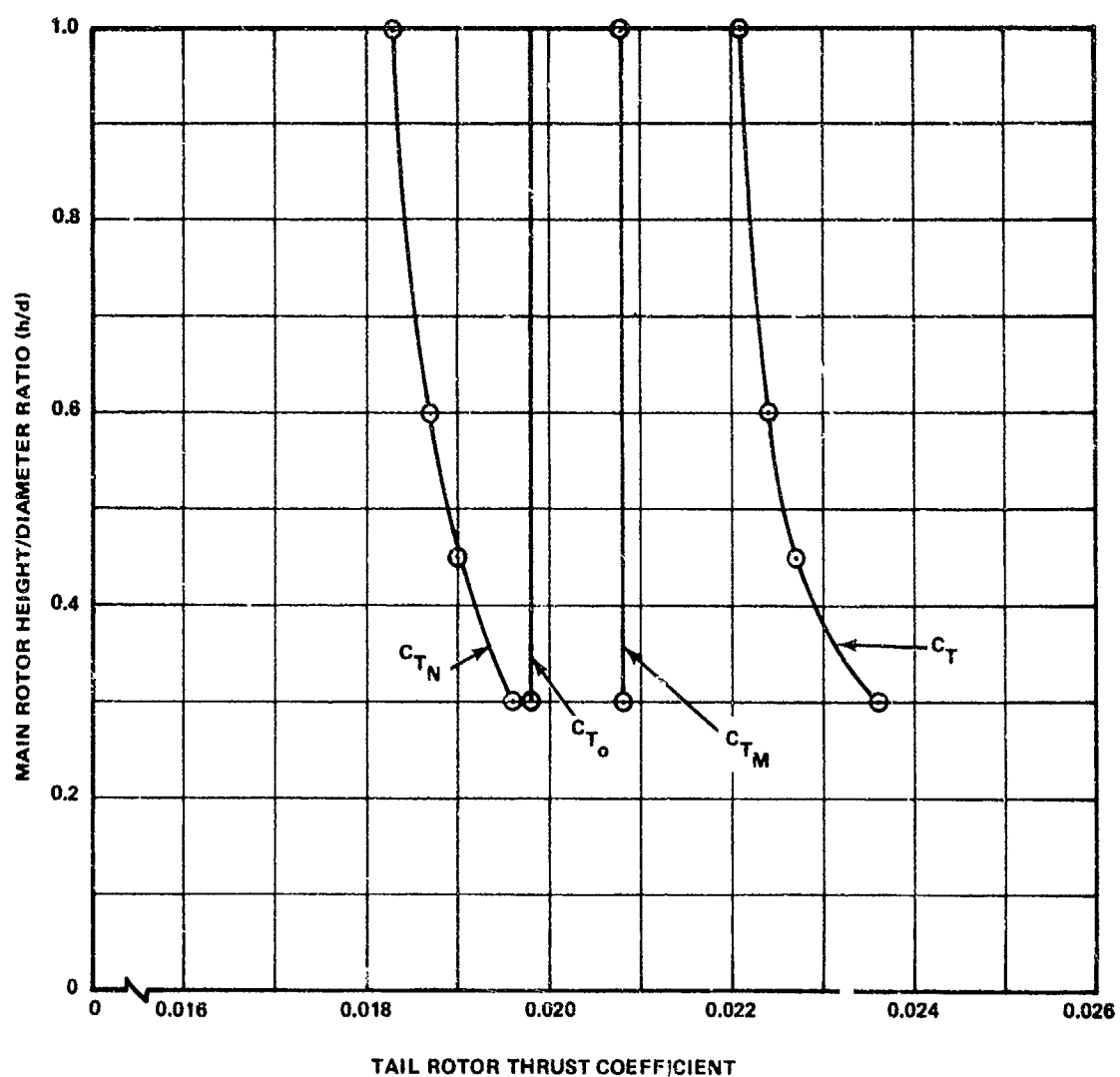This expression is included in Figure 14-2.

240

Figure 21. Variation of Tail Rotor Thrust With Main Rotor Height at V = 35 kn.
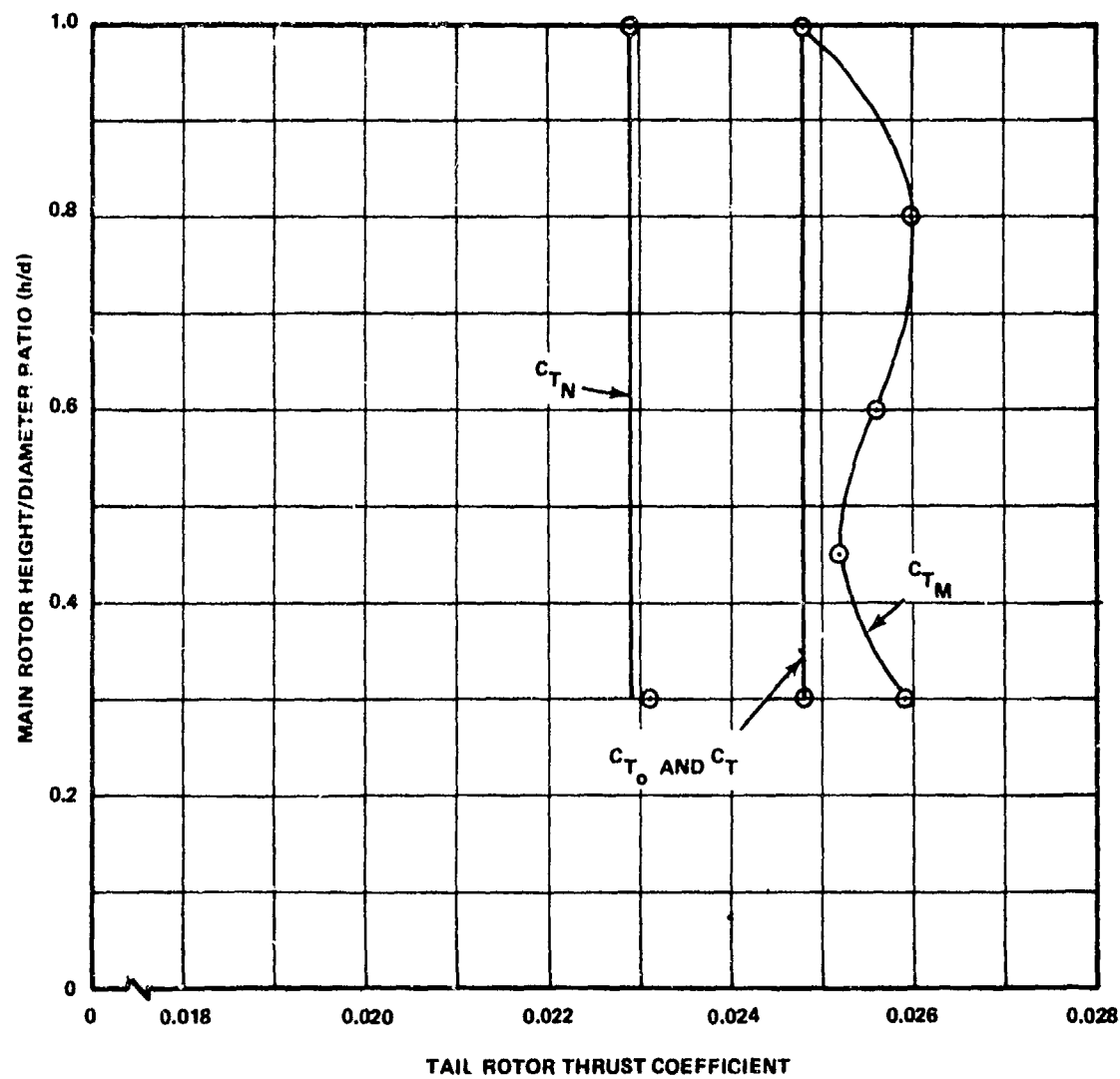
241

Figure 22. Variation of Tail Rotor Thrust With Main Rotor Height at V = 0 kn.

242

16.0 DESIGN POWER

Figure 16-1 of Guideline 16 shows the factor to multiply isolated tail rotor power to obtain tail rotor power in the presence of main rotor and fin. The data shown on this curve was determined as follows:

1. Very little difference in the thrust power ratio between isolated tail rotor and tail rotor in the presence of main rotor data was noted during Boeing tests.

2. Considerable difference in such ratio was noted when the fin was installed in the presence of main and tail rotor.

3. Therefore, Table VII shows comparative data for:

    ● Tail rotor in presence of main rotor

    ● Tail rotor in presence of both main rotor and fin

4. Such power data was corrected to a constant value of C_T or $C_{T_N} = 0.023$ by the same method shown on page 215.

5. K_p was calculated then as shown in Table VII.

6. Values of K_p for other values of $\bar{A}$ were obtained by assuming that the fin loss (and thus net thrust) varied directly with fin blockage factor, $\bar{A}$. Thus the power multiplying factor, K_p, will vary as the fin blockage factor to the 3/2 power.

7. The preceding data is all based on a constant $h/d = 0.30$, $\theta = 20^\circ$ ($C_\sigma \simeq 2.0$), pusher configuration, $s/r = 0.45$, $\psi = 0^\circ$ or 60° and $\bar{A} = 0.203$. Future tests should be conducted to obtain more basis for the K_p multiplying factor. This factor may apply only to the initial part of a maneuver, for when the aircraft rotates to a new azimuth, such a factor may no longer be applicable.

    However, it is inserted as a part of the Guidelines because such power variations were observed during the Boeing tests of Reference 2.

243

TABLE VII. TAIL ROTOR IN PRESENCE OF MAIN ROTOR

(A) TAIL ROTOR IN PRESENCE OF MAIN ROTOR

			$\psi = 60°$				$\psi = 0°$	
1	2	3	4	5	6	7	8	9
V	C_T	C_P	C_{PREF}	$\dfrac{C_T}{C_{PREF}}$	C_T	C_P	C_{PREF}	$\dfrac{C_T}{C_{PREF}}$
0	0.0259	0.0059	0.00503	4.572	0.0259	0.0059	0.00503	4.572
20	0.0225	0.00488	0.00504	4.563	0.0255	0.00577	0.00494	4.655
35	0.0208	0.00442	0.00514	4.474	0.0256	0.00584	0.00497	4.627

(B) TAIL ROTOR IN PRESENCE OF MAIN ROTOR AND FIN

			$\psi = 60°$					$\psi = 0°$		
10	11	12	13	14	15	16	17	18	19	20
V	C_{TN}	C_P	C_{PREF}	$\dfrac{C_{TN}}{C_{PREF}}$	K_P	C_{TN}	C_P	C_{PREF}	$\dfrac{C_{TN}}{C_{PREF}}$	K_P
0	0.0231	0.00484	0.00485	4.472	0.964	0.0231	0.00484	0.00485	4.742	0.964
20	0.0198	0.00447	0.00596	3.859	1.182	0.0238	0.00525	0.00499	4.61	1.009
35	0.0194	0.00510	0.00658	3.495	1.28	0.0241	0.00585	0.00545	4.22	1.09

Calculations
Col. (15) K_P = (5)/(14)
Col. (20) K_P = (9)/(19)

Conditions
h/d = 0.30, θ = 20°, Pusher, s/r = 0.45,
C_{TREF} = 0.023, $\bar{A}$ = 0.203
C_{PREF} based on C_{TREF}